

# Fetal Susceptibility to Porcine Reproductive and Respiratory Syndrome Virus

A Thesis Submitted to the  
College of Graduate and Postdoctoral Studies  
In Partial Fulfillment of the Requirements  
For the Degree of Doctor of Philosophy  
In the Large Animals Clinical Sciences  
University of Saskatchewan  
Saskatoon

By  
**Carolina Maciel Malgarin**

© Copyright Carolina Maciel Malgarin, January 2021. All rights reserved.  
Unless otherwise noted, copyright of the material in this thesis belongs to the author.

### **Permission to use**

In presenting this thesis/dissertation in partial fulfillment of the requirements for a Postgraduate degree from the University of Saskatchewan, I agree that the Libraries of this University may make it freely available for inspection. I further agree that permission for copying of this thesis/dissertation in any manner, in whole or in part, for scholarly purposes may be granted by the professor or professors who supervised my thesis/dissertation work or, in their absence, by the Head of the Department or the Dean of the College in which my thesis work was done. It is understood that any copying or publication or use of this thesis/dissertation or parts thereof for financial gain shall not be allowed without my written permission. It is also understood that due recognition shall be given to me and to the University of Saskatchewan in any scholarly use which may be made of any material in my thesis/dissertation.

### **Disclaimer**

Reference in this thesis/dissertation to any specific commercial products, process, or service by trade name, trademark, manufacturer, or otherwise, does not constitute or imply its endorsement, recommendation, or favoring by the University of Saskatchewan. The views and opinions of the author expressed herein do not state or reflect those of the University of Saskatchewan, and shall not be used for advertising or product endorsement purposes. Requests for permission to copy or to make other uses of materials in this thesis/dissertation in whole or part should be addressed to:

Head of the Department of Large Animals Clinical Sciences  
52 Campus Drive, Western College of Veterinary Medicine  
University of Saskatchewan  
Saskatoon, Saskatchewan, S7N 5B4, Canada  
OR  
Dean  
College of Graduate and Postdoctoral Studies  
University of Saskatchewan  
116 Thorvaldson Building, 110 Science Place  
Saskatoon, Saskatchewan S7N 5C9 Canada

## Abstract

Porcine Reproductive and Respiratory Syndrome (PRRS) is a swine disease caused by PRRS Virus (PRRSV), which besides respiratory disease, can also lead to reproductive failure. The extent of the reproductive disease can be highly variable within individual litters, demonstrating great variation in PRRSV susceptibility and resistance to the virus among litters, while intrauterine growth retarded (IUGR) fetuses have lower viral loads in both fetal thymus and in endometrium, indicating larger fetuses as more susceptible to transplacental PRRSV infection. Our hypothesis was that naturally occurring resistance/resilience to PRRSV infection and disease characteristic can be explained through the combination of techniques, such as fetal phenotype, metabolomics, and gene expression. We started by characterizing the temporal movement of PRRSV following maternal inoculation. It was observed that endometrium becomes infected as soon as 2 days post-inoculation (DPI), while fetal placenta and fetal serum presented viral RNA by 5 DPI. Demised fetuses due to PRRSV infection could be identified after 12 days of maternal infection, which established an ideal time point for future research. While this project was conducted, additional sampling of the endometrium and placenta was performed to determine the number of samples and analysis method required for an accurate, yet feasible viral load and histopathologic investigation. It was concluded that at least three random collected samples from each tissue are needed for both analyses, while these samples can be processed as a pool for viral RNA quantification. Moving forward on our objectives, a fetal metabolomics investigation was conducted and found differences in the metabolome of infected fetuses when compared to controls, as well as of IUGR fetuses related to normal developing fetuses. Most disturbances were related to amino acids pathways and lipid molecules, indicating differences in both nutritional transport ways and apoptosis pathways. To test the apoptosis pathway and the historically suggested hypoxia in PRRSV infected fetuses, two studies study between resilient and susceptible fetuses were conducted: 1) TUNEL staining of fetal tissues to detect apoptosis, and 2) expression of target genes in both apoptosis and hypoxia pathway. The results indicate that at 12 DPI both apoptosis and hypoxia were occurring in the fetal heart, while only apoptosis seems to affect the fetal brain; fetal thymus appears to be protected from these events. At 21 DPI, liver and thymus present with increased apoptosis in the highly infected animals, while only meconium-stained fetuses displayed apoptosis in the heart. In conclusion, fetal phenotype,

metabolomics, and gene expression were able to identify naturally occurring PRRSV resilient or susceptible fetuses.

## **Acknowledgements**

I would like to thank all the people without whom I would not have made it through my PhD degree, especially my supervisor Dr. John Harding, whose insights, incredible knowledge, and great supervision steered me through this research. A special thanks to all my committee members, Dr. Susan Detmer, Dr. Daniel MacPhee, Dr. Suraj Unniappan, and all the LACS department people that aided in making it all happen.

Thanks to all my colleagues in the Harding's Lab, who took the time to share their knowledge and skills with me, teach me, and support me through my development as a grad student for the past five years of study. I am also very grateful to the Vet Microbiology Department for "adopting" me in all their fun, food-filled potlucks, making these last few years much more enjoyable.

My biggest thanks to my family for all the support you have shown me through this program, even from the distance of 10,000 km! For my friends that kept me sane and encouraged to keep going forward. And for my husband Evan, thanks for all your support, encouragement, pep talks, and all the happiness we find in each other.

## Table of Contents

Permission to use.....	i
Disclaimer .....	i
Abstract.....	ii
Acknowledgements .....	iv
Table of Contents .....	v
List of Tables .....	ix
List of Figures.....	x
List of Additional files .....	xii
<b>1. Introduction and Literature Review.....</b>	<b>1</b>
<b>1.1. Reproductive physiology in the pig – placentation, transport of nutrients .....</b>	<b>1</b>
1.1.1. <i>Anatomical structures and function of the swine placenta .....</i>	<i>1</i>
1.1.2. <i>Placentation, fetal isolation and development.....</i>	<i>3</i>
1.1.3. <i>Placental transport mechanisms.....</i>	<i>5</i>
1.1.4. <i>Intrauterine growth retardation (IUGR) .....</i>	<i>6</i>
<b>1.2. Reproductive PRRS .....</b>	<b>7</b>
1.2.1. <i>PRRSV infection in pregnant sows and gilts.....</i>	<i>7</i>
1.2.2. <i>Events occurring at the maternal-fetal interface .....</i>	<i>8</i>
1.2.3. <i>Events occurring within fetuses .....</i>	<i>9</i>
<b>1.3. PRRSV detection and investigative methods.....</b>	<b>11</b>
1.3.1. <i>Classic diagnostic and investigative tools .....</i>	<i>11</i>
1.3.2. <i>Innovative methods – the “-omics” revolution.....</i>	<i>13</i>
<b>1.4. Rationale, hypothesis, objectives.....</b>	<b>16</b>

<b>2. Classification of fetal resilience to porcine reproductive and respiratory syndrome (PRRS) based on temporal viral load in late gestation maternal tissues and fetuses .....</b>	<b>18</b>
<b>2.1. Abstract.....</b>	<b>19</b>
<b>2.2. Introduction .....</b>	<b>19</b>
<b>2.3. Materials and methods.....</b>	<b>21</b>
2.3.1. <i>PRRSV propagation.....</i>	<i>21</i>
2.3.3. <i>Experimental procedures.....</i>	<i>22</i>
2.3.4. <i>Fetal preservation and sample collection.....</i>	<i>22</i>
2.3.5. <i>Quantification of PRRSV RNA.....</i>	<i>23</i>
2.3.6. <i>Classification of resistant, resilient and susceptible fetuses.....</i>	<i>24</i>
2.3.7. <i>Data analysis .....</i>	<i>24</i>
<b>2.4. Results .....</b>	<b>25</b>
2.4.1. <i>PRRSV transmission across maternal and fetal tissues by day post inoculation....</i>	<i>27</i>
2.4.2. <i>Classification of resistant, resilient and susceptible fetuses.....</i>	<i>35</i>
<b>2.5. Discussion.....</b>	<b>44</b>
<b>2.6. Conclusions .....</b>	<b>47</b>
<b>3. Samples sizes required to accurately quantify viral load and histologic lesion severity at the maternal-fetal interface of PRRSV-inoculated pregnant gilts.....</b>	<b>57</b>
<b>3.1. Abstract.....</b>	<b>58</b>
<b>3.2. Introduction .....</b>	<b>58</b>
<b>3.3. Materials and methods.....</b>	<b>60</b>
3.3.1. <i>Animal experiment and sample collection.....</i>	<i>60</i>
3.3.2. <i>PRRSV RNA extraction and sample pooling .....</i>	<i>60</i>
3.3.3. <i>Quantitative PCR.....</i>	<i>61</i>
3.3.4. <i>Histopathology.....</i>	<i>62</i>
3.3.5. <i>Data analysis .....</i>	<i>63</i>
<b>3.4. Results .....</b>	<b>64</b>
3.4.1. <i>PRRSV RNA quantification.....</i>	<i>64</i>
3.4.2. <i>Histopathology.....</i>	<i>69</i>
<b>3.5. Discussion.....</b>	<b>80</b>

<b>4. Fetal metabolomic alterations following porcine reproductive and respiratory syndrome virus infection .....</b>	<b>86</b>
<b>4.1. Abstract.....</b>	<b>87</b>
<b>4.2. Introduction .....</b>	<b>88</b>
<b>4.3. Material and methods .....</b>	<b>89</b>
4.3.1. <i>Phenotypic fetal susceptibility groups .....</i>	<i>89</i>
4.3.2. <i>Metabolomic techniques .....</i>	<i>91</i>
4.3.3. <i>Statistical and pathway analyses .....</i>	<i>93</i>
<b>4.4. Results .....</b>	<b>94</b>
4.4.1. <i>Metabolomic profiles associated with disease progression.....</i>	<i>94</i>
4.4.2. <i>Metabolomic profiles associated with altered fetal development and PRRSV infection 110</i>	
4.4.3. <i>Exploring PRRS IUGR group diversity .....</i>	<i>128</i>
<b>4.5. Discussion .....</b>	<b>132</b>
<b>4.6. Conclusions .....</b>	<b>135</b>
<b>5. Fetal hypoxia and apoptosis following maternal porcine reproductive and respiratory syndrome virus (PRRSV) infection .....</b>	<b>137</b>
<b>5.1. Abstract.....</b>	<b>138</b>
<b>5.2. Background.....</b>	<b>139</b>
<b>5.3. Material and Methods.....</b>	<b>140</b>
5.3.1. <i>Experiment 1: Apoptosis in fetal tissue at 21 DPI.....</i>	<i>140</i>
5.3.2. <i>Experiment 2: Apoptosis and hypoxia gene expression in fetal tissues at 12 DPI143</i>	
<b>5.4. Results .....</b>	<b>148</b>
5.4.1. <i>Experiment 1: Differences in apoptosis in fetal tissues at 21 DPI.....</i>	<i>148</i>
5.4.2. <i>Experiment 2: Apoptosis and hypoxia gene expression in fetal tissues at 12 dpi. 152</i>	
<b>5.5. Discussion .....</b>	<b>159</b>
<b>5.6. Conclusions .....</b>	<b>164</b>
<b>6. General discussion, conclusions and future directions .....</b>	<b>169</b>

7. References..... 177

## List of Tables

<b>Table 2-1:</b> Descriptive summary of fetal infection rates and viral load in tissues by days post inoculation.....	29
<b>Table 3-1:</b> PRRSV RNA concentration, coefficients of variation, and levels of agreement for endometrial and placental samples and pools.....	65
<b>Table 3-2:</b> Distribution of histologic lesion scores in endometrium and placenta in tissues used to assess inter-rater agreement.....	70
<b>Table 3-3:</b> Levels of agreement in lesion severity scores between pathologists as determined by the kappa inter-rater statistic.....	73
<b>Table 3-4:</b> Levels of agreement in lesion severity scores within pathologists as determined by the kappa inter-rater statistic.....	74
<b>Table 4-1:</b> Metabolites with significant differences among fetal PRRS disease progression groups.....	97
<b>Table 4-2:</b> Metabolites with significant differences between contrasting PRRSV-infected and IUGR phenotypic groups.....	112
<b>Table 5-1:</b> Porcine specific primer sequences used to assess fetal apoptosis and hypoxia. ....	146
<b>Table 5-2:</b> Spearman’s rank correlation test results between liver or thymus (TUNEL foci counts or sizes) and maternal-fetal interface (MFI) lesion severity* .....	151

## List of Figures

<b>Figure 2.1:</b> Median serum PRRSV RNA concentration in gilt sera. ....	26
<b>Figure 2.2:</b> Viral load heat maps by tissue and fetal preservation. ....	32
<b>Figure 2.3:</b> Fetal preservation status by position and days post inoculation. ....	34
<b>Figure 2.4:</b> Susceptible, resistant and resilient fetal matrix. ....	36
<b>Figure 2.5:</b> Classification of resistant, resilient, susceptible fetuses using a random forest model. .....	39
<b>Figure 2.6:</b> PRRSV RNA concentration (viral load) by IUGR group in fetal tissues and sera. ..	43
<b>Figure 3.1:</b> Viral load concordance. ....	68
<b>Figure 3.2:</b> Endometrial lesion concordance. ....	76
<b>Figure 3.3:</b> Placental lesion concordance. ....	78
<b>Figure 4.1:</b> Metabolite profiles of four disease progression fetal phenotypes. ....	96
<b>Figure 4.2:</b> Metabolite profile of control (CTRL) and uninfected (UNINF) contrast. ....	101
<b>Figure 4.3:</b> Metabolite profile of uninfected (UNINF) and high-viral load (HVL-VIA) contrast. .....	104
<b>Figure 4.4:</b> Metabolite profile of high-viral load (HVL-VIA) and meconium-stained fetuses (MEC) contrast. ....	108
<b>Figure 4.5:</b> Visual summary of the most significant metabolite changes associated with disease progression. ....	109
<b>Figure 4.6:</b> Metabolite profiles of four IUGR x PRRV-infected. (A) Two component PLS-DA score plot of all groups with individual fetuses represented by dots; (B) Variance Importance in Projection (VIP) score plot displaying the 15 most important metabolites differentiating the groups with colored side bar displaying the relative metabolite concentration in each group. ..	111
<b>Figure 4.7:</b> Metabolite profile of control-normal development fetuses (CON-N) and control- IUGR fetuses (CON-IUGR). ....	118
<b>Figure 4.8:</b> Metabolite profile of control-normal development fetuses (CON-N) and PRRS- infected normal development fetuses (PRRS-N). ....	120
<b>Figure 4.9:</b> Metabolite profile of control-IUGR (CON-IUGR) and PRRS-infected IUGR fetuses (PRRS-IUGR). ....	124
<b>Figure 4.10:</b> Metabolite profile of PRRS-infected normal development fetuses (PRRS-N) and PRRS-infected IUGR fetuses (PRRS-IUGR). ....	127

<b>Figure 4.11:</b> Analysis of the PRRSV-IUGR group as two subgroups based on PRRS viral concentration.....	129
<b>Figure 4.12:</b> Visual summary of the most significant metabolite changes associated with PRRSV-infection of fetuses with normal development or intrauterine growth retardation (IUGR). .....	131
<b>Figure 5.1:</b> TUNEL staining in three fetal tissues of PRRSV-infected fetuses. ....	149
<b>Figure 5.2:</b> Box-and-whisker plot of TUNEL positive foci counts and sizes by group. ....	150
<b>Figure 5.3:</b> Apoptosis and hypoxia gene expression in fetal brain.....	153
<b>Figure 5.4:</b> Apoptosis and hypoxia gene expression in fetal heart. ....	155
<b>Figure 5.5:</b> Apoptosis and hypoxia gene expression in fetal thymus. ....	157
<b>Figure 5.6:</b> Summary of gene expression fold changes by fetal tissues and group. Heat map of group median gene expression fold changes associated with apoptosis (CASP 3, 7, 8, 9; RIPK 1, 3), hypoxia (HIF1a, VEGF, LDHA, NOS2, NOX1), and infection (IDO1) by tissue and fetal phenotype.....	158
<b>Figure 6.1:</b> Timeline of infection and disease progression following PRRSV maternal inoculation.....	175

**List of Additional files**

**Additional file 2.1:** Fetal preservation categories..... 50

**Additional file 2.2:** Viral concentration by days post inoculation in endometrium. .... 51

**Additional file 2.3:** Viral concentration by days post inoculation in placenta. .... 52

**Additional file 2.4:** Viral concentration by days post inoculation in umbilical cord. .... 53

**Additional file 2.5:** Viral concentration by days post inoculation in sera. .... 54

**Additional file 2.6:** Viral concentration by days post inoculation in thymus..... 55

**Additional file 2.7:** Viral concentration by days post inoculation in amniotic fluid. .... 56

**Additional file 3.1:** Visual rendition of the maternal-fetal interface (MFI) of a single fetus showing locations of pieces collected for assessment of viral load (PCR Pc 1-5) and severity of endometrial and placental lesions (Histo Pc 1-3) following PRRSV-infection..... 84

**Additional file 3.2:** Box plot of PRRSV concentration of the 5 individual pieces of endometrium (A) and placenta (B) used to generate the virtual pools in silico and the pool of RNA and tissue homogenate. .... 85

**Additional file 5.1:** TUNEL staining in three fetal tissues of uninfected control fetuses. Scant cells with TUNEL positive staining are observed at higher magnification of fetal thymus (B) and liver (D), but not in heart (F). .... 166

**Additional file 5.2:** Experiment 1 (21 DPI) PRRSV RNA concentration by fetal group..... 167

**Additional file 5.3:** Experiment 2 (12 DPI) PRRSV RNA concentration by fetal group..... 168

## List of abbreviations

ADMA	Asymmetric dimethylarginine
ALA	Alpha-linoleic acid
Alpha-AAA	Alpha-aminoadipic acid
AMN	Amniotic fluid
ARA	Arachidonic acid
BRN	Brain
Bs	Biosynthesis
Buta	Butanoate
C0	Carnitine
C141	Tetradecenoyl carnitine
C2	Acetylcarnitine
CASP3	Caspase 3
CASP7	Caspase 7
CASP8	Caspase 8
CASP9	Caspase 9
CHLA	Chlorophyll
cis-OH-Pro	Cis-4-Hydroxy-L-proline
CON-IUGR	Control, intra-uterine growth retarded fetus
CON-N	Control, normal development fetus
CTRL	Fetuses from control (non-inoculated) gilts
Deg	Degradation
DI-MS	Direct infusion mass spectrometry
DPI	Days post infection
END	Endometrium
Glyo	Glyoxylate
GPL	Glycerophospholipid
GSH	Glutathione
HIF1a	Hypoxia-inducible Factor 1 subunit alpha
HRT	Heart
HVL-MEC	High viral load meconium-stained fetuses.

HVL-VIA	Viable high viral load fetuses
IDO1	Indoleamine 2,3-dioxygenase 1
INF	Infected
LDHA	Lactate dehydrogenase a
LVL	Low viral load fetuses
LVR	Liver
LysoPC	Lysophosphocholine
MEC-B	Meconium-staining on the body
MEC-F	Meconium-staining on the face
Met	Metabolism
MFI	Maternal-fetal interface
NMR	Nuclear magnetic resonance
NOS2	Nitric oxide synthase 2
NOX1	NADPH oxidase 1
PC	Phosphocholine
PCA	Principal component analysis
PLC	Placenta
PLS-DA	Partial least square – discriminant analysis
Por	Porphyrin
Prop	Propanoate
PRRS-IUGR	PRRSV infected, intra-uterine growth retarded fetus
PRRS-N	PRRSV infected, normal development fetus
PRRSV2	Porcine reproductive and respiratory syndrome virus 2
RIPK1	Receptor-interacting serine/threonine-protein kinase 1
RIPK3	Receptor-interacting serine/threonine-protein kinase 3
RT-qPCR	Quantitative reverse transcription PCR
SeC	Selenocompound
SER	Serum
SM	Sphingomyelin
THY	Thymus

TUNEL	Terminal deoxynucleotidyl transferase DUTP nick end labeling
UMB	Umbilical cord
UNINF	Uninfected fetuses from inoculated gilts (Experiment 2)
VEGFa	Vascular endothelial growth factor A
VIP	Variable importance in projection

# 1. Introduction and Literature Review

## 1.1. Reproductive physiology in the pig – placentation, transport of nutrients

The female pig is a non-seasonal polyestrous mammal that gives birth to multiple offspring at each pregnancy (polytocous). The regular cycle lasts 21 days on average (range 18-24 days), with a pregnancy length of around 114 days and a uterine physiology that takes around 20-25 days to recover following birth. The dam will exhibit estrus again a week after weaning, and it lasts from 2 to 3 days, being affected by environmental and genetic factors. After being bred, either by natural mating or artificial insemination (AI), fertilization occurs in the following 2-6 hours, which will lead to a series of anatomical and physiological events in the dam's reproductive tract.<sup>1-3</sup>

### 1.1.1. Anatomical structures and function of the swine placenta

The swine placenta, formed individually after fertilization, is classified<sup>1-3</sup> as:

- Chorioallantoic (apposition of chorion and allantois);
- Diffuse (regarding its form), as it has the chorionic villi uniformly distributed over the entirety of chorion's surface and closely spaced;
- Pleated (interdigitation model);
- Cross flow to counter-current blood flow; and
- Epitheliochorial (regarding the layers of inter-hematic membrane), composed by six layers: maternal blood vessel endothelium, connective tissue, uterine epithelium, trophoblast, fetal connective tissue and fetal blood vessel endothelium.

After formation, most of the placental layers remain the same until the end of pregnancy, however, they can change in thickness during different stages of gestation in order to increase or decrease the diffusion distance of pregnancy products between maternal and fetal vasculatures.<sup>2-4</sup> There are two structures, however, that do disappear early in gestation, the yolk sac and the choriovitelline region.<sup>2,4</sup> Due to the epitheliochorial nature of the swine placenta, the attachment is superficial. Thus, maternal tissues are kept intact during birth and placental separation, characterising an adecidua placenta.<sup>2-4</sup>

Placental formation relies on endometrial modifications in the dam, while the conceptus gives origin to the chorion and its functional unit, the chorionic villus, which are finger-like

projections on the chorion's surface protruding towards the endometrium.<sup>5</sup> The chorionic villi distribution help to classify the type of placenta as diffuse.<sup>3,5</sup> After the maternal and fetal tissue interaction has been successfully established, placental development starts, originating three different zones by the end of the first third of gestation: the central placental zone (adjacent to the fetus, also characterized as the highly vascular placenta – HVP); the two paraplacental zones (the immediate lateral zones to the fetus, also referred to as the less vascular placenta – LVP); and the necrotic tips at the terminal ends (the uterine area between placentas with no placenta attached).<sup>3,6,7</sup>

At 30 days of gestation, the trophoblast is formed by a high columnar type of cells, being taller in the depth of the chorionic troughs, decreasing their height on the sides and summit of ridges. The long microvilli on the apical surface of the trophoblast cell interdigitates with the uterine epithelium cell, while the round nucleus of the trophoblast cell locates in the basal area.<sup>3</sup> The trophoblast cells are closely apposed by tight junctions - located on the basal lamina. Capillaries are separated from the epithelial basal lamina by the mesenchymal tissues.<sup>3</sup> By day 58, mid-gestation, the trophoblast cells structure and positions have drastically changed, with capillaries now deeply indenting the lateral side and summit of ridges of the fetal epithelium, with vessels often present surrounded by the trophoblastic cells.<sup>3</sup> The basal lamina of the capillaries has fused with the trophoblast basal lamina, forming a single lamina. There is a decrease in height of the trophoblast cells on the sides and tops of the ridges, especially where the capillaries protrude into the epithelium. In contrast, the trophoblast cells at the base of the ridges are narrow high columnar.<sup>3</sup> Friess<sup>3</sup> also reported that, in the last third of gestation (days 100 and 110), the fetal vessels indent further into the trophoblast, and cell height is further reduced. In conjunction with maternal capillaries projecting in between the uterine epithelial cells and the thinning of the uterine epithelium, it leads to a marked decrease of the transplacental intervacular distance.<sup>3,8</sup>

At gestation day 30, contrary to the fetal epithelial cells, the height of the uterine epithelial cells do not change markedly.<sup>3</sup> Between the uterine epithelium of the microvilli, pinocytotic invaginations can be observed. The nuclei of those cells are elongated or oval in shape, with a more irregular outline than the fetal cell nuclei. Finger-like processes protrude from the cells to intercellular channels between neighbour cells.<sup>3</sup> The uterine epithelium sits on a well-defined basal lamina, while maternal vessels are separated by connective tissue.<sup>3</sup> Fewer changes

are noticed by day 58, contrary to the fetal side. The height of the cells can slightly decrease, however, as previously, the lateral and basal membranes are still highly convoluted, presenting intercellular channels.<sup>3</sup> By the final stage of pregnancy, the uterine epithelium shows a considerable reduction of its height, the nuclei are still round or oval,<sup>3</sup> and the neighbour uterine cells are separated by a complex system of intercellular channels that allow communication between cells.<sup>3</sup>

A remarkable characteristic of the swine placenta is the presence of areolae, located over the openings of the uterine glands, which are dome-shaped and look like circular marks on the chorionic surface.<sup>2,3,9,10</sup> Areolar glands in the areolae are specialized columnar to cuboidal epithelium responsible for the maternal-fetal substance transfer.<sup>2</sup> Areolae are formed by both maternal and fetal tissue where the uterine glands open and “uterine milk” (histotrophic secretions) is stored.<sup>11,12</sup> The epithelium has a high absorptive potential due to the high columns of epithelium, forming long microvilli, vesicles and tubular system.<sup>2,10,12</sup> The areola can be further divided into two types:

- Regular areolae: accumulates histotrophic secretions from only one uterine gland. When observed on the fetal membranes they can present as opaque, translucent, circular spots. Each placenta can have up to 7,000 regular areolae, measuring a diameter of 3 – 8 mm.<sup>13,14</sup>
- Irregular areolae: accumulate histotrophic secretions from several uterine glands. They present with indistinct boundaries due to the aperture of more than one uterine glands. Each placenta can have up to 1,500 irregular areolae, each measuring up to 15 times the size of the regular areolae.<sup>13,14</sup>

### *1.1.2. Placentation, fetal isolation and development*

After fertilization of the oocyte, the initial stage of embryonic development starts and after the cleavage divisions are done, the blastocyst is formed and remains growing, giving origin to the trophoblast and the inner cell mass (ICM) cell populations. Around days 7-8, the embryo hatches from the zona pellucida into the lumen of the uterus and undergoes significant growth. Eventually, the inner cell mass will develop into the body of the embryo, while the trophoblastic cells will form the chorion.<sup>5</sup> An additional layer of cells (primitive endoderm) starts to develop just beneath the inner cell mass, forming the inside lining of the trophoblast, while the mesoderm starts to form in between this primitive endoderm and the ICM (soon to be embryo).

During the next few days the blastocyst will elongate into a filamentous thread form, which will grow to 1 meter in length by day 16. Extraembryonic membranes at the pre-attachment stage are essential for embryo survival and attachment to the uterus following maternal recognition of pregnancy and are originated from the trophoblast, primitive endoderm, extra-embryonic mesoderm, and the embryo<sup>5</sup>:

- Yolk sac: formed by the evagination of the primitive endoderm into the ICM. It's the first structure to develop and to regress as the embryo develops.
- Chorion: originated by the "fusion" of the trophoblast with the mesoderm on the outer side, projecting around the embryo, to create a sac around the conceptus.
- Amnion: the sac structure formed by the chorion projection surrounding the embryo, filled with fluids to mechanically protect the embryo and also prevent attachment of the developing tissues to each other.
- Allantois: originates from the primitive gut of the embryo to collect embryonic liquid wastes. It continues to expand as the embryo develops and, eventually, it will fuse with the chorion, forming the allantochorion (fetal placenta that will attach to the uterus).

The preimplantation/pre-attachment stage embryos migrate and space themselves in both uterine horns between days 4 and 12, allowing the estrogen produced by the conceptus to be distributed over the entire uterine surface.<sup>15,16</sup> This process, known as embryo distribution, is uniform along the uterine horns and the equally spaced distribution of embryos throughout the uterine horns is facilitated by a range of events, including contractions of the myometrium, embryo orientation, and a diverse set of molecular activities.<sup>15,17,18</sup> By day 15 of gestation, spacing of the conceptuses is complete and the implantation progresses until day 18 of gestation.<sup>15,17</sup> The process of implantation is defined by the attachment of the blastocyst to the uterus through maternal and embryonic layers juxtaposition, leading to a firm adhesion of the trophoblast to the maternal epithelium by day 20.<sup>19</sup>

Following implantation, the development and regression of the yolk sac and the development and migration of the allantois into the elongated chorion which will become the functional placenta occur. The chorioallantois gets filled with allantoic fluid, helping in the implantation process and stimulating the uterine and placental growth.<sup>3,5,20</sup>

Placental areolae start to develop in close proximity to the uterine glands around gestation day 15 and it is observable by day 30 of gestation,<sup>3</sup> while the rest of the chorioallantois

surface starts to develop microscopic folds around day 35.<sup>20</sup> The HVP zone appears to start the microfold process at 27 days of pregnancy, earlier than the LVP zones, which start around day 32.<sup>21</sup> However, there are no differences in fold length and depth between the two zones, as the microfolds become narrower and deeper.<sup>21</sup>

Also around 27 days, the necrotic tips become identifiable as placental membranes that are not attached to either the uterus nor to the adjacent fetus, and remain similar by day 42, despite their possible entanglement.<sup>21</sup> Necrotic tips remain present until the end of gestation and, later in gestation, are able to adhere to necrotic tips of neighbouring fetuses.<sup>7</sup> Placental length, weight, and surface area, as well as number of areolae continue to increase until gestation days 50 to 70, but change little thereafter.<sup>22</sup> The angiogenic development, however, continues to increase the capillary volume of placenta close to term.<sup>23</sup>

### *1.1.3. Placental transport mechanisms*

The placenta can have different exchange mechanisms for different needs, ranging from simple diffusion, facilitated diffusion, to active transport<sup>3,5,8</sup>:

- Simple diffusion: transfer of materials, such as gases and water that pass from high to low concentrations.
- Facilitated diffusion: transport of glucose, amino acids and other metabolically relevant materials using specific carrier molecules.
- Active transport: transport using active pumps for materials such as amino acids.
- Endocytosis/Pinocytosis: an energy expending process occurring in the areola to transfer materials from the maternal uterine glands to the fetus, such as uteroferrin in the histotroph.

Not every material is able to cross the placenta, such as many maternal proteins, lipids, large peptide hormones (small molecular weight hormones might be able to cross the placenta). However, some toxic and pathogenic materials are able to cross the placenta with relative ease, such as ethyl alcohol, opiate drugs, barbiturates, viruses, and some bacteria.<sup>5</sup> Many factors can affect the nutrient transport efficiency of the placenta. Maternal and fetal blood flow, the interactive surface area, and the capillaries distance between dam and fetus are some examples of physical factors, which can affect nutrient transport.<sup>8</sup>

The porcine placenta can be divided into two different areas, the areolar and the interareolar (the rest of the placenta surface) areas.<sup>8</sup> As previously discussed, the areola is the

structure that takes up uterine gland secretions (the histotroph). The interareolar areas are defined by the adhesion of the fetal epithelium layer to the maternal endometrial epithelium.<sup>8</sup> As gestation evolves, this bilayer becomes thinner so fetal and maternal capillaries come closer together, although they never penetrate the epithelial cell layers.<sup>8</sup> Due to the cross-countercurrent fashion on opposite sides of the fetal and maternal capillaries, solutes are exchanged between dam and fetus within the axis perpendicular to the surface of the placenta.<sup>24</sup>

A transcriptomic investigation on solute carrier (SLC) genes expressed by trophoblastic cells indicated that a large number of genes related to transport of glucose, amino acids, lipids, vitamins, and minerals are present in both short cuboidal and tall columnar cells, having a preference for the short and wide cuboidal cells, probably due to their closeness to other cells and the greater surface area for nutrient exchange.<sup>8</sup> The genes identified might be responsible for the influx of substrates into the cell, out of the cell, or both, depending on location and environment.<sup>8</sup>

#### *1.1.4. Intrauterine growth retardation (IUGR)*

Fetal development and growth are complex events occurring in the intrauterine space and are influenced by the environment, the dam (age, maturity), genetics, epigenetics, and other factors.<sup>25</sup> Maternal nutrition and uterine capacity to adequately support conceptus life, growth and development are indicated as main aspects regulating the size of the fetus. Some insults suffered by the dam and/or fetus can also determine fetal development depending on the gestation stage, nature, duration, and severity of the insult.<sup>25</sup>

Intrauterine growth retardation (IUGR) is a condition well documented among livestock species by its natural occurrence and is characterized as the impaired growth and development of the conceptus and its organs during gestation, as well as postnatally.<sup>25</sup> It can be identified as having body weight lower than the mean body weight for gestational age by one standard deviation.<sup>26</sup> Substantial research has investigated how to prevent retarded development, as IUGR fetuses have increased pre-weaning morbidity and mortality rates, decreased feed efficiency, and will produce a low quality carcass, since they will carry the retarded development throughout life.<sup>25</sup>

As the placenta has a vital role in nutrient transport, it is expected that the placenta of IUGR fetuses may be another factor influencing affected animals. When compared to a normal

body weight fetus, both placenta and the related endometrium of an IUGR fetus can present altered expression of around 50 proteins each. These proteins are related to energy metabolism, transport of nutrients, stress response, nutrient metabolism, cell proliferation and apoptosis, as well as cell morphology and motility, with mainly negative effects on IUGR fetuses.<sup>26</sup> For example, it has been observed that an enriched placental vasculature tends to result in a more uniform litter with more efficient fetal growth.<sup>27</sup> However, placental vascularization is mainly controlled by the vascular endothelial growth factor (VEGF), which was observed to be downregulated in IUGR porcine fetuses on gestation days 60, 90, and 110 compared to normal body weight fetuses.<sup>26</sup>

## 1.2. Reproductive PRRS

Porcine reproductive and respiratory syndrome (PRRS) is a swine disease caused by PRRS virus (PRRSV), an *Arteriviridae* family member, which typically presents with mild to severe respiratory disease in growing pigs and infected newborns, mild respiratory and reproductive failure in pregnant gilts and sows. In addition to mild respiratory disease in boars, a decrease in semen quality following disease is expected, while for the sows, premature farrowing, late term abortions, stillborn or weak piglets and mummified fetuses, followed by high preweaning mortality,<sup>28,29</sup> due to malnutrition, respiratory disease, and secondary infections. Congenitally infected animals are also PRRSV spreaders, hosting a long lasting infection that will impact the animal's performance throughout growing and finishing.<sup>30</sup> The syndrome was first described in the late 1980s in North America and in the early 1990s in Europe, and was initially called “the mystery swine disease”, or “blue-ear pig disease”.<sup>28,29</sup>

Both species, PRRSV1 (mainly distributed in Europe) and PRRSV2 (mostly present in North America and Asia) belong to the genus *Porarterivirus*. The two original strains used to characterize those two current species presented around 44% of nucleotide sequence variation. It has also been observed that the intra-species diversity can reach 30% for PRRSV1 and more than 21% for PRRSV2, displaying the high rate of variation that is intrinsic to PRRSV.<sup>31</sup>

### 1.2.1. PRRSV infection in pregnant sows and gilts

Reproductive failure caused by PRRSV occurs when the pregnant gilt or sow becomes infected in the last trimester of gestation.<sup>31,32</sup> During infection, the macrophage glycoprotein

receptor Sialoadhesin (Sn) helps the virus enter host cells by endocytosis, having the viral genome introduced into the cytosol aided by the transmembrane glycoprotein CD163, where it will start its replication cycle.<sup>29,31</sup> As PRRSV has a restricted tropism to monocyte-derived cells, it starts replicating in macrophages and dendritic cells, resulting in serum viremia by one day post infection, and rapidly spreading.<sup>31</sup> Following the acute phase of infection, around 7-14 days after infection, virus titers start to decrease in the affected tissues and serum, but the virus continues to replicate in lymphoid tissues, such as lymph nodes and the tonsil. Viral levels will decrease until PRRSV is cleared from the host.<sup>29</sup>

During infection the gilt may develop respiratory symptoms and pneumonia, as well as lethargy, anorexia, return to estrus, abortions and birth of mixed litters with alive and dead fetuses,<sup>33,34</sup> although not all infected animals present with clinical signs.<sup>31</sup> Less common signs in sows and gilts include agalactia, incoordination, and the increase of other endemic conditions.<sup>31</sup> The mortality due to PRRSV infection in this phase is low, 1-4%, and mostly associated to pulmonary edema or cystitis/nephritis. After recovering, most females will have lower conception rates on the subsequent breeding.<sup>31</sup> The immune response and pathology of the PRRSV-infected pregnant gilt has been extensively investigated and reported elsewhere<sup>29,35-39</sup>, while herein we focus on the reproductive tract events.

### *1.2.2. Events occurring at the maternal-fetal interface*

*1.2.2.1. Virus replication and transplacental transmission:* After maternal infection and viral replication in the lungs and lymphoid tissues, the virus is carried in the blood stream, probably by infected macrophages or as free viral particles, until it arrives at the endometrium.<sup>40</sup> From the maternal side of the maternal-fetal interface (MFI), the virus crosses the placenta and is transmitted to the fetus. Three hypotheses for this transmission of the virus from endometrium to placenta have been proposed by Lager<sup>41</sup> and reviewed by Karniychuk<sup>40</sup>:

- cell-to-cell transmission (infected endometrial macrophage moves through the endometrial epithelial cell to the trophoblast cell to infect placental macrophages);
- transmission via free viral particles (independent from macrophage) through or in between endometrial epithelial cells and trophoblast cells; and

- cell-associated virus in or on endometrial macrophages migrating from endometrium to placenta.

*1.2.2.2. Gross and histologic lesions:* How the virus crosses the MFI is not completely understood, but it is known that Sn<sup>+</sup>CD163<sup>+</sup> macrophages are the target cells for PRRSV replication in the MFI. These macrophages are present at the MFI even in non-infected gilts, but increase in number after infection.<sup>42-45</sup> The intensive viral replication in the target cells at the fetal implantation sites during viremia causes apoptosis of infected and non-infected surrounding cells, especially in the fetal placenta mesenchyme<sup>46</sup> and on the endometrium-placenta junctions.<sup>45</sup>

It was observed that inflammatory cell infiltrates are closely associated with the number of PRRSV immunopositive cells in the endometrial placental junction<sup>47</sup> and a lymphoplasmacytic and histiocytic endometritis was the most commonly observed lesion at the MFI.<sup>34,39,48</sup> Additionally, the number of terminal deoxynucleotidyl transferase dUTP nick end labeling (TUNEL - cellular apoptosis detection staining) positive cells on the MFI was positively related to RNA PRRSV concentration and the severity of vasculitis in the uterine tissues.<sup>45</sup> This association of lesions, apoptosis and viral load, and the fact that inoculated gilts also have higher numbers of CD8 positive cells (uterine natural killer cells) which can contribute to placental detachment,<sup>44</sup> are speculated to be the major causative factor for fetal death. Viral replication in the MFI was shown to be important for the outcome of reproductive PRRS, being positively related to viral RNA concentration in the fetal serum and thymus<sup>48,49</sup> and also associated with the decline in fetal preservation status.<sup>37</sup>

### *1.2.3. Events occurring within fetuses*

*1.2.3.1. Virus replication and transplacental transmission:* After crossing all the MFI barriers, the virus congenitally infects the progeny, resulting in mummified fetuses, abortion, dead fetuses and live but weak-born piglets.<sup>31,33</sup> The virus is able to replicate in fetal tissues, with thymus indicated as the primary fetal site of viral replication. A pro-inflammatory fetal response is known to be articulated after 20 DPI associated with the expression of IFN-gamma and TNF-alpha.<sup>50</sup> PRRSV-positive cells can be detected in the fetal umbilical cord, amniotic fluid, sera,

heart, thymus, liver, spleen, inguinal and mesenteric lymph nodes, and lungs from intrauterine infected fetuses.<sup>46,50</sup> In addition, viral replication within fetuses and the spread of PRRSV to adjacent fetuses seem to be key factors in the pathogenesis of reproductive PRRS, as it was observed that an infected or dead fetus can increase the probability of other adjacent fetuses becoming infected or dying.<sup>37</sup>

*1.2.3.2. Gross and histologic lesions:* Although the disease leads to fetal death, fetal lesions are uncommon and mostly not definitive to the diagnostics of PRRS.<sup>31,51</sup> Since the first experiments performed in the early 1990's, the most cited lesion in fetuses is the vasculitis and edema of the umbilical cord,<sup>34,39,48,50</sup> which suggests low blood influx leading to death by hypoxia<sup>34,48</sup> and may be associated with fetal meconium-staining.<sup>39</sup>

The percentage of fetuses observed with umbilical lesions varies greatly between experiments, ranging from 5.9%<sup>39</sup> to 33%.<sup>34</sup> These differences can be due to the different methods of lesion observation, where the first study observed it microscopically<sup>39</sup> (histopathology of small sections), while the second one did it macroscopically<sup>34</sup> (gross pathology, analyzing the entire umbilical cord).

Although at lower rates, other lesions are also observed in PRRSV affected fetuses in both field and experimental infections, such as lymphocytic myocarditis, myocardial fibrosis, arteritis, encephalitis, perivascular cuffing and gliosis, interstitial pneumonia, periportal hepatitis, thymus atrophy and enlarged lymph nodes. These lesions can be related to PRRS viral load in the MFI and with fetal meconium-staining.<sup>34,39,48,50,51</sup>

Because of the lack of significant fetal lesions in many dead fetuses, the presence of lesions in the MFI such as endometritis, myometritis, placentitis, placental arteritis and placental detachment from the endometrium have been suggested as possible reasons for fetal death.<sup>34,46,52</sup> However, results from recent challenge experiments do not fully support placental detachment as a cause of fetal death, based on the observation that placental detachment was not related to the odds of meconium staining or to placental viral load. Furthermore, placental detachment did not progress over time following infection.<sup>53</sup> Nonetheless, some maternal factors have been investigated and it was observed that interleukin 10 (IL10) and natural killer cells (NK cells) levels in gilt sera prior to PRRSV inoculation were negatively associated to fetal mortality rate (protective effect), while interferon alpha (IFN $\alpha$ ) levels were positively associated to fetal

mortality rate.<sup>37</sup> Similarly, T helper cell levels following inoculation (6 DPI) was also observed as protective of fetal death in that study.

### **1.3. PRRSV detection and investigative methods**

Detection and identification of PRRSV can be achieved through the employment of different methods and used for a variety of activities. For example, faster and less specific tests can be used in a commercial diagnostic lab for quickly reporting results to the industry, while more time consuming and strain specific assays might be employed in academic research. As the reproductive and the respiratory forms of PRRS affect different systems, here I focus on the tools especially used to investigate reproductive PRRS.

The suspicion that a sow farm is infected with PRRSV likely starts by observing an increase in abortions, premature births, repeated estrus cycles, born-weak piglets, and/or other common reproductive symptoms.<sup>31</sup> As these are common clinical signs of other reproductive diseases, caused by a variety of pathogens, differential diagnosis is required by the identification of the agent.<sup>31</sup> Reproductive PRRS mostly presents without any gross lesions either in the sow or the aborted/stillborn fetuses, thus, collection of samples for lab analysis is essential.

#### *1.3.1. Classic diagnostic and investigative tools*

*1.3.1.1. Virus isolation:* PRRSV is more likely to be recovered from infected animals between 4 and 7 days post infection (DPI), as the virus reaches its peak. By 28-35 DPI, virus cannot be recovered from most samples, although it persists in the tonsil and lymph nodes.<sup>31</sup> As samples can vary widely in their viral concentration, they should be kept refrigerated (4°C) and submitted for analyses immediately after collection. Virus isolation (VI) should be performed on both PAMs (porcine alveolar macrophages) and/or sublines of the African monkey kidney cell line (MA-104) observing cytopathic changes, and the success of VI can be confirmed either by viral detection using reverse transcriptase polymerase chain reaction (RT-PCR) or immunoassays (fluorescent antibody, immunohistochemistry).<sup>31,54</sup>

*1.3.1.2. Detection of virus:* PRRSV can be detected by a diverse range of assays that were especially developed for this virus and can be specific to a certain strain, as well as less specific

tests that can detect a variety of strains or species. Many tissues can be fixed in 10% formalin, such as lung, tonsil, lymph nodes, heart, brain, thymus, spleen, and kidney, to enable detection of antigens by immunohistochemistry (IHC) coupled with the tissue histopathology exam. For PRRSV, antigen detection samples are best analysed between 4 and 14 DPI as the virus reaches its replication peak. Frozen sections can also be employed for viral detection by fluorescent antibody (FA) for a fast and cheap detection. However, due to its inability to detect genetically diverse isolates and later stages of infection, it is rarely employed nowadays. Both IHC and FA employ antibodies for PRRSV detection and their results can be confirmed by VI or RT-PCR<sup>31</sup>. Used not only for detection but also for quantification (or semi quantification), is the reverse-transcription real-time PCR (RT-qPCR) assay. Widely used and available as commercial kits or in-house developed assays, it is the diagnostic test of choice for suspected PRRSV infected fetuses. It is a relatively fast, highly specific and sensitive assay.<sup>31</sup> As this test is based on the viral genetic material, it detects and quantifies viral RNA in the sample, but it does not differentiate an active infection from an inactivated virus. The diagnostic assay should be used for serum samples during the first two weeks post infection when the animal reaches peak viremia, otherwise, other tissues such as lymph nodes and tonsil should be analysed.<sup>31</sup>

*1.3.1.3. Detection of antibody:* Differently from the previous assays, techniques that detect PRRSV antibodies do not have the virus as their principal target. Rather, the host response is the main focus. Antibodies formed in response to PRRSV infection can be detected in oral fluids or, more commonly, in serum. The ideal serological test will display the host seroconversion in response to infection by comparing the results from a sample collected either before infection and then during the acute phase or comparing a sample during the acute phase to a sample collected during the convalescent phase, although depending on the goal of the investigation, two samples are not always required. However, the assays are not able to differentiate natural infection immunity from vaccination generated immunity in most cases. The most common serological assay employed in PRRSV diagnostics is the enzyme-linked immunosorbent assay (ELISA), a fast and convenient assay that bases its detection on targeting antibodies to the nucleocapsid antigens of both species of PRRSV.<sup>31</sup> Indirect fluorescent antibody (IFA) detects PRRSV-specific antibody (IgM and IgG), starting at 5 DPI to 28 DPI for

IgM and from 9 DPI up to 5 months after infection for IgG. Sensitivity, however, will depend on the similarity between the PRRSV strain from the field and the strain(s) used in the assay.<sup>31</sup>

### *1.3.2. Innovative methods – the “-omics” revolution*

As science and technology evolves and improves, so do investigative methods. With robotic machines facilitating high-throughput processing and analyses of samples and bioinformatics aiding the analysis of larger datasets, the study of the “totality” of the studied field (or “-ome”, e.g. genome is the study of the whole set of genes from an organism) has advanced.<sup>55</sup>

*1.3.2.1.* Genomics studies the set of genes from an organism by gene sequencing and applies sequencing results to structure, function, evolution, mapping, and editing of the genome. The most common uses of genomics in livestock are in studies and activities related to improvement of breeding and disease resistance.<sup>56</sup> In the PRRS context, genomics has allowed researchers to investigate viral diversity,<sup>57</sup> has enabled advancements in understanding epigenetics and host response to PRRSV infection,<sup>58,59</sup> allowed genome-wide association studies (GWAS) to investigate single nucleotide polymorphisms (SNP) possibly associated to fetal PRRSV susceptibility, and it has even made possible the development of PRRSV-resistant pigs.<sup>60</sup> The use of genomics are less commonly used for commercial animal diagnostics than in research. However, as the technique becomes more common and databases increase, the tendency is for it to be more widely used.<sup>61</sup>

*1.3.2.2.* Transcriptomics provide detection and quantification of gene expression in a given tissue, allowing the investigation of gene functions pertaining to a particular trait or pathophysiologic state. Currently, the most commonly used assay to characterize gene expression profiles is the RNAseq, a next-generation sequencing (NGS) technology applied to mRNA sequencing, detection of novel and rare transcripts, novel protein isoforms, and others in a single experiment.<sup>56</sup> Whole blood transcriptional responses has been used to demonstrate differences in transcriptomic profiles of pregnant gilts infected with PRRSV2 with low or high fetal mortality.<sup>62</sup> Moreover, the use of RNA-seq allowed the investigation of differentially

expressed genes (DEGs) between groups of fetuses to determine their responses following PRRSV exposure.<sup>63</sup>

*1.3.2.3.* Metabolomics is the study of the small molecules resulting from biological metabolic processes. It represents the biochemical reactions that were occurring in the animal system at the time of sample collection, being a snapshot of the current events.<sup>64</sup> Metabolomic studies may investigate specific compounds or pathways (targeted metabolomics) or a global approach to detect and measure as many compounds as possible (untargeted metabolomics).<sup>64</sup> These techniques can be used to study and compare alterations in biochemical pathways among different treatment groups, such as healthy animals to sick animals, and to analyze how the animal physiologically responds to those alterations. It can also be used in the investigation of biomarkers for various aims, or in pharmaceutical development.<sup>64</sup>

Being different from other ‘omics such as genomics or proteomics, metabolomics also considers the environmental effects in which the animal is exposed to and possible causal changes to its phenotype, also enabling a link between genotype and phenotype.<sup>64</sup> Many of the metabolites found during the analyses might be in accordance with physiological pathways or not be relevant for the studied subject. While only a few metabolites might be significantly related to the investigation, it is important to recognize the pathways these selected metabolites are involved in to determine their real relevance.<sup>65</sup>

Different analytical techniques can be used on biological samples to identify and quantify various classes of metabolites. To serve the purpose of this thesis and for conciseness, the following explained techniques are specific to the ones employed in our metabolomics project (Chapter 4).

- Direct infusion mass-spectrometry (DI-MS) is a technique based on the measurement of mass-to-charge ratio of detected ions. The direct infusion method eliminates the liquid or gas chromatography (LC, GC) step for a higher throughput method.<sup>66</sup>

- Nuclear magnetic resonance (NMR) is based on the structural and chemical properties of the molecules, when analyzed under a very strong magnetic field, that measures their absorption of radiofrequency radiation by different nuclei. The spectral peaks generated by NMR can indirectly quantify the amount of that specific molecule, whereas the pattern of the peaks will identify the metabolite.<sup>67</sup>

1.3.2.3.1. Metabolomics analysis: As metabolomics is a novel technique, a brief explanation is warranted to support the understanding of Chapter 4. Because the raw data generated by both analyses are prone to biases, it has to pass through spectral processing before statistical analyses in order to improve the signal quality, e.g. baseline correction, noise filtering, peak detection and alignment, normalization and deconvolution.<sup>67</sup> In the end, a data table, known as a “feature quantification matrix” (FQM), is generated where the columns will present the metabolites related to the different samples in the rows.<sup>67</sup>

As these are very complex, high-dimensional data, strong strategies for features identification and assessment are needed.<sup>65</sup> Analyses generally begin with univariate analysis, using common techniques such as the Student’s *t*-test, analysis of variance (ANOVA) or correlation analysis that independently analyzes each metabolite across two or more groups resulting in easy interpretation of their individual significance. Univariate analyses, however, will not account for correlations between metabolites from the same pathway or among the different groups.<sup>67</sup>

Following univariate analyses, multivariate analyses can be performed to identify relationship patterns, since the multivariate statistical techniques account for all the metabolomic features together. Unsupervised methods, such as Principal Component Analysis (PCA) can be undertaken but does not take into account the type or class of the targeted samples. PCA transforms the metabolomics features into linearly uncorrelated vector variables, called principal components, which reflect underlying physiological processes. The variance explained by the first component is maximized while the subsequent components explain increasingly reduced amounts of variance while minimizing the covariance between the components.<sup>67</sup> Eigenvalues are calculated which detail the proportionate amount of variance captured by each principal component. The results are expressed in terms of loading factors which represent the individual contribution of each variable to each principal component, and score plots which show the principal component scores for individual animals.<sup>65,67</sup>

Supervised analytical methods, such as Partial Least Squares (PLS) regression, use labels to associate the phenotype of interest to the sample feature or combinations of features, while decreasing other sources of variation.<sup>65,67</sup> PLS-discriminant analysis (PLS-DA) maximizes the variation in the metabolomics data among treatment group.<sup>65,67</sup> The loadings represent a measure

of how much each feature contributes to the discrimination of the different sample groups. The variables are ranked by how well they explain the variance among treatment group.<sup>65,67</sup> PLS-DA also produces a variable importance in projection (VIP) score, which is a weighted sum of squares of the PLS loading factors that takes into account the amount of explained group variance for each component.<sup>65</sup> Validation and significance of the model can be assessed by calculating the goodness of fit (R<sup>2</sup>) and the predictive ability (Q<sup>2</sup>) values along with the permutation *P*-value.

The final step is the pathway analyses, which focuses on influential metabolites identified by the VIP scores to investigate which biochemical pathway(s) the most significant metabolite(s) belongs to as well as its function(s).<sup>65</sup> Several biological databases can be used for this, including the Human Metabolome Database (HMDB), Kyoto Encyclopedia of Genes and Genomes (KEGG), small molecule pathway database (SMPDB), Edinburgh Human Metabolic Network (EHMN), WikiPathways, and MetaCyc.<sup>67</sup> The platform MetaboAnalyst, for example, is able to generate a pathway analysis plot, which combines a topography and pathway impact analyses to provide a “big picture” of the metabolic pathways that better distinguish the groups analyzed. Information obtained from pathway analyses include the type and chemical structure of the molecule, the metabolic route where it is produced and its influence on the pathway. Based on that, specific pathways are identified that have the most biological relevance to the topic of interest.

#### **1.4. Rationale, hypothesis, objectives**

PRRSV has the ability to infect pregnant pigs, cross the placental barrier, infect and initiate disease in fetuses affecting the growth and survivability of many. Numerous studies have focused on the maternal response to PRRSV infection or on the events in the MFI, and suggested that fetal resilience to PRRSV infection is more related to inherent individual fetal traits, rather than maternal traits. After maternal infection is confirmed, even if the whole MFI is infected, fetal infection is not guaranteed. Some fetuses might become infected and some of these might die, while other fetuses escape infection and disease altogether. The hypothesis for this program was that the reasons for this desirable, naturally occurring resistance/resilience to infection and disease characteristic can be explained through the combination of techniques, such as fetal phenotyping, gene expression analysis and metabolomics studies.

To assess the hypothesis, the objectives were: 1) to characterize the timeline of PRRSV infection and disease progression across the maternal-fetal interface and fetal tissues; 2) to assess the subsequent effects on the fetal metabolome following PRRSV infection; and 3) to investigate the roles of hypoxia and apoptosis in PRRSV infected fetal tissues.

## **2. Classification of fetal resilience to porcine reproductive and respiratory syndrome (PRRS) based on temporal viral load in late gestation maternal tissues and fetuses**

This chapter presents the starting point for this research investigating fetal susceptibility to PRRSV and the assessment of PRRSV RNA concentration in a diverse set of maternal and fetal tissues at five different time points following maternal inoculation. A timeline of transplacental PRRSV transmission is established, while disease progression is investigated.

**Copyright:** Chapter 2 has been published and is reproduced here with the permission of the copyright owner (2018 Elsevier B.V.).

**Citation:** Malgarin CM, Nosach R, Novakovic P, Suleman M, Ladinig A, Detmer SE, MacPhee DJ, Harding J. Classification of fetal resilience to porcine reproductive and respiratory syndrome (PRRS) based on temporal viral load in late gestation maternal tissues and fetuses. *Virus Res.* 2019;260:151-162. doi:10.1016/j.virusres.2018.12.002

### **Authors' contributions:**

CMM: sample collection, tissue viral RNA extraction, RT-qPCR analysis, statistical analysis, manuscript preparation; RN: sample collection, RNA extraction, RT-qPCR; PN, MS, AL, SD, DJM, JH: experimental design, sample collection; JH: project and financial management, statistical analysis, manuscript preparation.

## 2.1. Abstract

Although porcine reproductive and respiratory syndrome virus (PRRSV) readily crosses the maternal fetal interface (MFI) in third trimester, fetal resilience varies within litters. The aim of this study was to characterize PRRSV-2 concentration in MFI and fetuses at five time points after experimental inoculation of late gestation gilts and use this information to classify potentially resistant, resilient and susceptible fetuses. The secondary objective was to verify the relationship between PRRS viral load and intrauterine growth retardation (IUGR). Three PRRSV-inoculated pregnant gilts and 1 sham-inoculated control were euthanized at five time points in days post infection (DPI; 2, 5, 8, 12, 14). The preservation status of each fetus was determined and MFI samples adjacent to the umbilical stump of each fetus, as well as serum, thymus, umbilical cord and amniotic fluid were collected. Viral load was quantified using probe-based reverse-transcriptase quantitative PCR (RT-qPCR) targeting PRRSV NVSL 97-7895 ORF7. Our result show the MFI was largely PRRSV infected by 2 DPI and virus was first detected in fetal sera and umbilical cord by 5 DPI, and in fetal thymus and amniotic fluid by 8 DPI. This indicates that PRRSV-2 quickly crossed the placenta and traveled toward the fetus via umbilical circulation within one week of the dam's inoculation. Fetal compromise was first observed on 8 DPI and increased progressively through to 14 DPI. However, several factors were associated with fetal resilience. The random forest model identified that 'viral load in fetal thymus' and duration of infection ('DPI') as the most important factors predicting fetal resilience and resistance. Moreover, IUGR fetuses had lower viral load and were less frequently compromised or dead compared to non-IUGR and average cohorts. Understanding the mechanisms of fetal resilience to PRRSV will improve selection strategies for replacement gilts.

**Keywords:** Swine, Virus, Transmission, Resistance, Random forest, Intrauterine growth retardation

## 2.2. Introduction

Porcine reproductive and respiratory syndrome virus 2 (PRRSV) belongs to the order Nidovirales, family Arteriviridae, genus Porartevirus and causes a disease with worldwide distribution that affects pigs of all ages.<sup>31</sup> Besides the well-studied respiratory disease, PRRSV can also cause reproductive losses associated with fetal death, abortions and birth of weak piglets<sup>31,33</sup> making PRRS one of the costliest swine diseases in North America with

approximately 45% of annual losses associated with the reproductive disease.<sup>68</sup> PRRSV replication in the maternal-fetal interface (MFI) is biologically important for the outcome of reproductive PRRS since it is positively related to viral RNA concentration in the fetal serum and thymus<sup>48</sup> and also one of the determinants of fetal preservation status.<sup>37</sup> How and when the virus crosses the MFI is not completely understood, but it is known that Sn+CD163+ macrophages are the target cells for PRRSV replication in the MFI.<sup>42-45,69</sup> Three hypotheses for the possible routes of transmission of the virus from endometrium (END) to placenta (PLC) have been proposed by Lager and Mengeling<sup>41</sup> and reviewed by Karniychuk and Nauwynck<sup>40</sup>: 1) a cell-to-cell transmission with virus transiting through infected END macrophages to END epithelium to fetal trophoblastic epithelium to PLC macrophages; 2) as free viral particles through or between END epithelium and trophoblast epithelial cells; and 3) as infected macrophage-associated virus migration from END to PLC. After transmission to fetuses, the virus replicates in fetal tissues with thymus (THY) reported as the primary site of viral replication.<sup>50</sup> Our research group has previously shown that the severity of PRRS can be highly variable within individual litters, and PRRSV RNA concentration in fetal thymus, serum (SER), PLC and END differs across preservation category.<sup>49</sup> Fetal meconium-staining of the skin, a condition associated with fetal stress in which the fetus is covered in fecal material, is an early clinical indicator of PRRSV-induced fetal compromise and is associated with the presence of fetal lesions<sup>39,53</sup> and severity of apoptosis in the MFI.<sup>45</sup> Meconium staining varies in severity and distribution in infected litters<sup>49</sup> as does fetal susceptibility and resistance to the virus.<sup>49</sup> Fetal infection is a strong predictor of fetal compromise and death<sup>37</sup> and viral replication within fetuses and clustering within litters appear to be important in the pathogenesis of reproductive PRRS because fetal infection and death increases the probability of adjacent fetuses becoming PRRSV-infected or dying.<sup>37</sup> A previous study determined that intrauterine growth retarded (IUGR) fetuses have lower PRRS viral load (VL) in THY and adjacent MFI than non-IUGR and larger fetuses when collected at 21 days post inoculation (DPI),<sup>70</sup> potentially indicating a mechanism of fetal resilience. Understanding the sequential movement of PRRSV across all reproductive and fetal tissues is important to more fully understand disease progression, further characterize the effects of IUGR on VL, as well as identify potential mechanisms of fetal resistance and resilience. The current study aimed to: a) characterize by RT-qPCR the temporal movement of PRRSV across the MFI and into fetal tissues within two weeks of maternal inoculation in late

gestation; b) determine when the first signs of fetal compromise occur; c) develop an algorithm to classify and/or identify resistant, resilient and susceptible fetuses; and d) confirm the relationship between fetal resistance/resilience to IUGR to understand how this condition potentially impacts transmission and susceptibility.

## **2.3. Materials and methods**

### *2.3.1. PRRSV propagation*

A virulent PRRSV-2 (formerly type 2) strain (NVSL 97-7895 ; GenBank Accession No. AF325691) was propagated for an experimental challenge by infecting PRRSV susceptible MARC-145 cells as previously described.<sup>71,72</sup> The culture conditions were set at 37 °C under 5% CO<sub>2</sub> and maintained in Modified Eagle Medium (MEM) supplemented with 7% heat-inactivated fetal bovine serum, 0.25 µg/ml fungizone, 100 U/ml penicillin, and 10 µg/ml streptomycin. Cytopathic effects (CPE) were observed at 24, 48 and 72 h post infection. The infected culture was frozen at -80 °C after 72 h with >70–75% CPE and viral titration was conducted using MARC-145 for calculating tissue culture infective dose 50 (TCID<sub>50</sub>) as previously described.<sup>73</sup>

### *2.3.2. Animals*

Twenty purebred Landrace gilts were purchased from a high health, PRRSV-free farm rearing pigs using husbandry and vaccination protocols compliant with the National Farm Animal Care Council 2014 Code of Practice ([http://www.nfacc.ca/pdfs/codes/pig\\_code\\_of\\_practice.pdf](http://www.nfacc.ca/pdfs/codes/pig_code_of_practice.pdf)) and the Canadian Pork Excellence Program (<http://www.cpc-ccp.com/canadian-pork-excellence>). Six months old gilts were selected, puberty stimulated, estrus synchronized and inseminated with Yorkshire semen using single sire matings. At ~80 days of gestation, gilts were transferred to biocontainment level 2 animal care facilities at the University of Saskatchewan. After five days of acclimation, blood was collected via jugular venipuncture, and 15 gilts blocked by sire were inoculated (INOC) with 4 mL of 1x10<sup>5</sup> TCID<sub>50</sub> of NVSL 97-7895 ; 2 mL intramuscularly and 1 mL into each nostril. Five gilts housed in a separate room were similarly mock inoculated with minimum essential medium (CTRL).

### 2.3.3. *Experimental procedures*

One CTRL and three INOC gilts were humanely euthanized and sampled at each of five different DPI (2, 5, 8, 12, and 14). On the day of sample collection, the dams and litters were collected one at a time, starting with the CTRL gilt, with the aim of completing all fetuses within 45 min of death to maintain mRNA quality. Gilts were euthanized by intravenous administration of pentobarbital sodium (Euthanyl Forte®, Bimeda-MTC Animal Health Inc., Canada) followed by cranial-captive bolt shot, pithing, and exsanguination. Blood was collected from each gilt in plain, anti-coagulant free tubes. The abdominal cavity was opened by a ventral midline incision, the reproductive lymph node collected, and the gravid reproductive tract removed and placed in a trough where maternal blood was washed from the external surface.

### 2.3.4. *Fetal preservation and sample collection*

The uterine horns were opened from ovarian tip (right and left) to the uterine body along the anti-mesometrial border. The fetuses were numbered sequentially in each horn, starting from the one closest to each ovary; R1 for the right side and L1 for the left, and progressing to the body of the uterus. An umbilical clamp was placed on each fetal cord to prevent cross-contamination and loss of fetal blood. The preservation status of each fetus was categorized as viable (VIA=live, normal skin color), meconium-stained (MEC=live, normal skin covered with meconium) and decomposed (DEC=dead, pale skin, sometimes edematous). Meconium staining was further characterized by severity based on the distribution of meconium; either on the face only (MEC-F), or face and body (MEC-B) (Additional file 2.1). Mummified fetuses (dehydrated, dark brown color, crown-rump length<20 cm) were not sampled because they were deemed to have died due to other reasons prior to the time of inoculation. Fetuses were placed on individual trays, weighed and crown-to rump length measured. Following dissection, the brain and liver were also weighed individually to assess the degree of IUGR based on the brain:liver ratio (with greater brain:liver indicative of IUGR; a.k.a. “brain sparing”). Fetal blood from the axillary artery, amniotic fluid (AMN) from stomach, and THY were collected from each fetus. Blood was refrigerated until serum separation. Serum and AMN were frozen and stored at -80 °C, whereas THY was snap frozen in liquid nitrogen. A 3x3 cm section of uterus adjacent to the umbilical stump was collected, washed of blood, and placed (PLC side up) in a plastic weigh boat on ice for 10 min. The PLC was manually separated from the END with forceps and

multiple 0.5 to 1.0 cm pieces of both tissues were stored at  $-80^{\circ}\text{C}$ . An approximately 3 cm section of the umbilical cord of each fetus was cut 2 to 5 cm from the placental attachment and similarly stored.

### 2.3.5. *Quantification of PRRSV RNA*

PRRSV RNA extraction and RT-qPCR reaction were performed as previously described.<sup>49</sup> Briefly, viral RNA was extracted using commercial kits (RNeasy MiniKit, Qiagen, Toronto, Canada) and a QIAcube extraction robot (Qiagen) from 30 mg of tissue sample after homogenization using lysis buffer (Qiagen RLT buffer plus beta-mercaptoethanol) and steel microspheres. Extraction of SER and AMN was performed manually using 140  $\mu\text{L}$  of sample and the Qiampr Viral RNA kit (Qiagen). For each procedure, a known positive control and an extraction negative control were run simultaneously. Specific primers, previously designed for the PRRSV strain NVSL 97-7895<sup>49</sup> were used: PRRS-2 F - 5'- TAATGGGCTGGCATTCTCCT -3', PRRS-1R - 5'-ACACGGTCGCCCTAATTG -3', probe PRRS-P1 - 5' HEX-TGTGGTGAATGGCACTGATTGRCA-BHQ2 3'. The plasmid HindIII pCR2.1TOPO-NVSL containing a 446 bp sequence of ORF-7 was used for the standard curve (five points:  $10^7$ ,  $10^5$ ,  $10^3$ ,  $10^2$ ,  $10^1$  run in triplicate on each plate). Each RT-qPCR reaction consisted of BioRad iTaq Universal Probes 1-Step Kit (10  $\mu\text{L}$ /reaction), water (8  $\mu\text{L}$ /reaction), forward and reverse primers (0.5  $\mu\text{L}$ /reaction), probe (0.5  $\mu\text{L}$ /reaction), and reverse transcriptase enzyme (BioRad) (0.5  $\mu\text{L}$ /reaction). For each 96 well plate, 35 samples were run in duplicate, along with three extraction negative controls, a positive control, and a RT-qPCR NTC. The RT-qPCR reaction consisted of reverse transcription for 30 min at  $50^{\circ}\text{C}$  for cDNA synthesis, followed by a PCR initial activation step of 10 min at  $95^{\circ}\text{C}$ , 40 cycles of denaturation for 30 s at  $95^{\circ}\text{C}$ , and annealing/extension for 30 s at  $59^{\circ}\text{C}$ . SPC charts were used to monitor the variability of the positive controls in each run. If the Ct standard deviation between the duplicates was higher than 1.5 or if one of the two duplicates had a negative Ct, the samples were re-analyzed. Incongruent negative results (e.g. a negative fetal SER result with a positive THY result) were repeated to confirm negativity. Results were reported as  $\log_{10}$  target RNA concentration per mg of tissue or  $\mu\text{L}$  of SER/AMN. Heat maps were created to visualize changes in VL by fetus across tissues and DPI.

### 2.3.6. *Classification of resistant, resilient and susceptible fetuses*

Fetal resistance, resilience and susceptibility to PRRSV infection were determined using previous definitions as guidelines.<sup>49,74,75</sup> As an initial step, the average PRRSV RNA concentration in fetal PLC, UMB, SER, THY, AMN was calculated and plotted against fetal preservation score (0=VIA, 1=MEC-F, 2=MEC-B, 3=DEC) (X-axis) for all fetuses from inoculated gilts. Breakpoints of 1.5 for fetal preservation score and 3.5 log<sub>10</sub> copies/mg or µL for average VL were used to distinguish four quadrants representing fetal resistance, resilience, susceptibility or ultra-susceptibility in the bottom-left, top-left, top-right, and bottom right quadrants, respectively. A classification approach was then used to determine which variables were most important in predicting fetal resistance, resilience and susceptibility. Random Forest classifier models<sup>76</sup> (RandomForestClassifier from sklearn.ensemble) were constructed in a Jupyter notebook and plotted using a confusion matrix (confusion\_matrix from sklearn.metrics). The data (205 inoculated fetuses from all DPI) was split into training and test datasets in a 70:30 ratio (train\_test\_split from sklearn.cross\_validation). A full model of 100 trees (100 permutations) was created by including potential predictor variables of fetal resistance, resilience and susceptibility: DPI, sex, categorized brain:liver ratio (-1 = Z score < 1 SD from the mean; +1 = Z score > 1 SD from the mean; 0 = Z score between -1 and +1 SD), and VL in sera and each fetal tissue (dichotomized according to natural break points in the data: 0 =< 4 log<sub>10</sub> copies/mg or µL; 1 => 4 log<sub>10</sub> copies/mg or µL). Given that fetal preservation score was initially used to classify fetal resistance, resilience and susceptibility, it was not included in the full model. Although average VL in tissues and sera was also used to initially classify fetuses, the full model included each individual tissue separately with the goal of identifying the most important tissue(s) for classification. Precision, recall and F1 scores, and the relative importance of each variable were determined. Variables with the lowest relative importance value were removed in a backward stepwise manner until the most parsimonious model with greatest precision, recall and F1 scores was obtained.

### 2.3.7. *Data analysis*

Descriptive and statistical analyses were performed using Stata 14 (Stata-Corp, College Station, TX). Fetal IUGR was categorized using the brain:liver weight ratio at each DPI (separately for inoculated and CTRL litters), where fetuses with brain:liver one or more standard

deviation below and above the mean were classified as non-IUGR and IUGR, respectively. Fetuses with brain:liver between -1 and +1 SD were considered average (AVG). Kruskal-Wallis with post hoc Dunn tests were performed to assess significant differences in VL in all the tissues amongst the three IUGR groups for each DPI. A Sidak test was used to adjust *P*-value to account for multiple comparisons. Differences in the frequency of compromised (MEC and DEC) versus VIA fetuses across IUGR groups were evaluated using an Exact test. For all analyses, *P* < 0.05 was considered statistically significant a priori.

#### **2.4. Results**

Five of the 15 inoculated gilts had a decreased appetite for one or two days, but no other clinical signs related to PRRSV-infection were observed. PRRSV RNA was not detected in any gilt sera prior to inoculation or in any CTRL gilt sera, fetal sera or tissue. Inoculated gilts were viremic from 2 to 14 DPI, having the viral concentration peak at 5 DPI (Figure 2.1). The study included 276 fetuses in total with 205 from inoculated gilts. The litter size was 13.8 in average. In control gilts, 70/ 71 (98.6%) fetuses were VIA and 1/71 (1.4%) was MEC. In inoculated gilts, 158/205 (77.1%) fetuses were VIA, 37/205 (18%) were MEC-F, 3/205 (1.5%) were MEC-B, and 7/205 (3.4%) were DEC.

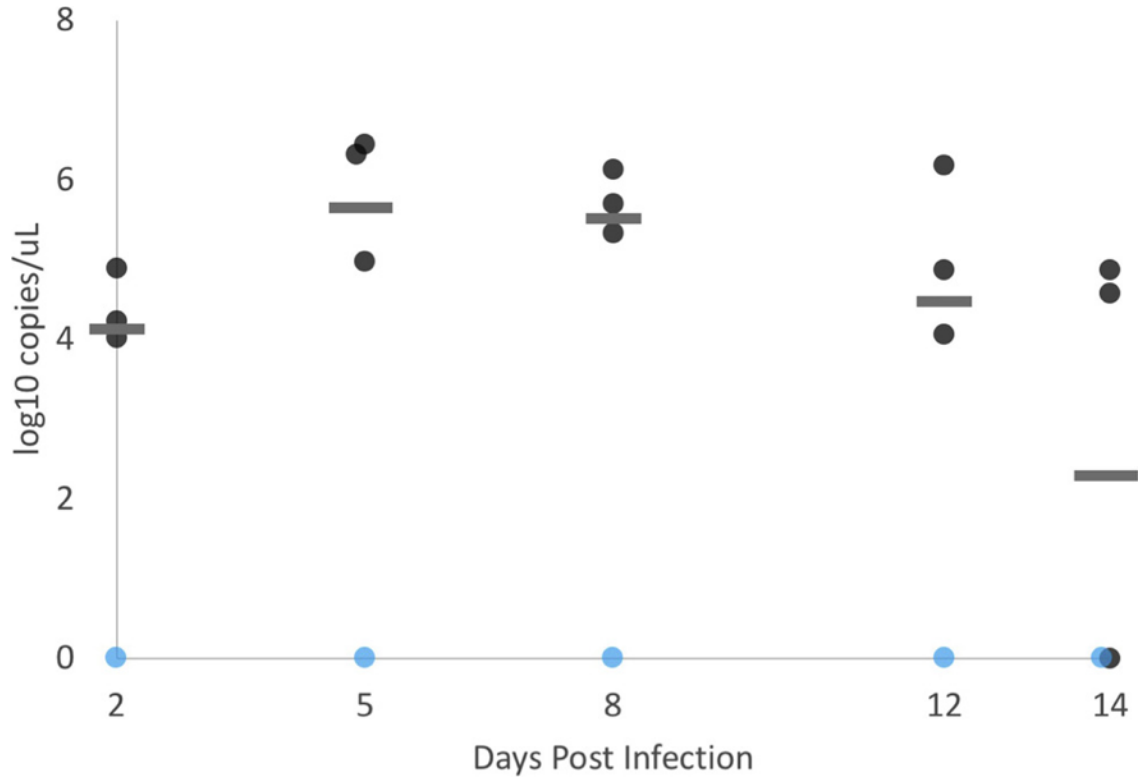


**Figure 2.1:** Median serum PRRSV RNA concentration in gilt sera.

PRRSV RNA concentration ( $\log_{10}/\mu\text{L}$  sera) in inoculated gilts between 2 and 14 days post inoculation (DPI) quantified using a probe-based RT-qPCR specific for NVSL 97- 7895. Horizontal bars represents the median value of three gilts. Control gilts are represented in light blue and inoculated gilts in dark grey. Different gilts are represented each day. All gilts were positive at 2 DPI. Peak levels were noted on 5 DPI which gradually decrease over 14 DPI. Viral RNA in sera at 0 DPI and from all control gilts were negative. Overlapping data points have been “jiggled” for visual representation.

#### 2.4.1. *PRSSV transmission across maternal and fetal tissues by day post inoculation.*

Heat maps (**Figure 2.2A-E**) were developed to visually assess the concentration of PRRSV RNA detected in maternal and fetal samples at each DPI and to identify temporal patterns in infection. On each, the identity of each gilt was listed in the left column and the fetal position in the uterine horn along the top row with the PRRSV RNA concentration ( $\log_{10}$ /mg or  $\mu\text{L}$ ) of each fetus presented in corresponding cells arranged in sections for each tissue. Cells were coloured on a scale from light yellow (low VL) to dark red (high VL). Descriptive statistics including number of RNA positive fetuses, median and mean VL are presented in **Table 2.1** by tissue and DPI. Trends across DPI are discussed below. Additional files 2.2 to 2.7 show PRRSV RNA concentration in fetuses, similar to **Figure 2.2**, except using heat maps organized by tissue, rather than DPI. The preservation status of individual fetuses (VIA, MEC-F, MEC-B, DEC) by DPI was temporally assessed (**Figure 2.3A**) with fetal PRRS severity represented along a light to dark grey color scale. The mean PRRSV RNA concentration increased in all tissues as fetal preservation progressed stepwise from VIA to MEC-F, MEC-B and finally to DEC (**Figure 2.3B**).

	<b>2 DPI</b>	<b>5 DPI</b>	<b>8 DPI</b>	<b>12 DPI</b>	<b>14 DPI</b>
<b><i>Endometrium</i></b>					
Number (%) positive fetuses/total	29/34 (85)	43/43(100)	43/43(100)	49/49(100)	28/36 (78)
Mean (SE) viral load	3.8 (0.1)	3.2 (0.2)	6.2 (0.2)	6.6 (0.1)	3.9 (0.1)
Median (IQR) viral load	4.4 (0.4)	2.5 (2.7)	6.5 (1.2)	6.5 (0.7)	5.2 (0.7)
<b><i>Placenta</i></b>					
Number (%) positive fetuses/total	32/34 (94)	37/43 (86)	42/43 (98)	48/49 (98)	21/36 (58)
Mean (SE) viral load	2.8 (0.1)	3.0 (0.1)	4.0 (0.2)	4.0 (0.2)	2.1 (0.6)
Median (IQR) viral load	2.8 (0.6)	3.5 (0.8)	3.9 (1.4)	3.7 (1.3)	2.8 (4.9)
<b><i>Umbilical cord</i></b>					
Number (%) positive fetuses/total	0	4/43 (9)	5/43 (12)	13/49 (26)	13/36 (36)
Mean (SE) viral load	-	1.8 (0.5)	3.2 (0.8)	3.2 (0.5)	3.5 (0.5)
Median (IQR) viral load	-	1.5 (1.1)	3.2 (3.0)	3.8 (3.8)	2.3 (2.7)
<b><i>Serum</i></b>					
Number (%) positive fetuses/total	0	17/43 (39)	17/43 (39)	36/49 (73)	19/36 (53)
Mean (SE) viral load	-	1.9 (0.1)	3.0 (0.6)	3.1 (0.4)	3.5 (0.5)
Median (IQR) viral load	-	1.9 (0.5)	1.8 (1.1)	2.2 (1.7)	2.6 (2.4)
<b><i>Thymus</i></b>					
Number (%) positive fetuses/total	0	0	4/43 (9)	8/49 (16)	6/36 (17)
Mean (SE) viral load	-	-	5.1 (1.0)	5.5 (0.6)	6.0 (0.4)
Median (IQR) viral load	-	-	5.6 (2.8)	5.7 (2.3)	6.2 (0.6)
<b><i>Amniotic fluid</i></b>					
Number (%) positive fetuses/total	0	0	2/43 (5)	13/49 (26)	9/36 (25)

Mean (SE) viral load	-	-	4.2 (2.1)	4.1 (0.6)	4.2 (0.6)
Median (IQR) viral load	-	-	4.2 (4.2)	3.7 (3.3)	3.7 (2.3)

---

**Table 2-1:** Descriptive summary of fetal infection rates and viral load in tissues by days post inoculation.

DPI=days post inoculation, SE=standard error, IQR=interquartile range. The prevalence of infection increases across DPI (left to right). Viral load in fetal tissues decreases proportionally as distance from endometrium increased (top to bottom).

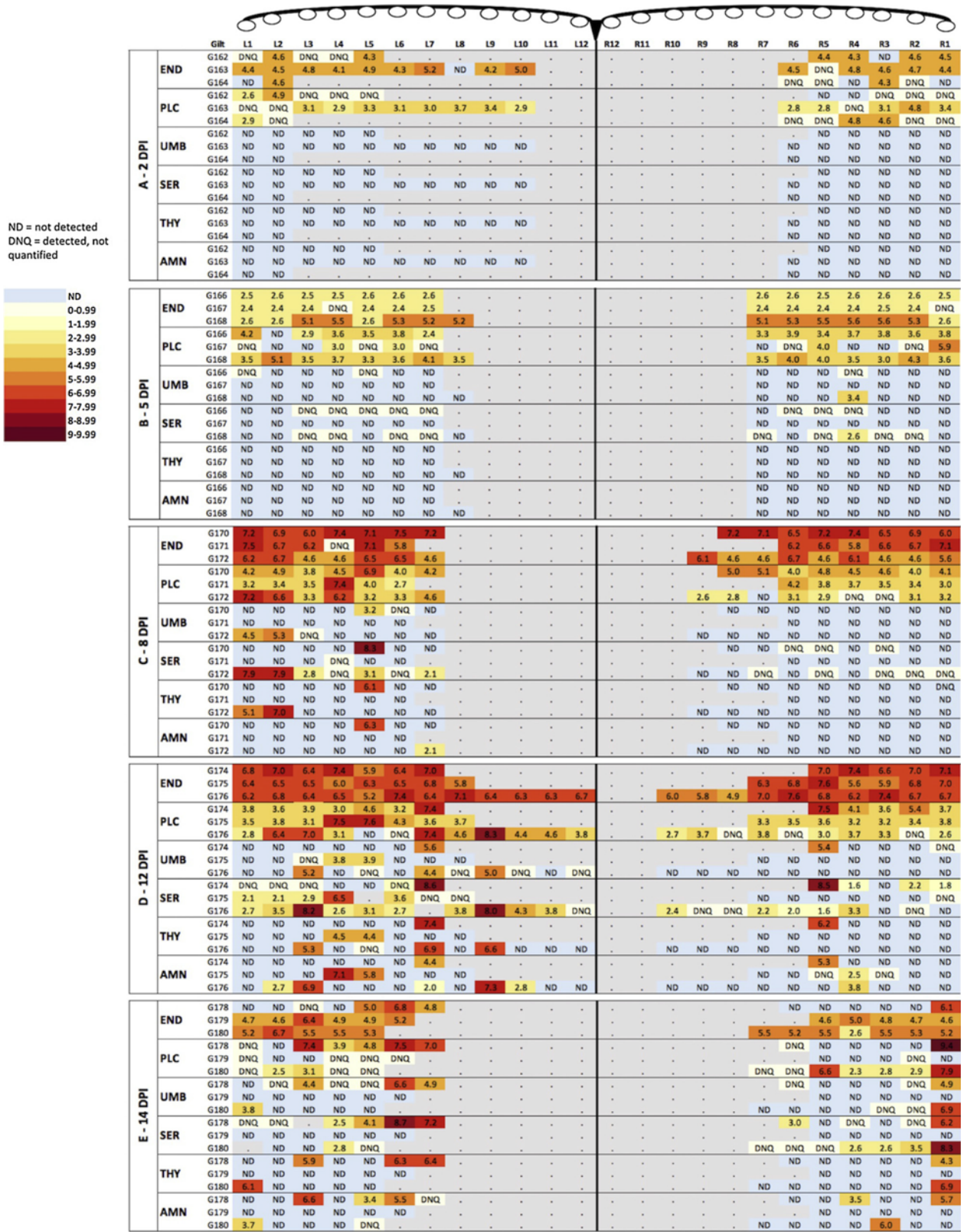
2.4.1.1. *Two days post-inoculation (Figure 2.2A, Figure 2.3):* The END and PLC were promptly infected after inoculation. PRRSV RNA was detected in either END, PLC or both tissues of all 2 DPI fetuses indicating an efficient mechanism(s) for maternofetal transmission. Quantifiable levels of virus were detected in the majority of fetuses in END (22/34; 65%) and PLC (18/34; 52%) with VL typically in the 3–4 log<sub>10</sub>/mg range (lower end of quantifiable range) indicating viral replication was well established in these tissues. No PRRSV RNA was detected in UMB, SER, THY and AMN indicating the PLC is the initial site of PRRSV replication. All the fetuses were VIA.

2.4.1.2. *Five days post-inoculation (Figure 2.2B, Figure 2.3):* The first evidence of PRRSV infection in UMB and SER was at 5 DPI. PRRSV RNA was detected in 4/43 (9%) of UMB and 17/43 (40%) of SER samples, most at DNQ levels. All 43 fetuses were VIA and all fetal THY and AMN samples remained negative at 5 DPI. The fetuses of one gilt (G167) had notably lower levels (prevalence and concentration) of viral RNA in PLC compared to the two other 5 DPI litters and no evidence of PRRSV infection in any fetal tissue, possibly suggesting a greater level of gilt-level resistance and/or resilience.

2.4.1.3. *Eight days post-inoculation (Figure 2.2C, Figure 2.3):* At 8 DPI, the first compromised fetuses were observed as well as the evidence of PRRSV infection of THY and AMN. Five fetuses in the uterine locations of one litter (G170) showed facial meconium staining; four with no or low VL in fetal tissues and SER, and one with high VL in SER, THY and AMN. The latter fetus (G170-L5) was pale in appearance in addition to being meconium stained. There was a single DEC fetus (G171-R1) that had blood-tinged, sticky exudate on its face, distinctly different from meconium staining. PRRSV RNA was detected in all END samples and 42/43 PLC samples. The prevalence of infection was greater in SER (17/43; 40%) than in THY (4/43; 9%) or AMN (2/43; 4.5%). The highest VL was observed in the pale fetus. Five other fetuses with quantifiable levels of virus in fetal tissues were in a single litter suggesting greater litter-level susceptibility. PRRSV RNA was not detected in the DEC fetus. Whether or not this death was a consequence of PRRSV infection is unknown.

2.4.1.4. *Twelve days post-inoculation (Figure 2.2D, Figure 2.3):* Forty-one percent (20/49) of fetuses were compromised, compared to under 14% (6/43) at 8 DPI. Four fetuses were DEC; two in each of two litters. Sixteen fetuses were MEC (16/49, 33%); all confined to face. Ten of 20 compromised fetuses were in a single litter suggesting greater litter-level susceptibility. PRRSV RNA was detected in the SER of all except one MEC fetus but was only sporadically detected in fetal tissues (UMB, THY, AMN). However, PRRSV RNA was detected in the fetal tissues of numerous VIA fetuses in seemingly random locations, and typically in more than one tissue of each fetus. The exception was three fetuses in one litter (G175-R3/4/5) in which PRRSV RNA was detected in AMN but not in UMB, SER or THY. This pattern is suggestive of interfetal transmission from an index (R4) fetus to its neighbours R3 and R5. The greatest PRRSV RNA detection frequency was in SER (36/47; 77%).

2.4.1.5. *Fourteen days post-inoculation (Figure 2.2E, Figure 2.3):* Clinical signs were more severe than at 12 DPI with fifty-eight percent of fetuses (21/36) showing compromise, including the first evidence of severe levels of meconium staining on face and/or body of 19/36 (53%) fetuses. These fetuses, along with two DEC, had high VL in all fetal tissues. The fetuses in one inoculated gilt (G179) appeared to be largely resistant to PRRSV infection. In spite of high VL in all END samples, no virus was detected in UMB, SER, THY or AMN of any fetus. PRRSV RNA in PLC was not detected in seven and was ultralow (DNQ) in four of the eleven fetuses in this litter. However, meconium staining was observed on the face of one fetus and on the body of another fetus in this litter.



Individual cells represent the PRRSV RNA concentration ( $\log_{10}$  copies per mg or  $\mu\text{L}$ ) in various maternal and fetal samples. Five blocks (A–E) each represent a different day post-inoculation (DPI) from 2 to 14. Fetal location within the left (L) and right (R) uterine horns is specified along the header (L1-L12, R1-R12). Each row represents a litter with gilt identity listed in the left column. Viral load is indicated numerically in each cell and by cell color, with light blue signifying “non-detected” (ND), pale yellow signifying “detected, not quantified” (DNQ), and quantifiable samples represented on a color gradient from light yellow (for lowest concentration) to dark red (highest concentration). Color intensity increases from top to bottom coinciding with greater viral load in more tissues at higher DPI. END=endometrium, PLC=placenta, UMB=umbilical cord, SER=fetal sera, THY=fetal thymus, AMN=amniotic fluid.



A) Fetal preservation status by position and days post inoculation (DPI). The table shows the status of individual fetuses (Gilt, G162-G180) across 14 DPI, categorized by days post inoculation (2, 5, 8, 12, 14 DPI). The status is recorded for 12 positions on the left (L1-L12) and right (R1-R12) uterine horns. The percentage of compromised fetuses is also indicated.

DPI	gilt	L1	L2	L3	L4	L5	L6	L7	L8	L9	L10	L11	L12	R12	R11	R10	R9	R8	R7	R6	R5	R4	R3	R2	R1	% compromised
2 DPI	G162	V	V	V	V	V	.	.	.	.	.	.	.	.	.	.	.	.	.	.	V	V	V	V	V	0%
	G163	V	V	V	V	V	V	V	V	V	V	.	.	.	.	.	.	.	.	V	V	V	V	V	V	0%
	G164	V	V	.	.	.	.	.	.	.	.	.	.	.	.	.	.	.	.	V	V	V	V	V	V	0%
5 DPI	G166	V	V	V	V	V	V	V	.	.	.	.	.	.	.	.	.	.	V	V	V	V	V	V	V	0%
	G167	V	V	V	V	V	V	V	.	.	.	.	.	.	.	.	.	.	V	V	V	V	V	V	V	0%
	G168	V	V	V	V	V	V	V	V	.	.	.	.	.	.	.	.	.	V	V	V	V	V	V	V	0%
8 DPI	G170	V	V	V	F	F	V	V	.	.	.	.	.	.	.	.	.	F	F	V	V	V	F	V	V	33%
	G171	V	V	V	V	V	V	V	.	.	.	.	.	.	.	.	.	.	V	V	V	V	V	V	D	8%
	G172	V	V	V	V	V	V	V	.	.	.	.	.	.	.	.	V	V	V	V	V	V	V	V	V	0%
12 DPI	G174	V	V	V	V	F	F	F	F	.	.	.	.	.	.	.	.	.	.	F	F	V	V	V	V	42%
	G175	V	V	V	D	D	V	V	V	.	.	.	.	.	.	.	.	.	V	V	V	V	V	V	V	13%
	G176	V	F	D	F	F	F	D	F	F	V	F	V	.	.	F	V	V	V	F	V	V	V	V	F	62%
14 DPI	G178	V	F	D	F	V	B	F	.	.	.	.	.	.	.	.	.	.	.	F	F	V	F	F	F	77%
	G179	B	V	V	F	V	V	.	.	.	.	.	.	.	.	.	.	.	.	.	V	V	V	V	V	18%
	G180	D	F	V	F	F	.	.	.	.	.	.	.	.	.	.	.	F	F	F	F	V	V	B	75%	

B) Fetal Preservation Score and PRRSV RNA concentration (log<sub>10</sub> copies per mg or μL) by tissue and fetal preservation score.

Fetal Preservation Score	n	PRRSV RNA concentration (log <sub>10</sub> copies per mg or μL)					
		END	PLC	UMB	SER	THY	AMN
VIA	158	3.4 (2.7)	2.2 (1.9)	0.2 (0.7)	0.6 (1.4)	0.1 (0.8)	0.2 (0.8)
MEC-FACE	37	5.2 (2.5)	3.6 (2.6)	1.1 (1.9)	2.7 (2.6)	1.1 (2.3)	1.0 (2.1)
MEC-BODY	3	5.5 (1.1)	5.1 (4.4)	4.5 (3.9)	5.7 (4.9)	4.4 (3.8)	1.8 (3.2)
DEC	7	5.9 (1.0)	5.7 (3.0)	3.7 (1.7)	4.9 (4.3)	4.7 (2.3)	4.6 (2.8)

205

PRRSV RNA concentration (log<sub>10</sub>/mg or uL)



ND 0-0.99 1-1.99 2-2.99 3-3.99 4-4.99 5-5.99 6-6.99 7-7.99 8-8.99 9-9.99

**Figure 2.3:** Fetal preservation status by position and days post inoculation.

A) The fetal preservation status of individual fetuses is shown by their relative position in the right (R) or left (L) uterine horn. Fetal meconium staining of face and/or body and death/decomposition increased progressively from 8 days post-inoculation (DPI). B) Mean (SD) PRRSV RNA concentration by tissue and fetal preservation score.

Fetal preservation scores: V=viaible, F=meconium staining restricted to the face, B=meconium staining on face and body, DEC=decomposed/dead fetus. END=endometrium, PLC=placenta, UMB=umbilical cord, SER=fetal serum, THY=fetal thymus, AMN=amniotic fluid.

## 2.4.2. *Classification of resistant, resilient and susceptible fetuses*

2.4.2.1. *Classification of fetal susceptibility by DPI:* All fetuses at 2 and 5 DPI were VIA with no or low VL. Although they fell into the bottom left quadrant of the fetal resilience matrix (**Figure 2.4A-B**) it was too early to classify as resistant. By contrast, at 8, 12 and 14 DPI (**Figure 2.4C-E**), a select number of fetuses fell into the resilient (top left), susceptible (top right) or ultra-susceptible (bottom right) quadrants. At 8 DPI, this was mainly due to individual fetuses with high VL, whereas at 12 and 14 DPI high VL and fetal preservation score contributed to their classification. The overall proportion of resistant fetuses decreased with duration of infection; from 86% (37/43) at 8 DPI to 42% (15/36) at 14 DPI (**Figure 2.4D-F**).

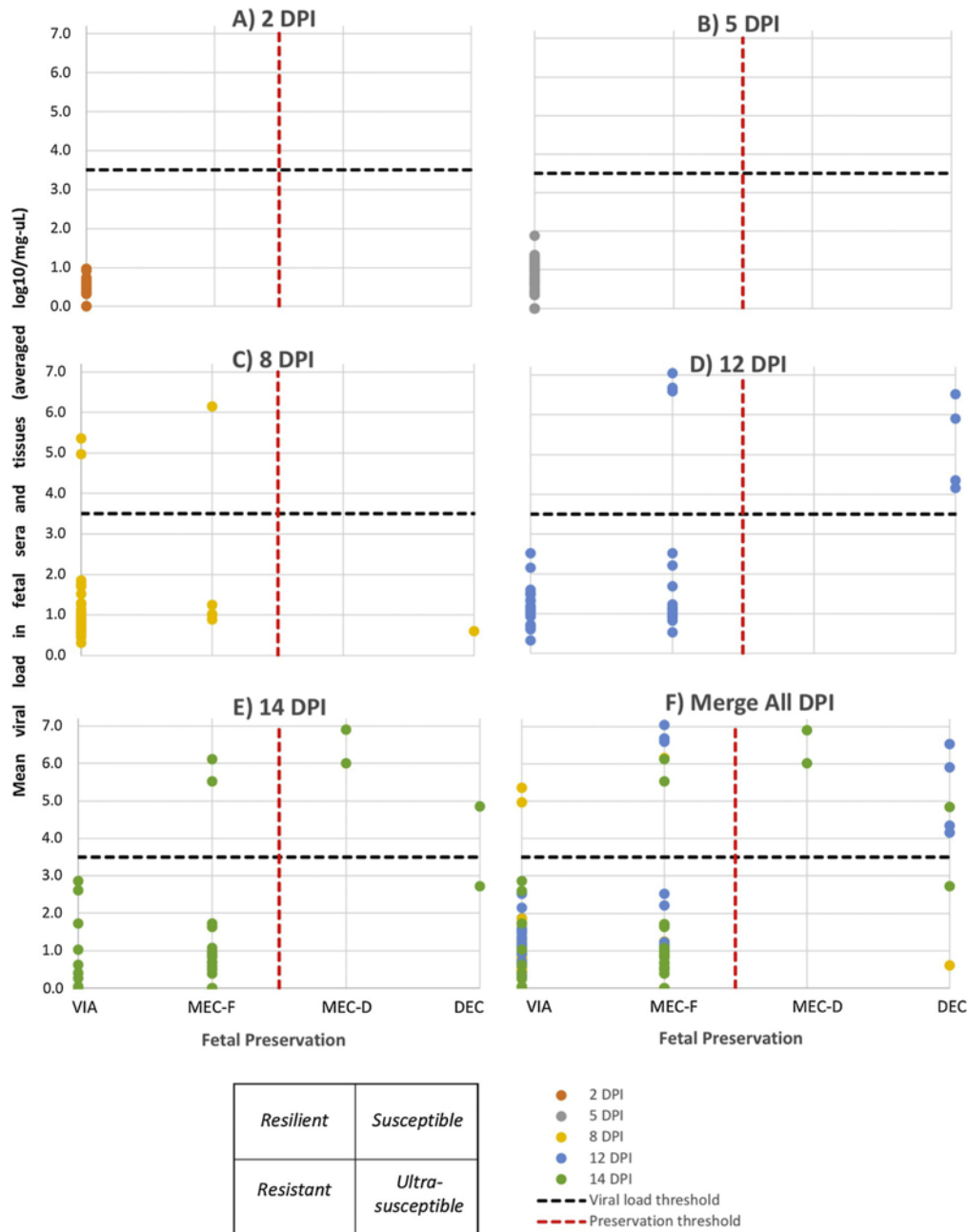
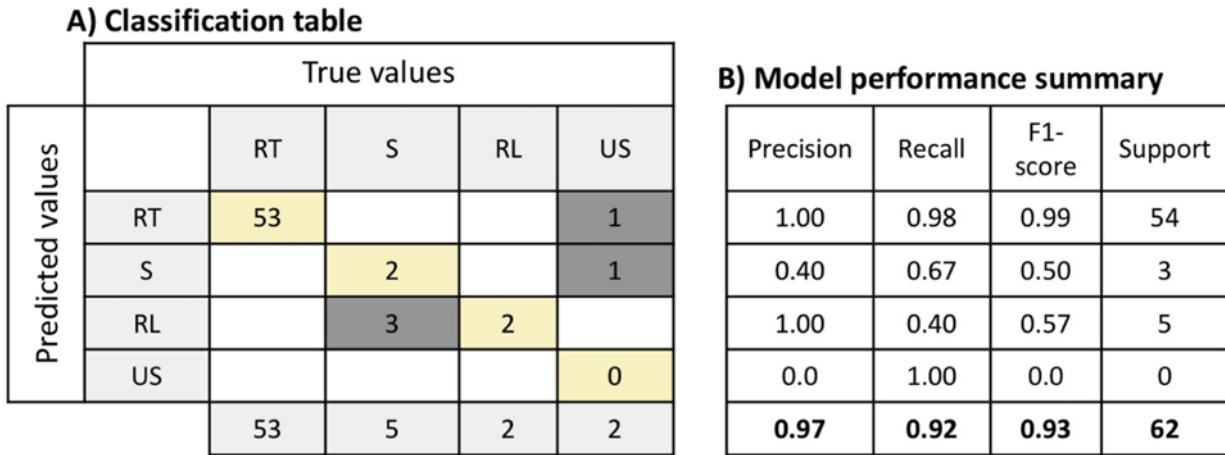


**Figure 2.4:** Susceptible, resistant and resilient fetal matrix.

Plots showing relative susceptibility of fetuses to PRRS virus based on mean RNA PRRSV concentration in fetal sera and tissues (placenta, umbilical cord, thymus, amniotic fluid) plotted on Y axis against fetal preservation category (VIA=viaible, MEC-F=meconium staining restricted to face, MEC-B=meconium staining on face and body, DEC=decomposed) on X axis. Resistant, resilient, susceptible and ultra-susceptible fetuses are positioned in the bottom-left, top-left, top-right, and bottom-right quadrants, respectively. Dashed lines represent break point thresholds for

fetal preservation score (vertical/red) and mean fetal PRRSV RNA concentration (horizontal/black). From 8 DPI onwards, select fetuses are found in the resilience, susceptible and ultrasusceptible quadrants due to changes in their viral load and/or fetal preservation score. DPI=days post inoculation.

2.4.2.2. *Factors associated with susceptibility classification:* The random forest approach determined which fetal factor(s): DPI, sex, brain:liver ratio, and VL in fetal SER, PLC, UMB, THY and AMN were the strongest predictors of fetal resilience as initially classified using the 2x2 fetal resilience (**Figure 2.4F**). The F1 score (average of precision and recall for resistant, resilient, susceptible and ultra-susceptible categories) in the full model was 0.92 and increased to 0.93 following the stepwise removal of: sex, brain:liver ratio, and VL in END, PLC, AMN, UMB and SER. Viral load in END and PLC were the first factors to be removed from the model indicating these tissues were least important determinants of classification. Viral load in AMN and UMB were correlated with THY and SER and when removed from the model had no impact on prediction accuracy. The most parsimonious (final) model contained only DPI and VL in THY. When THY was replaced by SER or DPI was removed, prediction accuracy decreased indicating DPI and THY are the most important predictors of fetal resistance and resilience in this study; however, susceptibility and ultra-susceptibility were poorly predicted by these two factors (**Figure 2.5A**). The precision score (0.97) of the final model exceeded the recall score (0.92) indicating the model had higher specificity and was biased towards producing false negative results (misclassifying true positives) (**Figure 2.5B**). This was most evident with the susceptible group where the final model misclassified 3/5 susceptible fetuses as resilient, and misclassified both ultra-susceptible fetuses. Thus, additional variables or factors are required to better characterize susceptibility. Of the features remaining in the final model, high VL in fetal thymus, non-detectable VL in fetal thymus, and DPI=14 were the more influential as indicated by their high feature relative importance scores (**Figure 2.5C**).



**C) Relative feature importance**

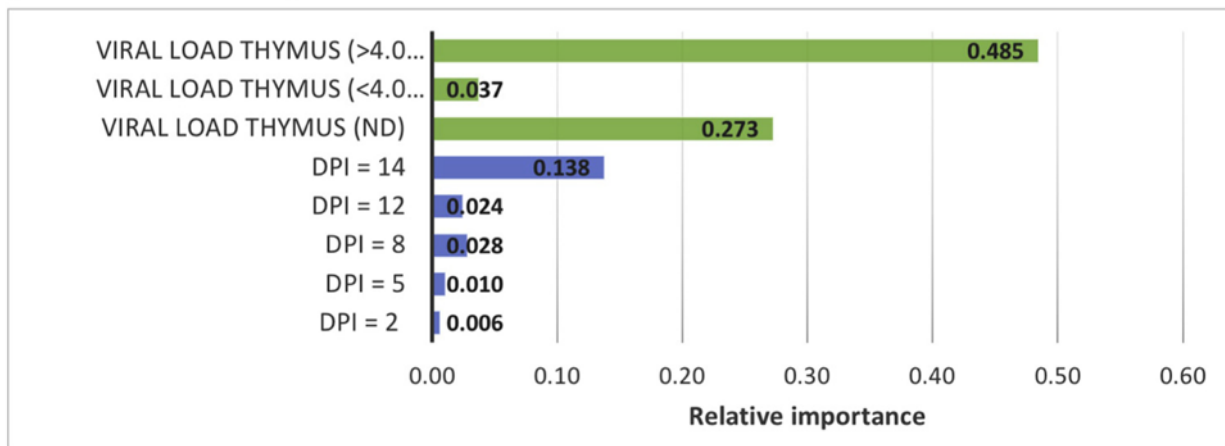


**Figure 2.5:** Classification of resistant, resilient, susceptible fetuses using a random forest model. A forest of 100 trees was created and 205 fetuses from PRRSV inoculated litters were classified using a 70:30 split between training and test datasets. A) Classification matrix of true versus predicted fetuses for each of four susceptibility categories (RT=resistant, S=susceptible, RL=resilient, US=ultra-susceptible). The model was most effective at classifying resistant and resilient fetuses (yellow boxes along diagonal), but misclassified most susceptible and ultra-susceptible fetuses (dark grey boxes). B) Model performance summary: ‘precision’ (specificity), ‘recall’ (sensitivity) and ‘F1-score’ (average of recall and precision) indicate the overall accuracy of 0.93 for the random forest model. ‘Support’ represents the number of predicted fetuses in each category. C) After developing the full model, a backwards stepwise removal of least important variables (pruning) was performed to create a parsimonious model. The relative importance of variables (features) left in the model is shown and indicates that thymic viral load >4 log<sub>10</sub>/mg or

not detected (negative) and 14 days post inoculation (DPI) were the most important features required for classification. By contrast, fetal sex, brain:liver ratio (IUGR), and viral load in endometrium, placenta, fetal sera, amniotic fluid and umbilic cord were not important predictors of fetal susceptibility, resilience or resistance in this study.

2.4.2.3. *Relationship of IUGR to VL and fetal preservation:* The brain: liver ratio averaged 1.34 ( $\pm 0.34$ ; SD) across all fetuses and was significantly greater in fetuses of non-inoculated versus inoculated gilts (CTRL=1.44  $\pm$  0.35; INOC=1.31  $\pm$  0.33;  $P= 0.006$ ). Because the brain: liver ratio changes in accordance with fetal growth, the mean brain: liver ratio was calculated for each DPI (only INOC gilts): 2 DPI = 1.15 ( $\pm 0.22$ ), 5 DPI = 1.26 ( $\pm 0.29$ ), 8 DPI = 1.54 ( $\pm 0.24$ ), 12 DPI = 1.37 ( $\pm 0.33$ ), and 14 DPI = 1.36 ( $\pm 0.44$ ). Using plus or minus 1 SD as breakpoints to identify IUGR and non-IUGR fetuses, respectively, 21/203 (10.8%) fetuses were classified as non-IUGR, 155/203 (76.4%) as average (AVG), and 27/203 (13.3%) as IUGR in PRRSV inoculated litters (2 fetuses did not have their brain or liver weighed). There was a trend towards more non-IUGR fetuses being compromised (MEC or DEC) compared to AVG and IUGR fetuses when all five DPI were combined ( $P= 0.06$ ), but this was largely the result of group differences observed at 12 DPI. Non-IUGR fetuses had significantly higher VL in UMB, SER and AMN than IUGR or AVG fetuses at 14 DPI, and in THY across all days. There were no differences of VL in END and PLC amongst the three groups (**Figure 2.6**)

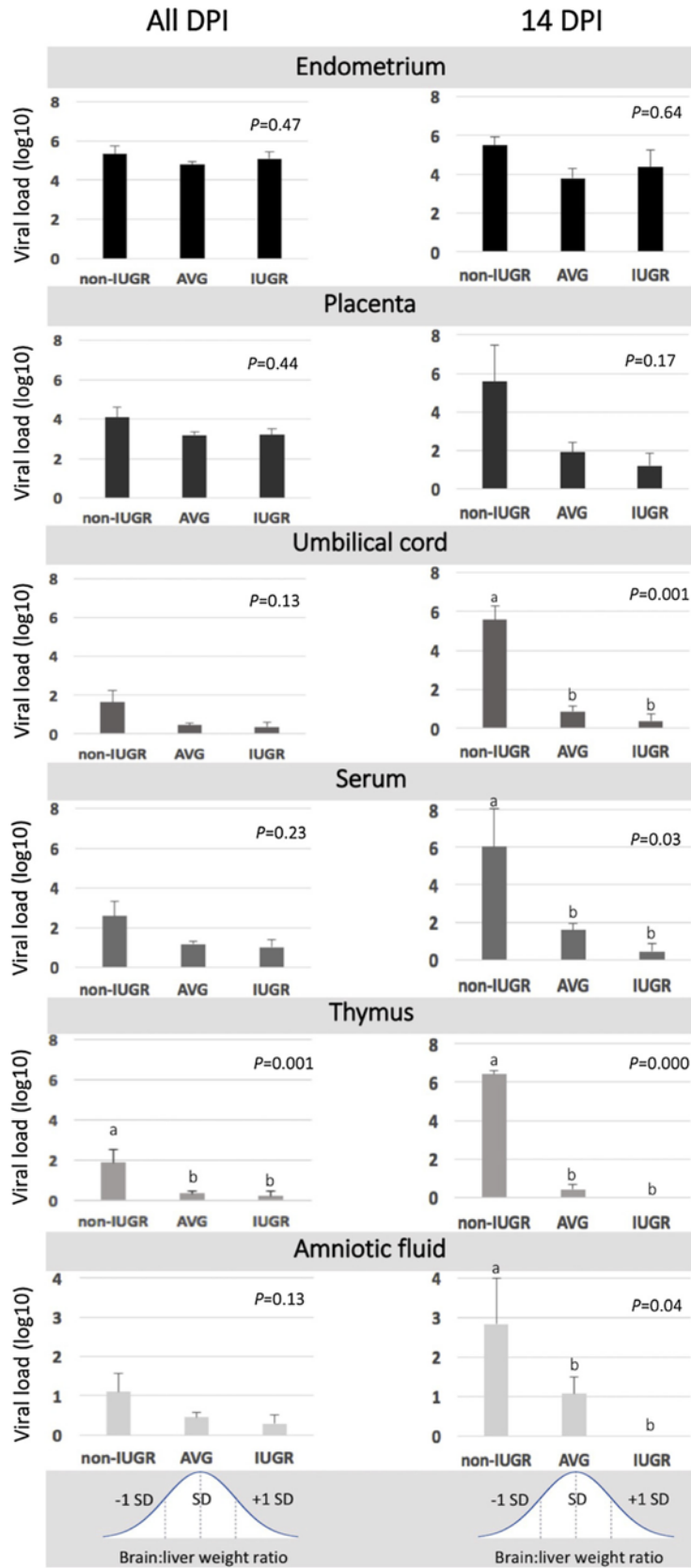


**Figure 2.6:** PRRSV RNA concentration (viral load) by IUGR group in fetal tissues and sera. Bar plots show the difference in viral load in endometrium, placenta, umbilical cord, fetal serum, thymus and amniotic fluid averaged across all days post inoculation (DPI; left) and at 14 DPI (right). The belt shape curves beneath the bar plots indicate how the three IUGR groups were defined: IUGR = < -1 SD below mean, non-IUGR = > 1 SD above mean, AVG = between -1 and +1 SD from the mean. Compared to IUGR and average fetuses, viral load in non-IUGR fetuses was significantly greater in THY across all DPI, and in umbilical cord, serum and amniotic fluid at 14 DPI.

## 2.5. Discussion

This study investigated the rate of PRRSV transmission across the maternal-fetal interface and the development of fetal compromise at five different time points post inoculation. Although our research group has undertaken a number of PRRSV2 pregnant gilt challenge experiments in the past, the results reported herein are novel in terms of investigating maternofetal transmission across range of termination days, assessment of viral load across multiple fetal tissues and elucidation of the pathogenesis and potential factors associated with fetal PRRSV resistance/ resilience. In spite of the small number of fetuses spread over five termination time points (14 post inoculation days), several important conclusions can be drawn from the study. The rapidity at which the END and PLC were infected cannot be under-emphasized and has implications for investigating potential routes of transplacental transmission of the virus. Nearly all END and PLC samples were infected at 2 DPI. Early endometrial infection was expected, as infected gilts are viremic at 1 DPI,<sup>77</sup> but the rapid infection of PLC indicates that the mechanism of transplacental infection is likely efficient and initiates concurrently with viremia. While macrophage-associated transmission of virus from END to PLC has been proposed,<sup>40</sup> PRRSV may use several routes to transmit into fetuses. The interdigitations of the dual epithelial layers of the porcine MFI prevents the transmission of large macromolecules, but allows for the efficient exchange of nutrients and gasses across short diffusion distances.<sup>19</sup> Inflammation, apoptosis or necrosis of maternal uterine epithelium and fetal trophoblast may alter cell membrane and tight junction integrity allowing direct transmission within or between cells. However, even before epithelial cell integrity is affected, extracellular vesicles may provide an efficient, rapid mechanism of viral transmission across the MFI. Extracellular vesicles are important carriers of lipids, proteins and nucleic acids and play a vital role in fetal-maternal communication in humans<sup>78,79</sup> and pigs.<sup>80</sup> Bidirectional shuttling of extracellular vesicles containing miRNAs between fetal trophoblast and maternal endothelial cells has been demonstrated in vitro and may be a “trojan horse” method of transmission. Exosomes have been implicated in the transmission of PRRSV, having been shown to contain viral genomic RNA and partial viral proteins, and establish productive infections in PK-15 and Marc-145 cells in vitro.<sup>81</sup> It is important to note that steps were taken to prevent the cross contamination of placenta with maternal blood during sample collection, to reduce the likelihood of false positive PCR results of PLC.

However, separating the placenta from endometrium is a delicate process, and when poorly performed can result in small amounts of endometrium adhering to the placental portion of the sample (unpublished data). To minimize the risk of contaminating the placental samples, this task was limited to a small team of experienced and proficient technicians. Furthermore, viral presence was assessed in a subset of fetuses across all DPI using immunofluorescent analyses that confirmed the presence of PRRSV antigen in placental tissue on 2 DPI.<sup>72</sup> Moreover, there was a moderate correlation between PRRSV RNA concentration (assessed using RT-qPCR) and viral antigen spot counts (assessed using immunofluorescence) in END and PLC.<sup>72</sup> After placental infection, the virus presumably replicates in permissive placental macrophages until it enters the fetal circulation. We observed the first evidence of viral RNA in UMB and fetal sera at 5 DPI. The positivity of the umbilical cord indicates PRRSV migrates from the placenta to the fetus through the umbilical blood circulation. In spite of that, we observed detection of virus in AMN within some fetuses, but not in their UMB or SER, suggesting the possibility of horizontal viral transmission through the placental membranes instead of the umbilical cord circulation. A previous study indicated that PRRSV may be transmitted from fetus to fetus via sibling microchimeric cells, crossing in between adjacent extremities of the fetal allantochorion.<sup>82</sup> Thymus is the putative primary fetal site for virus replication.<sup>50</sup> Our results clearly show that PLC is the initial fetal tissue for PRRSV replication, as it was infected within 2 days of inoculation, reaching high VL prior to any other fetal tissue. The first positive THY and AMN samples were detected at 8 DPI, demonstrating that the virus replicates in other fetal locations at first. However, THY may become the main fetal site of viral replication after about one week of infection, as it reached high VL quickly. The high PRRSV RNA concentration in THY when first detected indicates that the virus was possibly replicating there prior to 8 DPI. Unfortunately, we did not quantify PRRSV RNA concentration in THY or other systemic fetal sites between 5 and 8 DPI.

The first signs of fetal compromise were observed at 8 DPI, implying that the virus requires about one week of infection and replication to initiate whatever cascade of events jeopardizes fetal health and survival. Unexpectedly, the first observed DEC fetus was RT-qPCR negative in all fetal tissues and had no evidence of vasculitis and placental detachment, and only minimal placentitis based on assessments reported by Novakovic et al.<sup>53</sup> While the mechanism of fetal death is complex and poorly understood, this fetus is clearly an outlier and may have died

for a reason unrelated to PRRSV infection. The number of MEC and DEC fetuses steadily increased after 8 DPI, and more severe meconium staining of face and body was generally associated with higher PRRSV RNA concentration. Categorizing meconium staining based on location (face or face and body) was useful in this study to demonstrate the progression of disease over time. We believe that fetuses with deposits of meconium on their faces and bodies would likely die within a few days if pregnancy was continued without interruption. A previous study in which PRRSV infected pregnant gilts were euthanized at 21 DPI had more than 40% dead fetuses<sup>49</sup> compared to only 8% and 5% at 12 and 14 DPI, respectively in this study, emphasizing how rapidly the maternofetal environment decays.

Fetal resistance, resilience and susceptibility have not been formally defined in the context of PRRSV infection but may help lead to new control strategies if mechanisms of resistance are understood. In the present study, susceptible fetuses were easily identified as non-viable (MEC or DEC) with high VL in multiple fetal tissues. Resistant and resilient fetuses were harder to identify. Viable fetuses with high VL across multiple tissues were considered resilient, defined as the ability of the animal to not become compromised despite high infections<sup>75</sup> or sustained performance in the face of infection.<sup>74</sup> By contrast, resistance implies an animal's ability to exert control over the pathogen's life cycle, or replication in the case of PRRSV.<sup>74</sup> Resistance is typically relative rather than absolute, as observed in the present study. Resistant fetuses were VIA with negative or low VL in the majority of tissues. This is clearly an ideal characteristic to achieve and based on the results of this study, appear to occur at the fetal or gilt level. For example, the litter of G179 was almost completely RT-qPCR negative at 14 DPI. While high VL and the presence of fetal lesions are definitive risk factors for meconium staining,<sup>37,53</sup> it was not a factor in these fetuses. It is possible that these fetuses were responding to physiologic changes related to the infection of PLC and/or END, as has been previously elucidated.<sup>62</sup> As resistance does not need to be complete,<sup>74</sup> achieving partial resistance (reduction in VL or a proportion of negative animals, or both) might be a more achievable goal in the swine industry. However, we acknowledge that because animals were terminated earlier in this study than many reproductive PRRS studies and natural swine pregnancy (115 days), it is difficult to predict how many of the fetuses classified as resistant or resilient would have died if the pregnancy continued to term. Using fetal VL and fetal preservation status as an initial classification system allowed visualization of susceptible, resistant and resilient fetuses in a 2x2

matrix. While the fetuses occupied multiple quadrants at 8 and 12 DPI, the random forest classification model strongly indicated that 14 DPI was a more important feature for accurate classification than earlier DPI ( $\leq 12$ ). Moreover, VL in THY was a more important classifier than VL in SER or other fetal tissues. It must be noted that the random forest analysis was undertaken herein on a very small dataset with a limited number of variables, some highly correlated. While showing proof of concept in classifying fetal susceptibility, resistance and resilience, it is necessary to perform similar analyses on larger and more complex datasets to improve confidence in these findings. Although sparsely used in veterinary epidemiology, random forest models have been used with success to study relevant swine industry health-related problems such as swine influenza, salmonellosis, and biosecurity effectiveness.<sup>68,83-86</sup> A previous study unexpectedly showed that non-IUGR (“larger”) fetuses have higher VL compared to fetuses experiencing IUGR.<sup>70</sup> Here, we confirmed that non-IUGR fetuses have higher VL in all the fetal tissues at 14 DPI, but not in END and PLC, indicating that the consequences of IUGR only affect the fetus. The absence of IUGR group differences before 14 DPI is likely because insufficient time had elapsed for transplacental infection and viral replication in the fetal tissues. IUGR is a condition where individual fetuses are deprived of nutrients and, thus, have a restricted growth in the uterus. There are many factors that can lead to this condition, such as genetics, endocrine and environmental disruption. When it occurs, it favors brain development at the expense of other organs.<sup>87</sup> It was demonstrated that IUGR fetuses have altered placental structures, which can lead to alterations in nutrient absorption from the dam.<sup>26</sup> This concept might be applicable to transplacental PRRSV infection. The fact that IUGR fetuses have smaller PLC might result in fetuses that are less prone to infection. However, determining if any structural or cellular changes occur in IUGR tissues may lead to method(s) to prevent or reduce transmission to non-IUGR animals.

## **2.6. Conclusions**

This was the first temporal study assessing PRRSV RNA concentration in fetal tissues at five different time points over 14 days post-inoculation to investigate the progression of PRRSV infection and disease. Our results confirmed that the maternal-fetal interface (END, PLC) is promptly infected at 2 DPI after maternal inoculation and that PRRSV replicates in PLC before entering the fetal circulation on 5 DPI. Fetal compromise was first observed on 8 DPI and

increased progressively through 14 DPI. Although samples were not assessed each day between 2 and 14 DPI, we affirm that the virus takes around a week to sufficiently replicate in fetal tissues to induce fetal compromise. Variation in fetal resistance, resilience and susceptibility, most strongly associated with VL in fetal THY compared to other fetal tissues, was first evident beginning at 8 DPI, but was more clearly discernable at later DPI. Viral load in fetal tissues was greater in non-IUGR fetuses, confirming previous research, but brain: liver ratio was not a predictor of fetal resilience, resistance or susceptibility. Collectively, these findings shed new light on the mechanics of fetal PRRSV infection and resilience.

## **Declarations**

**Ethics approval:** This study was approved by the University of Saskatchewan Animal Research Ethics Board and adhered to the Canadian Council on Animal Care guidelines for humane animal use (protocol #2016002). The infected pregnant gilts were closely monitored for clinical signs and a human intervention point checklist was established to monitor the gilts for critical conditions post-inoculation. It was not feasible to monitor fetal conditions after the viral inoculation, but fetal compromise death was expected to occur at the later time points. We selected termination points that were prior to when a high rate of fetal death was expected. Gilts were euthanized with intravenous sodium pentobarbital overdose followed by pithing and exsanguination. Fetuses were euthanized as humanely as possible given that pentobarbital sodium crosses the MFI rapidly<sup>88,89</sup> and enters fetal circulation prior to the onset of hypoxia and asphyxia.

**Availability of data and material:** Data will be made available to researchers with a legitimate hypothesis and objectives. Please contact the corresponding author.

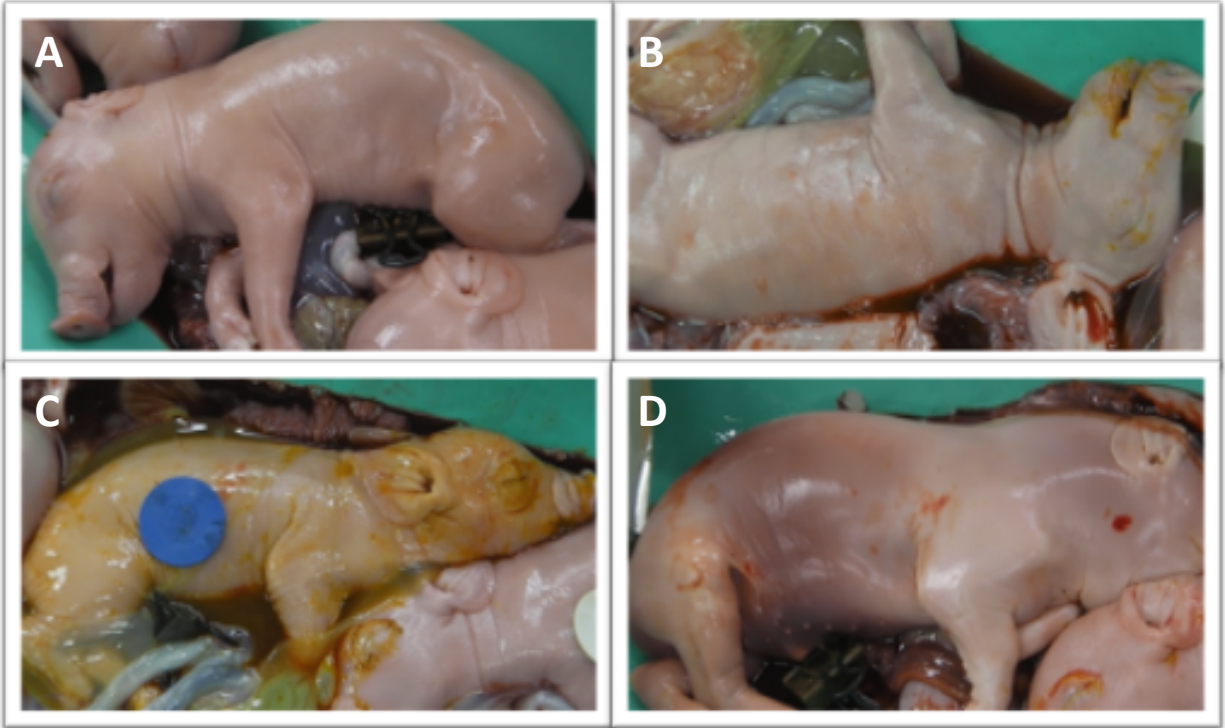
**Competing interests:** The authors declare no conflicts of interest with respect to the research, authorship and/or publication of this article.

**Funding:** This project was supported by Genome Canada (grant #345169) and Genome Prairie (Saskatchewan Ministry of Agriculture; grant #20150329), along with administrative support provided by Genome Alberta and the University of Saskatchewan. The funding agencies had no involvement in study design, implementation, analyses or interpretation of the results.

**Acknowledgements:** We express special acknowledgment to numerous personnel (technicians, graduate students, summer students, colleagues) who helped in the preparation and

implementation of this study. Animal Care was contracted to VIDO-Intervac, Saskatoon. Necropsies were performed at the Prairie Diagnostic Services, Saskatoon.

### **Additional files**



**Additional file 2.1:** Fetal preservation categories.

Image A shows a viable fetus (VIA; G172-L2); B shows a fetus with meconium staining restricted to its face (MEC-F; G17-R2); C shows a fetus with meconium staining distributed on face and body (MEC-B; G178-L6); and D shows a decomposed/dead fetus (DEC; G180-L1).



DPI	Gilt	L1	L2	L3	L4	L5	L6	L7	L8	L9	L10	L11	L12	R12	R11	R10	R9	R8	R7	R6	R5	R4	R3	R2	R1					
2	G161	ND								ND	ND	ND	ND	ND																
2	G162	DNQ	4.592	DNQ	DNQ	4.324	-	-	-	-	-	-	-								4.449	4.346	ND	4.615	4.487					
2	G163	4.439	4.549	4.784	4.130	4.940	4.272	5.167	ND	4.215	5.021	-	-							4.482	DNQ	4.814	4.609	4.691	4.428					
2	G164	ND	4.611	-	-	-	-	-	-	-	-	-	-							DNQ	DNQ	ND	4.282	DNQ	ND					
5	G165	ND	ND	ND	ND	ND	ND	-	-	-	-	-	-						ND											
5	G166	2.542	2.572	2.534	2.548	2.557	2.559	2.587	-	-	-	-	-						2.586	2.562	2.546	2.562	2.580	2.581	2.527					
5	G167	2.428	2.425	2.401	DNQ	2.423	2.387	2.458	-	-	-	-	-							2.410	2.367	2.449	2.429	2.490	2.363	DNQ				
5	G168	2.565	2.582	5.108	5.907	2.596	5.266	5.179	5.179	-	-	-	-							5.108	5.298	5.507	5.569	5.569	5.266	2.554				
8	G169	ND	-	-	-	-	-							ND	ND	ND	ND	ND	ND											
8	G170	7.179	6.895	6.043	7.378	7.086	7.474	7.176	-	-	-	-	-							7.176	7.086	6.461	7.179	7.378	6.461	6.895	6.043			
8	G171	7.474	6.668	6.210	DNQ	7.062	5.838	-	-	-	-	-	-								6.210	6.626	5.838	6.626	6.668	7.062				
8	G172	6.197	6.669	4.570	4.570	6.540	6.540	4.570	-	-	-	-	-								6.055	4.571	4.570	6.669	4.570	6.055	4.571	4.570	5.642	
12	G173	ND	-	-							ND	ND	ND	ND	ND	ND														
12	G174	6.846	7.013	6.399	7.355	5.949	6.368	7.036	-	-	-	-	-								6.986	7.428	6.611	6.982	7.149					
12	G175	6.436	6.536	6.506	5.957	6.250	6.497	6.765	5.803	-	-	-	-								6.296	6.803	7.639	5.615	5.909	6.778	6.952			
12	G176	6.194	6.774	6.406	6.511	5.153	7.376	6.439	7.086	6.440	6.260	6.345	6.680								5.962	5.850	4.923	6.981	7.558	6.815	6.213	7.352	6.677	6.749
14	G177	ND	ND	ND	ND	ND	ND	-	-	-	-	-	-							ND	ND	ND	ND	ND	ND					
14	G178	ND	ND	DNQ	ND	5.039	6.771	4.780	-	-	-	-	-								ND	ND	ND	ND	ND					
14	G179	4.747	4.575	6.445	4.925	4.887	5.244	-	-	-	-	-	-								4.577	5.047	4.831	4.735	4.585					
14	G180	5.156	6.711	5.519	5.457	5.316	-	-	-	-	-	-	-								5.519	5.191	5.519	2.563	5.463	5.335	5.156			

**Additional file 2.2:** Viral concentration by days post inoculation in endometrium.

Viral RNA concentration ( $\log_{10}$  /mg) in endometrium at each of five days post infection (gilts in rows, fetuses in columns). The endometrium is infected 2 days post inoculation (DPI). PRRSV concentration rapidly increases thereafter. G179 appears largely resistant to virus at 14 DPI. ND = not detected; DNQ = detectable, not quantifiable.

DPI	G#	L1	L2	L3	L4	L5	L6	L7	L8	L9	L10	L11	L12	R12	R11	R10	R9	R8	R7	R6	R5	R4	R3	R2	R1		
2	G161	ND	-	-	-	-	-	-	-	-	-	ND	ND	ND	ND	ND	ND										
2	G162	2.643	4.853	DNQ	DNQ	DNQ	-	-	-	-	-	-	-	-	-	-	-	-	-	ND	ND	DNQ	DNQ	DNQ	DNQ		
2	G163	DNQ	DNQ	3.091	2.905	3.253	3.087	3.011	3.719	3.385	2.851	-	-	-	-	-	-	-	2.848	2.825	DNQ	3.121	4.821	3.391	4.821		
2	G164	2.911	DNQ	-	-	-	-	-	-	-	-	-	-	-	-	-	-	-	DNQ	DNQ	4.773	4.588	DNQ	DNQ	4.773		
5	G165	ND	ND	ND	ND	ND	ND	-	-	-	-	-	-	-	-	-	-	-	ND								
5	G166	4.200	ND	2.944	3.642	3.518	3.753	2.401	-	-	-	-	-	-	-	-	-	-	3.327	3.949	3.366	3.701	3.753	3.552	3.848		
5	G167	DNQ	ND	ND	2.999	DNQ	2.963	DNQ	-	-	-	-	-	-	-	-	-	-	ND	DNQ	3.967	ND	ND	DNQ	5.861		
5	G168	3.460	5.105	3.451	3.665	3.261	3.638	4.131	3.486	-	-	-	-	-	-	-	-	-	3.465	4.004	3.986	3.456	3.045	4.329	3.560		
8	G169	ND	ND	ND	ND	ND	ND	-	-	-	-	-	-	-	-	-	-	-	ND								
8	G170	4.198	4.911	3.803	4.463	6.867	3.998	4.178	-	-	-	-	-	-	-	-	-	-	5.031	5.112	3.982	4.750	4.531	4.632	3.978	4.058	
8	G171	3.235	3.351	3.533	7.389	3.984	2.668	-	-	-	-	-	-	-	-	-	-	-	4.173	3.824	3.699	3.521	3.413	3.012	3.012		
8	G172	7.233	6.560	3.318	6.197	3.240	3.345	4.612	-	-	-	-	-	-	-	-	-	-	2.630	2.766	ND	3.087	2.933	DNQ	3.113	3.241	
12	G173	ND	-	-	-	-	-	-	-	-	ND																
12	G174	3.842	3.557	3.908	3.031	4.618	3.164	7.369	-	-	-	-	-	-	-	-	-	-	-	-	7.503	4.125	3.590	5.350	3.747		
12	G175	3.478	3.803	3.082	7.481	7.584	4.338	3.623	3.651	-	-	-	-	-	-	-	-	-	3.330	3.467	3.591	3.213	3.197	3.395	3.789		
12	G176	2.832	6.428	6.966	3.092	ND	DNQ	7.435	4.551	8.251	4.355	4.611	3.753	-	-	-	-	-	2.702	3.700	DNQ	3.825	2.972	3.711	3.273	DNQ	2.635
14	G177	ND	ND	ND	ND	ND	ND	-	-	-	-	-	-	-	-	-	-	-	ND								
14	G178	DNQ	ND	7.377	3.889	4.827	7.453	6.981	-	-	-	-	-	-	-	-	-	-	DNQ	ND	ND	ND	ND	ND	9.642		
14	G179	DNQ	ND	ND	DNQ	DNQ	DNQ	-	-	-	-	-	-	-	-	-	-	-	-	DNQ	ND	ND	DNQ	ND	ND		
14	G180	DNQ	2.511	3.108	DNQ	DNQ	-	-	-	-	-	-	-	-	-	-	-	-	DNQ	DNQ	6.591	2.318	2.784	2.855	7.903		

**Additional file 2.3:** Viral concentration by days post inoculation in placenta.

Viral RNA concentration ( $\log_{10}$  /mg) in placenta at each of five days post infection (gilts in rows, fetuses in columns). Similar to endometrium, the placenta is largely infected 2 days post inoculation (DPI). Thereafter, the PRRSV concentration rapidly increases but at a slower rate than in endometrium. ND = not detected; DNQ = detectable, not quantifiable.

DPI	Gilt	L1	L2	L3	L4	L5	L6	L7	L8	L9	L10	L11	L12	R12	R11	R10	R9	R8	R7	R6	R5	R4	R3	R2	R1
2	G161	ND	ND	ND	-	-	-	-	-	-	-	-	-	ND	ND	ND	ND	ND							
2	G162	ND	ND	ND	ND	ND	-	-	-	-	-	-	-	-	-	-	-	-	-	ND	ND	ND	ND	ND	
2	G163	ND	ND	ND	ND	-	-	-	-	-	-	-	-	ND	ND	ND	ND	ND							
2	G164	ND	ND	-	-	-	-	-	-	-	-	-	-	-	-	-	-	-	-	ND	ND	ND	ND	ND	
5	G165	ND	ND	ND	ND	ND	ND	-	-	-	-	-	-	-	-	-	-	-	ND	ND	ND	ND	ND	ND	
5	G166	DNQ	ND	ND	ND	DNQ	ND	ND	-	-	-	-	-	-	-	-	-	-	ND	ND	ND	DNQ	ND	ND	
5	G167	ND	-	-	-	-	-	-	-	-	-	-	ND	ND	ND	ND	ND	ND							
5	G168	ND	ND	-	-	-	-	-	-	-	-	-	ND	ND	ND	3.380	ND	ND							
8	G169	ND	-	-	-	-	-	-	-	-	-	-	ND	ND	ND	ND	ND	ND							
8	G170	ND	ND	ND	ND	3.171	DNQ	ND	-	-	-	-	-	-	-	-	-	ND	ND	ND	ND	ND	ND	ND	
8	G171	ND	ND	ND	ND	ND	ND	-	-	-	-	-	-	-	-	-	-	-	ND	ND	ND	ND	ND	ND	
8	G172	4.544	5.306	DNQ	ND	ND	ND	ND	-	-	-	-	-	-	-	-	-	ND	ND	ND	ND	ND	ND	ND	
12	G173	ND	ND	ND	ND	-	-	-	-	-	-	-	ND	ND	ND	ND	ND	ND							
12	G174	ND	ND	ND	ND	ND	ND	5.562	-	-	-	-	-	-	-	-	-	-	-	5.381	ND	ND	ND	DNQ	
12	G175	ND	ND	DNQ	3.849	3.909	ND	ND	ND	-	-	-	-	-	-	-	-	-	ND	ND	ND	ND	ND	ND	
12	G176	ND	ND	5.195	ND	DNQ	ND	4.448	DNQ	5.035	DNQ	ND	DNQ	-	-	-	-	-	ND	ND	ND	ND	ND	ND	
14	G177	ND	ND	ND	ND	ND	ND	-	-	-	-	-	-	-	-	-	-	-	ND	ND	ND	ND	ND	ND	
14	G178	ND	DNQ	4.448	DNQ	DNQ	6.623	4.910	-	-	-	-	-	-	-	-	-	-	DNQ	ND	ND	ND	DNQ	4.890	
14	G179	ND	ND	ND	ND	ND	ND	-	-	-	-	-	-	-	-	-	-	-	ND	ND	ND	ND	ND	ND	
14	G180	3.838	ND	ND	ND	ND	-	-	-	-	-	-	-	-	-	-	-	-	ND	ND	ND	DNQ	DNQ	6.885	

**Additional file 2.4:** Viral concentration by days post inoculation in umbilical cord.

Viral RNA concentration ( $\log_{10}/\text{mg}$ ) in umbilical cords at each of five days post infection (gilts in rows, fetuses in columns). The first evidence of PRRSV infection is at 5 days post inoculation (DPI). Thereafter, umbilical cord infection appears to be sporadic. ND = not detected; DNQ = detectable, not quantifiable.



DPI	Gilt	L1	L2	L3	L4	L5	L6	L7	L8	L9	L10	L11	L12	R12	R11	R10	R9	R8	R7	R6	R5	R4	R3	R2	R1
2	G161	ND	ND	ND	ND	ND	ND	ND	ND	ND	ND	ND	ND	ND	ND										
2	G162	ND	ND	ND	ND	ND	ND	ND	ND	ND	ND	ND	ND	ND	ND										
2	G163	ND	ND	ND	ND	ND	ND	ND	ND	ND	ND	ND	ND	ND	ND										
2	G164	ND	ND	ND	ND	ND	ND	ND	ND	ND	ND	ND	ND	ND	ND										
5	G165	ND	ND	ND	ND	ND	ND	ND	ND	ND	ND	ND	ND	ND	ND										
5	G166	ND	ND	DNQ	DNQ	DNQ	DNQ	DNQ	DNQ	ND	ND	ND	ND	ND	ND	ND	ND	ND	ND	ND	ND	ND	ND	ND	ND
5	G167	ND	ND	ND	ND	ND	ND	ND	ND	ND	ND	ND	ND	ND	ND										
5	G168	ND	ND	DNQ	DNQ	ND	DNQ	DNQ	ND	ND	ND	ND	ND	ND	ND	ND	ND	ND	ND	ND	2.552	DNQ	DNQ	ND	ND
8	G169	ND	ND	ND	ND	ND	ND	ND	ND	ND	ND	ND	ND	ND	ND										
8	G170	ND	ND	ND	ND	8.336	ND	ND	ND	ND	ND	ND	ND	ND	ND	ND	ND	ND	ND	ND	ND	ND	ND	ND	ND
8	G171	ND	ND	ND	DNQ	ND	ND	ND	ND	ND	ND	ND	ND	ND	ND	ND	ND	ND	ND						
8	G172	7.938	7.887	2.771	DNQ	3.060	DNQ	2.072	ND	ND	ND	ND	ND	ND	ND	ND	ND	ND	ND	ND	ND	ND	ND	ND	ND
12	G173	ND	ND	ND	ND	ND	ND	ND	ND	ND	ND	ND	ND	ND	ND										
12	G174	DNQ	DNQ	DNQ	ND	ND	DNQ	8.640	ND	ND	ND	ND	ND	ND	ND	ND	ND	ND	ND	ND	8.476	1.603	ND	2.201	1.820
12	G175	2.144	2.086	2.909	6.535	ND	3.630	DNQ	DNQ	ND	ND	ND	ND	ND	ND	ND	ND	ND	ND	ND	ND	ND	ND	ND	DNQ
12	G176	2.672	3.467	8.212	2.590	3.088	2.668	ND	3.779	8.017	4.259	3.825	DNQ	ND	2.421	DNQ	DNQ	2.162	1.951	1.627	3.270	ND	DNQ	ND	ND
14	G177	ND	ND	ND	ND	ND	ND	ND	ND	ND	ND	ND	ND	ND	ND										
14	G178	DNQ	DNQ	ND	2.516	4.135	8.662	7.165	ND	ND	ND	ND	ND	ND	ND	ND	ND	ND	ND	2.965	ND	DNQ	ND	DNQ	6.225
14	G179	ND	ND	ND	ND	ND	ND	ND	ND	ND	ND	ND	ND	ND	ND										
14	G180	ND	ND	ND	2.828	DNQ	ND	ND	ND	ND	ND	ND	ND	ND	ND	ND	ND	ND	ND	ND	2.563	2.573	3.533	8.338	ND

**Additional file 2.5:** Viral concentration by days post inoculation in sera.

Viral RNA concentration ( $\log_{10}$  /mg) in sera at each of five days post infection (gilts in rows, fetuses in columns). Similar to the umbilical cord, the first evidence of PRRSV infection is at 5 days post inoculation (DPI). Thereafter, the within litter infection rate increases and is greater than in umbilical cord. ND = not detected; DNQ = detectable, not quantifiable.



DPI	Gilt	L1	L2	L3	L4	L5	L6	L7	L8	L9	L10	L11	L12	R12	R11	R10	R9	R8	R7	R6	R5	R4	R3	R2	R1
2	G161	ND	ND	ND	-	-	-	-	-	-	-	-	-	ND	ND	ND	ND	ND							
2	G162	ND	ND	ND	ND	ND	-	-	-	-	-	-	-	-	-	-	-	-	-	-	ND	ND	ND	ND	ND
2	G163	ND	ND	ND	ND	-	-	-	-	-	-	-	-	ND	ND	ND	ND	ND							
2	G164	ND	ND	-	-	-	-	-	-	-	-	-	-	-	-	-	-	-	-	ND	ND	ND	ND	ND	
5	G165	ND	ND	ND	ND	ND	-	-	-	-	-	-	-	-	-	-	-	-	ND	ND	ND	ND	ND	ND	
5	G166	ND	ND	ND	ND	ND	ND	-	-	-	-	-	-	-	-	-	-	-	ND	ND	ND	ND	ND	ND	
5	G167	ND	-	-	-	-	-	-	-	-	-	-	ND	ND	ND	ND	ND	ND							
5	G168	ND	ND	-	-	-	-	-	-	-	-	-	ND	ND	ND	ND	ND	ND							
8	G169	ND	ND	ND	ND	ND	ND	-	-	-	-	-	-	-	-	-	-	-	ND	ND	ND	ND	ND	ND	
8	G170	ND	ND	ND	ND	6.067	ND	ND	-	-	-	-	-	-	-	-	-	ND	ND	ND	ND	ND	ND	DNQ	
8	G171	ND	ND	ND	ND	ND	-	-	-	-	-	-	-	-	-	-	-	-	ND	ND	ND	ND	ND	ND	
8	G172	5.147	7.015	ND	ND	ND	ND	ND	-	-	-	-	-	-	-	-	-	ND	ND	ND	ND	ND	ND	ND	
12	G173	ND	ND	ND	ND	-	-	-	-	-	-	-	ND	ND	ND	ND	ND	ND							
12	G174	ND	ND	ND	ND	ND	ND	7.424	-	-	-	-	-	-	-	-	-	-	-	6.229	ND	ND	ND	ND	
12	G175	ND	ND	ND	4.513	4.413	ND	ND	ND	-	-	-	-	-	-	-	-	-	ND	ND	ND	ND	ND	ND	
12	G176	ND	ND	5.295	ND	DNQ	ND	6.922	ND	6.648	ND	ND	ND	-	-	-	-	-	-	ND	ND	ND	ND	ND	
14	G177	ND	ND	ND	ND	ND	ND	-	-	-	-	-	-	-	-	-	-	-	ND	ND	ND	ND	ND	ND	
14	G178	ND	ND	5.853	ND	ND	6.315	6.420	-	-	-	-	-	-	-	-	-	-	-	ND	ND	ND	ND	4.298	
14	G179	ND	ND	ND	ND	ND	ND	-	-	-	-	-	-	-	-	-	-	-	-	ND	ND	ND	ND	ND	
14	G180	6.113	ND	ND	ND	ND	-	-	-	-	-	-	-	-	-	-	-	-	-	ND	ND	ND	ND	6.901	

**Additional file 2.6:** Viral concentration by days post inoculation in thymus.

Viral RNA concentration ( $\log_{10}$  /mg) in fetal thymus at each of five days post infection (gilts in rows, fetuses in columns). The first evidence of PRRSV infection is at 8 days post inoculation (DPI). Thereafter, fetal infection of thymus appears to be sporadic. ND = not detected; DNQ = detectable, not quantifiable.



DPI	Gilt	L1	L2	L3	L4	L5	L6	L7	L8	L9	L10	L11	L12	R12	R11	R10	R9	R8	R7	R6	R5	R4	R3	R2	R1
2	G161	ND	ND	ND	ND	-	-	-	-	-	-	-	-	ND	ND	ND	ND	ND							
2	G162	ND	ND	ND	ND	ND	-	-	-	-	-	-	-	-	-	-	-	-	-	-	ND	ND	ND	ND	ND
2	G163	ND	ND	ND	ND	-	-	-	-	-	-	-	-	ND	ND	ND	ND	ND							
2	G164	ND	ND	-	-	-	-	-	-	-	-	-	-	-	-	-	-	-	-	ND	ND	ND	ND	ND	
5	G165	ND	ND	ND	ND	ND	ND	-	-	-	-	-	-	-	-	-	-	-	ND	ND	ND	ND	ND	ND	
5	G166	ND	-	-	-	-	-	-	-	-	-	-	ND	ND	ND	ND	ND	ND							
5	G167	ND	-	-	-	-	-	-	-	-	-	-	ND	ND	ND	ND	ND	ND							
5	G168	ND	ND	-	-	-	-	-	-	-	-	-	ND	ND	ND	ND	ND	ND							
8	G169	ND	-	-	-	-	-	-	-	-	-	-	ND	ND	ND	ND	ND	ND							
8	G170	ND	ND	ND	ND	6.307	ND	ND	-	-	-	-	-	-	-	-	-	ND	ND	ND	ND	ND	ND	ND	
8	G171	ND	ND	ND	ND	ND	ND	-	-	-	-	-	-	-	-	-	-	-	-	ND	ND	ND	ND	ND	
8	G172	ND	ND	ND	ND	ND	ND	2.064	-	-	-	-	-	-	-	-	-	-	-	ND	ND	ND	ND	ND	
12	G173	ND	ND	ND	ND	-	-	-	-	-	-	-	ND	ND	ND	ND	ND	ND							
12	G174	ND	ND	ND	ND	ND	ND	4.403	-	-	-	-	-	-	-	-	-	-	-	5.323	ND	ND	ND	ND	
12	G175	ND	ND	ND	7.117	5.820	ND	ND	-	-	-	-	-	-	-	-	-	-	ND	DNQ	2.485	DNQ	ND	ND	
12	G176	ND	2.734	6.927	ND	ND	ND	1.969	ND	7.264	2.790	ND	ND	-	-	-	-	-	ND	ND	3.764	ND	ND	ND	
14	G177	ND	ND	ND	ND	ND	ND	-	-	-	-	-	-	-	-	-	-	-	ND	ND	ND	ND	ND	ND	
14	G178	ND	ND	6.571	ND	3.395	5.483	DNQ	-	-	-	-	-	-	-	-	-	-	ND	ND	3.502	ND	ND	5.738	
14	G179	ND	ND	ND	ND	ND	ND	-	-	-	-	-	-	-	-	-	-	-	-	ND	ND	ND	ND	ND	
14	G180	3.682	ND	ND	ND	DNQ	-	-	-	-	-	-	-	-	-	-	-	-	ND	ND	ND	ND	5.965	ND	

**Additional file 2.7:** Viral concentration by days post inoculation in amniotic fluid.

Viral RNA concentration (log10 /mg) in amniotic fluid at each of five days post infection (gilts in rows, fetuses in columns). The first evidence of PRRSV infection is at 8 days post inoculation (DPI). Thereafter, infection appears to be sporadic. ND = not detected; DNQ = detectable, not quantifiable.

### **3. Samples sizes required to accurately quantify viral load and histologic lesion severity at the maternal-fetal interface of PRRSV-inoculated pregnant gilts**

Whereas Chapter 2 served to determine a timeline of transplacental transmission and disease progression, Chapter 3 aims to investigate suitable methods for investigating the maternal-fetal interface (MFI). It concludes that at least three samples from endometrium and/or placental from PRRSV inoculated pregnant gilts should be collected for an accurate viral RNA concentration analysis, however, these multiple tissues from the same gilt can be homogenized prior to RT-qPCR investigation.

**Copyright:** This Chapter has been published. The copyright of this Chapter belong to the Journal of Veterinary Diagnostic Investigation (SAGE Publications).

**Citation:** Malgarin CM, Zarate JB, Novakovic P, Detmer SE, MacPhee DJ, Harding J. Samples sizes required to accurately quantify viral load and histologic lesion severity at the maternal-fetal interface of PRRSV-inoculated pregnant gilts. J Vet Diagn Invest, 2020. In press.

**Authors' contribution:** CMM: experimental design, sample collection, tissue viral RNA extraction, RT-qPCR analysis, statistical analysis, manuscript preparation; PN, JBZ: histopathologic evaluation, sample collection; SED, DJM, JH: experimental design, sample collection; JH: project and financial management, statistical analysis, manuscript preparation.

### 3.1. Abstract

Porcine reproductive and respiratory syndrome (PRRS) is transmitted vertically, causing fetal death in late gestation. Spatiotemporal distribution of virus at the maternal-fetal interface (MFI) is variable, and accurate assessment of viral concentration and lesions is thus subject to sampling error. Our objectives were: 1) to assess whether viral load and lesion severity in a single sample of endometrium (END) and placenta (PLC), collected near the base of the umbilical cord (the current standard), are representative of the entire organ; and 2) to compare sampling strategies and evaluate if spatial variation in viral load can be overcome by pooling of like-tissues. Spatially distinct pieces of END and PLC of 24 fetuses from PRRSV-2-infected dams were collected. PRRSV RNA quantified by RT-qPCR was compared in 5 individual pieces per fetus and in respective pools of tissue and extracted RNA. Three distinct pieces of MFI were assessed for histologic severity. Concordance correlation and kappa inter-rater agreement were used to characterize agreement among individual samples and pools. The viral load of individual samples and pools of END had greater concordance to a referent standard than did samples of PLC. Larger pool sizes had greater concordance than smaller pool sizes. Average viral load and lesion severity did not differ by location sampled and no technical advantages of pooling tissues versus RNA extracts were found. We conclude that multiple pieces of MFI tissues must be evaluated to accurately assess lesion severity and viral load. Three pieces per fetus provided a reasonable balance of cost and logistic feasibility.

**Key words:** concordance; endometrium; maternal-fetal interface; placenta; PRRSV; swine.

### 3.2. Introduction

Porcine reproductive and respiratory syndrome (PRRS) is an economically devastating disease affecting the pork industry.<sup>68</sup> Discovered in 1991, the causative viruses, PRRSV-1 and PRRSV-2, have worldwide distribution, but are separate species<sup>90</sup> with origins in the European Union and United States, respectively. A feature of the Arteriviridae family is its genome plasticity; there exist many different strains across a spectrum of virulence including a highly pathogenic lineage of PRRSV-2 that emerged with devastating effects in southeast Asia since the mid-2000s.<sup>91</sup> Neither species of virus is zoonotic nor infects other livestock or mammals. In naive infected pigs, disease is characterized by interstitial pneumonia accompanied by immune suppression in post-natal animals and reproductive losses (abortion, fetal death, congenital

infection, weak neonates, higher preweaning mortality) in pregnant animals infected during the third trimester.<sup>40</sup> The virus replicates in macrophages expressing the CD163 cell surface receptor,<sup>46</sup> and following infection of late-gestation females, viremia and endometritis rapidly develop whereas placentitis and placental detachment develop more slowly.<sup>53</sup> Although the mechanism of in-utero transmission is not understood completely, the virus crosses the placenta within a few days,<sup>72</sup> progressively infecting fetal placenta, umbilical cord, and the fetus.<sup>92</sup>

Swine have diffuse epitheliochorial placentation with each fetus compartmentalized in its own placental unit. The chorion and allantois fuse and vascularize in early gestation forming the chorioallantois (allantochorion); the tips of the elongated chorion that fail to fuse become necrotic.<sup>93</sup> The latter may be a mechanism by which PRRSV may transmit between fetuses.<sup>82</sup> The allantochorion superficially adheres to the endometrium and together forms an expansive network of interdigitating primary and secondary folds with underlying respective maternal and placental vasculatures.<sup>3</sup>

Not all fetuses within a given litter are equally susceptible to PRRSV, and infected viable, dead, and uninfected fetuses are known to co-exist in the same litter.<sup>49</sup> However, infection and fetal death cluster within a litter,<sup>37</sup> either by coincidence or possibly related to regional structural or physiologic features of the porcine maternal-fetal interface (MFI; defined as endometrium with adherent fetal allantochorion). The distribution of PRRSV particles<sup>46</sup> and endometrial lesions<sup>34</sup> [Novakovic, unpublished] vary within and between fetuses, posing challenges for diagnostic and research sampling protocols, particularly those requiring accurate quantification of viral load and lesion severity of the MFI.

Although viral RNA concentration in MFI and the severity of endometrial lesions<sup>45,53</sup> potentially contribute to fetal demise, there is no assessment to our knowledge showing that a single sample per fetus, either randomly or systematically collected, is representative of the entire MFI. Given the size of each placental unit and heterogeneity of fetal outcome following PRRSV infection, it is necessary to examine each fetus to assess viability, lesion severity, and viral load. With litter sizes averaging ~15 total born in contemporary sows, sample numbers can quickly become overwhelming in a large experiment, therefore judicious and efficacious sampling is required. Sampling a single site or tissue per fetus is practical and efficient at the time of collection and also requires fewer resources during the laboratory analyses, but, if accuracy is paramount, it is important to determine the optimal number of tissue pieces per fetus

that should be assessed. Our objectives were to determine: 1) optimal sample numbers required to accurately quantify PRRSV RNA concentration and histologic lesion severity across the entire endometrial and placental surface per fetus; 2) if viral load and lesion severity differ by location of MFI sampled; and 3) if pooling of collected MFI tissues or RNA extracts prior to RT-qPCR testing improves the accuracy of quantification compared to testing multiple tissue pieces individually.

### **3.3. Materials and methods**

#### *3.3.1. Animal experiment and sample collection*

We used tissues collected from a previously described PRRSV challenge experiment,<sup>53,72,92</sup> adhering to principles established by the Canadian Council on Animal Care and approved by the Animal Research Ethics Board at the University of Saskatchewan (Certification 20160023). Briefly, 15 purebred Landrace gilts from a PRRSV-naive farm were experimentally inoculated intranasally and intramuscularly (total dose  $1 \times 10^5$  TCID<sub>50</sub>) with PRRSV-2 strain NVSL 97-7895 at  $86 \pm 0.4$  days of gestation. Five control gilts were mock-inoculated. On each of 5 post-inoculation days (2, 5, 8, 12, and 14 dpi), 1 control and 3 PRRSV-inoculated gilts were euthanized using barbiturate overdose followed by cranial captive bolt stunning and exsanguination. Fetuses were removed from the gravid reproductive tract and their placement in the left or right uterine horn recorded. The preservation status of each fetus was assessed as viable, meconium-stained, or decomposed, according to pre-established guidelines.<sup>49</sup> The respective proportion of MFI supporting each fetus was removed while maintaining its identity with the fetus. We used tissues from 4-6 randomly selected fetuses per litter that had been subjected to more intensive sampling. From each of these intensively sampled fetuses, 3 spatially distinct pieces (Pc 1-3) of MFI tissue were collected into 10% neutral-buffered formalin, then processed routinely for hematoxylin and eosin stained tissue sections. Five unique pieces (Pc 1-5) were collected for quantification of viral load by RT-qPCR (Additional file 8).

#### *3.3.2. PRRSV RNA extraction and sample pooling*

After manually separating the placenta (PLC) from endometrium (END), the PRRSV RNA concentration was quantified in both tissues as described previously, using an in-house

probe-based assay specifically designed for the inoculum strain, NVSL 97-7895.<sup>92</sup> As a preliminary step, the central MFI piece adjacent to the umbilical stump (Pc1) was tested for all intensively sampled fetuses (n = 68) across 15 PRRSV-infected litters. These results were used to select a subset of 24 fetuses (11 female, 13 male) in which viral load was assessed in all 5 pieces of END and PLC (240 pieces in total). These intensively sampled fetuses were categorized into 3 groups (8 per group) based on their fetal preservation score and RNA concentration of Pc1: a) meconium-stained or decomposed fetuses, b) viable fetuses with consistent viral load in PLC and END, and c) viable fetuses with inconsistent viral load in PLC and END. In this context, “consistent” referred to fetuses in which the viral loads in END and PLC were similar (i.e., both had high or low viral load), whereas “inconsistent” referred to fetuses in which the viral load differed between these 2 tissues (i.e., one had high VL and the other had low VL). The purpose of categorizing fetuses was to ensure that the subset was representative of the entire fetal population. High viral load was considered as  $\geq 4 \log_{10}$  viral particles/mg of tissue, and low viral load was  $< 4 \log_{10}$ .

Individual pieces of END and PLC (30 mg) were homogenized by shaking with lysis buffer in a vial containing a steel ball (30 Hz for 4 min). Thereafter, 600  $\mu\text{L}$  of each homogenate was robotically extracted using a commercial kit as per the manufacturer’s instructions (RNeasy MiniKit; Qiagen).

Two pools of pieces were also generated. A “tissue pool” was made by combining 120  $\mu\text{L}$  of each END or PLC homogenate from the 5 individual pieces per fetus into a 600  $\mu\text{L}$  pool that was thoroughly mixed and extracted as described above. A “RNA pool” was made by combining 5  $\mu\text{L}$  of extracted RNA from each of the 5 individually extracted pieces per fetus. These were thoroughly mixed and the PRRSV RNA quantified using RT-qPCR. RNA concentration and purity (A260/A280 ratio  $\geq 2$ ) were assessed using 2  $\mu\text{L}$  of the sample by spectrophotometry (NanoDrop spectrophotometer; Thermo Fisher Scientific).

### 3.3.3. *Quantitative PCR*

We used a probe-based PCR protocol specific to PRRSV strain NVSL 97-7895 that amplified a highly conserved region of ORF7. The PCR primers and protocol has been described in detail previously.<sup>49</sup> Briefly, plasmid HindIII pCR2.1TOPO-NVSL containing a 446-bp sequence of ORF7 was used for the 5-point standard curve ( $10^7$ ,  $10^5$ ,  $10^3$ ,  $10^2$ ,  $10^1$ ) run in

triplicate on each plate. Samples were run in duplicate on 96-well plates (35 samples/plate) that also contained appropriate no template, positive control (pool of PRRSV-positive tissues), and RT-qPCR controls. A statistical process control (SPC) chart was used to monitor the positive control sample across plates. Individual samples were re-run if the C<sub>q</sub> standard deviation between the duplicates was >1.5 or if 1 of the 2 duplicates had no Ct. Negative results were re-run to confirm the absence of viral RNA. Results were reported as log<sub>10</sub> target RNA concentration per mg of tissue. The limits of quantification were defined by the least and most concentrated standards. Samples were recorded as negative if target RNA was not detected, or DNQ (detected, but not quantifiable) if target RNA was detected but the concentration was below the least concentrated standard.

#### 3.3.4. *Histopathology*

Lesions were assessed in each of 3 pieces of MFI (Additional file 3.1) collected from 87 intensively sampled fetuses (42 female, 45 male) independently by 2 pathologists (P Novakovic, J Zarate) blinded to group identity, fetal preservation status, and times of infection. Eight-mm long tissue cross sections were cut to fit inside a standard 4-well tissue cassette in the same order each time. Both PRRSV-infected and control litters were included (range 3-6 per litter). A score was generated for characteristic lesions produced by PRRSV, specifically endometritis, placentitis, endometrial vasculitis, and placental detachments, as described in detail previously.<sup>39,53</sup> The lymphocytic-to-lymphohistiocytic inflammatory cell infiltrate in endometrium and placenta was predominantly composed of lymphocytes admixed with small numbers of histiocytes and rare plasma cells. This infiltrate was scored: normal (0) no inflammatory cell infiltrate, minimal (1) <10% of section contains inflammatory cell infiltrate, mild (2) 10%–25% of tissue contains inflammatory cell infiltrate, moderate (3) 25%–50% of section contains inflammatory cell infiltrate, and severe (4) >50% of section contains inflammatory cell infiltrate. Vasculitis, with and without perivasculitis, was defined by the presence of ≥3 inflammatory cells within these locations. Accompanying changes of edema, vascular or endothelial degeneration, and vacuolation were very slight in most cases and not considered. The distribution of vasculitis was evaluated separately in the endometrium and fetal placenta as: normal (0) no blood vessels inflamed, focal (1) <30% of blood vessels inflamed, multifocal (2) 30–70% of blood vessels inflamed, or diffuse (3) >70% of blood vessels inflamed.

The severity of placenta detachment was scored: normal (0) no detachment of placenta along the interdigitation area, mild (1) <25% of interdigitation area was detached, moderate (2) 25%–50% of interdigitation area was detached, and severe (3) >50% of interdigitation area was detached.

### 3.3.5. *Data analysis*

PRRSV RNA quantification: To determine the optimal number of pieces per fetus needed to accurately quantify viral load in END and PLC (analyzed separately), the average of the 5 individual pieces per fetus was used as the referent quantification (gold standard for this experiment) to which the viral load of individual and pooled pieces were compared. Pooled samples included the RNA and homogenized tissue pools described above as well as the viral load of virtual pools of 2, 3, and 4 individual pieces created in silico by averaging the viral load of the pairwise combinations of 5 individual pieces. Twenty-four virtual pools were created: 10 virtual pools of 2 pieces (Pc 1+2, 1+3, 1+4...4+5), 6 virtual pools of 3 (1+2+3, 1+2+4, 1+2+5...3+4+5), and 5 virtual pools of 4 pieces (1+2+3+4, 1+2+3+5...2+3+4+5). Lin concordance coefficients (rc) were calculated to compare the level of agreement in viral RNA concentration between individual pieces and pools to the referent sample, with higher values reflecting a stronger association between the pool and gold standard. A Dunn test was used to compare viral load across the 5 sampling locations. To compare variation in viral load across the 5 sampling locations, a Levene robust test was used.

PRRSV histologic lesion scores: Average lesion scores were compared between PRRSV-inoculated and control groups using a Mann-Whitney U test. To evaluate the level of agreement in lesion scores across the 3 pieces (PLC and END evaluated separately) and between the pathologists, a kappa statistic of inter-rater agreement was calculated. Qualitative terminology describing the level of agreement was defined<sup>94</sup>: fair ( $\kappa = 0.21-0.4$ ), moderate ( $\kappa = 0.41-0.6$ ), substantial ( $\kappa = 0.61-0.8$ ), almost perfect ( $\kappa = 0.81-1.0$ ). To determine the number of pieces required to accurately assess lesion severity, Lin concordance coefficients (rc) were calculated to assess agreement between individual pieces (2 pathologists each scoring 3 pieces) to the referent sample (average score of all 3 tissue pieces) for each PRRSV-related lesion. Pairwise combinations of pieces, representative of 1 pathologist scoring 2 or 3 pieces, and 2 pathologists scoring 1 or 2 pieces, were also assessed. Accuracy and precision were calculated using the bias-correction factor (C\_b) and Pearson correlation coefficient (r), respectively.<sup>95</sup> A Dunn test was

used to determine if lesion scores differed by the location in the MFI. All statistical analyses were performed with Stata v.15.

### 3.4. Results

#### 3.4.1. *PRRSV RNA quantification*

Median RNA concentrations for the individual pieces across the 5 locations were 5.1 (range 0.0-7.9) and 2.2 (0.0-10.3) log<sub>10</sub> target copies per mg for END and PLC, respectively. PRRSV RNA was not detected in 22 of 120 (18%) and 34 of 120 (28%) individual pieces of END and PLC, respectively. Median viral load and within-location variation in viral load did not differ by sampling location in either END and PLC (Additional file 3.2) suggesting that multiple pieces collected randomly or systematically would yield similar results.

For END and PLC, the viral load estimates for the virtual pools of all sizes were equivalent to the estimate for the 5 pieces tested individually (**Table 3.1**). The viral load estimates of larger pools had greater concordance with the viral load estimates of individual pieces than did smaller pools, with the most dramatic gains in concordance noted when 2 or more pieces of endometrium, or 3 or more placental pieces were pooled for a single PCR test (**Table 3.1, Figure 3.1**). Virtual pools of 4 pieces had near perfect agreement to the individual pieces, indicating no advantage of collecting more than 4 pieces per fetus for assessment of viral load. Concordance coefficients were greater for virtual pools of endometrium than virtual pools of placenta, particularly in smaller pool sizes, indicating greater heterogeneity of virus distribution in the placenta.

**Table 3-1:** PRRSV RNA concentration, coefficients of variation, and levels of agreement for endometrial and placental samples and pools.

		Single pieces	Virtual pools of 2	Virtual pools of 3	Virtual pools of 4	Virtual pools of 5	Pool of extracted RNA	Pool of homogenized tissues
Viral load* (mean)	<i>Endometrium</i>	6.37	6.37	6.38	6.37	6.37	6.29	6.54
Viral load* (median)		5.10	5.26	5.28	5.31	5.33	5.39	5.49
Viral load (CV%)		108.5	107.1	106.5	106.1	106.0	105.2	106.3
$r_c$ median		0.68	0.83	0.89	0.99	1.00	0.81	0.88
Precision		0.78	0.88	0.93	0.96	1.00	0.85	0.90
Accuracy		0.86	0.95	0.98	0.99	1.00	0.94	0.98
Viral load* (mean)	<i>Placenta</i>	8.25	8.27	8.23	8.27	8.27	6.19	6.43
Viral load* (median)		2.16	2.37	2.49	2.66	4.8	2.59	2.59
Viral load (CV%)		112.3	110.4	109.5	108.5	128.2	108.1	107.4
$r_c$ median		0.44	0.62	0.88	0.97	1.00	0.67	0.62

Precision	0.62	0.73	0.82	0.92	1.00	0.70	0.64
Accuracy	0.83	0.92	0.96	0.99	1.00	0.96	0.97

---

\*log<sub>10</sub> copies PRRSV RNA per mg tissue. r<sub>c</sub> = Lin robust concordance coefficient; product of r \* c<sub>b</sub>. Precision = Pearson correlation coefficient (r). Accuracy = bias correction factor (c<sub>b</sub>).

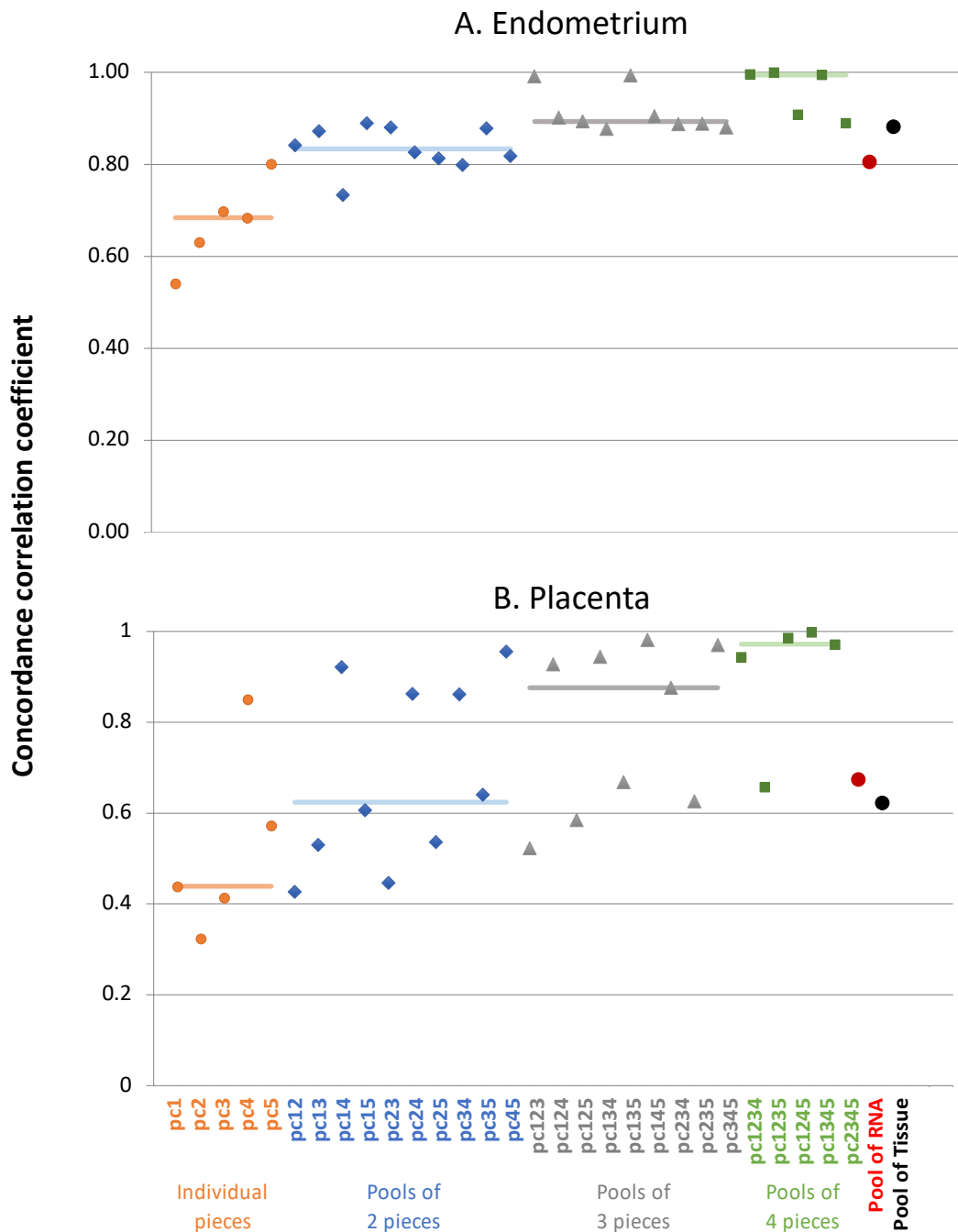


**Figure 3.1:** Viral load concordance.

Dot plot depicting the level of agreement (Y axis, Lin concordance correlation) in viral RNA concentration among individual pieces and pools (X axis, color-coded by pool size and type) to a referent standard for endometrium (A) and placenta (B). Horizontal lines represent the median concordance correlation coefficient value for that group of samples, with larger pool sizes showing greater agreement.

For endometrium, the mean viral load estimates of the tissue homogenate and RNA pools were within 0.25 log<sub>10</sub>/mg of the individual pieces and virtual pool averages. By contrast, the viral load estimates of the placental pools of homogenized tissues and RNA were ~2 log<sub>10</sub>/mg lower than the individual pieces and virtual pools (**Table 3.1**). Pooling homogenized endometrium had higher concordance than pooling the extracted RNA, but the opposite trend was evident for placenta (**Figure 3.1**). This suggests that there is no clear benefit to pooling either before or after extraction for MFI tissues. Expectedly, both the tissue homogenate and RNA pools had lower concordance with individual pieces than did the virtual pools. This is explained by the virtual pools being created in silico by averaging different combinations of the pieces tested individually, whereas the tissue and RNA pools were created by resampling the tissue pieces collected at post-mortem examination and therefore were different technical replicates.

Accuracy and precision were greater in END than PLC, and both increased with virtual pool size. Across all pool sizes, viral load estimates had greater accuracy than precision, although the gap between the 2 measures narrowed as virtual pool size increased. This result also suggests that viral load is heterogeneous in the MFI, especially in placenta.

#### 3.4.2. *Histopathology*

The severity of endometritis and placentitis was greater in PRRSV-infected compared to control fetuses (**Table 3.2**). Endometrial vasculitis was only present in PRRSV-infected samples, except for one control with a focal lesion. Vasculitis was not observed in placentas of either group. Mild placental detachments were observed in roughly one-third of fetuses (24 of 62 for control; 72 of 223 for PRRSV-infected) but median scores did not differ between PRRSV-infected and the non-infected group. However, pregnancies were terminated 2-14 dpi in our experiment, likely too early for placental detachment to occur in infected fetuses.

**Table 3-2:** Distribution of histologic lesion scores in endometrium and placenta in tissues used to assess inter-rater agreement.

	Distribution of lesion scores (number (%) of total cases)*					Group averages†			
						Median score (IQR) Control (n=62-63)	Median score (IQR) PRRSV (n=198-209)	Accuracy (C_b)	Precision (r)
	0	1	2	3	4				
Endometritis (n = 293)	<i>Normal</i> 38 (13%)	<i>Minimal</i> 93 (32%)	<i>Mild</i> 50 (17%)	<i>Moderate</i> 49 (17%)	<i>Severe</i> 63 (22%)	0.7 (0.4) <sup>a</sup>	2.7 (2.4) <sup>b</sup>	0.999 (0.002)	0.978 (0.019)
Placentitis (n = 279)	139 (50%)	123 (44%)	15 (5%)	2 (0.7%)	0 (0%)	0.3 (0.3) <sup>a</sup>	0.7 (0.7) <sup>b</sup>	0.966 (0.036)	0.819 (0.113)
Endometrial vasculitis distribution (n = 275)	<i>None</i> 138 (50%)	<i>Focal</i> 29 (10%)	<i>Multifocal</i> 53 (19%)	<i>Diffuse</i> 55 (20%)	-	0.0 (0.0) <sup>a</sup>	1.7 (2.3) <sup>b</sup>	0.998 (0.003)	0.969 (0.025)
Placental detachment (n = 285)	<i>None</i> 189 (66%)	<i>Mild</i> 96 (34%)	<i>Moderate</i> 0 (0%)	<i>Severe</i> 0 (0%)	-	0.0 (0.0)	0.0 (0.0)	0.943 (0.060)	0.784 (0.137)

\*Refer to Methods for full description of lesions. † superscripts (a, b) signify statistically significant differences in average lesion scores within row (Mann Whitney U test;  $P < 0.05$ )

The distribution of lesion scores at the umbilical stump (Pc 1, **Table 3.2**) helps to provide some context for interpreting the inter-rater agreement among the 3 pieces of MFI assessed for each fetus. Lesion severity did not significantly differ among the 3 locations sampled. Lesion scores were not equally distributed across all severity scores (0 to 4), thus the kappa values presented below should be interpreted cautiously. There was substantial agreement ( $\kappa = 0.61-0.8$ ) between the 2 pathologists for all lesion types (**Table 3.3**). There was lower agreement ( $\kappa < 0.50$ ) with respect to the lesion scores each pathologist assigned across location within the same fetus (**Table 3.4**). For endometritis and vasculitis distribution, the lesion scores of unaffected (score 0) and severely affected (scores 3-4) pieces were in moderate agreement, whereas lesion scores of the mildly and moderately (scores 1-2) affected pieces were in fair agreement. This result suggests that both pathologists were more consistent at scoring the extremes (normal, severe), or that endometrial lesion severity is heterogeneous across the MFI. For placental lesions (inflammation, detachment) there was poor-to-slight agreement in the pathologists' lesion scores across location, likely associated with great heterogeneity across the placenta.

**Table 3-3:** Levels of agreement in lesion severity scores between pathologists as determined by the kappa inter-rater statistic.

<b>Pairs of pieces</b>	<b>Pc 1+4</b>	<b>Pc 2+5</b>	<b>Pc 3+6</b>	<b><i>P</i>-value</b>
Endometritis	0.70	0.82	0.69	<0.001
Endometrial vasculitis	0.63	0.81	0.78	<0.001
Placentitis	0.64	0.59	0.68	<0.001
Placental detachment	0.77	0.77	0.66	<0.001

Two

pathologists scored the same 3 pieces of H&E-stained maternal-fetal interface for each fetus. Pathologist 1 scores are represented by pieces (Pc) 1-3. Pathologist 2 scores are represented by Pc 4-6. Kappa values for the same tissue piece assessed independently by both pathologists are in columns Pc 1+4, Pc 2+5, and Pc 3+6.

**Table 3-4:** Levels of agreement in lesion severity scores within pathologists as determined by the kappa inter-rater statistic.

<b>Pathologist 1</b>	<b>Lesion scores</b>					<b>All</b>	<b>P-value</b>
	<b>0</b>	<b>1</b>	<b>2</b>	<b>3</b>	<b>4</b>		
Endometritis	0.53	0.33	0.40	0.24	0.53	0.40	<0.001
Endometrial vasculitis	0.72	0.20	0.30	0.51	.	0.48	<0.001
Placentitis	0.25	0.15	0.0	.	.	0.19	0.001
Placental detachment	0.01	0.0	0.0	0.32	.	0.00	ns
<b>Pathologist 2</b>							
Endometritis	0.51	0.51	0.34	0.23	0.53	0.44	<0.001
Endometrial vasculitis	0.78	0.05	0.31	0.48	.	0.50	<0.001
Placentitis	0.18	0.05	0.14	0.0	.	0.11	0.023
Placental detachment	0.02	0.03	0.0	.	.	0.03	ns

Each of 3 pieces of maternal fetal interface were scored using ordinal scales by 2 pathologists blinded to group identity. Kappa values represent the level of agreement for each individual score (0-4) and overall scores (All). ns = not significant.

Regarding the optimal number of pieces and pathologists required to accurately assess lesion severity, the endometrial lesion scores of all individual pieces and pairwise combinations had high concordance with the referent sample (average lesion scores of 3 pieces by 2 pathologists, **Figure 3.2A-B**) and were both highly accurate and precise (**Table 3.2**). By contrast, placental lesion scores had lower concordance than endometrial lesions overall and improved when more pieces and pathologists were included (**Figure 3.3A-B**). Lesion scores were reasonably accurate but much less precise (**Table 3.2**). Interestingly, the evaluation of 3 pieces by either pathologist had superior concordance than if either pathologist evaluated 2 pieces. These results indicate that accurate assessment of placental lesions requires multiple pieces from multiple locations (the more the better, dependent on feasibility) but there is no measurable advantage of assessment by multiple pathologists.

Unlike placenta, the assessment of a single piece of endometrium, however, is sufficient to accurately assess the severity of endometritis and vasculitis distribution. This was likely the result of the diffuseness of the endometrial lesions compared to the heterogeneity and lower occurrence of placental lesions.

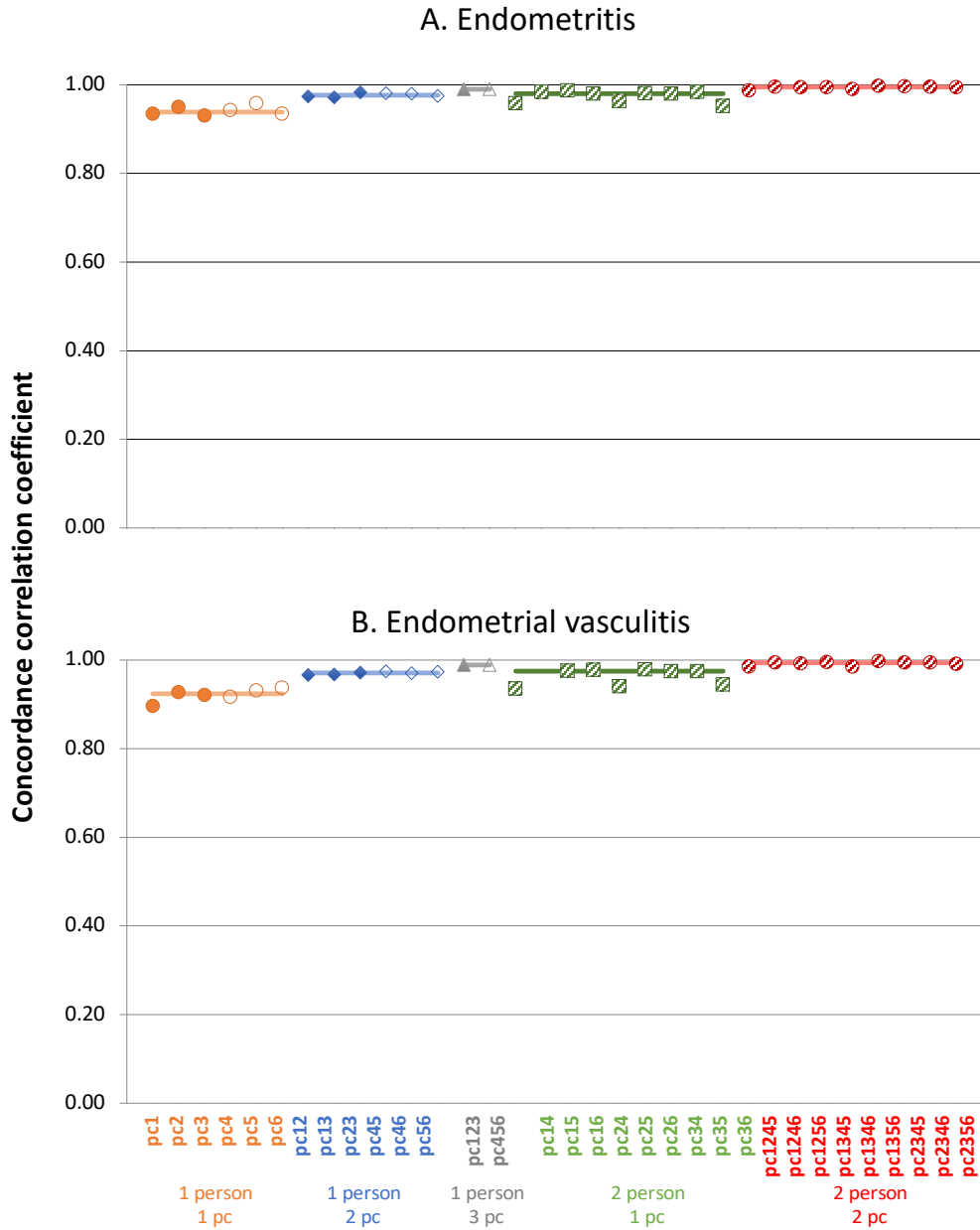


**Figure 3.2:** Endometrial lesion concordance.

Dot plot depicting the level of agreement (Y axis, Lin concordance correlation) in ordinal lesion scores among individual pieces and their pairwise combinations (X axis, color-coded by number of pieces examined and pathologists involved) to the referent standard for endometritis (A) and endometrial vasculitis distribution (B). The combinations of pieces and pathologists (X axis) were selected to mimic 1 or 2 pathologists requested to evaluate 1, 2, or 3 pieces each. Horizontal lines represent the median concordance correlation coefficient value for that group of

samples. Pieces 1-3 (solid markers) and 4-6 (open markers) were assessed by pathologist 1 and 2, respectively. Hatched markers represent combinations of pieces assessed by both pathologists. Endometrial lesion scores have high accuracy and precision regardless of the number of pieces and pathologists involved.

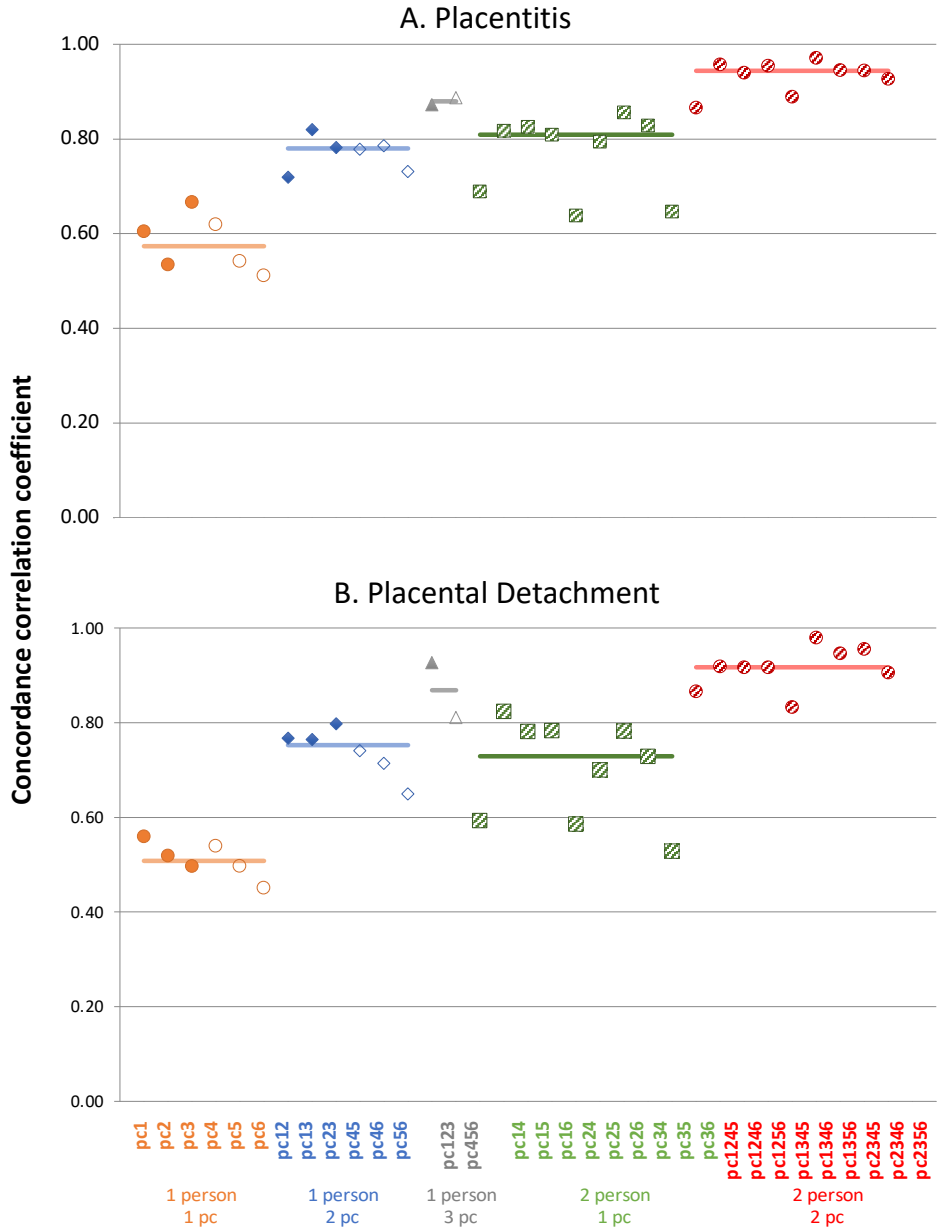


**Figure 3.3:** Placental lesion concordance.

Dot plot depicting the level of agreement (Y axis, Lin concordance correlation) in ordinal lesion scores among individual pieces and their pairwise combinations (X axis, color-coded by number of pieces examined and pathologists involved) to the referent standard for placentitis (A) and placental detachment (B). The combinations of pieces and pathologists (X axis) were selected to mimic 1 or 2 pathologists requested to evaluate 1, 2, or 3 pieces each.

Horizontal lines represent the median concordance correlation coefficient value for that group of samples. Pieces 1-3 (solid markers) and 4-6 (open markers) were assessed by pathologist 1 and

2, respectively. Hatched markers represent combinations of pieces assessed by both pathologists. Placental lesion scores have reasonably high accuracy but low precision.

### 3.5. Discussion

Contemporary sows are highly prolific, bearing litter sizes averaging  $\sim 14.9 (\pm 1.0)$  piglets, and the top 10% of farms averaged  $>16$  piglets per litter in North America in 2019.<sup>96</sup> Thus, diseases such as PRRS that can drastically reduce litter sizes can be financially devastating. It is estimated that pigs on  $\sim 45\text{-}70\%$  of US farms are infected with PRRSV<sup>97</sup>, with  $\sim 20\text{-}25\%$  of farms classified as positive “unstable”,<sup>98</sup> characterized by active circulation and shedding of PRRSV within the population of breeding females.<sup>68</sup> PRRSV is one of several causes of reproductive failure in swine, and diagnosis in individual animals, for instance following abortion, can be challenging, particularly in farms where the virus is known to pre-exist. Examination of the reproductive tract in cases of reproductive failure, including placentae and conceptae, may provide useful information regarding underlying causes of late-gestation reproductive failure, however with PRRS, lesions in fetuses are sparse<sup>34,39</sup> and not all fetuses within the litter are infected with virus.<sup>46,49</sup>

PRRSV-induced lymphohistiocytic endometritis is highly prevalent and develops rapidly following infection, but the severity of inflammatory infiltrate and vasculitis varies widely across the entire MFI.<sup>39,53</sup> However,  $\sim 20\%$  of endometrial samples may test negative for PRRSV RNA 2-3 wk post inoculation.<sup>49,92</sup> In a diagnostic setting, placenta is the only available sample, unless the sow is submitted with fetuses still in-utero. Therefore testing at least 3-5, randomly located pieces of placenta is likely sufficient for diagnosis. In a research setting in which accurate quantification of lesion severity and viral load at the MFI is required, it is relevant to understand how many pieces of MFI per fetus are required knowing that costs can increase substantially with increasing litter size. In our past research, a single piece of MFI collected adjacent to the umbilical stump of each fetus was collected and tested given the large number of animals ( $n = 1,400$ ) included in the evaluation.<sup>36</sup> Although this approach may be appropriate for large-scale screening, our present results indicate that when feasible, additional samples should be collected to improve accuracy and precision, but the number of pieces remains unclear.

Lin concordance correlation is a combined measure of the accuracy and precision of data to a referent standard.<sup>95</sup> Accuracy refers to how close estimates are to the true value, whereas precision refers to how close estimates are to each other regardless of how close they are to the true value. Although the concordance correlation is the most appropriate test for the present research, relevant questions including “what is an appropriate reference standard” and “what is a

sufficient correlation” are outstanding. Without a pre-existing gold standard (for viral load and lesion severity across tissue), the “average of all” was chosen as the best option.

Although greater concordance coefficient values are preferred, the optimum or target value largely depends on the research question, resources available to the project, and accuracy and precision required. Although arbitrary, our conclusions are based on our desire to achieve a concordance correlation  $\geq 0.90$ , with roughly equal measures of precision and accuracy. Our finding of greater accuracy and precision in larger pool sizes was expected. The fact that accuracy was greater than precision in both endometrium and placenta is indicative of the heterogeneity in viral load throughout the MFI, and supports the need for examining multiple pieces. In the absence of locational bias, the samples collected could be systematically or randomly collected if the selected number are representative of the entire organ.

Samples were collected at different days post infection (2, 5, 8, 12, and 14 dpi), and some of the variability might be the result of differences in viral load at these times. As the infection progresses and the virus establishes its presence in the host, viral load increases on average but also becomes more heterogeneous within an animal. Unfortunately, the number of fetuses we included at each time was not balanced and was too small to accurately characterize changes in viral load heterogeneity by day. The exact day of infection is rarely known in diagnostic cases, but is likely to be  $>7$  dpi, after clinical signs, fetal compromise, or abortion are first observed. This implies that diagnosticians should anticipate great viral load heterogeneity in diagnostic cases and err on the side of caution by collecting more, rather than fewer, samples of placenta or endometrium, then pool within an animal.

Although PRRSV infection clusters in litters, the clustering is unpredictable, and the heterogeneity of the placental viral load and lesions adds additional factors to consider. It is essential to sample as many fetuses as is practical to fully understand the impact of PRRSV across the entire litter. This is particularly important when examining placentae, because the placenta is more heterogeneous in terms of viral load and lesion severity than the maternal uterine layers, based on the results of our research. In terms of pathology assessments, the number of pathologists recruited is less important than the number of pieces examined per fetus. Our results indicate good agreement in semi-subjective lesion scores between 2 pathologists with reasonable expertise in examining PRRSV-affected reproductive tissues. As our results indicate, at least 3 pieces of placenta would be necessary for an accurate assessment of placental lesions

by 1 pathologist. If a pathologist lacks expertise or in cases in which a robust scoring methodology is unavailable, inter-pathologist agreement may be lower.

If it is necessary to collect multiple samples from all or many fetuses, the task of accurately assessing viral load and/or lesion severity quickly becomes unfeasible on a large scale. Thus, pooling becomes a necessity. Although there is no alternative but to evaluate pieces individually for histopathology, pooling of tissues is an alternative for assessment of viral load by RT-qPCR. Although the simplest way of pooling is to combine and homogenize small portions of tissue, this technique is prone to quantification error because the portions will invariably differ in weight and the viral load estimate will be biased towards the viral load of the largest pieces. We evaluated 2 methods of pooling for viral load quantification in our study. The most cost-effective method was by combining equal volumes of homogenized tissue, each with a roughly equivalent starting weight. The alternative, pooling of tissue pieces after extraction, was costlier in terms of reagent costs and time. Given that neither method provided contingently superior results, pooling of tissue homogenates is the logical recommendation.

The fetal placenta used for our study originated from dams 2-14 dpi and encompassed a wide range of viral load as well as PRRSV-negative samples. Although the heterogeneity of samples used may be perceived as a limitation, we believe this is reflective of the range of caseload a diagnostic laboratory may experience, which supports the external validity of our results.

The optimal number of samples to pool ultimately depends on the tissue, level of accuracy and precision required, and any logistical limitations associated with the task. Fewer pieces of endometrium are required compared to placenta for assessment of viral load and lesion severity, however, in smaller pools, individual outliers have greater impact. For our subsequent research, we chose tissue homogenates of 3 pieces as a reasonable balance of cost, feasibility, accuracy, and precision. With this strategy, the anticipated concordance correlation will be close to our target of 0.90. Although larger pools would have provided concordance  $>0.9$ , larger pools would only provide a practical benefit for placentae in terms of precision while adding substantially to the laboratory cost and workload. In spite of these results, past studies in which single pieces of tissue were assessed remain valid, but should be interpreted with some caution. Overall, our results offer insights on sampling techniques for future research projects and

diagnostic investigations related to PRRSV and possibly other transplacental reproductive viruses.

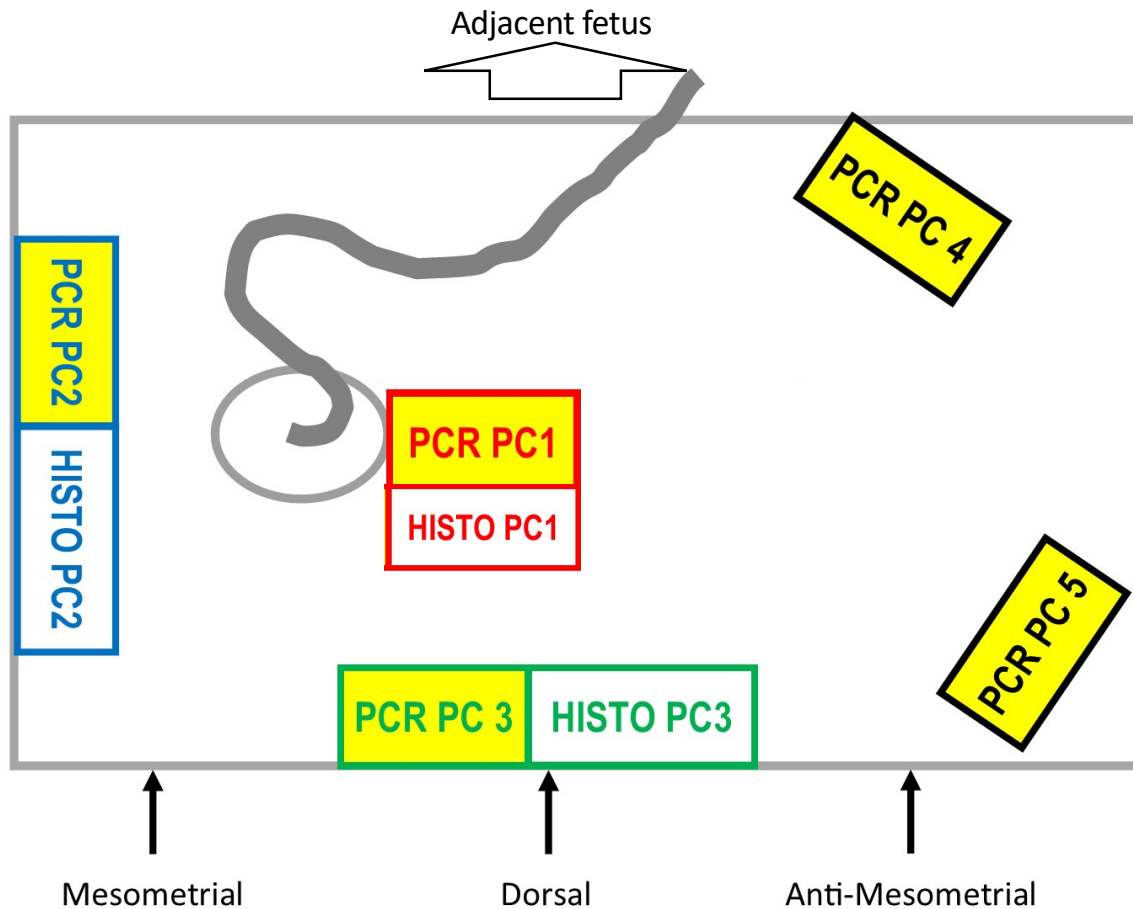
### **Declarations**

**Acknowledgments:** We thank the large number of technicians and students who assisted with the animal experiment enabling this research.

**Declaration of conflicting interests:** The authors declared no potential conflicts of interest with respect to the research, authorship, and/or publication of this article.

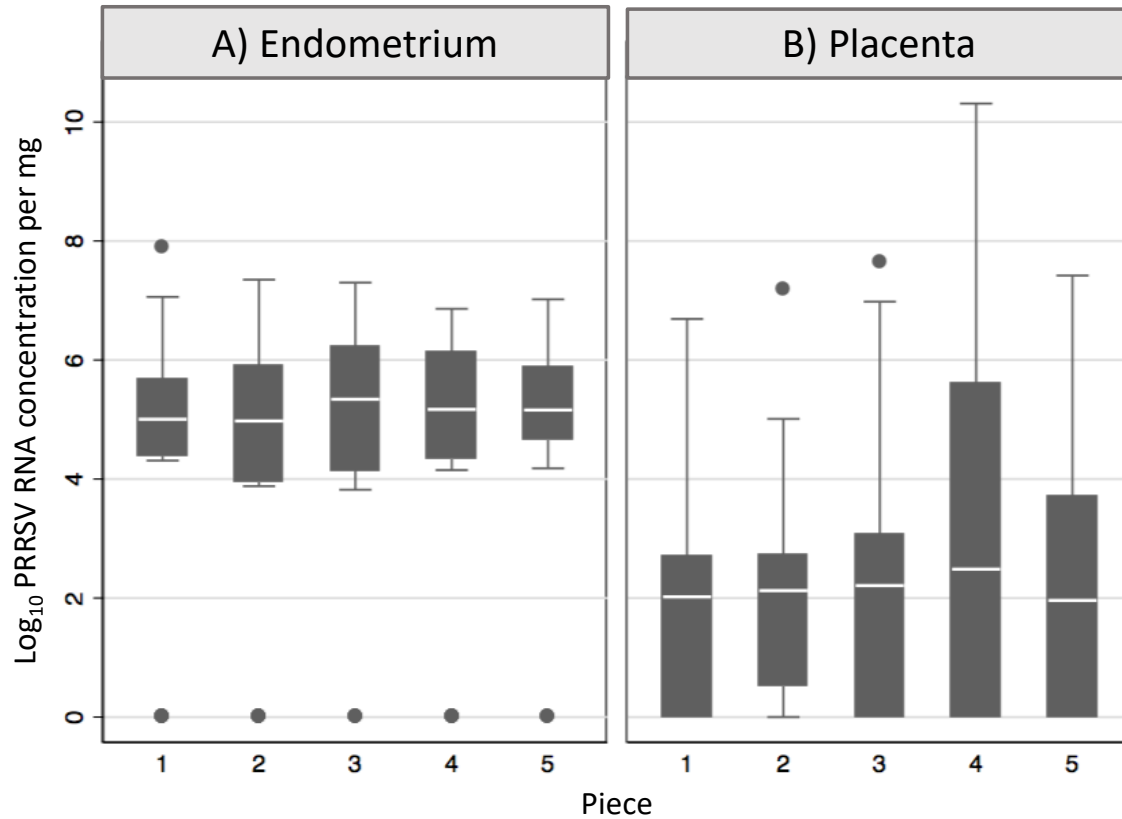
**Funding:** This project was supported by grants from Genome Canada (2014LSARP\_8202) and Genome Prairie (Saskatchewan Ministry of Agriculture 20150329) and administrative support from Genome Alberta and a Canada Foundation for Innovation John R. Evans Leaders Fund (Project 32512). The sponsors had no role in study design, execution, analysis, or interpretation of the results.

### **Additional files**



**Additional file 3.1:** Visual rendition of the maternal-fetal interface (MFI) of a single fetus showing locations of pieces collected for assessment of viral load (PCR Pc 1-5) and severity of endometrial and placental lesions (Histo Pc 1-3) following PRRSV-infection.

The umbilical cord and stump are depicted by the grey curved line and circle, respectively, and can be anywhere on the MFI but typically near the mesometrium. Pieces: 1 (red) immediately surrounding the umbilical attachment; 2 (blue) 10-15 cm from piece 1 and towards the anti-mesometrial side; 3 (green) 10-15 cm from piece 1 toward the ovary; 4 and 5 (black) anti-mesometrial side at corners of MFI; (yellow) PCR pieces were collected at least 10 cm apart; (white) histology pieces were adjacent to the PCR pieces.



**Additional file 3.2:** Box plot of PRRSV concentration of the 5 individual pieces of endometrium (A) and placenta (B) used to generate the virtual pools in silico and the pool of RNA and tissue homogenate.

Boxes represent the middle 50% of data, horizontal line is the median, vertical lines are defined by the upper adjacent value (largest observation that is  $\leq$  third quartile plus 1.5 times interquartile range (IQR) or  $\geq$  first quartile plus  $1.5 \times$  IQR). Dots are outside values that fall between  $\pm 1.5 \times$  IQR and  $\pm 3 \times$  IQR.

#### **4. Fetal metabolomic alterations following porcine reproductive and respiratory syndrome virus infection**

It has been previously observed that lesions and disruptions in the MFI following PRRSV infection are not sufficient by themselves to cause fetal death. Thus, a more fetal focused approach was adopted. This fourth chapter investigated differences in the metabolomic profile among PRRSV-infected and non-infected fetuses, as well as normally developed and intrauterine growth retarded (IUGR) fetuses. Significant differences were observed, helping to elucidate mechanisms involved in fetal compromise and death.

**Copyright:** This Chapter has been published. The copyright of this Chapter belongs to the Frontiers in Molecular Biosciences - Metabolomics journal.

**Citation:** Malgarin CM, MacPhee DJ, Harding JCS. Fetal Metabolomic Alterations Following Porcine Reproductive and Respiratory Syndrome Virus Infection. *Front Mol Biosci.* 2020;7.

#### **Authors' contribution:**

CMM: statistical analysis, data analysis, pathway investigation, data interpretation, manuscript preparation. JH: experiment design and sample collection, statistical analysis, data interpretation, manuscript preparation. DJM: contributed to interpretation of results and approved the manuscript.

#### 4.1. Abstract

PRRSV infection in third-trimester pregnant sows can lead to fetal death and abortions, although the mechanisms triggering these effects are not well understood. Since resistant and susceptible fetuses can coexist in the same litter, we propose that there may be differential mechanisms used by some fetuses to evade infection and/or disease progression. Our objectives were to investigate possible differences in the metabolome of PRRSV-infected and non-infected fetuses, as well as the interaction of altered intrauterine growth development and PRRSV infection to elucidate possible causes of fetal death following PRRSV infection. Near-term serum samples collected from fetuses on gestation day 106, 21 days post PRRSV-2 infection, were processed by direct flow injection mass spectrometry (DI-MS) and nuclear magnetic resonance (NMR) techniques. Experiment one investigated disease progression with 24 fetuses selected from each of four phenotypic groups: fetuses from non-inoculated gilts (CTRL); fetuses from inoculated gilts that escaped infection (UNINF); infected high viral load viable fetuses (INF); and infected high viral load meconium-stained fetuses (MEC). Experiment two investigated the interaction of intrauterine growth retardation (IUGR) and PRRSV infection by analyzing differences among: non-infected normal development (CON-N); CON-IUGR; PRRS infected normal development (PRRS-N); and PRRS-IUGR. Univariate and multivariate (PCA, PLS-DA) statistics determined group differences among various contrasts, and the most important metabolites associated with disease progression and fetal development. Significant differences in the metabolome were observed, especially between PRRSV-negative fetuses (CTRL and UNINF) and MEC fetuses, while INF fetuses appear to span both groups. The two metabolites with highest variable importance in projection (VIP) scores related to disease progression were alpha-amino adipic acid (alpha-AAA) and kynurenine (KYN), having the highest concentration in MEC and INF fetuses, respectively, compared to CTRL and UNINF. In experiment two, non-IUGR fetuses were found to have increased levels of lysoPCs, PCs and amino acids compared to IUGR fetuses, while the near complete absence of lysoPCs and PCs in IUGR fetuses, even during infection, indicate a distinctive response to infection compared to non-growth retarded fetuses. Possible markers of PRRSV fetal susceptibility, such as alpha-AAA, kynurenine and lysoPCs, are presented and discussed.

## 4.2. Introduction

In medical research, the development of global untargeted metabolomic techniques has provided tremendous insight into the cellular and biochemical processes occurring in healthy individuals, or those subjected to physiological stresses, neoplasia or infective diseases. The unique value stems from the fact that, unlike other ‘omic approaches like genomics, transcriptomics or proteomics, metabolomics provides a tool to directly measure biochemical response.<sup>64</sup> While metabolomics has been used in swine-related nutritional and reproductive research, the technique is less commonly employed to study host responses to veterinary infective diseases, and porcine diseases in particular. Although the utility of this approach lies primarily in hypothesis generation, recent studies have shed light on possible metabolic and physiologic changes following respiratory disease caused by *Mycoplasma hyopneumoniae*,<sup>99</sup> enteric disease cause by *Brachyspira hyodysenteriae*<sup>100</sup> and a potential interaction between the host and gut microbiome in the development of disease following infection with classical swine fever virus.<sup>101</sup>

Porcine reproductive and respiratory syndrome (PRRS) is a financially devastating Arteriviral disease<sup>68</sup> associated with systemic vasculitis, immunosuppression, and persistent infections in post-natal pigs. Infection of pregnant sows or gilts during the third trimester results in rapid endometritis and endometrial vasculitis<sup>53</sup> followed by rapid transmission across the diffuse epitheliochorial placenta within days of maternal infection.<sup>72,92</sup> Fetal infection can lead to death and abortions, however, there is vast heterogeneity in outcome within and between litters.<sup>49</sup> Pregnant gilts experience minor symptoms but have a significant endometritis, vasculitis and immune response following PRRSV infection<sup>35,38,39</sup> that may impact the efficiency of the placenta and thereby alter fetal metabolomics and compromise growth and viability. The mechanisms that trigger fetal death, as well as factors associated with variation in fetal susceptibility or resilience to viral infection, are not well understood. Since resilient and susceptible fetuses can coexist in the same litter, differential physiological mechanisms might underlie the ability of some fetuses to evade infection or resist disease progression. For example, previous large-scale research allowing the categorization of fetuses according to their phenotypic responses identified differences in genomic (e.g. fetal SNPs related to thymus viral load and fetal viability)<sup>102</sup> and transcriptomic (e.g. increased TREM1 signaling as disease progresses)<sup>62</sup> profiles of susceptible and resilient fetuses, indicating that events occurring within the fetal compartment

are important to the final outcome. Moreover, it has been observed that intrauterine growth-retarded (IUGR) fetuses, fetuses born with lower body weight relative to brain weight (i.e. “brain sparing”) when compared to its siblings, possess lower viral concentration after maternal inoculation than fetuses experiencing normal intrauterine growth.<sup>70</sup>

In spite of being a difficult compartment to access, understanding changes in the fetal metabolome may help explain the pathophysiology associated with disease progression and fetal death following both maternal and fetal PRRSV infection. Metabolomics may also help to identify differences between susceptible and resistant fetuses, including why IUGR fetuses appear to be more resistant to infection. With this background, the aim of this study was to identify key differences in the metabolomic profiles of fetuses representative of unique phenotypic susceptibility groups following maternal PRRSV infection, and observe how retarded fetal development may alter the metabolic profiles of PRRSV-infected fetuses.

#### **4.3. Material and methods**

The project was approved by the University of Saskatchewan’s Animal Research Ethics Board and adhered to the Canadian Council on Animal Care guidelines for humane animal use (permit #20110102).

The experimental protocol has been extensively described.<sup>49</sup> Briefly, 114 pregnant gilts were inoculated with PRRSV2 (NVSL 97-7895) at day 85 of gestation while 19 pregnant gilts were mock inoculated negative controls. Animals were humanely euthanized 21 days post inoculation (DPI), the gravid reproductive tract removed, and fetuses categorized as per their preservation status as: viable (VIA), meconium-stained (MEC), decomposed (DEC), and autolyzed (AUT). Blood was collected via the axillary artery from VIA and MEC fetuses and refrigerated after clot formation. Serum was separated the following morning then frozen at -80 °C pending further analysis. The PRRSV RNA concentration in fetal sera and thymus was quantified using an in-house RT-qPCR targeting NVSL 97-7895 and reported as logarithm base 10 DNA copies per  $\mu$ L sera or mg tissue.

##### *4.3.1. Phenotypic fetal susceptibility groups*

4.3.1.1. *Experiment 1 - Disease progression:* A subset of sera from fetuses representing four phenotypic severity groups (n = 24/group) were selected for untargeted metabolomic analyses as follow: 1) fetuses from non-inoculated control gilts (CTRL); 2) fetuses that escaped infection from PRRSV inoculated gilts, i.e. negative viral load (UNINF); 3) viable PRRSV-infected fetuses with high viral load (over 3.5 log<sub>10</sub>; mean 6.7 ±0.9 genome copies/mg) in fetal thymus (HVL-VIA); and 4) PRRSV-infected meconium-stained fetuses with high viral load (over 5 log<sub>10</sub>; mean 7.3 ±0.9 genome copies/mg) (MEC). A first batch of samples (48 samples; 12 per group) was submitted to The Metabolomics Innovation Centre (TMIC) at the University of Alberta to initially determine the within group variability across metabolites. This data was used to establish the sample size required and a second batch (48 samples; 12 per group) was submitted and tested subsequently. Fetuses from PRRSV-inoculated groups were randomly selected blocking by litter (one UNINF, HVL-VIA and MEC fetus from each of 24 litters). The CTRL group comprised of one randomly selected fetus from each of 19 non-infected gilts plus a second fetus from each of 5 randomly selected non-inoculated litters (24 in total). All serum samples submitted to the TMIC had been previously used to measure PRRSV RNA concentration, thus, had been thawed/re-frozen up to 3 times, admittedly a weakness of this study.

4.3.1.2. *Experiment 2 – Fetal IUGR:* A subset of fetuses investigating the interaction of intrauterine growth and maternal PRRSV infection status was selected using a 2 x 2 factorial design: 1) Non-IUGR (normal development) fetuses from non-inoculated control gilts (CON-N, n=23); 2) IUGR fetuses from non-inoculated control gilts (CON-IUGR, n=24); 3) Non-IUGR fetuses from PRRSV-infected gilts (PRRS-N, n=25); and 4) IUGR fetuses from PRRSV-infected gilts (PRRS-IUGR, n=24). IUGR was characterized based on the fetal brain:liver weight ratio as previously described,<sup>70</sup> with high brain:liver ratio representative of the brain sparing effect typifying IUGR fetuses. The IUGR and non-IUGR fetuses were selected at the opposing extreme ends of the brain:liver range, and averaged 1.75 ±0.52 and 0.64 ±0.11, respectively. The PRRSV infected fetuses had mean viral load of 4.7 ±3.2 log<sub>10</sub> RNA copies, however, not all fetuses in the PRRSV-IUGR group were infected (discussed below in more detail). Similar to experiment 1, an initial batch of sera (48 samples; 12 per group) was submitted to TMIC for the purpose of estimating the sample size, then a second batch of equal size was subsequently

submitted. Due to the relative sparsity of IUGR fetuses, they were selected from 28 PRRSV-infected and 19-non-infected litters (1-4 fetuses/litter) while including as many IUGR/non-IUGR matched littermates as possible. The final section included 33/47 matched control and 30/49 matched inoculated fetuses. All samples had been thawed/re-frozen up to three times for reasons describe above.

#### 4.3.2. *Metabolomic techniques*

Nuclear Magnetic Resonance (NMR) and Direct Flow Injection Mass Spectrometry (DI-MS) were performed following each submission to TMIC. The results from identical metabolites found in both assays were averaged.

4.3.2.1. *Sample preparation, NMR spectroscopy and compound quantification and identification:* To remove large molecular weight proteins and lipoproteins from the sera, which affects the identification of the small molecular weight metabolites by NMR spectroscopy, a deproteinization step involving ultra-filtration<sup>103</sup> was undertaken. Prior to filtration, the 3 KDa cut-off centrifugal filter units (Amicon Microcon YM-3) were rinsed five times each with 0.5 mL ultrapure water and centrifuged ( $13,000 \times g$  for 10 minutes) to remove residual glycerol bound to the filter membranes. Aliquots of each serum sample were then transferred into the centrifuge filter devices and spun ( $13,000 \times g$  for 20 minutes) to remove macromolecules from the sample. The filtrates were checked visually for any evidence of a compromised membrane and if observed the filtration process was repeated. The filtrates were collected and if the total volume was  $<600 \mu\text{L}$  an appropriate amount of 50 mM  $\text{NaH}_2\text{PO}_4$  buffer (pH 7) was added to bring the total volume to  $600 \mu\text{L}$ . For such samples, the dilution factor was used to correct the metabolite concentrations in the subsequent analysis. Subsequently,  $70 \mu\text{L}$  of deuterium oxide ( $\text{D}_2\text{O}$ ) and  $30 \mu\text{L}$  of buffer solution (12 mM disodium -2, 2-dimethyl-2-silcepentane-5-sulphonate, 730 mM imidazole, and 0.47%  $\text{NaN}_3$  in water) were added to the samples. The sample ( $700 \mu\text{L}$ ) was transferred to a standard NMR tube for subsequent spectral analysis. All  $^1\text{H}$ -NMR spectra were collected on a 500 MHz Inova (Varian Inc. Palo Alto, CA) spectrometer equipped with a 5 mm HCN Z-gradient pulsed-field gradient (PFG) room-temperature probe.  $^1\text{H}$ -NMR spectra were acquired at  $25^\circ\text{C}$  using the first transient of the NOESY- pre-saturation pulse sequence, chosen for its high degree of quantitative accuracy<sup>104</sup>. As previously described

by Bahado-Singh<sup>105</sup> (p. 1841) and Hage<sup>106</sup> (p. 13), all free induction decays (FID's) were zero-filled to 64 K data points and subjected to line broadening of 0.5 Hz. The singlet produced by the DSS methyl groups was used as an internal standard for chemical shift referencing (set to 0 ppm) and for quantification. All <sup>1</sup>H-NMR spectra were processed and analyzed using the Chenomx NMR Suite Professional Software package version 7.1 (Chenomx Inc, Edmonton, AB). The Chenomx NMR Suite software allows for qualitative and quantitative analysis of an NMR spectrum by manually fitting spectral signatures from an internal database to the spectrum. Specifically, the spectral fitting for metabolite was done using the standard Chenomx 500 MHz metabolite library. Typically, 90% of visible peaks were assigned to a compound and more than 90% of the spectral area could be routinely fit using the Chenomx spectral analysis software. Most visible peaks were annotated with a compound name previously shown to provide absolute concentration accuracy of greater than 90%. Each spectrum was processed and analyzed by at least two NMR spectroscopists to minimize compound misidentification and miss-quantification.

*4.3.2.2. Combined Direct Flow Injection and LC-MS/MS compound identification and quantification:* An untargeted quantitative approach using a combination of direct injection mass spectrometry (AbsoluteIDQ® Kit) with a reverse-phase LC-MS/MS Kit (BIOCRATES Life Sciences AG, Austria) was used. This kit was selected based on its capability to identify and quantify up to 180 different endogenous metabolites including amino acids, acylcarnitines, biogenic amines, glycerophospholipids, sphingolipids and sugars. Serum samples were analyzed with the AbsoluteIDQ kit as per the manufacturer's instructions. Briefly, samples were vortexed then centrifuged at 13,000 × g for 10 minutes. Ten µL was loaded onto the center of the filter on the upper 96-well kit plate and dried in a stream of nitrogen. Subsequently, 20 µL of a 5% solution of phenyl-isothiocyanate was added for derivatization. After incubation, the filter spots were dried using an evaporator. Extraction of metabolites was achieved by adding 300 µL methanol containing 5 mM ammonium acetate. Extracts were obtained by centrifugation into the lower 96-deep well plate, followed by dilution with kit MS running solvent. Mass spectrometric analysis was performed on an API4000 Qtrap® tandem mass spectrometry instrument (Applied Biosystems/MDS Analytical Technologies, Foster City, CA) equipped with a solvent delivery system. The samples were delivered to the mass spectrometer by a LC method followed by a direct injection (DI) method. The Biocrates MetIQ software was used to control the assay

workflow, including sample registration, calculation of metabolite concentrations and export of data for analysis. A targeted profiling scheme was used to quantitatively screen for known small molecule metabolites using multiple reaction monitoring, neutral loss and precursor ion scans. Forty different isotope-labelled internal standards (representing amino acids and biogenic amines) at 7 concentrations were used to create the calibration curves. Regression was used to calculate the R<sup>2</sup> for six repetitive preparations, which resulted in R<sup>2</sup> equal or higher than 0.990 for most metabolites. Accuracy of the measurements ranged between 80 – 115% for all analyses, while intra-day precision and accuracy of the standards remained <16% CV and ranging from 57 – 120%, respectively. Reproducibility of the assay was examined and scored between 4 - 37% CV, while inter-day accuracy ranged between 51 – 159%. All metabolites discussed herein are considered level 1 Identified Metabolites.

#### 4.3.3. *Statistical and pathway analyses*

Differences in metabolite levels resulting from running the two separate batches were accounted for by quality control (QC) samples and then centralizing the data (i.e. differences in the means of batches 1 and 2 for each metabolite were added to the batch 2 subject values). Thereafter, the analytical platform MetaboAnalyst (<https://www.metaboanalyst.ca/>) was used for all the statistical analyses. Data normalization was completed by log base 10 transformation and Pareto scaling followed by visualization of the normalized data using box plots and kernel density plots. Shapiro-Wilk tests were performed and because a proportion of the compounds were not normally distributed non- parametric univariate analysis was used to screen for the most significant (FDR < 0.01) metabolites to be included in multivariate analyses to identify metabolite alterations associated with each of the four phenotypic groups in each experiment.

MetaboAnalyst was also used to generate the pathway analysis plots, which combine the topography (Y axis) and pathway impact (X axis) analyses. The plots were re-formatted in R to also display the relative number of compounds in each pathway (bubble size) and the percentage of hits we detected in that pathway (bubble color scale). Pathways with *P*-values (log base10) and “pathway impact” higher than the mid-point for that contrast were labeled. The data generated from MetaboAnalyst was also used to produce boxplots of the significant (*P*-value<0.05) compounds leading those pathways.

Group differences were visualized using scatter plots following: a) unsupervised Principal Components Analysis (PCA) that maximized the data variance into few principal components; and b) supervised Partial Least Squares Discriminant Analysis (PLS-DA) that generated principle components maximizing variation among the phenotypic groups. PLS-DA model quality was assessed by 10-fold cross-validation, generation of the R2 and Q2 measures, and assessing the significance by permutations tests (2000 permutations). Variable Importance in Projection (VIP) scores were calculated to provide a relative ranking of metabolites, and the 15 most important metabolites responsible for group differences were further examined. A targeted pathway analysis was performed on the metabolites or groups of metabolites with VIP scores greater than 1. The Human Metabolome Database (<http://www.hmdb.ca/>) and the Kyoto Encyclopedia of Genes and Genomes (<https://www.genome.jp/kegg/>) were used to identify biochemical pathways specific to the high VIP metabolites. Those were followed by an extensive literature review to relate the most significant metabolites to their biological reactions, focusing especially on possible PRRS, IUGR and infectious diseases related pathways.

#### 4.4. Results

##### 4.4.1. Metabolomic profiles associated with disease progression

In total, 140 common metabolites (DI-MS: 108, NMR: 32) were detected. Seventy-eight were phosphocholines (PC) or lysophosphocholines (lysoPC), 22 were amino acids (AA), 15 were sphingomyelins (SM), and 25 were in other categories. Of these, 89 were identified by Kruskal-Wallis as having significant differences ( $FDR < 0.01$ ) among groups. Across all metabolites, profiles of the UNINF and MEC groups were the most distinct while being unique from each other, with metabolites largely positive/increased for MEC and negative/decreased for UNINF. The same pattern was observed following analyses by PCA and PLS-DA (2 components,  $R^2=0.68$ ,  $Q^2=0.54$ ) where clear differences ( $P < 5e-04$ ; 0/2000 permutations) in the metabolome were observed for the PRRSV negative groups (CTRL and UNINF) compared to the MEC fetuses, while the metabolome of HVL-VIA fetuses spanned both groups (**Figure 4.1A**). The metabolites with the greatest contribution (highest VIP scores) to disease progression and group separation were kynurenine and amino adipic acid (alpha-AAA), being of highest concentration in MEC and HVL-VIA fetuses compared to UNINF and CTRL (**Figure 10B**).

Thirteen other metabolites including amino acids (2), sphingomyelins (SMs; 4), phosphocholines (PCs; 4), lysophosphocholines (lysoPCs;1), acetic acid and histamine had VIP scores > 1.5 and were significantly different among groups. Levels were lower in PRRSV-negative fetuses compared to infected fetuses (HVL-VIA, MEC) with the exception of histamine and acetic acid. Individual group contrasts are described in more detail below and **Table 4.1** contains all the important metabolites indicating their significance, VIP score, and fold change (FC) between groups for each of the contrasts.

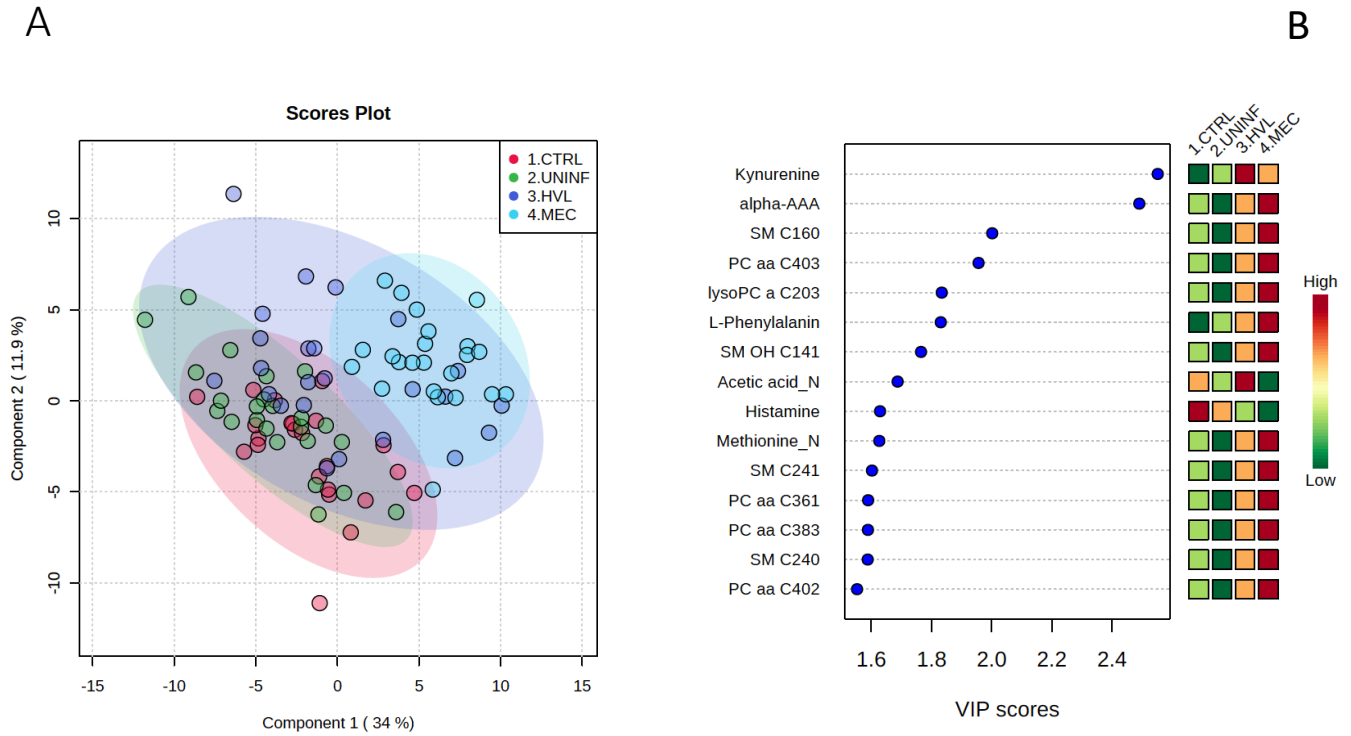


**Figure 4.1:** Metabolite profiles of four disease progression fetal phenotypes.

(A) Two component PLS-DA score plot of all groups with individual fetuses represented by dots. (B) Variance Importance in Projection (VIP) score plot displaying the 15 most important metabolites differentiating the groups with colored side bar displaying the relative metabolite concentration in each group. 1. CTRL: fetuses from non-inoculated control gilts; 2. UNINF: fetuses from PRRSV inoculated gilts that escaped infection, i.e. negative viral load; 3. HVL-VIA: viable PRRSV-infected fetuses with high viral load (over  $3.5 \log_{10}$ ; mean  $6.7 \pm 0.9$  genome copies/mg) in fetal thymus; and 4. MEC: PRRSV-infected meconium-stained fetuses with high viral load (over  $5 \log_{10}$ ; mean  $7.3 \pm 0.9$  genome copies/mg). Alpha-AAA=alpha-aminoadipic acid, lysoPC=lysophosphocholine, PC=phosphocholine, SM=sphingomyelin.

**Table 4-1:** Metabolites with significant differences among fetal PRRS disease progression groups.

Contrasts	CTRL vs UNINF			UNINF vs HVL-VIA			HVL-VIA vs MEC		
	VIP score	FDR	FC	VIP score	FDR	FC	VIP score	FDR	F C
ADMA	<1	ns	ns	1.58	0.025	ns	<1	ns	ns
Alpha-AAA		0.01	2.6		0.001	0.1	1.55	0.01	
	3.39	9	7	3.72		7		8	ns
C2	<1	ns	ns	1.72	0.012	ns	<1	ns	ns
Creatine	<1	ns	ns	1.34	0.012	ns	<1	ns	ns
Formate			ns		<0.00	ns	<1	ns	ns
	1.09	ns		2.08	1				
Histamine			ns			ns	1.38	0.00	ns
	<1	ns		<1	ns			3	
Kynurenine			ns		<0.00	0.1	<1		ns
	<1	ns		3.19	1	9		ns	
L-Glutamic acid		0.01	ns	<1		ns	<1	0.00	ns
	1.40	9			ns			6	
L-Phenylalanine			ns			ns	<1	ns	ns
	<1	ns		1.69	0.001				
L-Threonine		0.02	ns	<1	ns	ns	<1	ns	ns
	1.48	7							
lysoPC a C160			ns	<1	ns	ns	1.00	0.01	ns
	1.47	ns						7	
lysoPC a C170		0.03	ns	<1	ns	ns	<1	0.02	ns
	1.63	5						5	
lysoPC a C180			ns	<1	ns	ns	1.28	0.00	ns
	1.37	ns						4	
lysoPC a C181			ns	<1	ns	ns	1.43	0.00	ns
	1.22	ns						3	

lysoPC a C203	<1	ns	ns	1.16	ns	ns	1.44	0.00	ns
								3	
Methionine		0.04	ns		<0.00	ns	<1		ns
	1.06	3		1.98	1				ns
PC aa C360		0.03	ns	<1	ns	ns	<1	0.00	ns
	1.35	0						7	
PC aa C361			ns	<1	ns	ns	1.31	0.00	ns
	<1	ns						3	
PC aa C363			ns	<1	ns	ns	1.27	0.00	ns
	<1	ns						6	
PC aa C366		0.02	ns	<1	ns	ns	<1		ns
	1.54	7						ns	
PC aa C383			ns	<1	ns	ns	1.32	0.00	ns
	<1	ns						3	
PC aa C386		0.04	ns	<1	ns	ns	1.25	0.00	ns
	1.41	3						6	
PC aa C403			ns	1.08		ns	1.46	0.00	ns
	<1				ns			3	
PC aa C404			ns	<1	ns	ns	1.40	0.00	ns
	<1							5	
PC aa C405			ns	<1	ns	ns	1.34	0.00	ns
	<1							5	
PC aa C406			ns	<1	ns	ns	1.26	0.00	ns
	1.30	ns						6	
PC ae C380		0.03	ns	<1	ns	ns	1.25	0.00	ns
	1.43	5						9	
PC ae C386		0.04	ns	<1	ns	ns	<1	0.03	ns
	1.31	3						2	
PC ae C401		0.01	ns	<1	ns	ns	1.13	0.01	ns
	1.70	9						4	

PC ae C406	1.41	0.03	ns	<1	ns	ns	<1	0.00	ns
		5					7		
PC ae C422	1.30		ns	<1	ns	ns	1.26	0.00	ns
		ns					7		
PC ae C423	1.49	0.03	ns	<1	ns	ns	1.15	0.00	ns
		5					7		
SM C160	<1	ns	ns	1.62	0.025	ns	1.25	0.00	ns
							4		
SM C161	<1	ns	ns	1.23	ns	ns	1.12	0.00	ns
							5		
SM C180	<1	ns	ns	1.29	0.039	ns	1.02	0.00	ns
							5		
SM C240	<1	ns	ns	1.26	0.047	ns	1.12	0.00	ns
							4		
SM C241	<1	ns	ns	1.30	0.049	ns	1.05	0.00	ns
							5		
SM OH C141	<1	ns	ns	1.43	ns	ns	1.17	0.00	ns
							6		
SM OH C222	1.01		ns	1.22	ns	ns		0.03	ns
		ns					<1	0	

FC=fold change, FDR=false discovery rate, VIP=Variable Importance in Projection, ns=not significant

4.4.1.1. *Control versus Uninfected fetuses:* This contrast aimed to investigate the impact of maternal infection only and response by non-infected fetuses on fetal parameters. Pathways related to amino acid metabolism or biosynthesis were most impactful and/or significant (**Figure 4.2A**) with a number of key amino acids decreased in the UNINF group (**Figure 4.2B**). The global metabolomes of CTRL and UNINF fetuses trended towards significance ( $P=0.075$ ; 145/2000 permutations) based on PLS-DA (3 components,  $R^2=0.62$ ,  $Q^2=0.27$ ) showing marginal differences between groups (**Figure 4.2C**). As this contrast reflects fetal responses following PRRSV infection of the maternal-fetal interface (MFI), the differences although minimal, indicate that some fetuses are responding to endometrial infection without themselves being infected. The most important in variance metabolites between the CTRL and UNINF groups based on VIP score (although most are in between 1 and 2, not consider highly important) were alpha-AAA, amino acids (glutamic acid and threonine), lysoPCs (3), and some PCs (9). Alpha-AAA stood out as the most contributory metabolite distinguishing these groups (**Figure 4.2D**) and the only metabolite with a VIP score over 2.0. It was at higher concentration in the CTRL group.

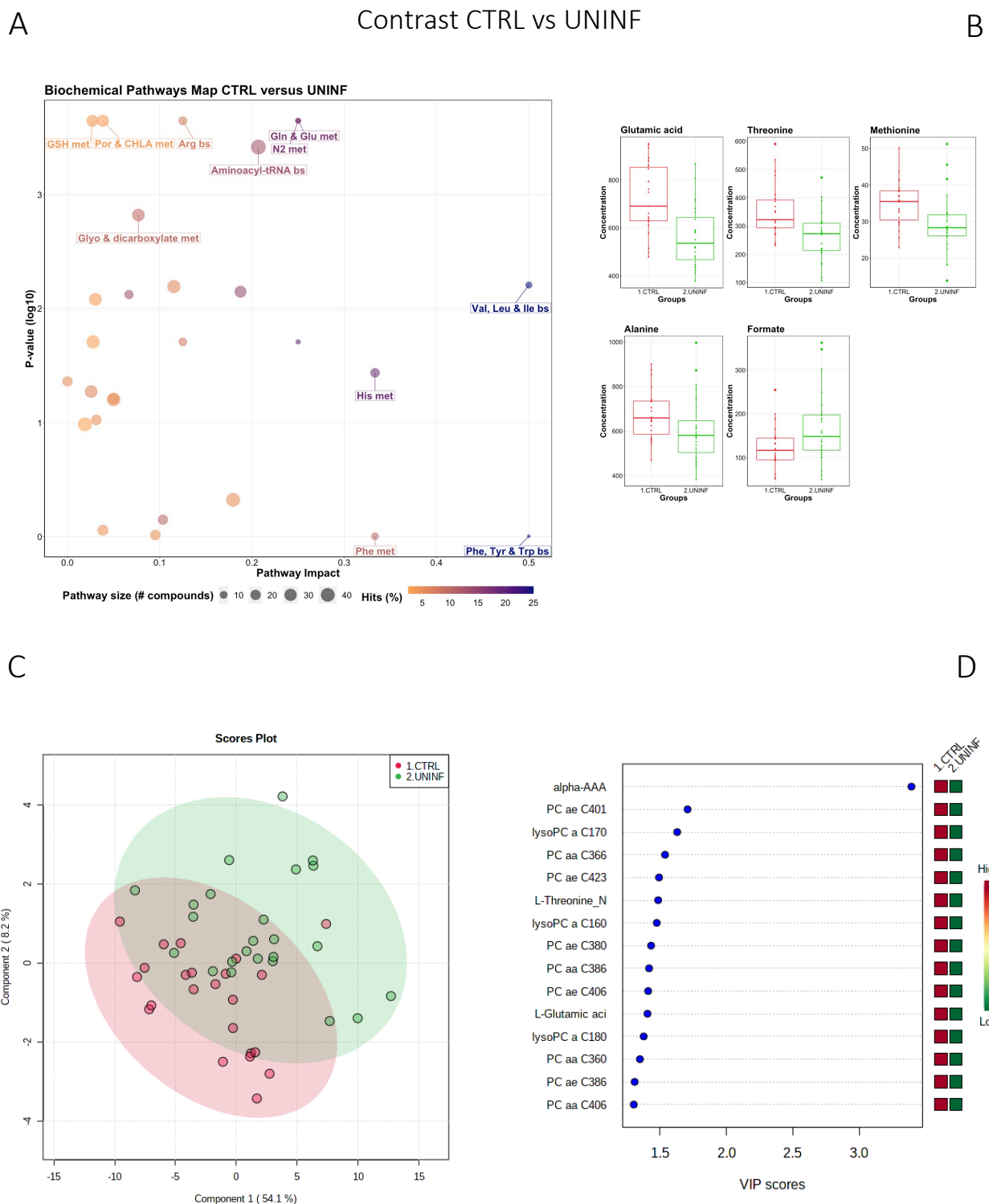


**Figure 4.2:** Metabolite profile of control (CTRL) and uninfected (UNINF) contrast. (A) Biochemical pathway plot displaying the most significant (Y-axis;  $P$ -value $<0.05$ ) and impactful (X-axis) pathways distinguishing the groups. Size of dot represents the size of the

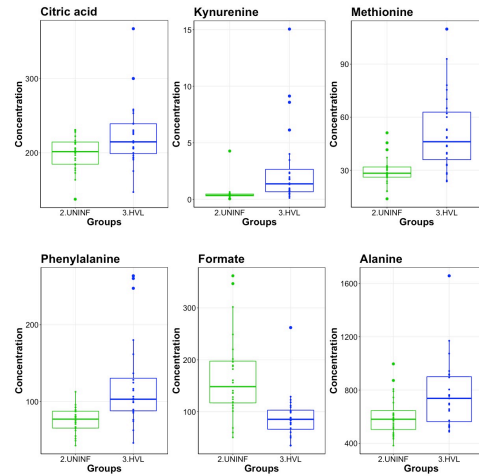
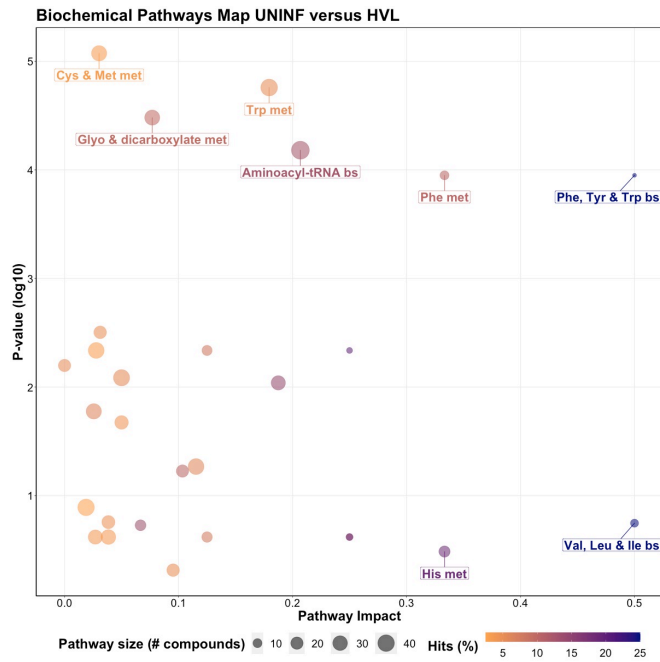
pathway (number of compounds). Dark colors (from light orange to dark purple) represent higher hits (percentage of the pathway detected in our study). (B) Boxplots of the concentration of significant ( $P$ -value $<0.05$ ) compounds distinguishing the groups. (C) Two component PLS-DA score plots with individual fetuses represented by dots. (D) Variance Importance in Projection (VIP) score plots displaying the 15 most important metabolites differentiating groups with colored side bar displaying the relative metabolite concentration in each group. 1. CTRL: fetuses from non-inoculated control gilts; 2. UNINF: fetuses from PRRSV inoculated gilts that escaped infection, i.e. negative viral load. Met=metabolism, bs=biosynthesis, deg=degradation, Por= Porphyrin, CHLA= chlorophyll, Glyo= Glyoxylate, Buta=Butanoate, GSH= Glutathione, GPL= Glycerophospholipid, ALA=alpha-Linoleic acid, ARA=arachidonic acid, SeC= Selenocompound, Prop=Propanoate. Alpha-AAA=alpha-aminoadipic acid, lysoPC= lysophosphocholine, PC=phosphocholine.

4.4.1.2. *Uninfected versus High Viral Load Viable fetuses:* This contrast was made to highlight the fetal response to PRRSV infection. Pathways mainly related to amino acid metabolism, but also sphingolipid metabolism, were most prominent in this contrast (**Figure 4.3A**), led by the compounds shown in **Figure 4.3B** including kynurenine. Group variation was much greater and significantly different ( $P < 5e-04$ ; 0/2000 permutations) in the HVL-VIA compared to the UNINF group (**Figure 4.3C**) on PLS-DA (2 components,  $R^2=0.52$ ,  $Q^2=0.41$ ), likely reflecting the heterogeneity within the HVL-VIA group in terms of individual variability in response or timing of fetal infection, or both. Infection of the fetus was mostly related to increased levels of kynurenine, alpha-AAA, acylcarnitine (C2), formate, amino acids (methionine, phenylalanine, and creatine), and asymmetric dimethylarginine (ADMA) among others. In addition to alpha-AAA, kynurenine also stood out as an important metabolite (VIP score  $>3$ ) distinguishing the HVL-VIA group (**Figure 4.3D**). With the exception of formate, all of the most important metabolites distinguishing these two groups were at greater concentration in the HVL-VIA group.

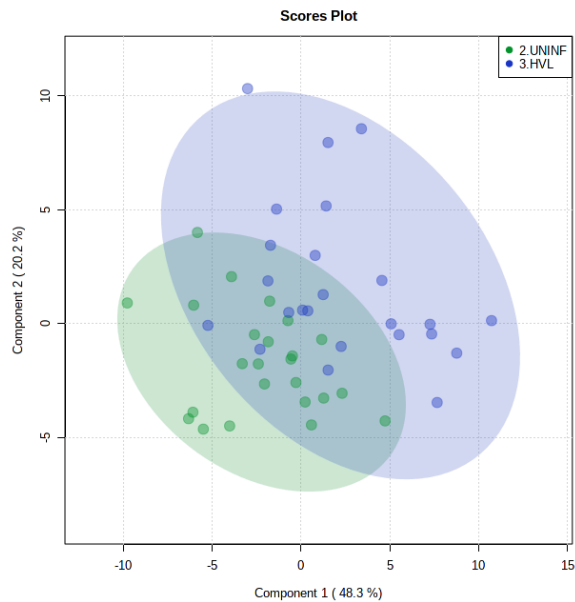
A

Contrast UNINF vs HVL-VIA

B



C



D

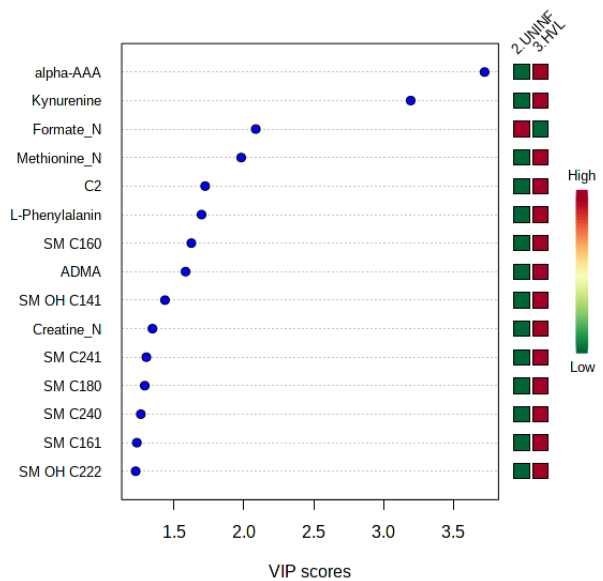


**Figure 4.3:** Metabolite profile of uninfected (UNINF) and high-viral load (HVL-VIA) contrast.

(A) Biochemical pathway plot displaying the most significant (Y-axis;  $P$ -value $<0.05$ ) and impactful (X-axis) pathways distinguishing the groups. Size of dot represents the size of the

pathway (number of compounds). Dark colors (from light orange to dark purple) represent higher hits (percentage of the pathway detected in our study). (B) Boxplots of the concentration of significant ( $P$ -value<0.05) compounds distinguishing the groups. (C) Two component PLS-DA score plots with individual fetuses represented by dots. (D) Variance Importance in Projection (VIP) score plots displaying the 15 most important metabolites differentiating groups with colored side bar displaying the relative metabolite concentration in each group. 2.UNINF: fetuses from PRRSV inoculated gilts that escaped infection, i.e. negative viral load; 3.HVL-VIA: viable PRRSV-infected fetuses with high viral load (over 3.5 log<sub>10</sub>; mean 6.7 ±0.9 genome copies/mg) in fetal thymus. Met=metabolism, bs=biosynthesis, deg=degradation, Por= Porphyrin, CHLA= chlorophyll, GSH= Glutathione, Glyo= Glyoxylate, Buta=Butanoate, ALA=alpha-Linoleic acid, ARA=arachidonic acid, SeC= Selenocompound, Prop=Propanoate. ADMA=asymmetric dimethylarginine, Alpha-AAA=alpha-aminoadipic acid, C2=acetylcarnitine, SM=sphingomyelin.

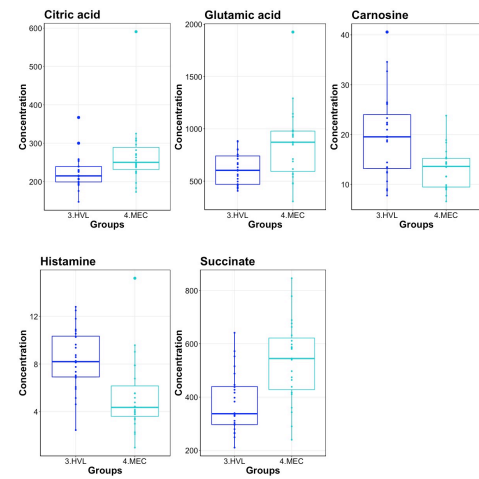
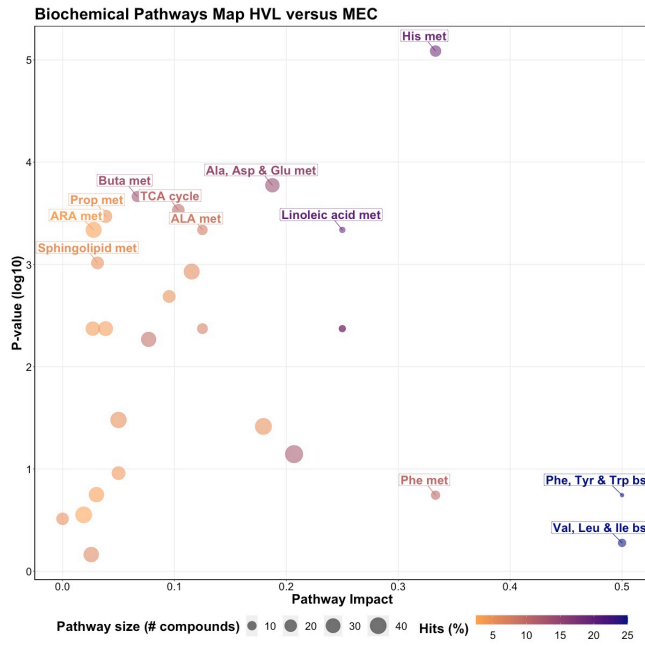
4.4.1.3. *High Viral Load Viable versus Meconium-Stained fetuses*: While all fetuses included in this contrast were highly infected, the contrast highlighted metabolic changes associated with fetal compromise represented by the presence of meconium staining on skin of the MEC fetuses. In addition to the amino acids and sphingolipid metabolism, the citrate cycle and the arachidonic acid metabolism pathways influential in this contrast (**Figure 4.4A-B**). The metabolome of the MEC group was more homogeneous and distinct than the HVL-VIA group based on PLS-DA (2 components,  $R^2=0.54$ ,  $Q^2=0.31$ ) ( $P=0.006$ ; 13/2000 permutations) (**Figure 4.4C**). Alpha-AAA, but not kynurenine, ranked the top 15 contributors to group separation (**Figure 4.4D**). While the top 15 contributors were comprised mainly of PCs and lysoPCs, many other metabolites including carnosine, glutamic acid, serotonin and succinate were significantly altered ( $FDR<0.05$ ) in the MEC group suggesting they are directly or indirectly associated with disease progression. Histamine was the only compound with higher concentration in the HVL-VIA group.

A summary of these contrasts to highlight the most important metabolite changes associated with disease progression is shown in **Figure 4.5**.

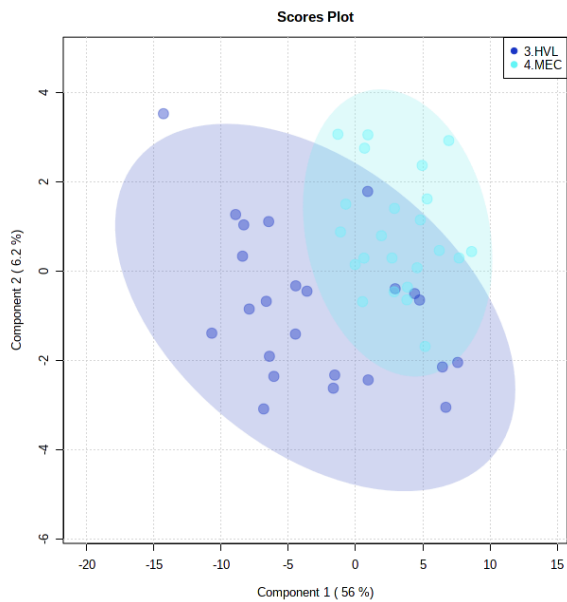
A

## Contrast HVL-VIA vs HVL-MEC

B



C



D

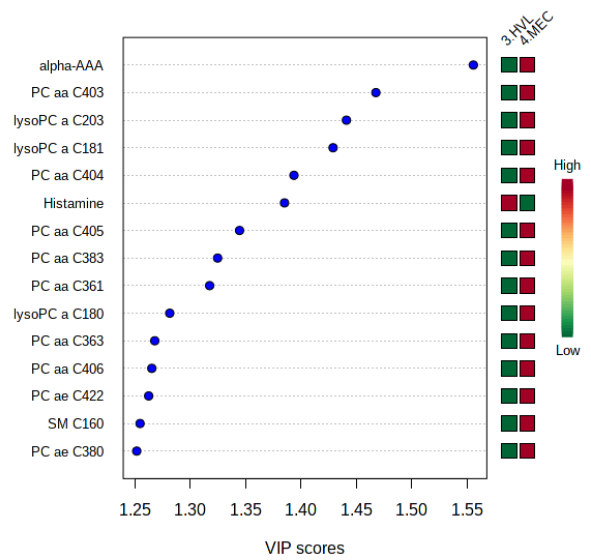


**Figure 4.4:** Metabolite profile of high-viral load (HVL-VIA) and meconium-stained fetuses (MEC) contrast.

(A) Biochemical pathway plot displaying the most significant (Y-axis;  $P$ -value $<0.05$ ) and impactful (X-axis) pathways distinguishing the groups. Size of dot represents the size of the pathway (number of compounds). Dark colors (from light orange to dark purple) represent higher hits (percentage of the pathway detected in our study). (B) Boxplots of the concentration of significant ( $P$ -value $<0.05$ ) compounds distinguishing the groups. (C) Two component PLS-DA score plots with individual fetuses represented by dots. (D) Variance Importance in Projection (VIP) score plots displaying the 15 most important metabolites differentiating groups with colored side bar displaying the relative metabolite concentration in each group. 3.HVL-VIA: viable PRRSV-infected fetuses with high viral load (over 3.5 log<sub>10</sub>; mean 6.7 ±0.9 genome copies/mg) in fetal thymus; 4.MEC: PRRSV-infected meconium-stained fetuses with high viral load (over 5 log<sub>10</sub>; mean 7.3 ±0.9 genome copies/mg). Met=metabolism, bs=biosynthesis, deg=degradation, Por= Porphyrin, CHLA= chlorophyll, GSH= Glutathione, GPL= Glycerophospholipid, ALA=alpha-Linoleic acid, ARA=arachidonic acid, SeC= Selenocompound. Alpha-AAA=alpha-aminoadipic acid, lysoPC= lysophosphocholine, PC=phosphocholine, SM=sphingomyelin.

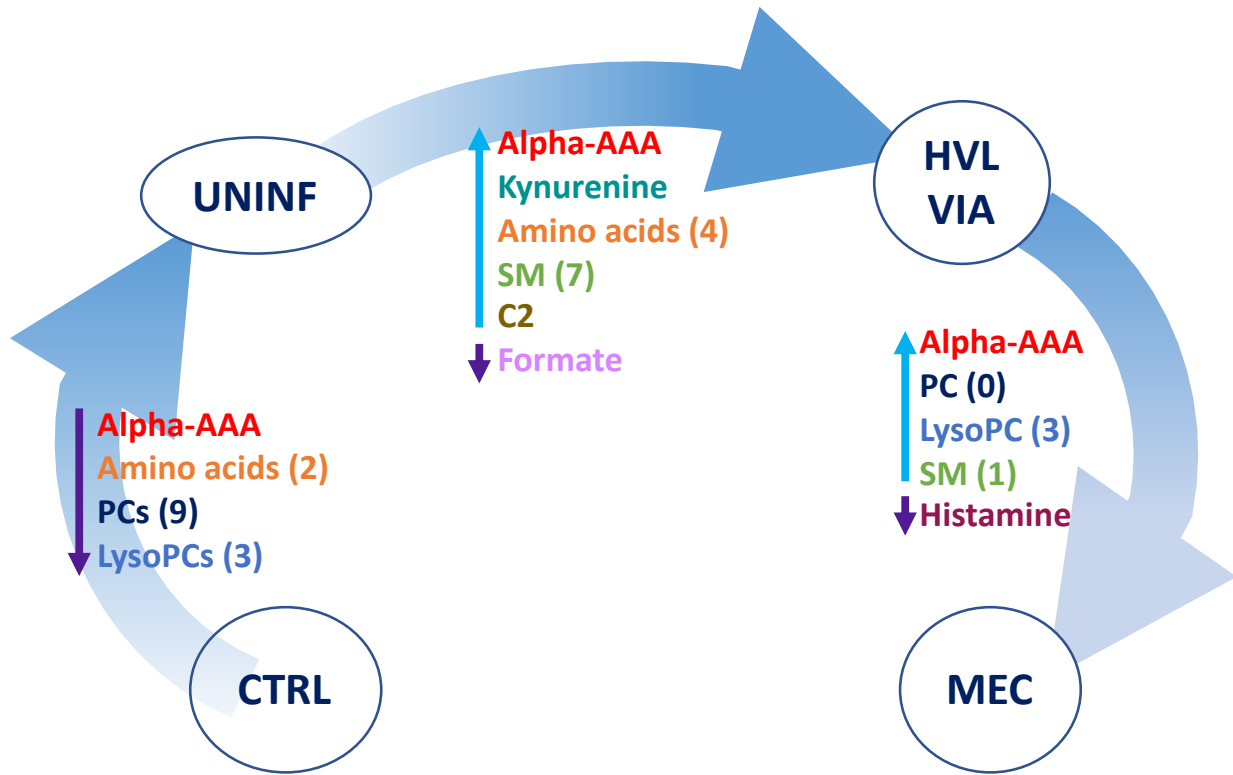


**Figure 4.5:** Visual summary of the most significant metabolite changes associated with disease progression.

1. CTRL: fetuses from non-inoculated control gilts; 2. UNINF: fetuses from PRRSV inoculated gilts that escaped infection, i.e. negative viral load; 3. HVL-VIA: viable PRRSV-infected fetuses with high viral load (over 3.5 log<sub>10</sub>; mean 6.7 ±0.9 genome copies/mg) in fetal thymus; and 4. MEC: PRRSV-infected meconium-stained fetuses with high viral load (over 5 log<sub>10</sub>; mean 7.3 ±0.9 genome copies/mg). Alpha-AAA=alpha-amino adipic acid, ADMA=asymmetric dimethylarginine C2=acetylcarnitine, lysoPC= lysophosphocholine, PC=phosphocholine, SM= sphingomyelin.

#### 4.4.2. *Metabolomic profiles associated with altered fetal development and PRRSV infection*

As previous research identified intrauterine growth rate as a predictor of infection, we next compared the global metabolome in a two by two experiment to investigate this relationship. In total, 141 common metabolites (DI-MS: 109, NMR: 32) were detected and 68 of these significantly differed (FDR < 0.01) among groups based on Kruskal-Wallis. Although there was substantial overlap among all four groups based on the PLS-DA analysis (3 components, R<sup>2</sup>=0.62, Q<sup>2</sup>=0.50), the metabolomes of non-infected (CON-N and CON-IUGR) fetuses were more homogeneous than the PRRSV-infected fetuses (**Figure 4.6A**) and significantly different from each other ( $P < 5e-04$ ; 0/2000 permutations). Across all four groups, the metabolites with highest VIP scores were mainly kynurenine, carnitines (C0 and C2), alpha-AAA, PCs and amino acids, being mostly higher in the PRRSV-infected fetuses (**Figure 4.6B**) and all presenting with VIP scores between 1.4 and 2.4. Specific contrasts were further investigated to elucidate the interaction between fetal development and infection status. Individual group contrasts are described in more detail below and **Table 4.2** highlights all the VIP metabolites indicating their significance, VIP score, and fold change (FC) between groups for each contrast.

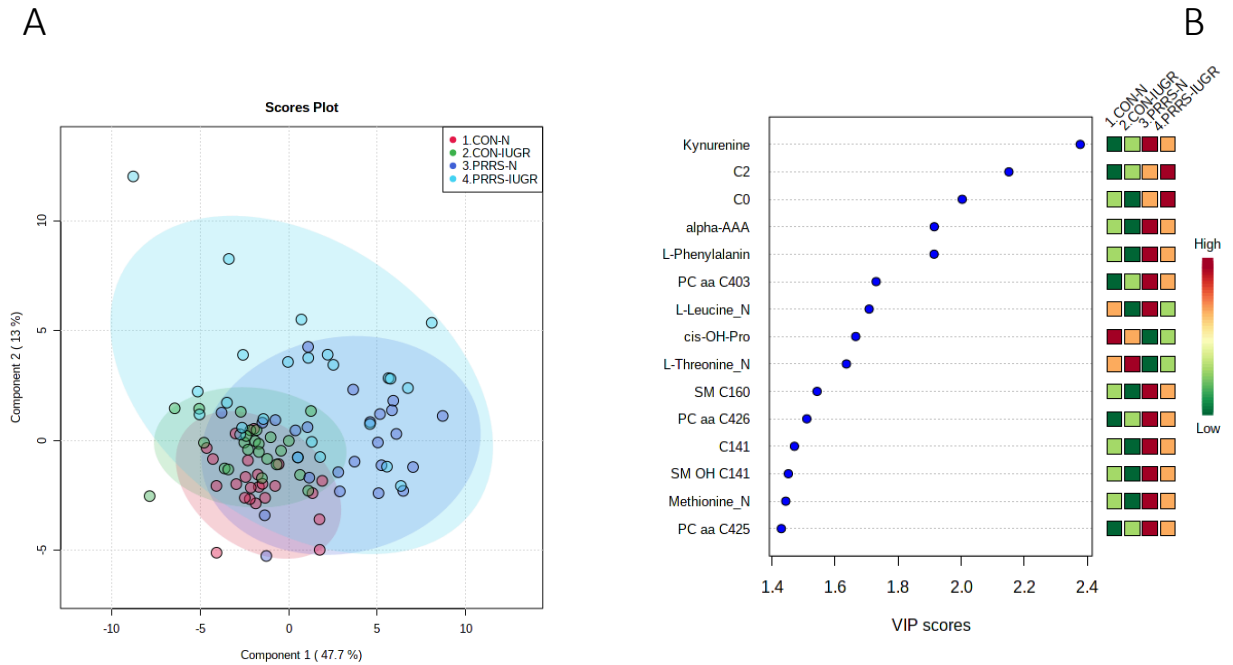


**Figure 4.6:** Metabolite profiles of four IUGR x PRRV-infected. (A) Two component PLS-DA score plot of all groups with individual fetuses represented by dots; (B) Variance Importance in Projection (VIP) score plot displaying the 15 most important metabolites differentiating the groups with colored side bar displaying the relative metabolite concentration in each group. 1.CON-N: non-IUGR (normal development) fetuses from non-inoculated control gilts; 2.CON-IUGR: IUGR fetuses from non-inoculated control gilts; 3.PRRS-N: non-IUGR fetuses from PRRSV-infected gilts; and 4.PRRS-IUGR: IUGR fetuses from PRRSV-infected gilts. Alpha-AAA=alpha-aminoadipic acid, C0=carnitine, C2=acetylcarnitine, cis-OH-Pro=cis-4-Hydroxy-L-proline, PC=phosphocholine, SM=sphingomyelin.

**Table 4-2:** Metabolites with significant differences between contrasting PRRSV-infected and IUGR phenotypic groups.

Metabolite	CON-N VS CON-IUGR			CON-N VS PRRS-N			CON-IUGR VS PRRS-IUGR			PRRS-N VS PRRS-IUGR		
	VIP score	FDR	FC	VIP score	FDR	FC	VIP score	FDR	FC	VIP score	FDR	FC
Alpha-AAA	<1	ns	ns	1.76	<0.00	0.42	1.74	ns	0.43	1.16	0.042	ns
					1							
C0	<1	ns	ns	<1	0.002	ns	2.27	0.003	ns	<1	ns	ns
C141	<1	ns	ns	1.24	<0.00	ns	1.43	ns	ns	<1	0.045	ns
					1							
C2	<1	ns	ns	<1	0.016	ns	2.05	ns	ns	<1	ns	ns
Cis-OH-Pro	<1	ns	ns	1.26	<0.00	ns	1.49	0.006	ns	<1	ns	ns
					1							
Glycine	1.17	ns	ns	<1	<0.00	0.47	1.36	ns	ns	<1	ns	ns
					1							
Histamine	<1	ns	ns	1.27	0.001	ns	<1	ns	ns	1.34	0.013	ns
Kynurenine	<1	ns	ns	1.08	<0.00	0.30	2.61	ns	0.24	<1	ns	ns
					1							
L-Alanine	1.30	0.005	ns	<1	0.006	ns	<1	ns	ns	<1	0.050	ns
L-Glutamine	2.04	<0.00	ns	<1	ns	ns	<1	ns	ns	<1	0.011	ns
		1										

L-Leucine	1.86	<0.001	ns	<1	ns	ns	1.51	ns	ns	1.31	ns	ns
L-Phenylalanine	<1	ns	ns	1.31	<0.001	ns	2.10	ns	ns	<1	ns	ns
L-Threonine	<1	ns	ns	<1	0.005	ns	1.75	0.036	ns	<1	ns	ns
LysoPC a c160	1.54	0.007	ns	<1	ns	ns	<1	ns	ns	1.38	0.010	ns
LysoPC a c161	1.31	ns	ns	<1	ns	ns	<1	ns	ns	1.14	0.026	ns
LysoPC a c170	1.56	0.004	ns	<1	ns	ns	<1	ns	ns	1.27	0.013	ns
LysoPC a c180	1.75	<0.001	ns	1.10	<0.001	ns	<1	ns	ns	1.70	0.008	ns
LysoPC a c181	1.62	0.009	ns	1.22	<0.001	ns	<1	ns	ns	1.58	0.010	ns
LysoPC a c182	1.76	0.007	ns	<1	0.026	ns	<1	ns	ns	1.47	0.010	ns
LysoPC a c203	1.45	ns	ns	1.36	<0.001	ns	1.40	ns	ns	1.37	0.019	ns
Methionine	<1	ns	ns	<1	0.004	ns	1.48	ns	ns	<1	ns	ns
PC aa C360	1.40	ns	ns	1.05	0.001	ns	<1	ns	ns	1.23	0.026	ns
PC aa C361	<1	ns	ns	1.36	<0.001	ns	<1	ns	ns	1.31	0.011	ns
PC aa C381	<1	ns	ns	1.36	<0.001	ns	<1	ns	ns	1.11	0.026	ns

PC aa C383	1.07	ns	ns	1.26	<0.00	ns	1.05	ns	ns	1.18	0.020	ns
					1							
PC aa C386	1.26	ns	ns	<1	0.003	ns	<1	ns	ns	1.43	0.011	ns
PC aa C403	<1	ns	ns	1.45	<0.00	0.49	1.14	ns	ns	<1	ns	ns
					1							
PC aa C404	<1	ns	ns	1.51	<0.00	0.49	<1	ns	ns	<1	ns	ns
					1							
PC aa C405	<1	ns	ns	1.48	<0.00	ns	<1	ns	ns	1.10	ns	ns
					1							
PC aa C406	<1	ns	ns	1.18	<0.00	ns	<1	ns	ns	1.35	0.014	ns
					1							
PC aa C424	<1	ns	ns	1.46	<0.00	0.49	<1	ns	ns	<1	ns	ns
					1							
PC aa C425	1.12	ns	ns	1.34	<0.00	ns	<1	ns	ns	<1	ns	ns
					1							
PC ae C423	1.43	0.021	ns	<1	0.004	ns	<1	ns	ns	1.29	0.019	ns
SM C160	<1	ns	ns	1.42	<0.00	ns	1.62	ns	ns	1.13	0.022	ns
					1							
SM C240	1.20	ns	ns	1.07	<0.00	ns	<1	ns	ns	1.20	0.014	ns
					1							
SM OH C141	<1	ns	ns	1.40	<0.00	ns	1.57	ns	ns	1.11	0.027	ns
					1							

SM OH C221	1.27	ns	ns	<1	0.002	ns	<1	ns	ns	1.29	0.011	ns
Tyrosine	<1	ns	ns	<1	ns	ns	2.15	0.036	ns	<1	0.026	ns
Valine	1.70	<0.001	ns	<1	ns	ns	<1	ns	ns	<1	ns	ns

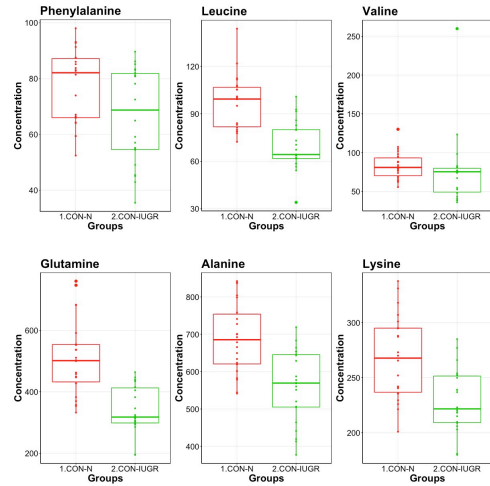
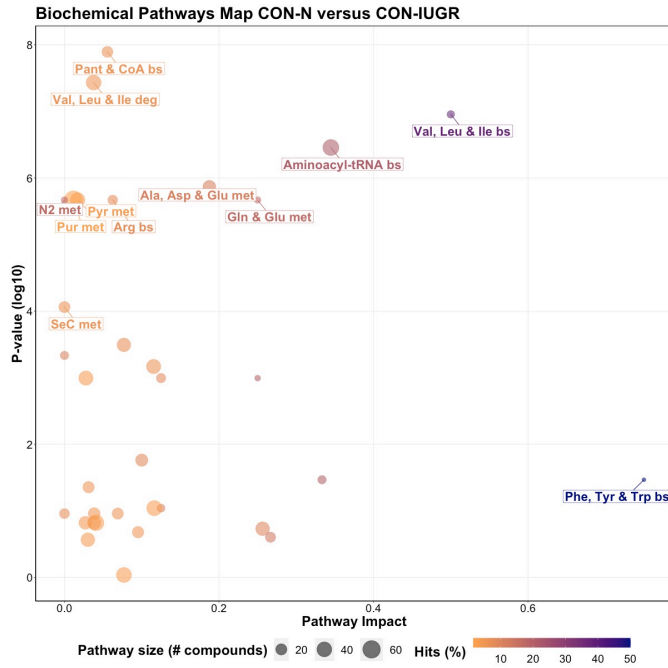
FC=fold change, FDR=false discovery rate, VIP=Variable Importance in Projection, ns=not significant

4.4.2.1. *Control-normal versus Control-IUGR*: This contrast aimed to display metabolomic differences between normal and IUGR fetuses (disparaging fetal development) prior to infection. The most influential pathways in this contrast related to amino acid metabolism or biosynthesis (**Figure 4.7A-B**). These groups were significantly different ( $P < 5 \times 10^{-4}$ ; 0/2000 permutations) based on the PLS-DA analysis (3 components,  $R^2=0.79$ ,  $Q^2=0.55$ ) (**Figure 4.7C**) and most metabolites were at greater concentration in the non-IUGR compared to IUGR fetuses, likely commensurate with greater growth rates. Metabolites contributing to group differences were amino acids (glutamine, leucine, valine, alanine), lysoPCs (7), PCs (3) and SM (1); all were increased in the non-IUGR fetuses (**Figure 4.7D**).

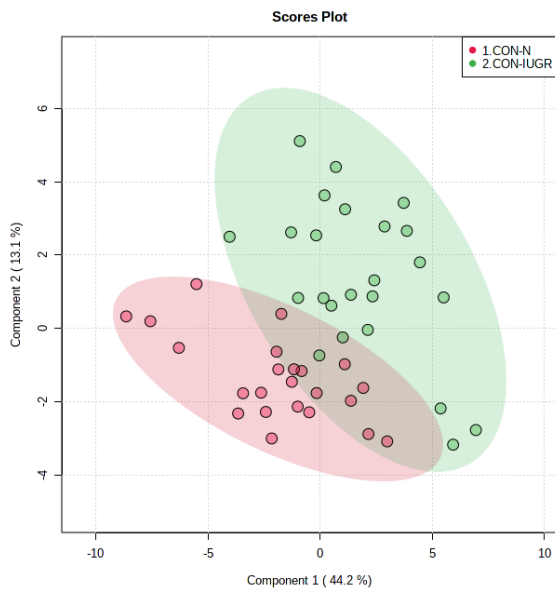
A

## Contrast CON-N vs CON-IUGR

B



C



D

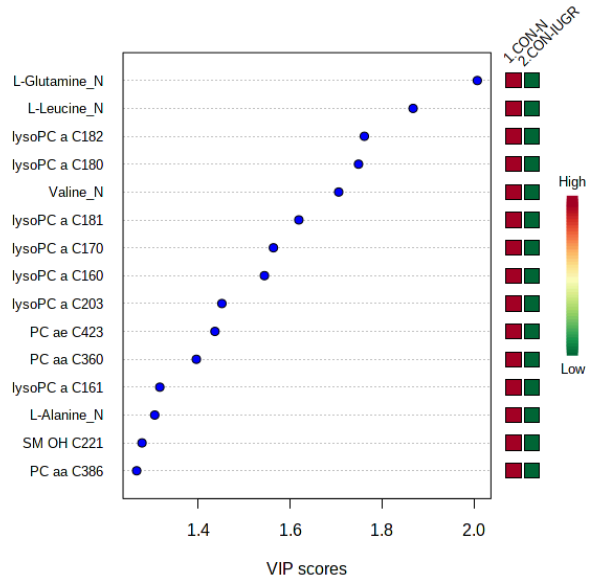


**Figure 4.7:** Metabolite profile of control-normal development fetuses (CON-N) and control-IUGR fetuses (CON-IUGR).

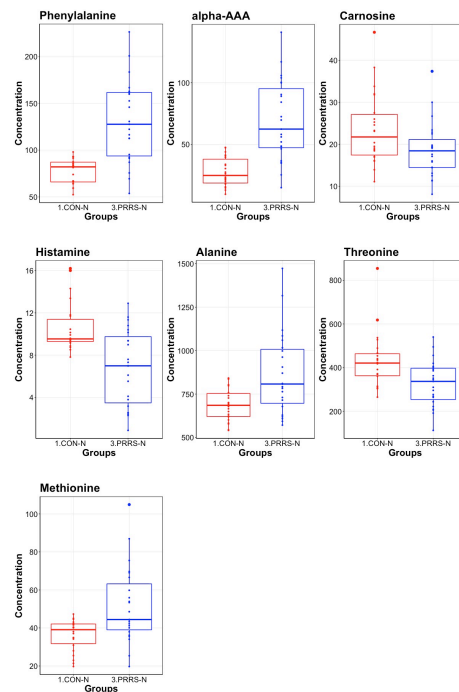
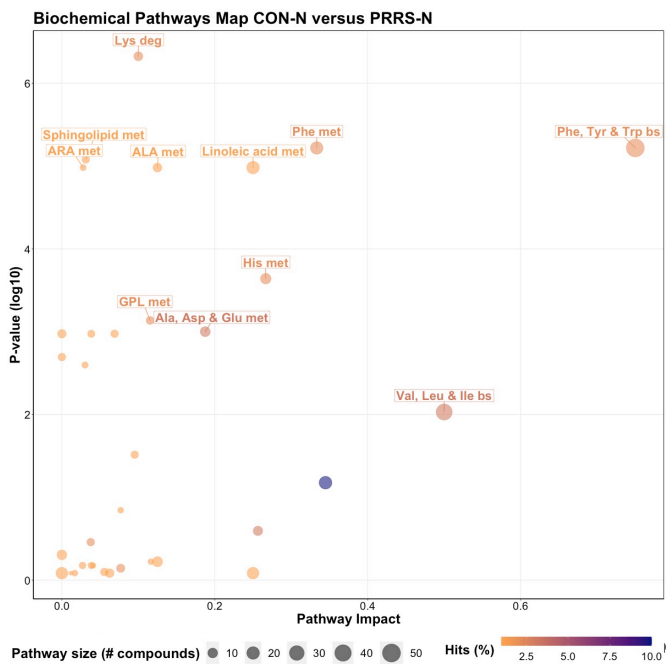
(A) Biochemical pathway plot displaying the most significant (Y-axis;  $P$ -value $<0.05$ ) and impactful (X-axis) pathways distinguishing the groups. Size of dot represents the size of the pathway (number of compounds). Dark colors (from light orange to dark purple) represent higher hits (percentage of the pathway detected in our study). (B) Boxplots of the concentration of significant ( $P$ -value $<0.05$ ) compounds distinguishing the groups. (C) Two component PLS-DA score plots with individual fetuses represented by dots. (D) Variance Importance in Projection (VIP) score plots displaying the 15 most important metabolites differentiating groups with colored side bar displaying the relative metabolite concentration in each group. 1.CON-N: non-IUGR (normal development) fetuses from non-inoculated control gilts; 2.CON-IUGR: IUGR fetuses from non-inoculated control gilts. Met=metabolism, bs=biosynthesis, deg=degradation, Por= Porphyrin, CHLA= chlorophyll, GSH= Glutathione, GPL= Glycerophospholipid, ALA=alpha-Linoleic acid, ARA=arachidonic acid, SeC= Selenocompound. LysoPC= lysophosphocholine, PC=phosphocholine, SM= sphingomyelin.

4.4.2.2. *Control-normal versus PRRS-normal*: This contrast highlighted differences between control and infected fetuses exhibiting normal fetal development. The most impactful pathways in this contrast related to amino acids sphingolipids and arachidonic acid metabolism (**Figure 4.8A-B**). Not surprisingly, the groups were significantly different ( $P < 5e-04$ ; 0/2000 permutations) based on the PLS-DA analysis (**Figure 8C**; 2 components,  $R^2=0.60$ ,  $Q^2=0.40$ ) and similar to the infected versus non-infected (CTRL x UNINF, UNINF x HVL-VIA) contrasts of the disease progression experiment described above (**Figures 4.2 and 4.3**), but with important differences. Firstly, kynurenine was not a prominent metabolite distinguishing group (**Figure 4.8D**) where it had the second highest VIP score in UNINF x HVL-VIA contrast. Secondly, phenylalanine was the only amino acid with a high VIP score in this contrast whereas there were five amino acids with high VIP scores in the CTRL x UNINF and UNINF x HVL-VIA comparisons. Alpha-AAA scored prominently in all, highlighting it as a major biomarker of PRRSV infection of the fetus, being consistently elevated in fetal sera following infection.

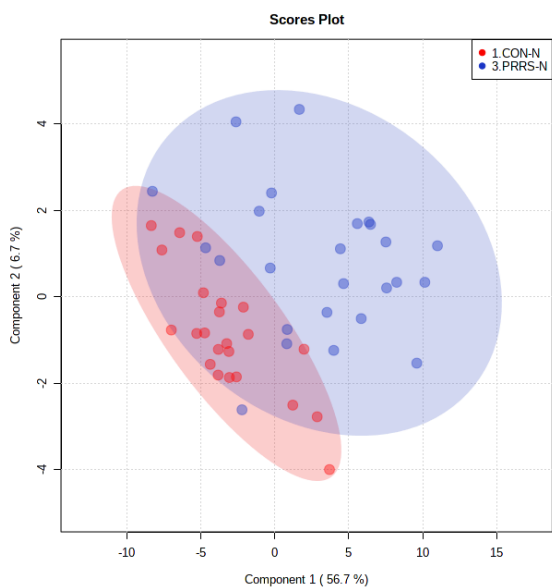
A

## Contrast CON-N vs PRRS-N

B



C



D

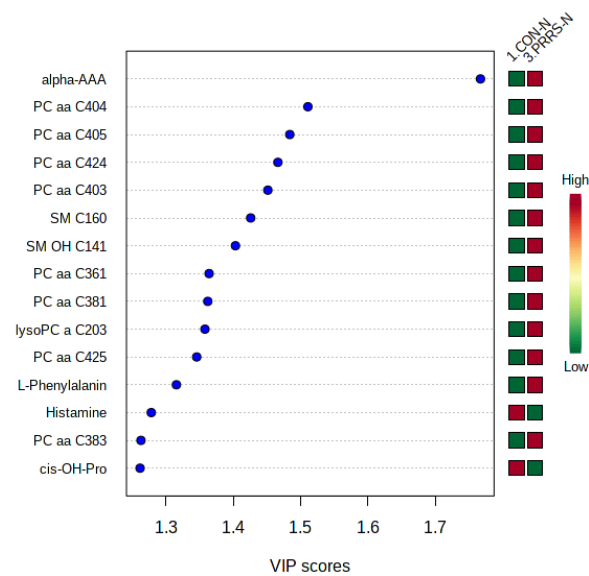


**Figure 4.8:** Metabolite profile of control-normal development fetuses (CON-N) and PRRS-infected normal development fetuses (PRRS-N).

(A) Biochemical pathway plot displaying the most significant (Y-axis;  $P$ -value<0.05) and impactful (X-axis) pathways distinguishing the groups. Size of dot represents the size of the

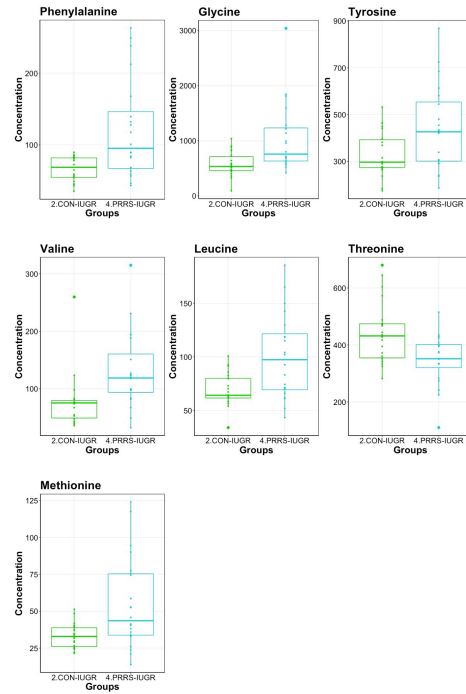
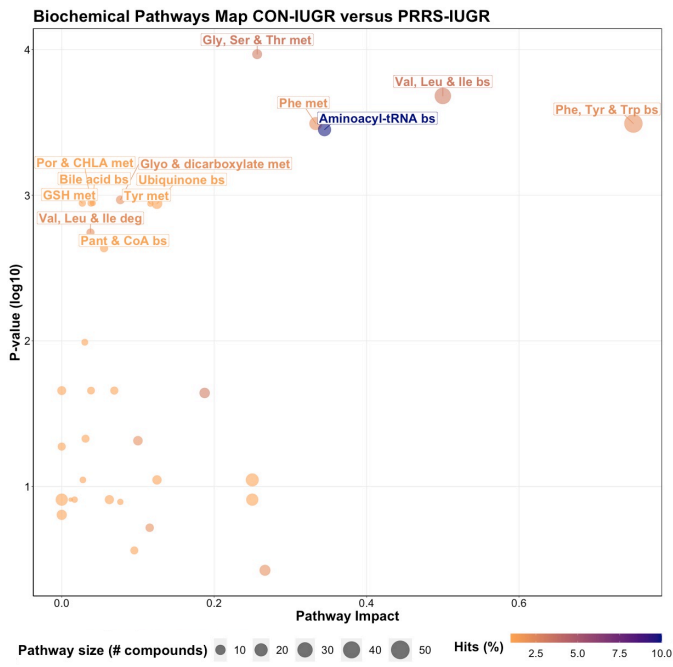
pathway (number of compounds). Dark colors (from light orange to dark purple) represent higher hits (percentage of the pathway detected in our study). (B) Boxplots of the concentration of significant ( $P$ -value<0.05) compounds distinguishing the groups. (C) Two component PLS-DA score plots with individual fetuses represented by dots. (D) Variance Importance in Projection (VIP) score plots displaying the 15 most important metabolites differentiating groups with colored side bar displaying the relative metabolite concentration in each group. 1.CON-N: non-IUGR (normal development) fetuses from non-inoculated control gilts; 3.PRRS-N: non-IUGR fetuses from PRRSV-infected gilts. Met=metabolism, bs=biosynthesis, deg=degradation, Por= Porphyrin, CHLA= chlorophyll, GSH= Glutathione, GPL= Glycerophospholipid, ALA=alpha-Linoleic acid, ARA=arachidonic acid, SeC= Selenocompound. Alpha-AAA=alpha-aminoadipic acid, cis-OH-Pro=cis-4-Hydroxy-L-proline, lysoPC= lysophosphocholine, PC=phosphocholine, SM= sphingomyelin.

4.4.2.3. *Control-IUGR versus PRRS-IUGR*: This contrast aimed to display the metabolic differences in response to infection in the fetal IUGR population. A number of amino acid related pathways were altered between these groups (**Figure 4.9A**) with amino acid levels typically greater in the PRRSV-infected group (**Figure 4.9B**). Group differences were significant ( $P=0.001$ ; 3/2000 permutations) based on the PLS-DA analysis (3 components,  $R^2=0.55$ ,  $Q^2=0.26$ ), possibly related to the extremely diverse global metabolome of the PRRS-IUGR group (**Figure 4.9C**) or that the PRRS response in IUGR fetuses was fundamentally different than the normally developed cohorts. Six of the top 15 VIP score metabolites distinguishing these groups were amino acids. Others included carnitines C0, C2, C14:1) and some lysoPCs and SMs (**Figure 4.9D**). Kynurenine had the highest VIP score, while alpha-AAA ranked 7th, scoring under 2.

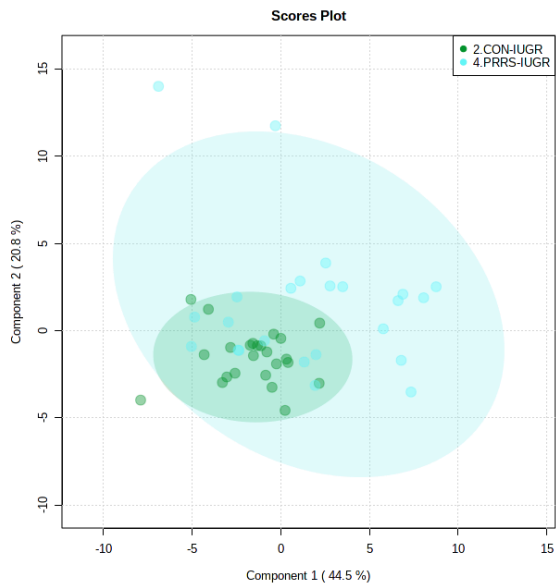
A

Contrast CON-IUGR vs PRRS-IUGR

B



C



D

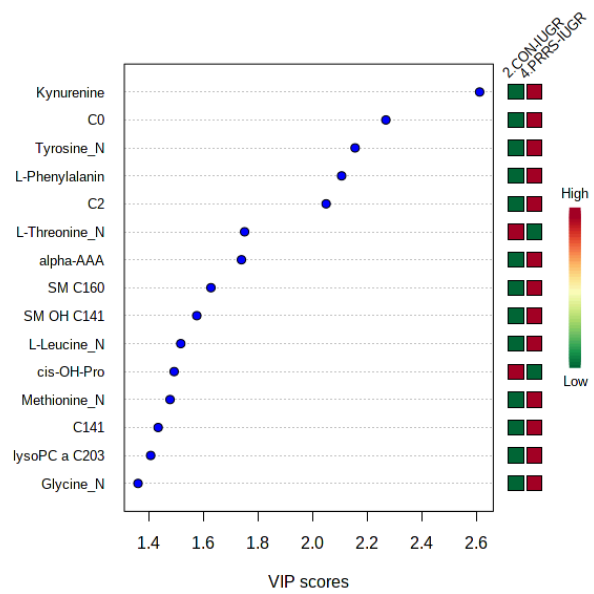


**Figure 4.9:** Metabolite profile of control-IUGR (CON-IUGR) and PRRS-infected IUGR fetuses (PRRS-IUGR).

(A) Biochemical pathway plot displaying the most significant (Y-axis;  $P$ -value $<0.05$ ) and impactful (X-axis) pathways distinguishing the groups. Size of dot represents the size of the pathway (number of compounds). Dark colors (from light orange to dark purple) represent higher hits (percentage of the pathway detected in our study). (B) Boxplots of the concentration of significant ( $P$ -value $<0.05$ ) compounds distinguishing the groups. (C) Two component PLS-DA score plots with individual fetuses represented by dots. (D) Variance Importance in Projection (VIP) score plots displaying the 15 most important metabolites differentiating groups with colored side bar displaying the relative metabolite concentration in each group. 2.CON-IUGR: IUGR fetuses from non-inoculated control gilts; 4.PRRS-IUGR: IUGR fetuses from PRRSV-infected gilts. Met=metabolism, bs=biosynthesis, deg=degradation, Por= Porphyrin, CHLA= chlorophyll, GSH= Glutathione, GPL= Glycerophospholipid, ALA=alpha-Linoleic acid, ARA=arachidonic acid, SeC= Selenocompound. C0: carnitine, C2: acetylcarnitine, C141=tetradecenoyl carnitine, cis-OH-Pro=cis-4-Hydroxy-L-proline, lysoPC= lysophosphocholine, SM= sphingomyelin.

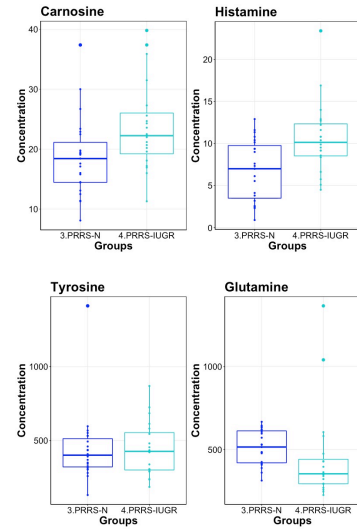
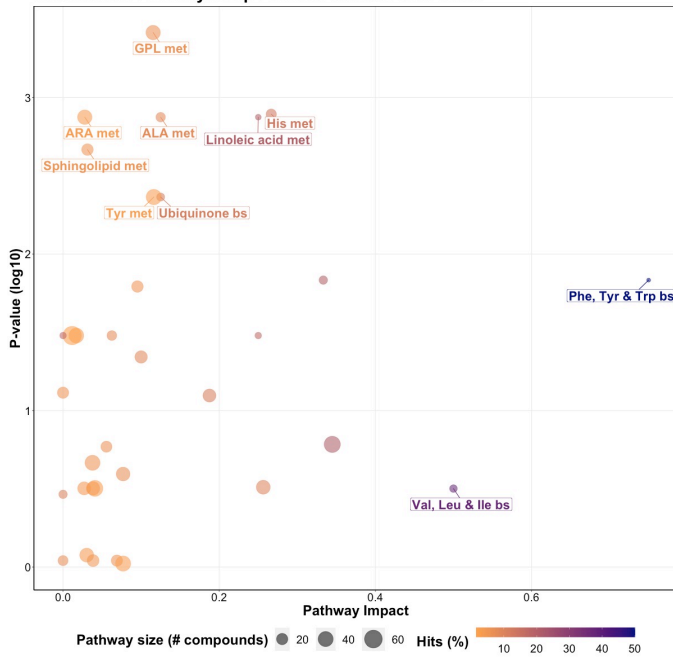
4.4.2.4. *PRRS-normal versus PRRS-IUGR*: This contrast highlighted differences between normal and IUGR fetuses after maternal PRRSV infection. The diverging pathways between these two groups were mainly related to amino acid metabolism, as well as sphingolipids and arachidonic acid metabolism (**Figure 4.10A**), however, only four amino acids differed significantly between group (**Figure 4.10B**), lower than other the previous contrasts. Whereas the IUGR versus non-IUGR contrast in control fetuses found three amino acids among the prominent metabolites distinguishing group, only one amino acid scored in the top 15 metabolites distinguishing non-IUGR and IUGR fetuses following maternal PRRSV infection (**Figure 4.10C-D**). Group separation and differences ( $P=0.001$ ; 2/2000 permutations) by PLS-DA analysis (4 components,  $R^2=0.73$ ,  $Q^2=0.54$ ) were mainly related to differences in lysoPCs, PCs, and SM concentration, all decreased in the PRRS-IUGR group, with the exception of histamine and cis-4-Hydroxy-L-proline (cis-OH-Pro).

A

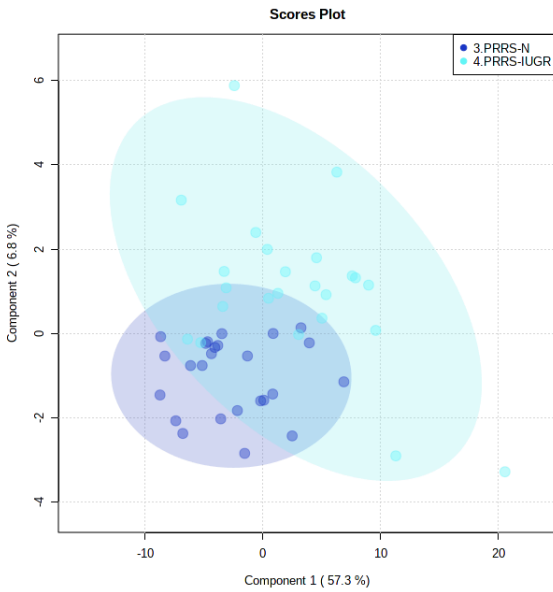
Contrast PRRS-N vs PRRS-IUGR

B

Biochemical Pathways Map PRRS-N versus PRRS-IUGR



C



D

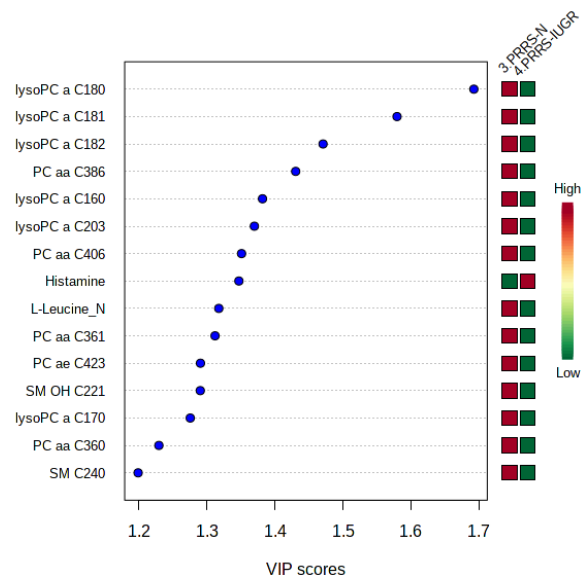


**Figure 4.10:** Metabolite profile of PRRS-infected normal development fetuses (PRRS-N) and PRRS-infected IUGR fetuses (PRRS-IUGR).

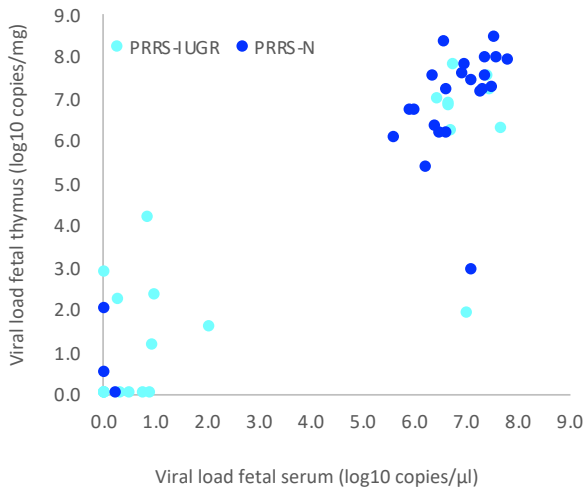
(A) Biochemical pathway plot displaying the most significant (Y-axis;  $P$ -value $<0.05$ ) and impactful (X-axis) pathways distinguishing the groups. Size of dot represents the size of the pathway (number of compounds). Dark colors (from light orange to dark purple) represent higher hits (percentage of the pathway detected in our study). (B) Boxplots of the concentration of significant ( $P$ -value $<0.05$ ) compounds distinguishing the groups. (C) Two component PLS-DA score plots with individual fetuses represented by dots. (D) Variance Importance in Projection (VIP) score plots displaying the 15 most important metabolites differentiating groups with colored side bar displaying the relative metabolite concentration in each group. 3.PRRS-N: non-IUGR fetuses from PRRSV-infected gilts; 4.PRRS-IUGR: IUGR fetuses from PRRSV-infected gilts. Met=metabolism, bs=biosynthesis, deg=degradation, Por= Porphyrin, CHLA= chlorophyll, GSH= Glutathione, GPL= Glycerophospholipid, ALA=alpha-Linoleic acid, ARA=arachidonic acid, SeC= Selenocompound. LysoPC= lysophosphocholine, PC=phosphocholine, SM= sphingomyelin.

#### 4.4.3. Exploring PRRS IUGR group diversity

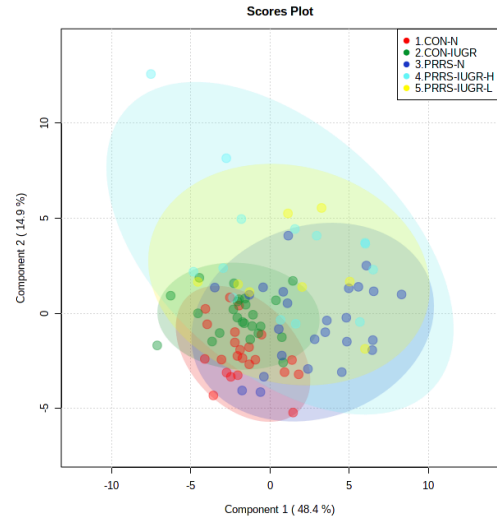
The wide heterogeneity of the PRRS-IUGR group prompted further investigation to determine if it was associated with viral infection. While all PRRS-N fetuses were PRRSV-infected and the majority (22/25) had high viral concentration in fetal serum and thymus, the PRRS-IUGR group was comprised of fetuses with high (10/24), low (9/24) or non-detectable (5/24) viral load in sera or thymus (**Figure 4.11A**), largely because IUGR fetuses are protected from PRRSV infection<sup>70</sup> and were sparse. After splitting the PRRS-IUGR into high (PRRS-IUGR-H) and low/negative (PRRS-IUGR-L) viral load subgroups, 78 metabolites significantly differed (FDR < 0.01) amongst the five groups based on Kruskal-Wallis testing and group differences were significant based on PLS-DA analysis (3 components, R<sup>2</sup>=0.60, Q<sup>2</sup>=0.40)( $P < 5e-04$ ; 0/2000 permutations)(**Figure 4.11B**). However, no significant ( $P=0.351$ ; 703/2000 permutations) differences between the high and low viral load subgroups were evident on the two-group PLS-DA contrast (3 components, R<sup>2</sup>=0.63, Q<sup>2</sup>=0.16) (**Figure 4.11C**). Kynurenine was the most distinguishing metabolite being higher in PRRSV-IUGR-H fetuses (**Figure 4.11D**) corresponding to higher levels of viral infection. There was a variety of other metabolites with high VIP scores including leucine and glutamine (increased in PRRS-IUGR-H subgroup), while creatinine and several lysoPC/PCs were all increased in PRRS-IUGR-L subgroup.

A summary of the most important metabolite alterations related to the interaction of PRRSV-infection and IUGR is shown in **Figure 4.12**.

A

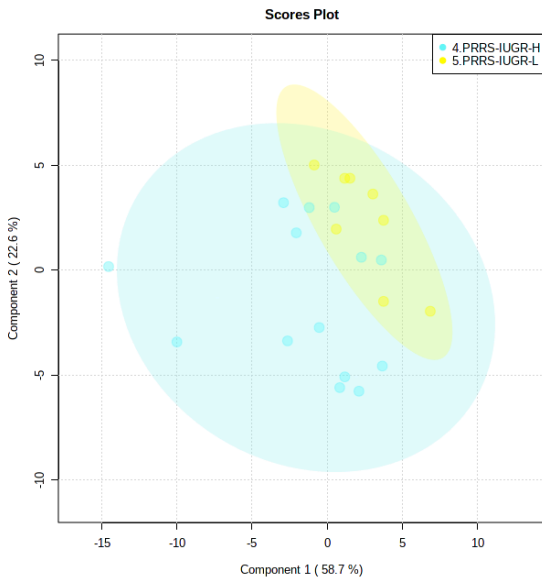


B



Contrast of high (H) vs low (L) viral load fetuses in PRRS-IUGR group

C



D

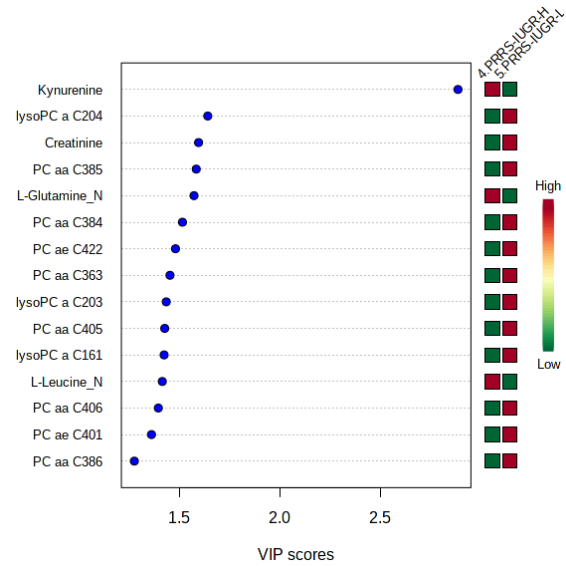


**Figure 4.11:** Analysis of the PRRSV-IUGR group as two subgroups based on PRRS viral concentration.

(A) PRRSV viral load in thymus and serum of PRRSV infected IUGR and non-IUGR/normal (N) fetuses. (B) Two component score plot PLS-DA plot of all PRRS x IUGR groups with

PRRS-IUGR subdivided into high (H) and low (L) viral load subgroups. (C) Two component PLS-DA score plots of the PRRS-IUGR high (H) and low (L) sub-groups only. (D) Variance Importance in Projection (VIP) score plots displaying the 15 most important metabolites differentiating high and low viral load groups with colored side bar displaying the relative metabolite concentration in each group. 1.CON-N: non-IUGR (normal development) fetuses from non-inoculated control gilts; 2.CON-IUGR: IUGR fetuses from non-inoculated control gilts; 3.PRRS-N: non-IUGR fetuses from PRRSV-infected gilts; 4.PRRS-IUGR-H: high viral load subgroup; and 5.PRRS-IUGR-L: low/negative viral load subgroup. lysoPC= lysophosphocholine, PC=phosphocholine.

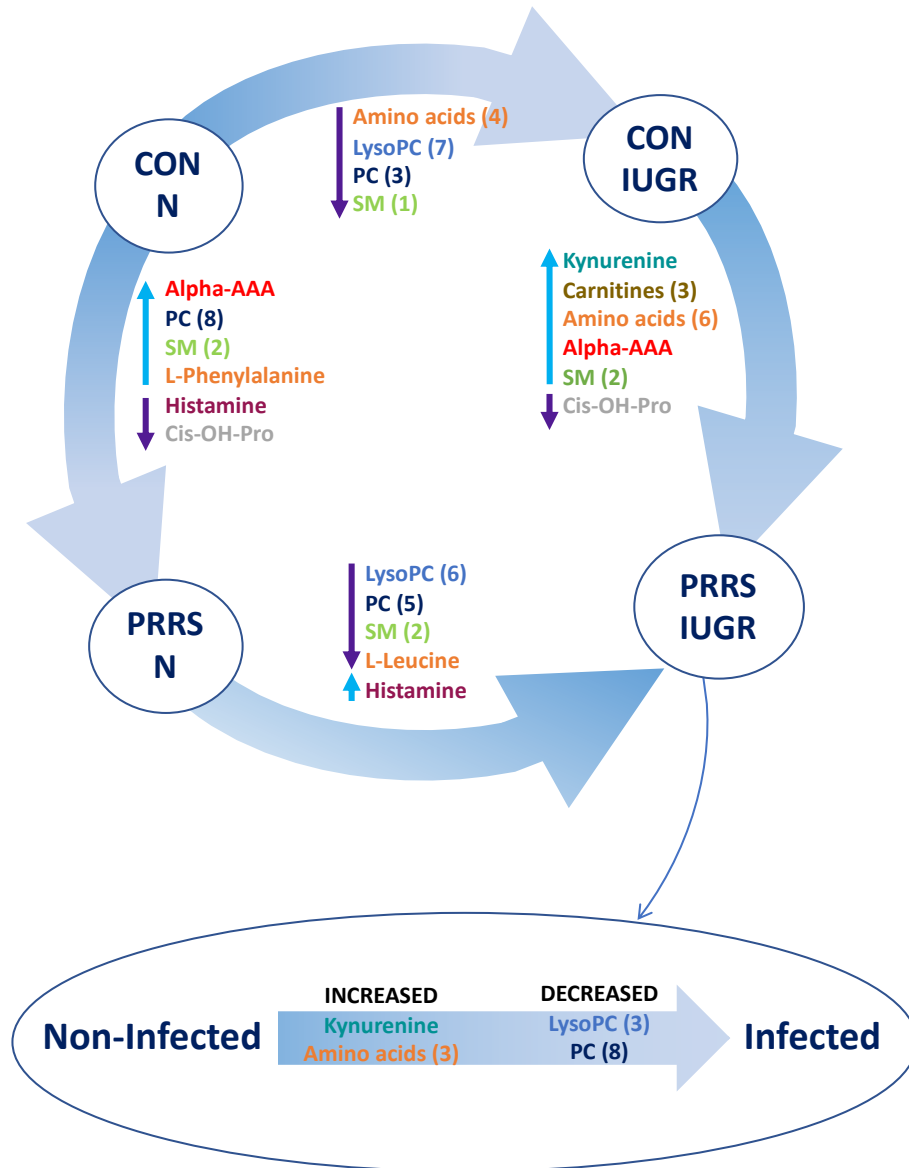


**Figure 4.12:** Visual summary of the most significant metabolite changes associated with PRRSV-infection of fetuses with normal development or intrauterine growth retardation (IUGR). 1.CON-N: non-IUGR (normal development) fetuses from non-inoculated control gilts; 2.CON-IUGR: IUGR fetuses from non-inoculated control gilts; 3.PRRS-N: non-IUGR fetuses from PRRSV-infected gilts; and 4.PRRS-IUGR: IUGR fetuses from PRRSV-infected gilts. Alpha-AAA=alpha-aminoadipic acid, cis-OH-Pro=cis-4-Hydroxy-L-proline, lysoPC=lysophosphocholine, PC=phosphocholine, SM= sphingomyelin.

#### 4.5. Discussion

This global metabolomics profiling utilized archived fetal serum to explore the progression of disease and the impact of fetal development following PRRSV infection. To our knowledge, this is the first research describing alterations in the global metabolome of fetal pigs during maternal PRRSV infection and one of the first studies to investigate fetuses experiencing IUGR which are naturally resilient to prenatal PRRSV infection. As such, it provides novel insights into PRRS virus infection as well as for infective diseases in pigs and other livestock species.

An important initial finding with respect to PRRS disease progression is that most of the VIP metabolites were at high levels in control fetuses (CTRL), lower in UNINF fetuses, and increased again in the PRRSV-infected groups (HVL-VIA and MEC). With respect to the interaction of PRRSV and fetal development, higher metabolite levels were observed in non-IUGR versus IUGR fetuses as well as in PRRSV-infected versus non-infected groups. These results suggest fetal responses are influenced by both factors.

Following maternal PRRSV-challenge, virus quickly infects the uterine tissues, then transmits across maternal uterine and fetal trophoblast epithelial layers to placental tissue and fetal circulation.<sup>92</sup> The rate of transplacental transmission varies and some fetuses escape infection while others succumb to infection resulting in varied fetal outcomes along a susceptibility-resilience spectrum.<sup>36</sup> UNINF fetuses are most resilient and dead fetuses most susceptible. In the present research, however, dead fetuses were not included because it was not possible to collect high quality blood samples. Thus, our proxy for susceptible fetuses were those affected by meconium staining of skin, a clinical sign associated with PRRS disease progression,<sup>49</sup> and imminent death in the most severe cases.

In spite of being more resilient to PRRSV-infection, UNINF fetuses responded to maternal infection in agreement with past research showing differentially expressed genes related to innate and inflammatory responses in fetal thymus following infection of the endometrium.<sup>63</sup> One of the most important metabolites distinguishing UNINF from CTRL fetuses was alpha-AAA. Alpha-AAA was also a predominant metabolite in other PRRSV-infected groups (HVL-VIA, PRRS-N, PRRS-IUGR) compared to non-infected (CTRL, CON-N, CON-IUGR). It is a key compound in the lysine biosynthesis and degradation pathways. A number of amino acid biosynthesis and degradation metabolism pathways were also significantly

altered between the PRRSV-infected and non-infected groups indicating a disruption in amino acids' pathways or the energy cycle (tricarboxylic acid cycle; TCA).

Although it is not yet completely understood how PRRSV crosses the maternal-fetal interface (MFI) to infect fetuses,<sup>40</sup> IUGR fetuses have lower viral loads than fetuses with normal intrauterine growth (non-IUGR).<sup>70,92</sup> Intrauterine growth retardation in swine may result from many genetic, epigenetic, maternal and environmental factors as previously reviewed.<sup>25</sup> Impaired placental growth is one of the most important factors associated with IUGR, which has a negative impact on placental size and blood flow, resulting in a lower nutrient transport to the fetus compared to its regular sized siblings. This likely explains the lower levels of metabolites in the IUGR groups in this study. It is also possible that virus enters the fetal compartment from the dam by transiting through the maternal and fetal epithelial layers. In fact, PRRSV is capable of entering and exiting trophoblastic epithelium *in vitro* by vesicle-mediated intercellular communication,<sup>107</sup> supporting this hypothesis. If fetal infection does rely on mechanisms of intercellular communication inherent to epithelial cells, the placental inefficiency underlying fetal growth retardation may be a protective factor against PRRSV transplacental infection. Consistent with placental inefficiency, many lysoPCs and PCs were decreased in UNINF, CON-IUGR and PRRS-IUGR fetuses. Biosynthesis of these compounds can be regulated by the availability of certain amino acids.<sup>108</sup> The lower amino acid levels (possibly some essential) in these groups compared to CON and non-IUGR groups might result in lower levels of the PCs and lyso PCs as well. Besides their natural biochemical pathway (glycerophospholipid metabolism),<sup>109</sup> lysoPCs and PCs can be used to synthesize arachidonic acid in response to tumor necrosis factor alpha (TNF-alpha). Arachidonic acid metabolism, which is significantly different between groups in most contrasts, is the precursor of eicosanoids, like prostaglandin E, among many others<sup>110</sup> that can work as pro-inflammatory molecules and the lack of those compounds might serve as a protective factor for the UNINF and IUGR fetuses or may reflect the lack of nutrition.

Several contrasts in the present study (UNINF vs HVL-VIA, CTRL-N vs PRRS-N, CON-IUGR vs PRRS-IUGR) demonstrate the fetus' first reaction to PRRSV-infection. While alpha-AAA was increased in fetuses following PRRSV-infection, kynurenine was the predominant metabolite increased in HVL-VIA fetuses. Kynurenine is a biproduct of tryptophan metabolism regulated by the enzyme Indoleamine 2,3-Dioxygenase (IDO1).<sup>111</sup> IDO1 can be induced by

increased levels of TNF-alpha, IFN-gamma and IFN-beta,<sup>63,112</sup> cytokines normally elevated in response to PRRSV infection.<sup>35,50,113</sup> Thus, the high levels of kynurenine would be expected following fetal infection and may be a potential biomarker for differentiating resilient from susceptible fetuses following PRRSV infection. Although alpha-AAA does not appear in the main metabolic pathways related to response to infection, its high concentration in PRRSV-infected groups implies it may be a potential biomarker to differentiate uninfected/control from infected fetuses.

The SM group of compounds was increased in the PRRSV-infected fetuses, and sphingolipid metabolism pathway significantly impacted in a number of groups contrasts. These compounds are part of lipid rafts on cell membranes, which are involved in PRRSV cell entry, replication and release in the host.<sup>114</sup> Thus, the elevated level of SMs might be a response to infection, causing a high recruitment of these compounds. Alternatively, as these are important to the viral replication cycle in the host and can change the availability and function of the receptor CD163,<sup>114</sup> animals with greater concentration of SMs on their cell surfaces may be more susceptible to infection.

The contrast HVL-VIA versus MEC reflects progression of disease to the point of compromise prior to fetal death. Most of the significantly different metabolites increased in MEC fetuses were PCs and SMs. SMs are compounds that crosslink a PC to ceramide.<sup>115</sup> During inflammation, increased levels of TNF-alpha activate the sphingomyelinase enzyme (SMase) which induces the breakdown of the SMs releasing ceramides<sup>116</sup> and PCs, explaining the higher levels of PCs observed in PRRSV-infected fetuses. Ceramides can play a key role in activating apoptosis and recently have also been linked to necroptosis (programmed cell necrosis).<sup>116,117</sup> Thus, activation of this pathway during a sustained inflammatory response would eventually lead to apoptosis of fetal cells, compromising fetal tissues.

Histamine was the only metabolite that was decreased in MEC compared to HVL-VIA fetuses. Histamine is a well-known compound involved in allergic responses which can lead to anaphylactic reactions and is released by mast cells in most tissues when in contact with an antigen.<sup>118</sup> It has been shown that mast cells can release histamine during an early primary response to viral infection.<sup>119</sup> While histamine was significantly decreased in MEC compared to HVL-VIA fetuses, it was also numerically increased in HVL-VIA versus UNINF fetuses

consistent with a response to PRRSV infection and highlighting its potential as a biomarker of fetal PRRSV infection.

Other contrasts and comparisons could be investigated using different combinations of the groups, however, we opted to focus on disease progression (uninfected to infected to high viral load to meconium staining in a stepwise manner) as per our objective for this study. Moreover, several other metabolites were significantly altered in specific contrasts, however, not all had a plausible biological link to PRRSV infection or fetal development. In spite of an extensive literature search, the mechanisms underlying some of the metabolite alterations observed in the phenotypic contrasts described herein were not readily apparent. Such examples include acetic acid, ethanol, glutamine, creatinine, and carnitine in the contrast between PRRS-IUGR H and -L groups. Thus, we have limited our discussion to the metabolic alterations we believe provide a meaningful addition to the current knowledge of PRRS pathogenesis. It's also important to acknowledge the limitations of the AbsoluteIDQ® p180 Kit used in this study, which is limited to detect only the groups of compounds included in the kit (comprised of 180 analytes in total). However, the kit was designed to be a reliable and robust tool to detect and quantify a broad spectrum of metabolites. Although the biochemical pathway maps provide a general vision of the differences between groups, it is important to acknowledge they are limited to the kit's targeted detection system.

#### **4.6. Conclusions**

For the first time, differences in the fetal metabolome of PRRSV-infected and non-infected fetuses were investigated. Clear differences were observed between contrasting resilience phenotypes, helping to elucidate mechanisms involved in fetal compromise and death. The lower levels of amino acids in UNINF fetuses possibly suggest a lower placental efficiency of these animals, which might protect them from PRRSV infection. Increased alpha-AAA and kynurenine levels in HVL-VIA fetuses are potential markers of susceptibility to PRRSV infection. The increased concentration of PCs in MEC fetuses may be a result of the degradation of the SMs and production of ceramides, and may be a marker of the compromised animals after viral infection. Fetuses experiencing normal in utero growth appear to have an increased level of lysoPCs, PCs and amino acids compared to IUGR fetuses, which might indirectly reflect greater intercellular communication across the maternal-fetal interface leading to higher risk of viral

infection, while the almost complete absence of lysoPCs and PCs, even during infection, in the IUGR animals may indicate a different and perhaps muted response to infection associated with fetal growth retardation. These results bring novel insights into some possible mechanisms occurring in fetuses at various stages following maternal viral infection as well as elucidating new potential markers of fetal resilience to PRRSV infection.

## **Declarations**

**Acknowledgements:** The authors gratefully acknowledge the assistance of Rupasri Mandal and BoemSoo of The Metabolomics Innovation Centre, University of Alberta, in addition to the VIDO/Intervac and the large number of technicians and students that assisted with the animal experiment enabling this research.

**Declaration and competing interests:** The authors declared no potential conflicts of interest regarding the research, authorship, and publication of this article.

**Funding:** This project was supported by grants from Genome Canada (Project 2014LSARP\_8202) and Genome Prairie (Saskatchewan Ministry of Agriculture, Project #346143) and administrative support from Genome Alberta. The sponsors had no role in study design, execution, analysis or interpretation of the results.

**Data availability:** The data has been uploaded to a public repository:  
[www.ebi.ac.uk/metabolights/MTBLS2249](http://www.ebi.ac.uk/metabolights/MTBLS2249).

## **5. Fetal hypoxia and apoptosis following maternal porcine reproductive and respiratory syndrome virus (PRRSV) infection**

As the results from Chapter 4 indicated disturbance in cell death related pathways and with a history of hypoxia being considered a putative cause for fetal death following PRRSV infection, this experiment aimed to investigate both apoptosis and hypoxia in fetal tissues to better understand fetal death mechanisms at 12 DPI. We identified the fetal heart is the most affected tissue after PRRSV fetal infection, displaying alterations in hypoxia and apoptosis related genes, as well as elevated DNA fragmentation (indication of apoptosis). Fetal brain presents with indications of apoptosis, while fetal thymus appears to be protected at this post-infection time point.

**Copyright:** This Chapter has been submitted for publication. The copyright of this Chapter will belong to the journal it is published in.

**Citation:** Malgarin CM, Moser F, Pasternak JA, Hamonic G, Detmer SE, MacPhee DJ, and Harding J. Fetal hypoxia and apoptosis following maternal porcine reproductive and respiratory syndrome virus (PRRSV) infection. *BMC Veterinary Research*, 2021. Submitted, November 26, 2020.

### **Authors' contribution:**

CMM: experimental design, sample collection, tissue RNA extraction, primer design, RT-qPCR analyses, TUNEL data analysis, statistical analysis, manuscript preparation; FM: sample collection, TUNEL staining, imaging, and quantification; JAP, GH, SED, DJM, JH: experimental design, sample collection; JAP: tissue RNA extraction, primer design; JH: principal investigator, project design and management, sample collection, financial management, statistical analysis, manuscript preparation.

## 5.1. Abstract

Mechanisms of fetal death following maternal PRRSV2 infection remain uncharacterized, although hypoxia from umbilical cord lesions and/or placental detachment due to apoptosis are hypothesized. We performed two experiments examining hypoxia and apoptosis in PRRSV-infected and non-infected, third-trimester fetuses to elucidate possible associations with fetal death. Fetuses were selected based on four phenotypic infection groups: fetuses from non-challenged control gilts (CTRL); low viral load fetuses (LVL; Exp 1) or uninfected fetuses (UNINF; Exp 2) from inoculated gilts; viable high viral load fetuses (HVL-VIA); and HVL meconium-stained fetuses (HVL-MEC). In experiment 1, paraffin embedded fetal tissues collected 21 days post maternal infection (DPI) were examined for DNA fragmentation associated with apoptosis. Positively stained foci were larger and more numerous ( $P<0.05$ ) in heart, liver, and thymus of HVL-VIA and HVL-MEC compared to CTRL and LVL fetuses. In experiment 2, group differences in gene expression within the hypoxia (HIF1a, IDO1, VEGFa, LDHA, NOS2, NOX1) and apoptosis (CASP3, CASP7, CASP8, CASP9, RIPK1, RIPK3) pathways were assessed by RT-qPCR in fetal tissues collected at 12 DPI. High viral load fetuses showed differential expression relative to the CTRL and UNINF ( $P<0.05$  for all). Brain tissue from HVL-VIA and HVL-MEC fetuses presented increased expression of CASP7, CASP8, RIPK3, HIF1a and IDO1. Fetal heart showed increased expression of CASP8, HIF1a, IDO and NOX1 and a decrease in NOS2 expression in infected groups. CASP7, CASP9, RIPK1 and RIPK3 were only increased in the heart of HVL-VIA while VEGFa was only increased for HVL-MEC fetuses. Thymus from HVL-MEC had decreased expression of CASP9 and there was increased IDO1 in all infected fetuses. There is strong evidence of apoptosis occurring in the heart, liver and thymus of highly viral load fetuses at 21 DPI. Furthermore, there was clear upregulation of apoptotic genes in the heart of high viral load infected fetuses and less prominent upregulation in the brain of PRRSV-infected fetuses, whereas thymus appears to be spared at 12 DPI. There was no strong evidence of hypoxia at 12 DPI in brain and thymus but some indication of hypoxia occurring in fetal heart.

**Key words:** swine, fetus, apoptosis, hypoxia, TUNEL, PRRS, gene expression.

## 5.2. Background

Porcine reproductive and respiratory syndrome (PRRS) remains the most impactful viral pig disease in North America due to the heavy financial burden it has caused the pork industry.<sup>68</sup> Responsible for 45% of the economic losses, the reproductive form of the disease following PRRSV infection of sows during late gestation is characterized by abortions, fetal death, weak-born fetuses, and high pre-weaning mortality.<sup>32</sup> The mechanisms of fetal disease are not entirely understood and few studies have explored this topic, in part due to the lack of obvious fetal lesions.<sup>34,51</sup> Following maternal infection, PRRSV rapidly infects the endometrium and crosses the epitheliochorial placenta to the fetus.<sup>72,92</sup>

We have previously reported that fetal serum is infected by 5 days after maternal inoculation (DPI) and fetal thymus by 8 DPI when fetal compromise first appeared.<sup>92</sup> Although gross and histopathologic lesions of infected fetuses have been characterized previously,<sup>34,39,48,51</sup> few studies have investigated possible mechanisms leading to fetal death after maternal PRRSV infection.

Due to the low frequency and inconsistency of fetal lesions, many studies have explored the maternal-fetal interface (MFI) for pathophysiological factors affecting fetal viability. Inflammatory lesions, placental detachment from endometrium, and apoptosis have been explored in both endometrium and placenta; however, none have proven directly responsible for fetal death.<sup>37,39,44-46,48,53</sup> Due to the infrequent but consistent finding of peri-vascular umbilical lesions in dead fetuses, hypoxia has also been proposed as a leading cause of fetal losses, due to the blood flow disruption.<sup>34,48</sup> This is supported by the observation that the odds of meconium-staining of fetal skin,<sup>39</sup> an indication of fetal stress and early clinical sign of fetal compromise, is associated with the presence of umbilical cord and fetal lesions.<sup>39</sup>

Apoptosis is a normal physiological process responsible for programmed cell death in a selective manner, which when deregulated can lead to pathology and death.<sup>120</sup> Frequently used to investigate apoptosis, the terminal deoxynucleotidyl transferase (TdT) dUTP nick end labeling (TUNEL) assay detects DNA fragmentation due to apoptosis. TUNEL has been previously applied in PRRSV studies to assess severity of apoptosis in infected tissues and to associate the severity of apoptosis to PRRSV viral load in placental tissue from infected pregnant gilts at 21 DPI.<sup>45</sup> In addition, this methodology has been used to demonstrate that PRRSV cell infection

not only results in apoptosis of the infected cells, but also induces apoptosis of surrounding non-infected cells at 10 DPI.<sup>46</sup>

Although the pathophysiologic events occurring in the endometrium and placenta following maternal infection may contribute to fetal compromise, fetal death may also involve events compartmentalized to the fetal side. The absence of fetal lesions in many compromised and dead fetuses<sup>39</sup> raises questions about events occurring at a cellular and subcellular level in fetal tissues. RNA-Seq has been utilized and shown that the fetal thymus responded to infection by mounting an innate immune response, followed by an inflammatory response.<sup>63</sup> In a targeted gene expression study,<sup>113</sup> IFNB, IFNG, CCL2, CCL5, CXCL10 and IL10, were upregulated in fetal tissues of high viral load fetuses at 21 DPI, although only CCL5 was elevated in more than one tissue from high viral load meconium-stained fetuses compared to high viral load viable fetuses, indicating that fetal immune response is not the main cause of fetal death. Nonetheless, a suppression of the cell cycle coupled with an increase in cardiac stress were found in the hearts of high viral load fetuses at 21 DPI.<sup>121</sup> More recently, differential expression analysis of some 283 immune related genes using the NanoString platform on placental and thymic tissues from fetuses at different stages of infection demonstrated response in either tissues was only initiated following infection of the fetus per se.<sup>122</sup>

With these indications that fetal demise might be influenced by events occurring not only on the maternal side, but also in the fetal compartment, we aimed to determine if there was evidence of apoptosis and hypoxia in fetal tissues and if it was more pronounced in compromised (meconium-stained) fetuses. We designed two studies, firstly to assess apoptosis in fetal tissues collected between PRRSV-infected and non-infected fetuses at 21 days post-infection (DPI); and secondly, to determine differences in gene expression related to apoptosis and hypoxia in PRRSV-infected and non-infected fetuses collected at 12 DPI. Both experiments used the best available tissues archived from PRRSV pregnant gilt challenge studies conducted at the University of Saskatchewan, Canada.

### **5.3. Material and Methods**

#### *5.3.1. Experiment 1: Apoptosis in fetal tissue at 21 DPI*

5.3.1.1. *Animals:* Animal work was conducted in strict accordance with the guidelines of the Canadian Council of Animal Care and with approval of the University of Saskatchewan's Animal Research Ethics Board (Protocol #20110102). This project has been described in detail elsewhere and complied to the ARRIVE Guidelines (<https://arriveguidelines.org/arrive-guidelines>) where feasible.<sup>49</sup> In short, 133 purebred Landrace gilts bred to York boars were transported, in bi-weekly repetitions, to a biocontainment level 2 (BCL2) animal facility at University of Saskatchewan at day 80 of gestation. After 5 days of acclimation, 114 randomly selected gilts were inoculated with  $1 \times 10^5$  TCID<sub>50</sub> PRRSV NVSL 97–7895; 2 mL intramuscular (IM) and 1 mL into each nostril. Nineteen gilts were mock inoculated with minimal essential medium to serve as control animals.

5.3.1.2. *Sample collection:* At 21 DPI, gilts were humanly euthanized by intravenous barbiturate overdose followed by cranial captive bolt and exsanguination. The uterus was removed, placed linearly and opened enabling fetal assessment. Fetuses were identified and numbered in accordance with their position in the right or left uterine horn. Their preservation status was determined as: viable (VIA live, normal skin color), meconium-stained (MEC; live, normal skin covered with meconium), decomposed (DEC; dead, pale skin, sometimes edematous), autolyzed (AUT; dead, pale or dark skin, friable or liquefied organs) or mummified (MUM; dehydrated, dark brown color, crown-rump length < 20 cm). Samples were not collected from AUT and MUM fetuses. From all other fetuses, liver (LVR), heart apex (HRT), and thymus (THY) were collected into 10% buffered formalin for routine histopathologic processing. Serum (SER) and THY were collected and frozen at -80 °C for PRRSV RNA quantification.

5.3.1.3. *PRRS virus quantification and group selection:* PRRSV was quantified in fetal THY and SER by RT-qPCR as previously described.<sup>49</sup> Briefly, RNA was extracted from 140 µL SER using the QIAamp Viral RNA mini kit (Qiagen Inc., Toronto, ON) or from 10–20 mg THY using the RNeasy extraction kit (Qiagen Inc.) according to the manufacturer's instructions. Primers targeting the C-terminal end of ORF7 of NVSL 97–7895 were designed and a HindIII linearized plasmid, pCR2.1TOPO-NVSL, containing a 446 bp sequence of ORF7 serial dilution was used as a standard curve. The Master mix (Brilliant II RT-qPCR Low ROX 1-Step Master Mix, Agilent technologies Canada Inc., Mississauga, ON) was used and the reactions were run

on a Stratagene MX3500P (Agilent Technologies, Mississauga, ON). Results were transformed to log (base 10). PRRSV-infected viable fetuses were further divided into a low viral load viable group (LVL-VIA, n=25) with viral load (VL) lower than 4.1 log<sub>10</sub> copies/μL or mg in both SER and THY (19/25 or 76% had less than 1 log), and a high VL viable group (HVL-VIA, n=25) group with viral load (VL) higher than 5.0 log<sub>10</sub> copies/μL or mg. In addition, a HVL-MEC group (n=25) was selected to represent the most PRRSV-susceptible set of fetuses. Viral load by group is graphically displayed in Additional file 2. In addition to meeting viral load criteria, nearly all fetuses had been included in a previous study<sup>45</sup> investigating apoptosis at the maternal fetal interface using the TUNEL assay. As much as possible, infected fetuses from multiple phenotypic groups were nested within litter. In fulfillment of these criteria, the 75 LVL-VIA, HVL-VIA and HVL-MEC fetuses originated from 48 PRRSV-challenged gilts (23 providing more than 1 fetal group). Control (CTRL) fetuses (n=25) were derived from 6 non-challenged gilts (4-5 per gilt) and all were included in the previous apoptosis study of MFI tissues.<sup>45</sup>

*5.3.1.4. TUNEL assay of fetal tissues:* As previously described,<sup>45</sup> formalin-fixed paraffin embedded fetal organ samples were deparaffinized and rehydrated, followed by protein digestion using Proteinase K solution (15 min). Hydrogen peroxide (3%) was applied (5 min) to block endogenous peroxidase activity, followed immediately by application of the equilibration buffer provided with the ApopTag Plus Peroxidase In Situ Apoptosis Detection Kit (Millipore Canada Ltd., Etobicoke, Ontario) for 10 sec at room temperature. Terminal deoxynucleotidyl transferase (TdT) enzyme was then applied at 37°C for 1 hour in a humidity chamber. Slides were rinsed and the signal was revealed using 3-Amino-9-Ethylcarbazole (AEC) chromogen for 15 min. The whole slides were scanned at 20X magnification using OlyVIA (Olympus Corp., Tokyo, Japan), and converted to JPEG format. Image conversion was conducted using ImageJ (version 1.50i) and the quantitative analysis of TUNEL positive staining was completed using ImagePro Premier software (Media Cybernetics, Inc., Rockville, MD, USA) using the parent-child application for ten random microscopic fields for heart, brain and thymus.

*5.3.1.5. Statistical analysis:* The raw count data was exported to Microsoft Excel and Stata (StataCorp, College Station, TX) to categorize TUNEL positive staining counts by foci size and to calculate the average foci size per μm<sup>2</sup> of tissue for each size category. Three size

categories were established: “large foci” above 23  $\mu\text{m}^2$ ; “medium foci” between 5 and 23  $\mu\text{m}^2$ ; and “small foci” below 5  $\mu\text{m}^2$ . The “small foci” category was removed from further analyses because they were considered artifacts, or not related to cell-associated PRRSV infection, as PRRSV infection is restricted to porcine alveolar macrophages or differentiated blood monocytes<sup>123</sup>, which measure between 15-20  $\mu\text{m}^2$ . Data was tested for normality using the Shapiro-Wilk test. Differences among the fetal groups in the number of positive TUNEL positive foci counts for each tissue were examined using Kruskal-Wallis and post hoc Dunn’s tests and a Benjamini-Hochberg multiple comparison adjustment. The strength of relationship between fold changes of each target gene and MFI lesions was assessed using Spearman’s rank correlation test, with significance  $P < 0.05$ , and correlation as: none ( $\rho = 0$ ), weak ( $0.1 < |\rho| < 0.3$ ), moderate ( $0.3 < |\rho| < 0.6$ ), strong ( $0.6 < |\rho| < 0.9$ ), and perfect ( $|\rho| > 0.9$ ) for both positive and negative correlations[41]. The pathologic evaluation and scoring of the MFI samples was previously published by Novakovic.<sup>45</sup>

### 5.3.2. *Experiment 2: Apoptosis and hypoxia gene expression in fetal tissues at 12 DPI*

5.3.2.1. *Animals:* Animal work was conducted in strict accordance with the guidelines of the Canadian Council of Animal Care and with approval of the University of Saskatchewan’s Animal Research Ethics Board (Protocol #20160023). This project has been described elsewhere.<sup>121</sup> Briefly, 36 purebred Landrace gilts bred to York boars were purchased at 80 days of gestation from the same high health, PRRSV-free farm as used in Experiment 1. For each of six weeks, six gilts were transferred to a BCL2 animal facility at the University of Saskatchewan. After five days of acclimation, five gilts blocked by sire were inoculated (INOC) as previously described for “Experiment 1”. One gilt housed in a separate room was similarly mock inoculated with minimum essential medium (CTRL). In total, 30 gilts were INOC and six gilts served as CTRL.

5.3.2.2. *Sample collection:* After 12 DPI, gilts were euthanized and necropsied as described for Experiment 1, as was fetal preservation classification and sample collection. In addition, placenta (PLC) was manually separated from the endometrium (END) and along with fetal brain (BRN) were snap frozen in liquid nitrogen.

5.3.2.3. *PRRS virus quantification and group selection:* Virus concentration was measured in PLC, SER and THY for each fetus, as previously described<sup>92</sup> and followed the same viral extraction procedures as Experiment 1. Thereafter, a one-step reverse transcriptase qPCR kit (iTaq Universal Probes 1-Step Kit, BioRad, Mississauga, Canada) was employed for the absolute quantification of viral RNA, using the same primers,<sup>49</sup> standard curve, and quality control samples as in Experiment 1. Based on the quantification results, the fetuses were further classified as uninfected (UNINF) representing the fetuses from inoculated gilts that had no detectable infection, and as high viral load (HVL) with viral load over 4.5 log<sub>10</sub> target RNA copies per mg or µL in PLC, SER, and THY. Tissues including brain (BRN, n=12/group, total=48), HRT (n=8-16/group, total=47) and THY (n=7-8/group, total=31) were selected from fetuses of four phenotypic groups based on the preservation status of the fetus and its viral load in PLC, SER, and THY: control fetuses from non-inoculated gilts (CTRL, n=30); viable fetuses from inoculated gilts that escaped infection (UNINF, n=33); viable high viral load fetuses (HVL-VIA, n=24); and high viral load meconium-stained fetuses (HVL-MEC, n=36) (Additional file 3). The number of fetuses per group differed slightly because final selection of samples for analyses was dependent on mRNA integrity, as explained below.

5.3.2.4. *mRNA extraction and cDNA library generation:* Under liquid nitrogen, the selected fetal tissues were individually ground and RNA extracted using a double precipitation method employing Trizol (Thermofisher Scientific, Carlsbad, Canada), followed by DNase (Thermofisher Scientific, Carlsbad, Canada) treatment. RNA purity was determined using nanodrop spectrophotometry (Thermofisher Scientific, Carlsbad, Canada) and a denaturing agarose gel electrophoresis was used to determine mRNA integrity.<sup>124</sup> Only high-quality samples with discrete 18S and 28S rRNA bands were further analyzed. A cDNA library was created using 2 µg of RNA following instructions for the High-Capacity cDNA Reverse Transcription kit (Thermofisher Scientific, Carlsbad, Canada).

5.3.2.5. *RT-qPCR:* Genes of interest were selected based on their involvement in response to infection (IDO1), hypoxia (HIF-1α, VEGF α, LDHA, NOS2, and NOX1) and apoptosis (CASP3, CASP7, CASP8, CASP9, RIPK1, and RIPK3). The primers were designed based on

the *Sus Scrofa* 11.1 genome assembly to match all transcript variants of the RefSeq mRNA sequences and positioned to span exon-exon junctions, when possible (**Table 5-1**). Eleven housekeeping genes (RPL19, HPRT1, GAPDH, ACTB, HMBS, YWHAZ, IPO8, STX5, SDHA, PPIA, and TBP ) previously designed<sup>113</sup> were tested in each tissue and the most stable ones were used for further analyses, as follow: brain – HPRT, IPO8, YWHAZ; heart – RPL19, SDHA, STX5; and thymus - RPL19, SDHA, STX5. All primers were tested and approved with efficiency over 90% and presenting a single peak melting curve. Samples were run in duplicate, each containing 20ng of cDNA, by real time PCR using the SsoFast EvaGreen Supermix (BioRad) and CFX qPCR system (BioRad), 95°C for 2 min followed by 40 cycles of 95°C for 10 sec and individual primer set melt temperature (**Table 5-1**) for 45 sec.

5.3.2.6. *Statistical analyses:* The geometric mean of the most stable housekeeping genes in each tissue was used to normalize the expression data. Fold change of each gene of interest was calculated using the  $2^{-\Delta\Delta C_t}$  method and univariate non-parametric analysis (Kruskal Wallis followed by pairwise Wilcoxon rank sum test and Bonferroni correction) was performed to determine group differences within genes. All statistical analyses were performed in R,<sup>125</sup> data visualization was conducted with the ggplot2<sup>126</sup> package and observed statistical differences ( $P < 0.05$ ) marked by unique superscripts. The strength of relationship between target genes fold changes and the MFI lesions was assessed using Spearman's rank correlation test as described above for "Experiment 1" using MFI lesion scores (unpublished data) based on the same scoring previously described.<sup>45</sup>

**Table 5-1:** Porcine specific primer sequences used to assess fetal apoptosis and hypoxia.

PATHWAY	TARGET	NCBI GENE ID	FORWARD PRIMER	REVERSE PRIMER	TM (°C)	LENGTH (BP)
Apoptosis	CASP3	397244	5'-GTGGGATTGAGACGGACAGT	5'-TTCGCCAGGAATAGTAACCA	60	114
			-3'	G-3'		
	CASP7	10015677 7	5'-TCGGTGCAAGACCCTTTTAG-	5'-GCCTGGAAGTGTGGAATAGG-	60	178
			3'	3'		
	CASP8	595105	5'-GGAAGTCTTTTCCGAATGA-	5'-AGCATGACCCTGTAGGCAGA-	60	126
			3'	3'		
	CASP9	10051891 3	5'-TCTGCCACACCTAGTGACA-	5'-ACAGCATTGGAGACCCTGAG-	60	171
			3'	3'		
RIPK1	10052475 1	5'-ATCCTGTACGGCAACTCTGG-	5'-GGTGGTGTTCGAAGATGG-	60	147	
		3'	3'			
RIPK3	10015326 3	5'-AATAGGCCCTCCTCCAAGA-	5'-CTCACGGACAGACAACAAGC-	60	162	
		3'	3'			

Infection	IDO1	10051987 7	5'-	5'-	60	139
			GCTGTCAGAGGGTCTGCTCT-	TGAAGGAACTCCACCCACAG-		
			3'	3'		
Hypoxia	HIF1 $\alpha$	396696	5'-	5'-	59	180
			GGCAGCAATGACACAGAAA	CTGATTGAGTGCAGGGTCAG-		
			C-3'	3'		
			5'-	5'-		
	VEGF $\alpha$	397157	CAACATCGCCATGCAGATTA	GCATTCACATTTGTTGTGCTG-	60	91
			-3'	3'		
			5'-	5'-		
	NOX1	10073982 2	TCCCTTTACCCTGACCTCTG-	TCCACCTCAATCCTTGGAAC-	60	132
			3'	3'		
			5'-	5'-		
	NOS2	396859	CTGTGAGACGTTTCGATGTCC-	GCTGCTGAGAGCTTTGTTGA-	59	139
			3'	3'		
			5'-	5'-		
	LDHA	407245	TTCACCCCCTAAGCTGTCAT-	TAAGCACTGTCCACCACCTG-	60	178
			3'	3'		

---

## 5.4. Results

### 5.4.1. Experiment 1: Differences in apoptosis in fetal tissues at 21 DPI

In total, 100 fetuses were analyzed for apoptotic foci in LVR, THY and HRT. Only one fetus (HVL) had no TUNEL positive staining in THY, although its LVR had many TUNEL positive TUNEL foci. Only 8 fetuses had TUNEL positive staining in the HRT, all belonging to the HVL-MEC group. TUNEL staining foci were moderately to widely distributed in fetal THY and LVR and less abundant in the fetal HRT (**Figure 5.1**). The limited TUNEL staining in the control group was within normal expectations (Additional file 1).

In the liver, TUNEL positive staining was distributed in all areas and found in hepatocyte nuclei (**Figure 5.1**). The mean size of TUNEL positive foci (**Figure 5.2A**) in the liver was significantly ( $P=0.0009$ ) larger in the HVL-VIA and HVL-MEC groups ( $20 \pm 6.7 \mu\text{m}^2$  and  $21 \pm 5 \mu\text{m}^2$ , respectively) compared to the CTRL and LVL groups ( $17 \pm 3 \mu\text{m}^2$  and  $16 \pm 4.2 \mu\text{m}^2$ , respectively). The number of TUNEL positive foci (**Figure 5.2B**) was significantly ( $P=0.0004$ ) greater in HVL-VIA and HVL-MEC fetuses (average  $86.9 \pm 107.4$  and  $68.3 \pm 32$ , respectively) compared to the CTRL (average  $48.9 \pm 36.8$ ) and LVL (average  $46.5 \pm 66.1$ ) groups.

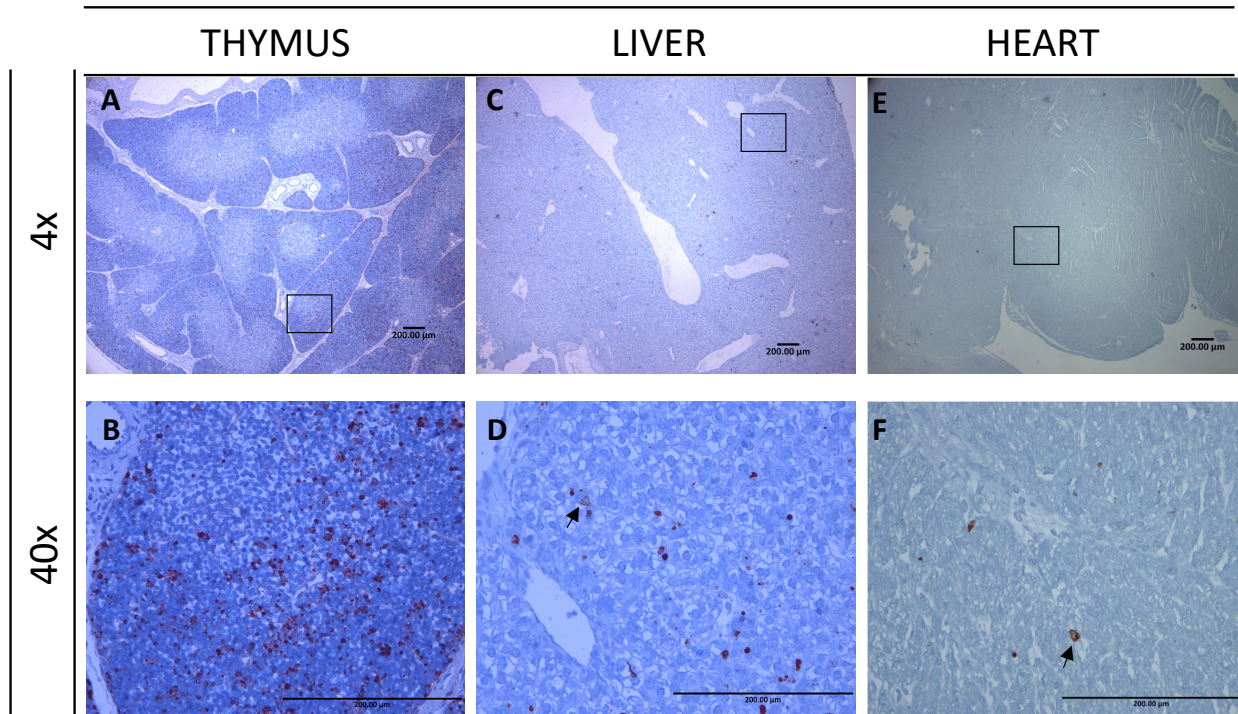


**Figure 5.1:** TUNEL staining in three fetal tissues of PRRSV-infected fetuses.

(A) Diffuse areas of apoptosis on fetal thymus; (B) Higher magnification fetal thymus to display apoptosis (arrow) in thymocytes; (C) Areas with multiple apoptosis staining on fetal liver; (D) Higher magnification fetal liver to display apoptosis (arrow) in hepatocytes; (E) Focal spots of apoptosis in the fetal heart (arrow); (F) Higher magnification fetal heart to display apoptosis (arrow) in myocytes.

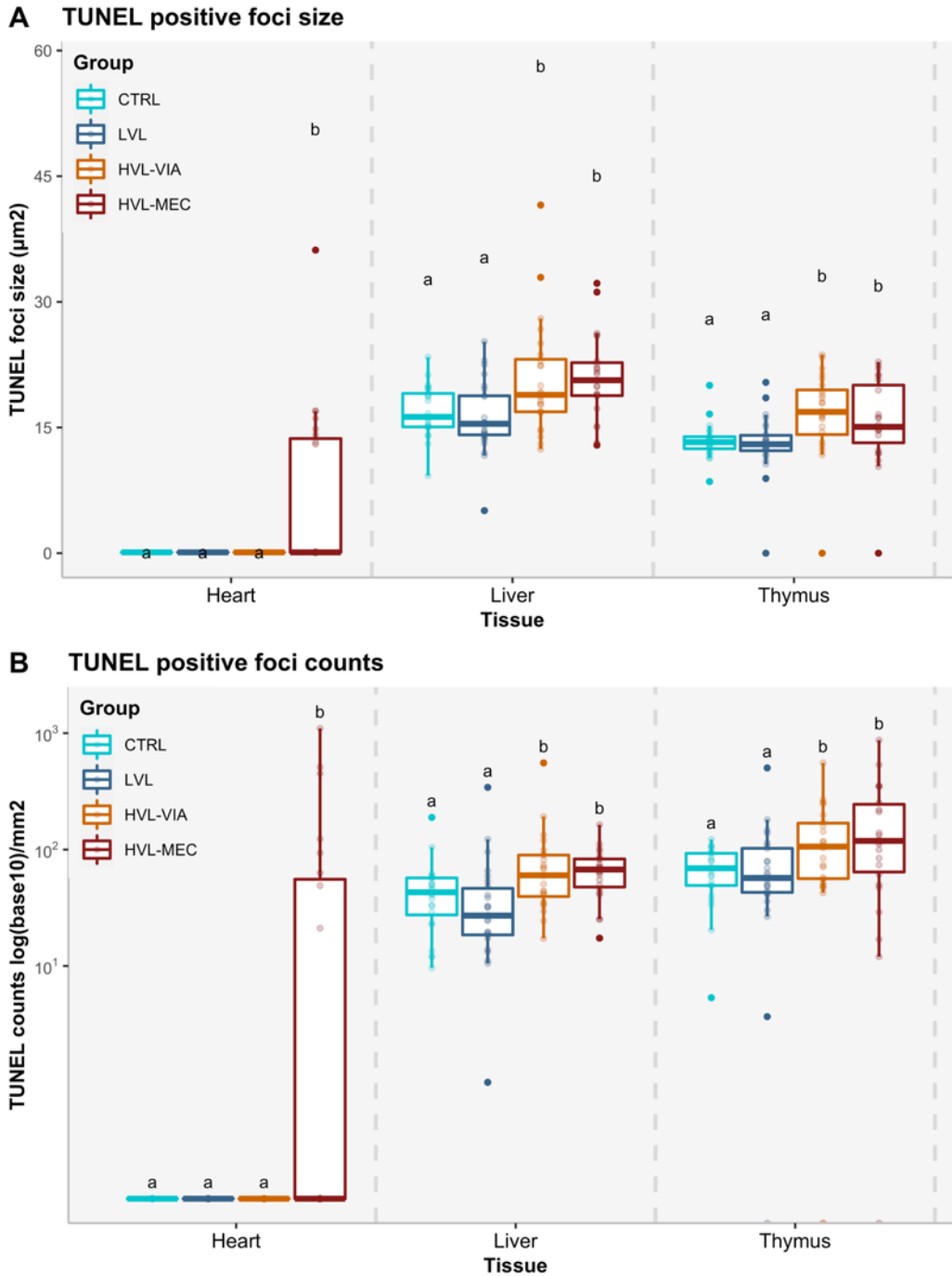


**Figure 5.2:** Box-and-whisker plot of TUNEL positive foci counts and sizes by group. The Y-axis presents the size or counts, the X-axis presents the tissues analyzed. Each group is represented by a different colour. (A) Size of TUNEL positive foci/ $\mu\text{m}^2$  in fetal heart, liver and thymus and (B) counts/ $\text{mm}^2$  of TUNEL positive staining.

In thymus, TUNEL positive cells were diffusely distributed along the cortical and cortico-medullar regions, located in the thymocytes, mostly as single cell staining and rarely presenting in clusters. The number of stained foci differed among groups ( $P=0.009$ ) with the CTRL and LVL groups having similar counts;  $66.2 \pm 29.6$  and  $87.5 \pm 95.7$  positive stained foci on average, compared to  $131.4 \pm 118.7$  and  $192.5 \pm 202.3$  positive stained foci for the HVL-VIA and HVL-MEC groups, respectively. Furthermore, the mean size of TUNEL positive foci in thymus was significantly ( $P=0.0002$ ) larger in the highly infected animals (HVL-VIA =  $16.8 \pm 5.9 \mu\text{m}^2$  and HVL-MEC =  $16.3 \pm 5.1 \mu\text{m}^2$ ) compared to the CTRL and LVL-VIA animals ( $13.5 \pm 2.1 \mu\text{m}^2$  and  $13.3 \pm 3.6 \mu\text{m}^2$ , respectively).

Only eight of the 100 fetal hearts, all from HVL-MEC fetuses, had any positive TUNEL staining and in these fetuses the staining was located in the cardiomyocytes. The mean number of TUNEL positive foci were  $301.5 \pm 373.9$  in HVL-MEC fetuses. The average size of positive stained foci was  $17.6 \pm 7.6 \mu\text{m}^2$  for HVL-MEC fetuses.

The TUNEL staining foci size on thymus tissues was significantly correlated ( $P<0.05$ ) to vasculitis distribution and severity in MFI, as well as endometrial inflammation, previously analysed for these animals<sup>45</sup>. Similarly, the foci counts on fetal liver were also correlated to vasculitis severity in MFI. Although the correlations were not strong (**Table 5-2**), it indicates a progression in or aggravation of in fetal disease concomitant with progression of lesion severity on the MFI.

**Table 5-2:** Spearman’s rank correlation test results between liver or thymus (TUNEL foci counts or sizes) and maternal-fetal interface (MFI) lesion severity\*

	LIVER		THYMUS	
	SIZE Rho/P-value	COUNTS Rho/P-value	SIZE Rho/P-value	COUNTS Rho/P-value
<b>Vasculitis distribution</b>	0.16 / 0.11	0.19 / 0.06	<b>0.21 / 0.04</b>	0.14 / 0.18
<b>Vasculitis severity</b>	0.18 / 0.07	<b>0.24 / 0.01</b>	<b>0.24 / 0.02</b>	0.17 / 0.10
<b>Endometrial inflammation</b>	0.16 / 0.11	0.13 / 0.18	<b>0.23 / 0.02</b>	0.15 / 0.15

<b>Myometrial inflammation</b>	0.01 / 0.90	0.00 / 0.98	0.05 / 0.59	-0.09 / 0.38
------------------------------------	-------------	-------------	-------------	--------------

---

\*MFI lesion scores as previously evaluated<sup>45</sup>

#### 5.4.2. *Experiment 2: Apoptosis and hypoxia gene expression in fetal tissues at 12 dpi*

A number of genes were significantly upregulated following fetal infection ( $P < 0.05$ ). The expression of IDO1 was significantly increased in the BRN of HVL-VIA and HVL-MEC fetuses, consistent with PRRSV infection (**Figure 5.3**). HIF-1 $\alpha$  was also significantly elevated in BRN of both PRRSV-infected groups, possibly indicating the activation of hypoxia mechanisms. Additionally, significant upregulation of CASP7, CASP8 and RIPK3 genes of HVL-VIA and HVL-MEC groups indicate the activation of the apoptosis pathway in fetal BRN. The expression of no other genes differed significantly from CTRL.

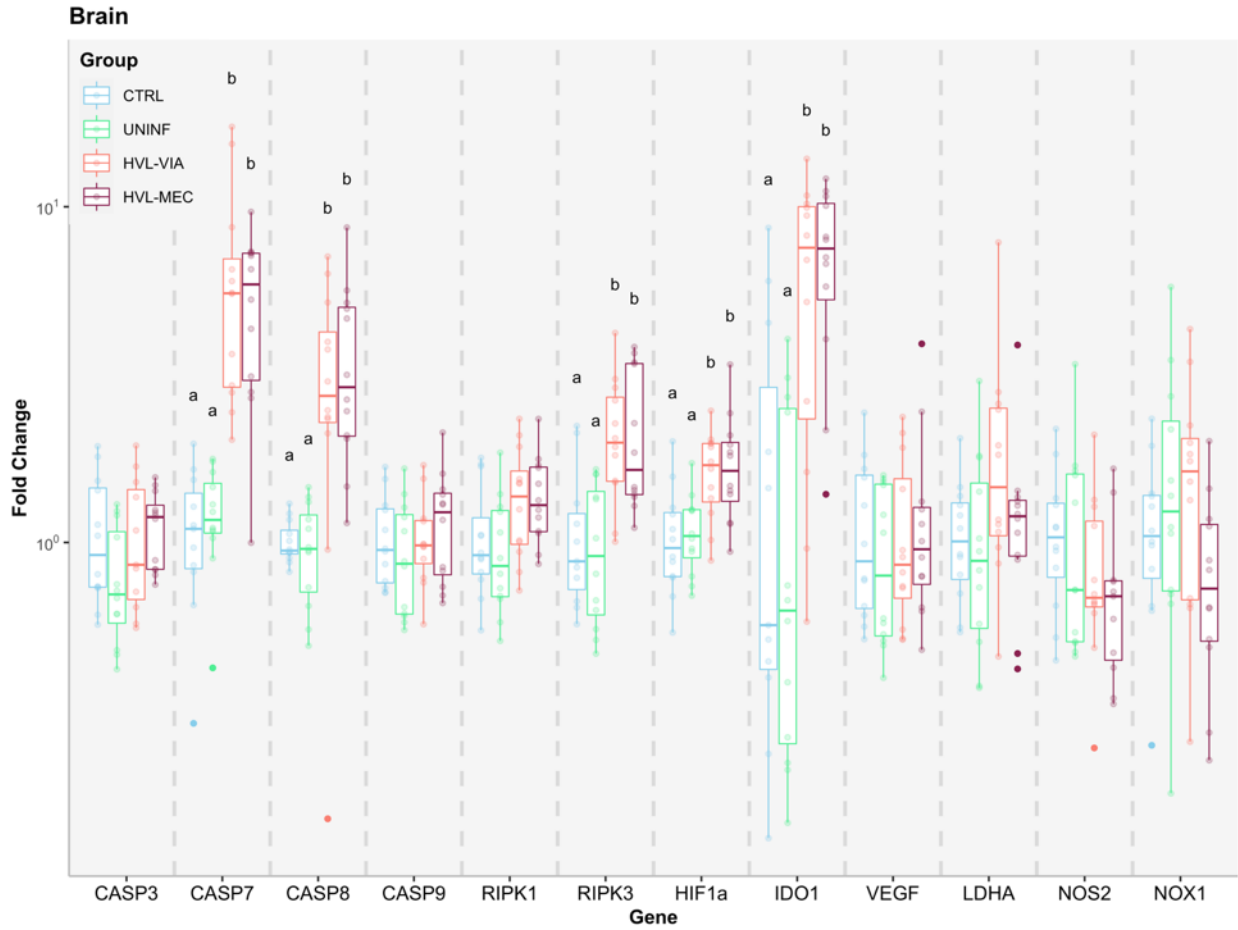


**Figure 5.3:** Apoptosis and hypoxia gene expression in fetal brain.

Box-and-whisker plot of twelve target genes analyzed in fetal brain for each of the four fetal phenotypic groups (represented by different colours). The Y-axis presents fold changes, the X-axis presents the targeted genes. Superscript letters indicate statistical differences among groups for individual genes ( $P < 0.05$ ).

Of the three tissues examined, fetal heart was the most affected (**Figure 5.4**). The expression of all tested genes except for CASP3 and LDHA were significantly ( $P < 0.05$ ) altered compared to CTRL. The marked upregulation of IDO1 (almost  $10^2$  fold change) in HVL-VIA and HVL-MEC fetuses is indicative of the infection of the HRT. The HVL-VIA group had the most significant upregulation of genes related to apoptosis (CASP7, CASP8, RIPK1, and RIPK3), whereas only CASP8 was significantly upregulated in HVL-MEC compared to both non-infected groups. CASP9 gene expression did not differ among HVL-VIA versus CTRL and UNINF groups but was significantly upregulated compared to HVL-MEC. With the exception of CASP8, HVL-MEC did not differ significantly from CTRL and also did not differ significantly from HVL-VIA in the expression of CASP7, CASP8 and RIPK1. The UNINF group had expression patterns similar to the CTRL group in most of the targeted genes but presented significant downregulation of CASP7. With regards to the hypoxia related genes, HIF-1 $\alpha$  was significantly upregulated in both HVL-VIA and HVL-MEC, while the UNINF group was intermediary between CTRL and the infected groups. The HVL-VIA group showed marked upregulated expression of NOX1, while HVL-MEC were intermediary between HVL-VIA and both non-infected groups. The only downregulated gene in the infected animals was NOS2, where HVL-MEC was significantly different from the CTRL group and HVL-VIA was intermediary between CTRL and HVL-MEC. The UNINF group was similar to the CTRL group in all genes related to hypoxia.

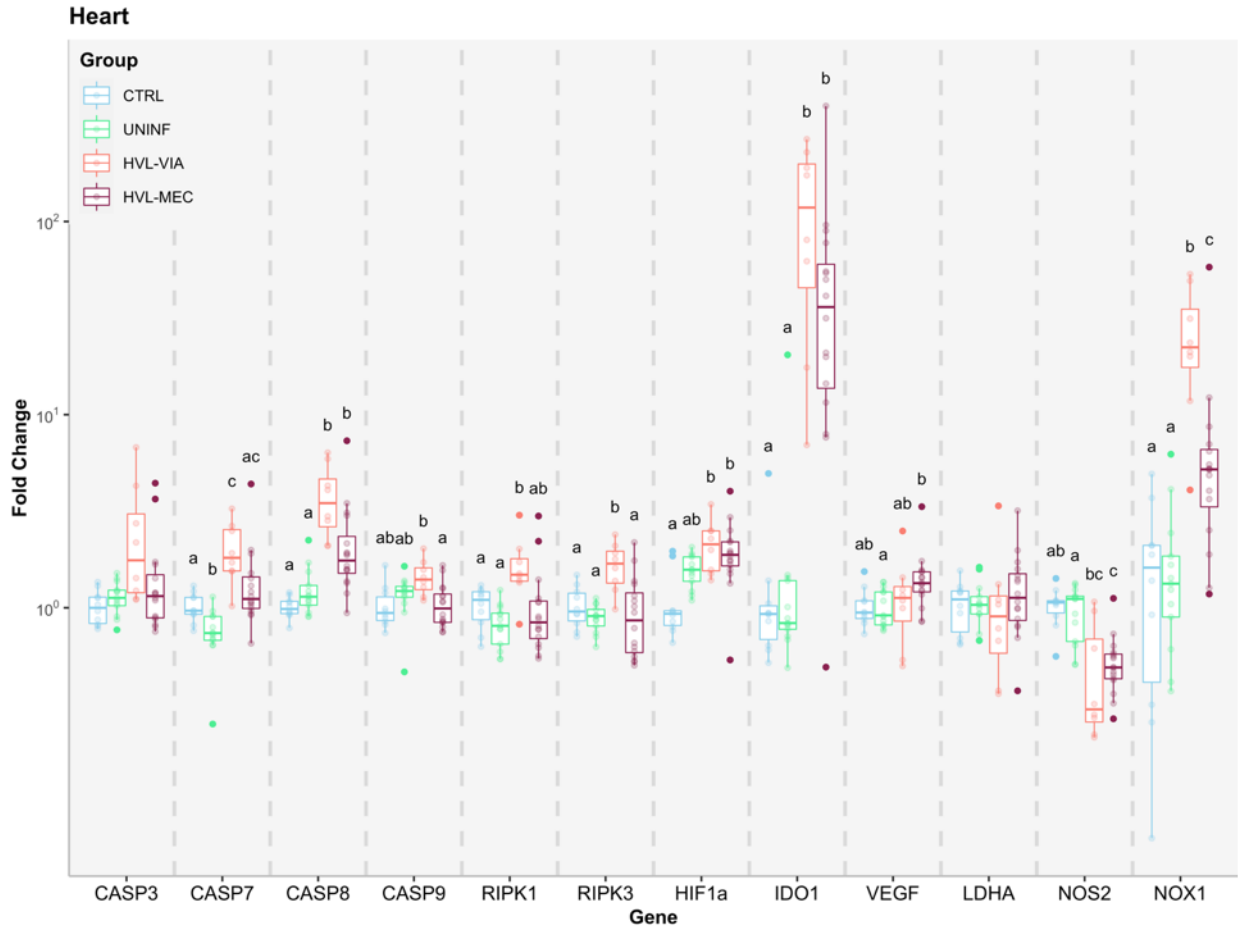


**Figure 5.4:** Apoptosis and hypoxia gene expression in fetal heart.

Box-and-whisker plot of twelve target genes analyzed in fetal heart for each of the four fetal phenotypic groups (represented by different colours). The Y-axis presents the fold change, the X-axis presents the targeted genes. Superscript letters indicate statistical differences among groups for individual genes ( $P < 0.05$ ).

Fetal thymus was the least affected tissue in this study (**Figure 5.5**). The HVL-VIA group had a significant upregulation of IDO1, consistent with PRRSV-infection. Expression of IDO1 was numerically increased in HVL-MEC except for one fetus in this group. There is no explanation for this outlier fetus (G189-R3), as the fetus was phenotypically representative of the group. Three UNINF and one CTRL fetus also had upregulated IDO1 expression despite being uninfected. The only other altered gene among groups was CASP9, which was significantly downregulated in HVL-MEC compared to the HVL-VIA, but neither of these groups differed from the CTRL and UNINF groups. Weak ( $\rho < 0.3$ ) correlation ( $P < 0.05$ ) was found between endometritis and HIF1a ( $\rho = 0.19$ ) and IDO1 ( $\rho = 0.18$ ), and between placental detachment and CASP3 ( $\rho = 0.30$ ) and NOS2 ( $-0.19$ ). No correlation was found between target genes and vasculitis in endometrium or placenta, and placentitis (unpublished data).

A heatmap summarizing the gene expression findings is presented in **Figure 5.6**.



**Figure 5.5:** Apoptosis and hypoxia gene expression in fetal thymus.

Box-and-whisker plot of twelve target genes analyzed in fetal thymus for each of the four fetal phenotypic groups (represented by different colours). The Y-axis presents the fold change, the X-axis presents the targeted genes. Superscript letters indicate statistical differences among groups for individual genes ( $P < 0.05$ ).

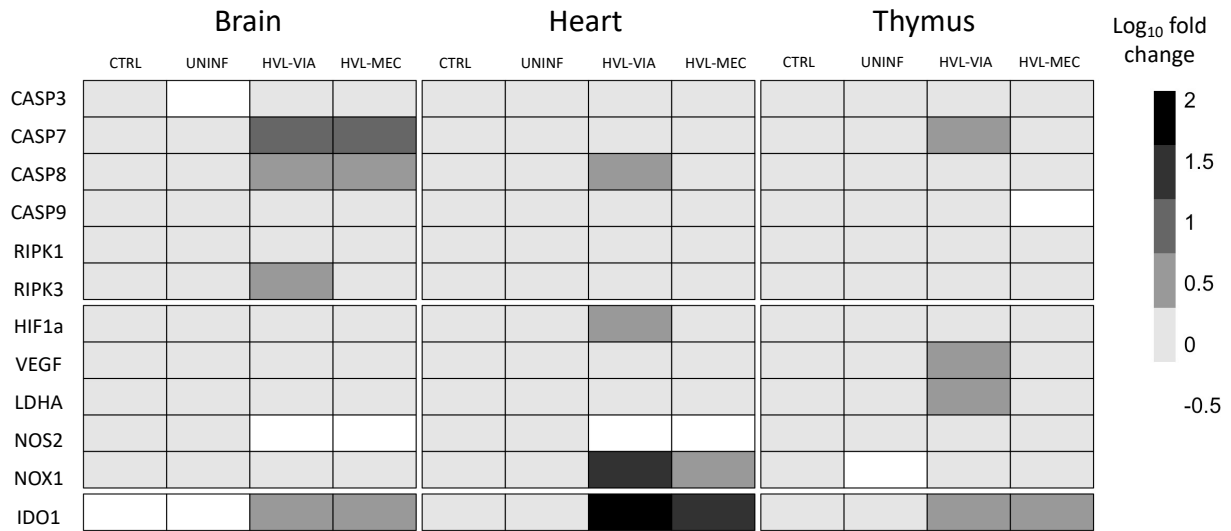


**Figure 5.6:** Summary of gene expression fold changes by fetal tissues and group. Heat map of group median gene expression fold changes associated with apoptosis (CASP 3, 7, 8, 9; RIPK 1, 3), hypoxia (HIF1a, VEGF, LDHA, NOS2, NOX1), and infection (IDO1) by tissue and fetal phenotype.

## 5.5. Discussion

Although first described over 30 years ago in North America, Europe and Asia (as reviewed by Christianson),<sup>28</sup> porcine reproductive and respiratory syndrome (PRRS) is still one of the most damaging diseases affecting the pork industry. The reproductive form of the disease is responsible for 45% of all economic losses caused by PRRS virus infection.<sup>68</sup> The infection of pregnant gilts and sows in their last third of gestation often results in only mild clinical signs in the dam, however, the litter can be severely affected by abortions, fetal death, weak born piglets and pre-weaning mortality.<sup>31</sup> The mechanisms of maternal uterine infection and transplacental transmission have been explored<sup>39,43–46</sup> and a few hypothesis about transplacental infection have been proposed and are reviewed in detail elsewhere.<sup>40</sup> In spite of the rapid development of severe endometritis, placentitis, and endometrial vasculitis subsequent to PRRSV infection, it is uncertain if those lesions result in fetal death, since fetuses present with minimal and non-lethal lesions when found dead.<sup>34,51</sup> However, previous studies have concluded that there is no relationship between MFI lesions or viral load and fetal death.<sup>48,53</sup> Thus, our goal was to investigate the fetal mechanisms that are potentially leading to compromise and death following PRRSV infection of third trimester fetuses.

Two separate animal experiments were conducted aiming to find possible insights into fetal death mechanisms following PRRSV infection. Our first experiment investigated apoptosis in fetal tissues after 21 days of maternal inoculation, using paraffin embedded samples from a previously described project<sup>49</sup> conducted in 2012. This was a follow up to our previous investigation in which apoptosis in the MFI (determined by TUNEL staining) was positively associated with PRRSV concentration in the fetal thymus and to meconium-staining of the fetus<sup>45</sup>. The results from this first experiment guided our second experiment that was designed to investigate an earlier stage of apoptosis at 12 days post-infection (12 DPI) through gene expression. The snap frozen tissues for this experiment were collected from a 2017 animal experiment. We also investigated the role of hypoxia as previous research suggested its involvement in fetal compromise<sup>34,48</sup>. Unfortunately, not all “Experiment 2” fetal samples collected yielded high quality mRNA, explaining the difference in tissue samples used between experiments.

The four fetal phenotypic groups selected for these experiments are representative of the evolution of PRRSV fetal infection and disease. The UNINF and LVL-VIA groups contained

either non-infected or very low viral load fetuses from inoculated/infected dams. These are considered the most resistant fetuses,<sup>121</sup> escaping infection entirely or sustaining a low rate of viral replication resulting in low levels of virus detectable in SER, THY, and PLC. UNINF fetuses are rather rare, although they would be of high value to the pork industry. Our use of the four fetal phenotypic groups also enabled investigation of the mechanisms that may contribute to fetal death and whether those mechanisms are initiated by maternal or fetal infection; i.e., if they are initiated only after the fetuses per se becomes infected or if there is a threshold of viral concentration to be achieved before disease starts.

Although it is unknown if UNINF fetuses would have been alive and healthy if gestation was taken to term (gestation day 115), they were more resistant than the HVL-VIA and HVL-MEC fetuses at the termination of the experiment (gestation day 106). By contrast, the HVL-VIA fetuses were the most tolerant or resilient fetuses<sup>121</sup> because in spite of high viral load, they remain viable. The HVL-MEC group was the most susceptible.<sup>121</sup> Fetal meconium-staining is largely recognized as a sign of multi-factorial in-utero distress that leads the fetus to defecate or regurgitate into the amniotic sac resulting in contamination of the skin (and sometimes lung) by this yellowish fecal matter. A positive relationship between high PRRSV viral load and meconium-staining of the fetus has been previously reported, indicating this is an initial step towards fetal compromise and death after infection.<sup>49</sup> The most susceptible fetuses are those that die following maternal PRRSV infection. Although decomposed and autolyzed fetuses were present in our challenge trials, we did not collect tissue samples from these fetuses because the mRNA quality was subpar.

In our first experiment, TUNEL staining in liver and thymus confirmed the association between DNA fragmentation and HVL-VIA and HVL-MEC fetuses that was previously observed.<sup>45</sup> where the number of TUNEL positive foci in the MFI were related to the HVL-VIA and HVL-MEC phenotypes at 21 DPI. The same relationship was found in fetal heart samples with HVL-MEC fetuses having greater counts of TUNEL positive foci than the CTRL, LVL-VIA and HVL-VIA groups. This result also agrees with a recent study investigating disruption of the fetal thyroid hormones in PRRSV-infected fetuses,<sup>121</sup> where the HVL-MEC group was more affected than the respective CTRL, UNINF, and HVL-VIA groups. The diffuse distribution of the apoptotic foci in the liver and thymus may indicate the apoptotic process is advanced in those tissues, possibly contributing to fetal demise.

By evaluating the size of TUNEL positive foci we aimed to determine any association with the progression of the disease and/or viral load of fetuses. Although no standards to characterize these findings by size exist to our knowledge, we hypothesize that it can, at least, indicate the abundance and extent of the apoptotic process in the affected tissues. Statistically, there were differences among the groups, where the highly infected animals (HVL-VIA and HVL-MEC in LVR and THY, HVL-MEC in HRT) presented with larger foci than the non-infected groups (UNINF, CTRL). We interpret these results as confirmation that the highly infected animals are in a more severe state of apoptosis, which may contribute to fetal demise or death.

Based on insights from the first experiment using 21 DPI tissues, we investigated an earlier timepoint (12 DPI) to assess gene expression of apoptosis initiators and executioners. Apoptosis is the programmed cell death, regulated by a family of cysteine proteases (caspases; CASP)<sup>120</sup> along two main pathways: intrinsic and extrinsic. The intrinsic pathway is very well-regulated and initiated by mitochondrial perturbation resulting from cellular stress or cytotoxic insults. It is mainly regulated by CASP-9, an initiator caspase, that subsequently activates the effector, CASP-3.<sup>120</sup> PRRSV activates the extrinsic apoptotic pathway after infecting the MFI,<sup>45,46</sup> which can be initiated via the TNF receptor (TNFR) family coupled to extrinsic signals. The extrinsic pathway is mainly regulated by the initiator, CASP-8, which subsequently activates CASP-3 and CASP-7.<sup>120</sup>

The TNFR and other inflammatory signals can also initiate the necroptosis pathway. Necroptosis is another form of programmed cell death that shares common reactions and processes with both apoptosis and necrosis. Also classified as a “programmed cell necrosis”, it is mainly regulated by the receptor-interacting protein kinases 1 and 3 (RIPK1 and RIPK3).<sup>127</sup> Although there are many cells and signals involved in the extrinsic apoptotic pathway and the necroptosis pathway, we focused our investigation on expression of the main genes involved in both (to which we will refer here simply as “apoptosis”) in fetal tissues after maternal PRRSV inoculation.

There was a remarkable difference in gene expression across tissues and phenotypic groups. Apoptosis related genes were typically over expressed in brain and heart of PRRSV-infected fetuses, confirming that infection induces cell death in fetal tissues. Importantly, this apoptotic fetal response is dependent on infection of the fetus, not by maternal infection as noted

by the lack of statistical difference between the UNINF and CTRL groups. It is also in general agreement with previous findings, where increased counts of apoptotic cells in the MFI were associated with increased fetal thymus PRRSV viral load.<sup>45</sup>

One of the most unexpected and potentially important findings is that heart was the most affected organ, presenting with the higher number of altered genes and higher fold change averages among the three analyzed tissues. This aligns with the findings of Pasternak,<sup>121</sup> where after fetal PRRSV infection genes related to cell cycle progression were downregulated and genes related to cell cycle inhibition were upregulated in the fetal heart. Moreover, this result partially agrees with our TUNEL findings, where evidence of apoptosis was only found in the hearts of HVL-MEC group, whereas gene expression was more consistently altered in HVL-VIA fetuses. Additionally, early experiments demonstrated the presence, albeit inconsistent, of virus in the heart of PRRSV challenged fetuses using culture recovery methods.<sup>50</sup> This finding is consistent with immune histochemical analysis of the postnatal heart of piglets following in utero infection.<sup>128,129</sup> The degree of apoptosis and gene expression changes in fetal heart following local infection may therefore be a key indicator of fetal outcome. Interestingly, fetal thymus, the putative primary site of PRRSV replication on the fetus,<sup>50</sup> despite presenting with greater counts and larger sizes of TUNEL positive foci in infected fetuses at 21 DPI, was surprisingly the least altered tissue, having only two out of 12 genes differentially expressed among groups of fetuses. This finding may be due to the early timepoint of sample collection, or to the fact that, as the main viral replication site, the immunosuppressing characteristics of the virus<sup>130</sup> are more influential in thymus than other tissues. Although thymus is considered a tissue of great importance in fetal PRRSV infection, it is not a vital organ for fetal survival in the acute stages of the disease and may therefore only be relevant in the experimental context as a measure of fetal infection.

Hypoxia, the deprivation of adequate levels of oxygen in a tissue, has been theorized as a potential cause of PRRSV-related fetal death based on the observation of umbilical cord lesions,<sup>34</sup> which were found to be associated with meconium-staining of the fetus.<sup>39</sup> As some umbilical cord lesions have been observed in dead fetuses from PRRSV infected dams, it is plausible that a reduced blood flow would lead to decreased levels of available oxygen for the fetus. Inflammatory lesions within the MFI and placental detachment may also lead to reduced maternal oxygen transfer to the progeny. These theories prompted our interest in testing the main

genes related to hypoxia and its consequences. HIF-1 $\alpha$ , a member of the hypoxia-inducible factors (HIFs), is a master regulator of the adaptive response to low levels of oxygen.<sup>131</sup> It is ubiquitously expressed and under normal conditions (normoxia), its subunits are hydroxylated by prolyl hydroxylases (PHD1-3) and go under proteasomal degradation by the von Hippel Lindau (VHL) E3 ubiquitin ligase complex.<sup>131</sup> However, during hypoxia the PHD enzymes are unable to function, suppressing HIF-1 $\alpha$  hydroxylation and stabilizing its subunits. From there, HIF-1 $\alpha$  can dimerize with HIF-1 $\beta$  and promote transcription of other hypoxia-responsive target genes such as vascular endothelial growth factor (VEGF $\alpha$ ), lactate dehydrogenase A (LDHA), nitric oxide synthase 2 (NOS2), and NADPH oxidase 1 (NOX1).<sup>131,132</sup> In fetal brain, expression of HIF-1 $\alpha$  was upregulated in highly infected fetuses (HVL-VIA and HVL-MEC) compared to CTRL and UNINF, however, none of the other hypoxia-responsive genes were altered. This might indicate an early response to hypoxia or no response at all. HIF-1 $\alpha$  can be also involved in the cell death cycle by activating expression of genes in the apoptosis pathway,<sup>133</sup> which may explain its upregulation. By contrast, the heart of highly infected fetuses presented with multiple altered genes in addition to HIF-1 $\alpha$ . The VEGF $\alpha$  gene was slightly increased in HVL-VIA (1.07 fold changes) and HVL-MEC (1.25 fold changes) groups, suggesting an increase in the proliferation and migration of vascular endothelial cells to provide a larger vascular network for oxygen exchange in response to hypoxia. Much greater differences in expression were observed in the NOX1 (NADPH oxidase 1) gene in the heart of infected animals. NOX1 is involved in many physiological pathways, but it is normally responsible for catalyzing the production of reactive oxygen species (ROS) involved in vascular system. ROS are produced in very low amounts under normal situations, however, ROS can be induced by an increase of NOX1 resulting in damage to cellular proteins, RNA, DNA and lipids. More importantly in this scenario, it impairs the PHD enzymes, decreasing the hydroxylation of HIF-1 $\alpha$ .<sup>134</sup> In any case the degree of disruption within this pathway is consistent with previous work by Pasternak et al. (2020)<sup>121</sup> showing the high degree of susceptibility of this critical organ to PRRSV infection.

The downregulation of inducible nitric oxide synthase gene (iNOS or NOS2) in the HVL-MEC fetuses (and a trend for the HVL-VIA group) was interesting and unexpected. The production of this enzyme can be induced by inflammatory cytokines such as TNF- $\alpha$  and INF- $\gamma$  that are present in sera of PRRSV infected fetuses at or over 19 DPI.<sup>50,113</sup> NOS2 induces dilatation of blood vessels in response to hypoxia in order to increase blood (and oxygen)

availability.<sup>135</sup> The unexpected result might indicate the levels of TNF- $\alpha$  and INF-gamma might not be sufficiently increased at the termination point (12 DPI) used in this project to cause the expected effects. As none of the hypoxia related genes were altered in THY, it is possible that this tissue is not experiencing any hypoxia. However, it's important to note that in mice the thymus was observed to be a naturally hypoxic tissue when compared to other organs and blood cells, enabling the thymus to be better adapted to hypoxia.<sup>136</sup> This may explain why the expected responses was not initiated. Moreover, as T cells have a lower activation in hypoxic environments,<sup>137</sup> this might be a factor that makes thymus a preferred tissue for PRRSV replication.

The only gene that presented a constant pattern throughout all the tissues was indoleamine 2, 3-dioxygenase 1 (IDO1), where its expression was consistently upregulated in highly infected fetuses. This enzyme facilitates tryptophan metabolism and the production of kynurenine,<sup>75</sup> which interestingly, was increased in HVL-VIA fetuses compared with UNINF fetuses.<sup>138</sup> Kynurenine is involved in the “metabolic immune regulation” mechanism and its gene expression can be regulated by TNF- $\alpha$  and INF-gamma, as reviewed by Richardson.<sup>75</sup> Because expression in the UNINF and CTRL groups were similar, we deduce that this response to infection is only elicited when the virus infects the fetus (not only the dam), confirming a fetal compartmentalized response to PRRSV infection.

## 5.6. Conclusions

The findings of this study bring new insights into fetal demise mechanisms after maternal inoculation with PRRSV. Apoptosis is clearly a compromising mechanism evident in multiple organs in the highly infected fetuses. It is plausible the observed apoptotic tendencies, particularly within the heart, contribute to fetal compromise and death beginning as early as 12 DPI and still evident at 21 DPI. Both HVL groups (-VIA and -MEC) displayed indications of an apoptotic process in the brain, while fetal heart is the most severely affected fetal organ following PRRSV infection, showing signs of hypoxia in addition to the apoptosis process.

## Declarations

**Animal ethics approval:** This study was approved by the University of Saskatchewan Animal Research Ethics Board and adhered to the Canadian Council on Animal Care guidelines for

humane animal use (Protocols 20110102 and 20160023). The infected pregnant gilts were closely monitored for clinical signs and a human intervention point checklist was established to monitor the gilts for critical conditions post-inoculation. It was not feasible to monitor fetal conditions after the viral inoculation, but fetal compromise death was expected to occur at the later time points. Gilts were euthanized with intravenous sodium pentobarbital overdose followed by cranial captive bolt and exsanguination. Fetuses were euthanized as humanely as possible given that pentobarbital sodium crosses the MFI rapidly and enters fetal circulation prior to the onset of hypoxia and asphyxia.

**Consent for publication:** not applicable

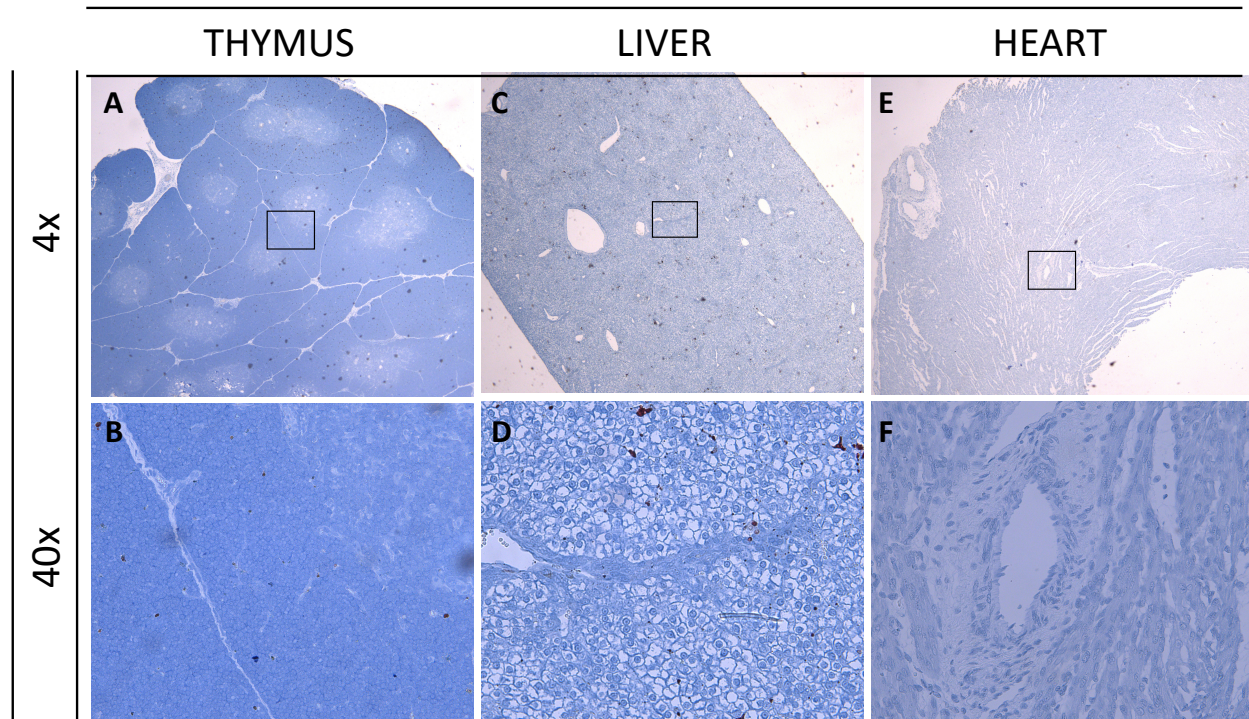
**Availability of data and materials:** The datasets analysed for Experiments 1 and 2 are available from the corresponding author on reasonable request.

**Competing interests:** The authors declare no conflicts of interest with respect to the research, authorship and/or publication of this article.

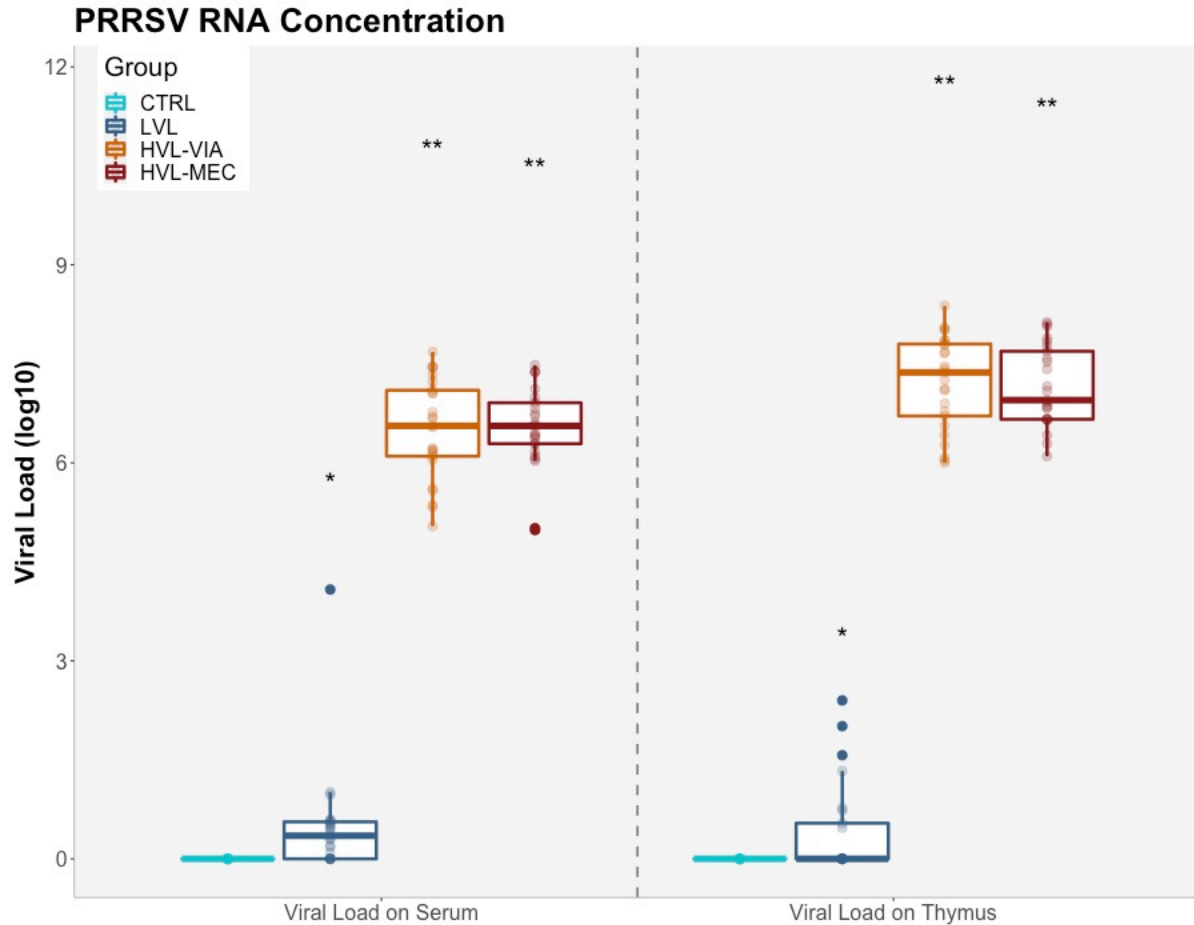
**Funding:** This project was supported by Genome Canada (grant #345169) and Genome Prairie (Saskatchewan Ministry of Agriculture; grant #20150329), along with administrative support provided by Genome Alberta and the University of Saskatchewan. The funding agencies had no involvement in study design, implementation, analyses or interpretation of the results.

**Acknowledgements:** We express special acknowledgment to numerous personnel (technicians, graduate students, summer students, colleagues) who helped in the preparation and implementation of this study. Animal Care was contracted to VIDO-Intervac, Saskatoon. Necropsies were performed at the Prairie Diagnostic Services, Saskatoon.

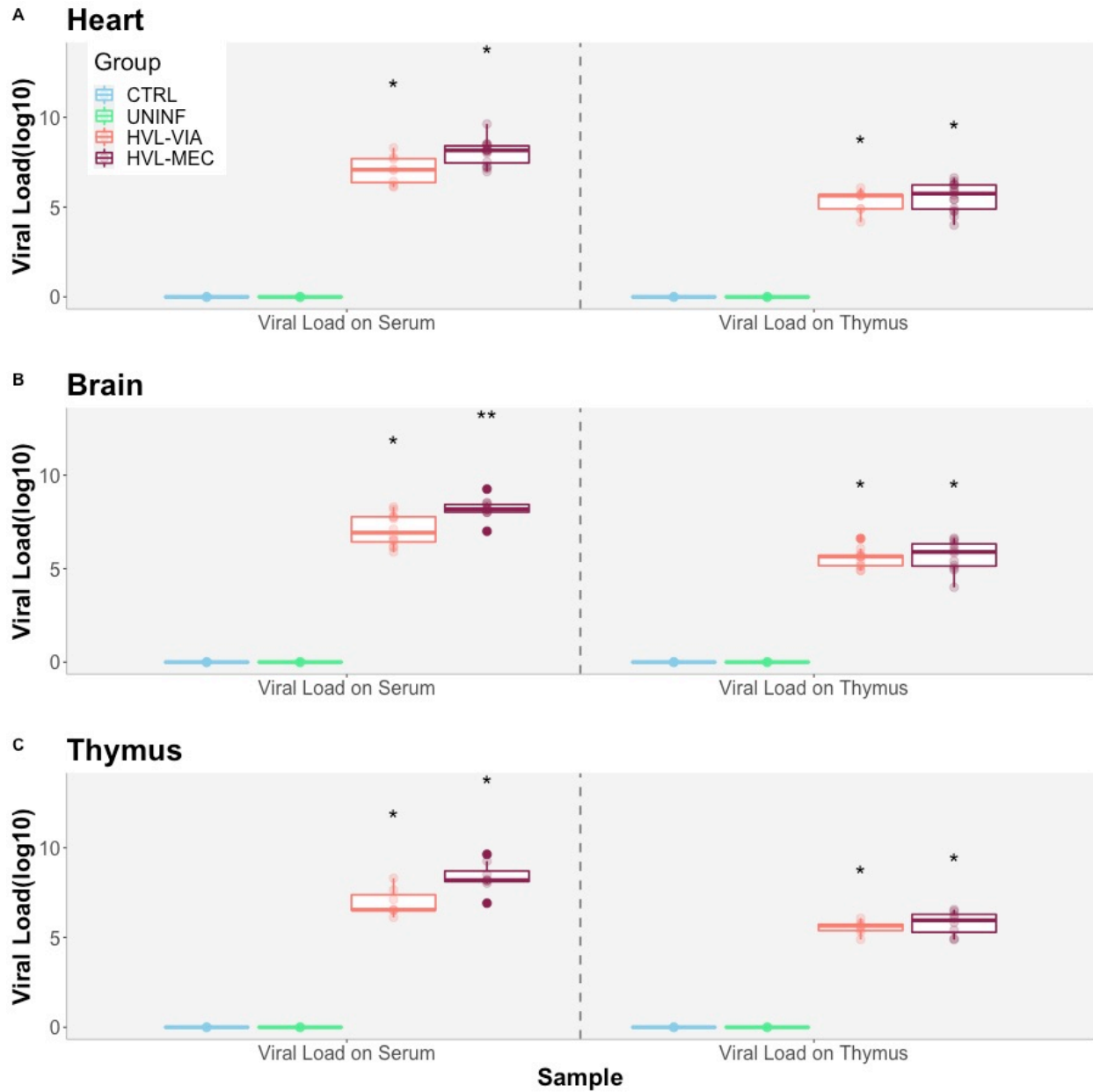
**Additional files**



**Additional file 5.1:** TUNEL staining in three fetal tissues of uninfected control fetuses. Scant cells with TUNEL positive staining are observed at higher magnification of fetal thymus (B) and liver (D), but not in heart (F).



**Additional file 5.2:** Experiment 1 (21 DPI) PRRSV RNA concentration by fetal group. Viral load expressed in log (base 10) in fetal serum (left) and thymus (right) for each of the four phenotypical fetal groups: non-infected control (CTRL), PRRSV-infected low viral load viable (LVL), PRRSV-infected high viral load viable (HVL-VIA), PRRSV-infected high viral load meconium stained (VHL-MEC).



**Additional file 5.3:** Experiment 2 (12 DPI) PRRSV RNA concentration by fetal group. Viral load expressed in log (base 10) in fetal serum (left) and thymus (right) for each of the four phenotypical fetal groups in heart (A), brain (B), and thymus (C): non-infected control (CTRL), uninfected fetuses from inoculated dams (UNINF), PRRSV-infected high viral load viable (HVL-VIA), PRRSV-infected high viral load meconium stained (VHL-MEC) fetuses.

## 6. General discussion, conclusions and future directions

The hypothesis underlying the presented studies was that the reasons for the naturally occurring resistance/resilience to reproductive PRRSV infection and disease severity can be explained by a combination of features including fetal phenotype, gene expression and metabolomics. Results of the studies presented herein provide evidence to support the hypothesis. In particular, there were differences in gene expression and metabolomic profiles between the more susceptible and more resilient fetuses (Chapters 4 & 5). In addition, our research advanced our understanding of the timeline of reproductive PRRSV infection and fetal disease (Chapter 2), and what is the best sampling strategy and analyses to better assess the events in the maternal-fetal interface (Chapter 3).

Since it was first described in the late 1980's as the "mystery swine disease",<sup>28,32,33</sup> countless questions regarding PRRS pathophysiology have been raised, many of which still unanswered. One of the greatest remaining "mysteries" revolves around the reproductive disease. Late term pregnant sows, normally asymptomatic or mildly symptomatic after PRRSV infection, present with abortions, dead fetuses, weak-born piglets and high pre-weaning mortality rates.<sup>32,41</sup> Earlier studies recognized the importance of investigating the maternal-fetal interface to better understand the causative factors associated with reproductive losses following viral infection. Endometritis, placentitis, and micro separations of the placenta after natural or experimental PRRSV inoculation were observed and reported.<sup>52,139</sup> From the beginning of PRRSV investigations, transplacental viral transmission from the dam to the litter was perceived to play a great role in the pathogenesis.<sup>33</sup> Since then, many studies have investigated the impact of PRRSV infection on the MFI to better understand the mechanisms leading to fetal death in the absence of fetal lesions.<sup>39,43,44,46,47,53,72</sup>

Chapter 2 of this thesis brought new perspectives on the infection timeline and when some of the most important events in reproductive PRRS occur. Within the limits of the experimental model we used, we now understand the rapidity of infection of the endometrium following maternal inoculation, the speed at which the virus spreads to fetal tissues, and the day of onset of fetal pathology on the litter. It became clear that there are possible fetal mechanisms in place to avoid placental infection in some fetuses (e.g. UNINF – uninfected fetuses from infected dams), protecting them from viral infection. These are extremely important findings when trying to understand the pathogenesis and mechanisms that lead to fetal death. One of the

limitations of this project, however, was the assessment of viral RNA concentration in the MFI by only one sample of endometrium and placenta.

Based on preliminary data, we hypothesized that both viral load and histological lesions could be heterogeneously present. Thus, Chapter 3 was designed to define the most accurate and feasible ways of sample collection and processing for MFI infection investigation. We were able to analyse endometrium and placenta separately, collected from five pre-established locations and comparing methods of processing and analysis. We concluded that at least three randomly located pieces of MFI and PLC tissue should be collected and analyzed for an accurate measurement of PRRSV viral load and histological assessment. However, as previously discussed in the introduction chapter, we also know that the lesions and disruptions in the MFI are not sufficient by themselves to cause fetal death. Thus, moving forward, a more fetal focused approach was adopted.

The first studies investigating dead fetuses from PRRSV infected sows reported that, although fetuses were being affected by the viral infection, they were not presenting with any pathognomonic lesions or even consistent lesions causing their demise.<sup>34,51,52</sup> Thus, an investigation of differences in the metabolome among fetuses considered resistant, resilient, or susceptible to PRRSV infection and disease was undertaken. We now understand that metabolomic changes in the fetus only start after fetal infection per se, following transplacental transmission. However, once the fetus became infected, disruptions in biochemical pathways initiated, mainly amino acid-related pathways became apparent, particularly tryptophan metabolism. Other disruptions involved the sphingolipids, phosphatidyl and lysophosphocholine metabolism, lipid molecules that have diverse roles in many cellular functions and signaling, including growth regulation, apoptosis, and inflammatory responses.<sup>116,140</sup> Fetuses with impaired growth and more resistant to infection by PRRSV<sup>70</sup> (IUGR fetuses) also presented with lower serum concentrations of amino acids, phosphatidyl and lysophosphocholine, when compared to normal growth fetuses, both prior to and post PRRSV infection (Chapter 4). Thus, these findings lead to the question of whether reduced metabolism, especially related to essential amino acids metabolism, might be a protective factor against PRRSV infection. If so, does that point to a resistance mechanism related to fetal nutrition in utero? It is possible that viral transmission can occur through more than one mechanism, i.e., via exosomes, via placenta, via nutritional glands. However, the exact routes of transplacental transmission are still under investigation and our

results do not aim to respond to that specific question, but rather provide further insights to initiate future studies.

Looking back to studies analysing dead fetuses from PRRSV infected dams, a study<sup>34</sup> identified umbilical cord lesions, as segmented or full length haemorrhages and edema, as an indication of fetal PRRSV infection. The authors added that meconium-staining of the fetus, abdominal and thoracic effusions, as well as edema around the kidney, spleen, and spiral colon mesentery can be related to PRRS fetal pathogenesis leading to fetal death.<sup>34</sup> Due to the lesions found in umbilical cord, the authors suggested that reduced fetal oxygenation associated with disrupted blood flow in the umbilical cord, was a first indication of fetal death caused by hypoxia.<sup>34</sup> These umbilical cord lesions were also associated with meconium-staining of the fetuses. A more recent study investigating fetal pathology following maternal PRRSV infection confirmed the inconsistency and low frequency of fetal lesions, but added the presence of fetal lesions (including follicular atrophy of mesenteric lymph nodes and lymphocytic perivascular cuffing in umbilical vessels) to umbilical cord lesions as factors increasing the likelihood of meconium-staining of the fetus.<sup>39</sup> Our results now confirmed that hypoxia was indeed evident in fetal heart, and was dependent on PRRSV fetal infection per se. Low levels of oxygenation in the heart can result in many different responses depending on the extent of hypoxia, its duration, and the individual animal biology. It can however, be a risk factor for (or a result of) heart ischemia, possibly leading to heart failure or myocardial infarction, which could potentially be a cause of fetal death.<sup>141</sup> Lymphocytic myocarditis, perivascular cuffing, and myocardiocyte degeneration and necrosis have been observed in compromised fetuses (3.9% of fetuses presented with cardiac lesions),<sup>34,39</sup> which supports this possibility. At least at an early stage of fetal infection, fetal brain and thymus seemed to still be protected from this process. Similarly, PRRSV infection affected the ability of the fetal heart to respond to thyroid hormone, greatly dysregulating cell-cycle progression, while the same intensity of effects were not observed in fetal brain.<sup>121</sup>

Previous studies<sup>39</sup> also demonstrated how PRRSV infection of the MFI is associated with fetal pathological lesions. Supporting these findings, another study<sup>45</sup> associated PRRSV infection of the MFI with apoptosis of the MFI, indirectly connecting progress of fetal lesions with increasing levels of apoptosis. Thus, we hypothesized that apoptosis in fetal tissues was a contributing fetal death mechanism. Our latest experiment found evidence of apoptosis in both early and late stages of fetal infection, again with the heart being the most affected organ

analyzed. Cardiomyocyte death is a well-controlled process, as these specialized cells have a lower rate of regeneration and self-repair, when compared to other cells.<sup>142,143</sup> It is currently understood that physiological levels of apoptosis in the healthy adult human heart are extremely low (0.01-0.001% counts of apoptotic myocyte nuclei per million nuclei counted),<sup>142</sup> implying greatly biological significance even with low apoptosis detection. The observed myocyte apoptosis in our studies might result from the hypoxia present in the fetal hearts and a more significant indication of cardiac pathology<sup>142,143</sup> as PRRSV fetal infection is able to promote cardiac stress.<sup>121</sup> Regardless of the cause of myocyte death, it is important to stress that any level of apoptosis in the heart tissue is detrimental. **Figure 6.1** presents an overall summary of main events occurring on the porcine maternal (top half, blue line) and fetal (bottom half, red line) compartments following PRRSV infection.

Most of the limitations of our studies were discussed in their own chapters, however, some general points are presented for discussion here. The results provided insights from an experimentally controlled environment infection, mostly free of other disease-causing agents and husbandry manipulations, thus, they may not reflect the exact conditions of commercial pig farms. As all of the projects were based on one specific PRRSV2 strain (NSVL-97-7895), caution should be taken when extrapolating these data to other PRRSV2 strains. Additionally, only gilts (no previous pregnancy), from the same commercial breeding company and female line (Landrace) served as maternal subjects, which aided in controlling variability factors, but possibly impedes generalization of the results. Furthermore, considering that fetuses were in different stages of infection, the results were a reflection of the sample collection time points, not representing the entirety of infection and disease progression in gestation. It is important to note that we aimed to classify fetuses as resistant, resilient or susceptible following maternal PRRSV-2 infection. The classification employed herein might not be in complete accordance with the traditional definition of “resistance” as is applied in different fields, because the fetuses classified herein, were not directly inoculated with the virus. Thus, we were not 100% confident that resistant fetuses were completely resistant to viral infection. However, we believe that those fetuses were partially resistant to viral infection, or partially resistant to disease development (after viral infection), relative to many of their littermates and neighbours that were often infected earlier, had greater viral load or were non-viable. As for some of the fetal focused projects, we cannot be definitive whether specific findings were causes or results of the disease,

since we cannot obtain day 0 samples, prior to maternal inoculation. Were these disruptions in affected fetuses a response to infection or did the fetal groups used had differences prior to infection that led to different disruptive response to infection? For example, did susceptible fetuses already have higher levels of kynurenine and lysophosphocholines that predisposed them to a higher infection, or were the higher levels an exclusive response following infection of those fetuses? Further studies are needed to provide those answers, however, as we have observed numerous differences in the fetal response following PRRSV infection, it appears that finding a natural fetal resistance/resilience mechanism to infection and disease is closer, and that is hopefully where future studies will lead.

In conclusion, these studies presented new insights into the temporal movement of PRRSV following maternal inoculation and fetal disease progression, as well as novel details on fetal death mechanics. Importantly, we have started to understand that PRRSV infection leads to a much more complex fetal cardiometabolic disorder with potential postnatal effects, that is understated by “reproductive and respiratory syndrome”. However, fetal PRRS investigations are not completed. Future studies can branch out in at least three directions from the findings presented in here:

- If we interpret these results as that there are fetal placental factors preventing the transplacental infection and that those factors are related to nutritional transport from dam to fetus, more emphasis on placental structure, nutrient transport, and functionality among resilient and susceptible fetuses following PRRSV infection would be advised. Most investigations so far have analyzed the MFI as a whole, however, we now have further advanced sample collection and analysis techniques, allowing for more specific studies.
- Results reported herein as well as the latest results from our reproductive PRRS research group (Chapter 5 and Pasternak, 2020)<sup>121</sup> present strong evidence of cardiometabolic compromise in highly infected and compromised fetuses. Thus, fetal death following PRRSV infection might be due to altered cardiac physiology. Further investigation on fetal hearts is strongly advised to better understand this condition, as well as for finding possible new ways of controlling or intervening on PRRSV infection. .
- To clarify if fetuses are truly resistant (in the traditional definition) to PRRSV-2 infection, additional experiments designed to directly inoculate fetuses across a range of viral concentrations in utero followed by sample collection in a timeline fashion should be undertaken.

The study would advance the knowledge on fetal resistance, resilience and susceptibility to PRRSV by testing the fetal ability to respond to viral infection. Furthermore, cardiac enzyme alterations and cardiovascular consequences could be monitored and investigated to further elucidate the mechanisms leading to fetal losses.

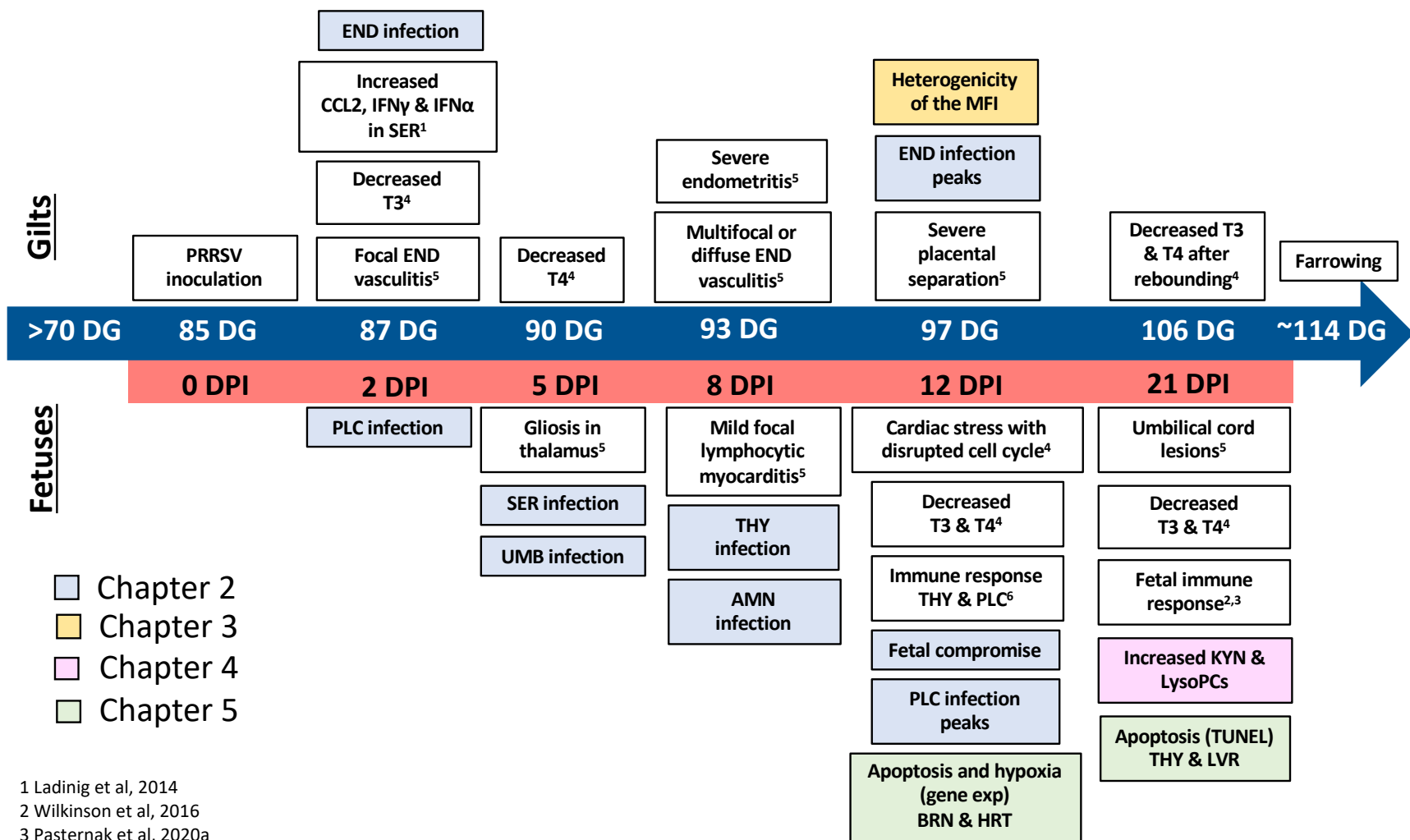


**Figure 6.1:** Timeline of infection and disease progression following PRRSV maternal inoculation.

The events start on the left of the image, at the beginning of the last third of gestation, when fetuses are most susceptible to PRRSV transplacental infection. The maternal timeline is based of days of gestation (DG), while the fetal timeline is based on days post-inoculation (DPI). Boxes of findings that belong to a chapter of this thesis are colour-coded, and findings from other studies are cited in the figure. DG = Days of gestation; DPI = days post-inoculation; PLC = placenta; SER = serum; UMB = umbilical cord; THY = thymus; AMN = amniotic fluid; BRN = brain; HRT = heart; LVR = liver.

## 7. References

1. Leiser R, Kaufmann P. Placental structure: in a comparative aspect. *Exp Clin Endocrinol Diabetes*. 2009;102(03):122-134.
2. Bertasoli B, Santos A, Paula R, Barbosa A, Jorge E. Swine placenta and placentation. *Brazilian J Biol Sci*. 2015;2(4):199-207.
3. Friess AE, Sinowatz F, Skolek-Winnisch R, Träutner W. The placenta of the pig - I. Finestructural changes of the placental barrier during pregnancy. *Anat Embryol (Berl)*. 1980;158(2):179-191.
4. Mossman HW. Comparative morphogenesis of the fetal membranes and accessory uterine structures. *Contrib Embriol*. 1937;26(158):133-247.
5. Senger PL. *Pathways to Pregnancy and Parturition*. 2nd ed. Current Conceptions; 2003.
6. Flood PF. Endometrial differentiation in the pregnant sow and the necrotic tips of the allantochorion. *J Reprod Fertil*. 1973;32(3):539.
7. Ashdown RR, Marrable AW. Adherence and fusion between the extremities of adjacent embryonic sacs in the pig. *J Anat*. 1967;101(2):269-275.
8. Vallet JL, McNeel AK, Miles JR, Freking BA. Placental accommodations for transport and metabolism during intra-uterine crowding in pigs. *J Anim Sci Biotechnol*. 2014;5(1):1-14.
9. Perry JS. Mammalian fetal membranes. *J Reprod Fertil*. 1981;62(2):321-335.
10. Friess AE, Sinowatz F, Skolek-Winnisch R, Träutner W. The Placenta of the Pig II The Ultrasound of the Areolae. *Anat Embryol (Berl)*. 1981;163:43-53.
11. Roth VL, Mossman HW. Vertebrate Fetal Membranes. Comparative Ontogeny and Morphology; Evolution; Phylogenetic Significance; Basic Functions; Research Opportunities. *Q Rev Biol*. 1988;63(1):89-89.
12. Olio RL, Lobo LM, Pereira MA, et al. Accessory Placental Structures—A Review. *Open J Anim Sci*. 2014;04(05):305-312.
13. Dantzer V, Leiser R. Microvasculature of regular and irregular areolae of the areola-gland subunit of the porcine placenta: structural and functional aspects. *Anat Embryol (Berl)*. 1993;188(3):257-267.
14. Miglino MA, Pereira FTV, Santos TC, Carvalho AF. A morfologia placentária dos suínos domésticos (Domestic swine placental morphology). *Arq ciênc vet zool UNIPAR*.

Published online 2001:71-76.

15. Anderson LL, Parker RO. Distribution and development of embryos in the pig. *J Reprod Fertil*. 1976;46(2):363-368.
16. Pope WF, Maurer RR, Stormshak F. Intrauterine Migration of the Porcine Embryo: Influence of Estradiol-17 $\beta$  and Histamine. *Biol Reprod*. 1982;27(3):575-579.
17. Dziuk P. Effect of migration, distribution and spacing of pig embryos on pregnancy and fetal survival. *J Reprod Fertil Suppl*. 1985;33:57-63.
18. Chen Q, Zhang Y, Elad D, et al. Navigating the site for embryo implantation: Biomechanical and molecular regulation of intrauterine embryo distribution. *Mol Aspects Med*. 2013;34(5):1024-1042.
19. Bazer FW, Johnson GA. Pig blastocyst-uterine interactions. *Differentiation*. 2014;87(1-2):52-65.
20. Vallet JL, Miles JR, Freking BA. Development of the pig placenta. *Soc Reprod Fertil*. 2009;66:265-279.
21. Wright EC, Miles JR, Lents CA, Rempel LA. Uterine and placenta characteristics during early vascular development in the pig from day 22 to 42 of gestation. *Anim Reprod Sci*. 2016;164:14-22.
22. Knight JW, Bazer FW, Thatcher WW, Franke DE, Wallace HD. Conceptus development in intact and unilaterally hysterectomized-ovariectomized gilts: interrelations among hormonal status, placental development, fetal fluids and fetal growth. *J Anim Sci*. 1977;44(4):620-637.
23. Bazer FW, Song G, Kim J, et al. Uterine biology in pigs and sheep. *J Anim Sci Biotechnol*. 2012;3(1):1-21.
24. Leiser R, Dantzer V. Structural and functional aspects of porcine placental microvasculature. *Anat Embryol (Berl)*. 1988;177(5):409-419.
25. Wu G, Bazer FW, Wallace JM, Spencer TE. Intrauterine growth retardation: Implications for the animal sciences. *J Anim Sci*. 2006;84(9):2316-2337.
26. Chen F, Wang T, Feng C, et al. Proteome differences in placenta and endometrium between normal and intrauterine growth restricted pig fetuses. *PLoS One*. 2015;10(11):e0142396.
27. Finch AM, Antipatis C, Pickard AR, Ashworth CJ. Patterns of fetal growth within Large

- White × Landrace and Chinese Meishan gilt litters at three stages of gestation. *Reprod Fertil Dev.* 2002;14(7):419.
28. Christianson WT, Joo HS. Porcine reproductive and respiratory syndrome: A review. *Swine Heal Prod.* 1994;2(2):10-28.
  29. Lunney JK, Fang Y, Ladinig A, et al. Porcine reproductive and respiratory syndrome virus (prrsv): pathogenesis and interaction with the immune system and Interaction with the Immune System. *Annu Rev Anim Biosci.* 2016;4(1):129-154.
  30. Done SH, Paton DJ, White MEC. Porcine reproductive and respiratory syndrome (PRRS): A review, with emphasis on pathological, virological and diagnostic aspects. *Br Vet J.* 1996;152(2):153-174.
  31. Zimmerman JJ, Dee SA, Holtkamp DJ, et al. Diseases of Swine. In: Zimmerman JJ, Karriker LA, Ramirez A, Schwartz KJ, Stevenson GW, Zhang J, eds. *Diseases of Swine.* Vol 11. 11th ed. Wiley-Blackwell; 2019:685-708.
  32. Mengeling WL, Lager KM, Vorwald AC. Temporal characterization of transplacental infection of porcine fetuses with porcine reproductive and respiratory syndrome virus. *Am J Vet Res.* 1994;55(10):1391-1398.
  33. Terpstra C, Wensvoort G, Pol JM. Experimental reproduction of porcine epidemic abortion and respiratory syndrome (mystery swine disease) by infection with Lelystad virus: Koch's postulates fulfilled. *Vet Q.* 1991;13(3):131-136.
  34. Lager KM, Halbur PG, Invest JVD. Gross and microscopic lesions in porcine fetuses infected with porcine reproductive and respiratory syndrome virus. *J Vet Diagn Invest.* 1996;8(1 996):275-282.
  35. Ladinig A, Lunney JK, Souza CJ, Ashley C, Plastow G, Harding JC. Cytokine profiles in pregnant gilts experimentally infected with porcine reproductive and respiratory syndrome virus and relationships with viral load and fetal outcome. *Vet Res.* 2014;45:113.
  36. Harding JCS, Ladinig A, Novakovic P, et al. Novel insights into host responses and reproductive pathophysiology of porcine reproductive and respiratory syndrome caused by PRRSV-2. *Vet Microbiol.* 2017;209:114-123.
  37. Ladinig A, Ashley C, Detmer SE, et al. Maternal and fetal predictors of fetal viral load and death in third trimester, type 2 porcine reproductive and respiratory syndrome virus infected pregnant gilts. *Vet Res.* 2015;46:107.

38. Ladinig A, Gerner W, Saalmüller A, Lunney JK, Ashley C, Harding JCS. Changes in leukocyte subsets of pregnant gilts experimentally infected with porcine reproductive and respiratory syndrome virus and relationships with viral load and fetal outcome. *Vet Res.* 2014;45(1):1-12.
39. Novakovic P, Harding JCS, Al-Dissi AN, Ladinig A, Detmer SE. Pathologic evaluation of type 2 porcine reproductive and respiratory syndrome virus infection at the maternal-fetal interface of late gestation pregnant gilts. *PLoS One.* 2016;11(3):e0151198.
40. Karniychuk UU, Nauwynck HJ. Pathogenesis and prevention of placental and transplacental porcine reproductive and respiratory syndrome virus infection. *Vet Res.* 2013;44(1):95.
41. Lager KM, Mengeling WL. Pathogenesis of in utero infection in porcine fetuses with porcine reproductive and respiratory syndrome virus. *Can J Vet Res.* 1995;59(3):187-192.
42. Van Gorp H, Van Breedam W, Delputte PL, Nauwynck HJ. Sialoadhesin and CD163 join forces during entry of the porcine reproductive and respiratory syndrome virus. *J Gen Virol.* 2008;89(12):2943-2953.
43. Karniychuk UU, Nauwynck HJ. Quantitative changes of sialoadhesin and CD163 positive macrophages in the implantation sites and organs of porcine embryos/fetuses during gestation. *Placenta.* 2009;30(6):497-500.
44. Karniychuk UU, De Spiegelaere W, Nauwynck HJ. Porcine reproductive and respiratory syndrome virus infection is associated with an increased number of Sn-positive and CD8-positive cells in the maternal-fetal interface. *Virus Res.* 2013;176(1-2):285-291.
45. Novakovic P, Harding JC, Al-Dissi AN, Detmer SE. Type 2 porcine reproductive and respiratory syndrome virus infection increases apoptosis at the maternal-fetal interface in late gestation pregnant gilts. *PLoS One.* 2017;12(3):e0173360.
46. Karniychuk UU, Saha D, Geldhof M, et al. Porcine reproductive and respiratory syndrome virus (PRRSV) causes apoptosis during its replication in fetal implantation sites. *Microb Pathog.* 2011;51(3):194-202.
47. Novakovic P, Harding JC, Ladinig A, Al-Dissi AN, MacPhee DJ, Detmer SE. Relationships of CD163 and CD169 positive cell numbers in the endometrium and fetal placenta with type 2 PRRSV RNA concentration in fetal thymus. *Vet Res.* 2016;47(1):76.
48. Ladinig A, Detmer SE, Clarke K, et al. Pathogenicity of three type 2 porcine reproductive

- and respiratory syndrome virus strains in experimentally inoculated pregnant gilts. *Virus Res.* 2015;203:24-35.
49. Ladinig A, Wilkinson J, Ashley C, et al. Variation in fetal outcome, viral load and ORF5 sequence mutations in a large scale study of phenotypic responses to late gestation exposure to type 2 porcine reproductive and respiratory syndrome virus. *PLoS One.* 2014;9(4):e96104.
  50. Rowland RR. The interaction between PRRSV and the late gestation pig fetus. *Virus Res.* 2010;154(1-2):114-122.
  51. Rossow KD, Laube KL, Goyal SM, Collins JE. Fetal microscopic lesions in porcine reproductive and respiratory syndrome virus-induced abortion. *Vet Pathol.* 1996;33(1):95-99.
  52. Stockhofe-Zurwieden N, Navarro Camarro JA, Grosse-Beilage E, Chavez J, Pohlenz J. Uterine and placental alterations in pregnant sows associated with the porcine epidemic abortion and respiratory syndrome (PEARS). *Zentralbl Vet B.* 1993;40(4):261-271.
  53. Novakovic P, Detmer SE, Suleman M, Malgarin CM, MacPhee DJ, Harding JCS. Histologic changes associated with placental separation in gilts infected with porcine reproductive and respiratory syndrome virus. *Vet Pathol.* 2018;55(4):521-530.
  54. Mengeling WL, Lager KM, Vorwald AC. Diagnosis of porcine reproductive and respiratory syndrome. *J Vet Diagn Invest.* 1995;7(1):3-16.
  55. Deusch S, Tilocca B, Camarinha-Silva A, Seifert J. News in livestock research - Use of Omics-technologies to study the microbiota in the gastrointestinal tract of farm animals. *Comput Struct Biotechnol J.* 2015;13:55-63.
  56. Kadarmideen HN. Genomics to systems biology in animal and veterinary sciences: Progress, lessons and opportunities. *Livest Sci.* 2014;166(1):232-248.
  57. Jiang Y, Li G, Yu L, et al. Genetic Diversity of Porcine Reproductive and Respiratory Syndrome Virus (PRRSV) From 1996 to 2017 in China. *Front Microbiol.* 2020;11(April).
  58. Dekkers J, Rowland RRR, Lunney JK, Plastow G. Host genetics of response to porcine reproductive and respiratory syndrome in nursery pigs. *Vet Microbiol.* 2017;209(November 2016):107-113.
  59. Waide EH, Tuggle CK, Serão NVL, et al. Genomic prediction of piglet response to infection with one of two porcine reproductive and respiratory syndrome virus isolates.

- Genet Sel Evol.* 2018;50(1):1-12.
60. Burkard C, Lilloco SG, Reid E, et al. Precision engineering for PRRSV resistance in pigs: Macrophages from genome edited pigs lacking CD163 SRCR5 domain are fully resistant to both PRRSV genotypes while maintaining biological function. *PLoS Pathog.* 2017;13(2):1-28.
  61. Georges M, Charlier C, Hayes B. Harnessing genomic information for livestock improvement. *Nat Rev Genet.* 2019;20(3):135-156.
  62. Wilkinson JM, Ladinig A, Bao H, et al. Differences in whole blood gene expression associated with infection time-course and extent of fetal mortality in a reproductive model of type 2 porcine reproductive and respiratory syndrome virus (PRRSV) infection. *PLoS One.* 2016;11(4):e0153615.
  63. Wilkinson JM, Bao H, Ladinig A, et al. Genome-wide analysis of the transcriptional response to porcine reproductive and respiratory syndrome virus infection at the maternal/fetal interface and in the fetus. *BMC Genomics.* 2016;17:383.
  64. Patti GJ, Yanes O, Siuzdak G. Metabolomics: the apogee of the omics trilogy. *Nat Rev Mol Cell Biol.* 2012;13(4):263-269.
  65. Xia J, Wishart DS. Web-based inference of biological patterns, functions and pathways from metabolomic data using MetaboAnalyst. *Nat Protoc.* 2011;6(6):743-760.
  66. Scalbert A, Brennan L, Fiehn O, et al. Mass-spectrometry-based metabolomics: Limitations and recommendations for future progress with particular focus on nutrition research. *Metabolomics.* 2009;5(4):435-458.
  67. Alonso A, Marsal S, Julià A. Analytical methods in untargeted metabolomics: State of the art in 2015. *Front Bioeng Biotechnol.* 2015;3(MAR):1-20.
  68. Holtkamp DJ, Kliebenstein JB, Neumann EJ, et al. Assessment of the economic impact of porcine reproductive and respiratory syndrome virus on United States pork producers. *J Swine Heal Prod.* 2013;21(2):72-84.
  69. Whitworth KM, Prather RS. Gene editing as applied to prevention of reproductive porcine reproductive and respiratory syndrome. *Mol Reprod Dev.* 2017;84(9):926-933.
  70. Ladinig A, Foxcroft G, Ashley C, Lunney JK, Plastow G, Harding JC. Birth weight, intrauterine growth retardation and fetal susceptibility to porcine reproductive and respiratory syndrome virus. *PLoS One.* 2014;9(10):e109541.

71. Ge M, Zhang Y, Liu Y, Liu T, Zeng F. Propagation of field highly pathogenic porcine reproductive and respiratory syndrome virus in MARC-145 cells is promoted by cell apoptosis. *Virus Res.* 2016;213:322-331.
72. Suleman M, Novakovic P, Malgarin CM, Detmer SE, Harding JCS, MacPhee DJ. Spatiotemporal immunofluorescent evaluation of porcine reproductive and respiratory syndrome virus transmission across the maternal-fetal interface. *Pathog Dis.* 2018;76(5):1-14.
73. Suleman M, Galea S, Gavard F, et al. Antigen encoded by vaccine vectors derived from human adenovirus serotype 5 is preferentially presented to CD8+ T lymphocytes by the CD8 $\alpha$ + dendritic cell subset. *Vaccine.* 2011;29(35):5892-5903.
74. Bishop SC, Woolliams JA. Genomics and disease resistance studies in livestock. *Livest Sci.* 2014;166:190-198.
75. Richardson LA. Understanding disease tolerance and resilience. *PLoS Biol.* 2016;14(7):e1002513.
76. Machado G, Mendoza MR, Corbellini LG. What variables are important in predicting bovine viral diarrhea virus? A random forest approach. *Vet Res.* 2015;46(1):85.
77. Zimmerman JJ, Karkiker LA, Ramirez A, Schwartz KJ, Stevenson GW. *Diseases of Swine.* 10th ed. (John Wiley & Sons 2012, ed.); 2012.
78. Cronqvist T, Tannetta D, Mörgelin M, et al. Syncytiotrophoblast derived extracellular vesicles transfer functional placental miRNAs to primary human endothelial cells. *Sci Rep.* 2017;7(1):4558.
79. Tong M, Chamley LW. Placental Extracellular Vesicles and Feto-Maternal Communication. *Cold Spring Harb Perspect Med.* 2015;5(3):a023028.
80. Bidarimath M, Khalaj K, Kridli RT, Kan FWK, Koti M, Tayade C. Extracellular vesicle mediated intercellular communication at the porcine maternal-fetal interface: A new paradigm for conceptus-endometrial cross-talk. *Sci Rep.* 2017;7(1):40476.
81. Wang T, Fang L, Zhao F, Wang D, Xiao S. Exosomes mediate intercellular transmission of porcine reproductive and respiratory syndrome virus (PRRSV). *J Virol.* Published online November 29, 2017:01734-17.
82. Karniychuk UU, Van Breedam W, Van Roy N, Rogel-Gaillard C, Nauwynck HJ. Demonstration of microchimerism in pregnant sows and effects of congenital PRRSV

- infection. *Vet Res.* 2012;43:19.
83. Cortiñas Abrahantes J, Bollaerts K, Aerts M, Ogunsanya V, Van der Stede Y. Salmonella serosurveillance: Different statistical methods to categorise pig herds based on serological data. *Prev Vet Med.* 2009;89(1-2):59-66.
  84. Larison B, Njabo KY, Chasar A, Fuller T, Harrigan RJ, Smith TB. Spillover of pH1N1 to swine in Cameroon: an investigation of risk factors. *BMC Vet Res.* 2014;10(1):55.
  85. Valdes-Donoso P, VanderWaal K, Jarvis LS, Wayne SR, Perez AM. Using machine learning to predict swine movements within a regional program to improve control of infectious diseases in the US. *Front Vet Sci.* 2017;4.
  86. White LA, Torremorell M, Craft ME. Influenza A virus in swine breeding herds: Combination of vaccination and biosecurity practices can reduce likelihood of endemic piglet reservoir. *Prev Vet Med.* 2017;138:55-69.
  87. Fowden AL, Forhead AJ. Endocrine mechanisms of intrauterine programming. *Reproduction.* 2004;127(5):515-526.
  88. Fishman RHB, Yanai J. Long-lasting effects of early barbiturates on central nervous system and behavior. *Neurosci Biobehav Rev.* 1983;7(1):19-28.
  89. RXmed. Barbiturates (Amobarbital).
  90. Adams MJ, Lefkowitz EJ, King AMQ, et al. Ratification vote on taxonomic proposals to the International Committee on Taxonomy of Viruses (2016). *Arch Virol.* 2016;161(10):2921-2949.
  91. Hou LiLi, TieZhu Z, XiuLing Y, et al. Molecular epidemiology of highly pathogenic porcine reproductive and respiratory syndrome virus in China. *Chinese J Vet Sci.* 2009;29(6):667-682.
  92. Malgarin CM, Nosach R, Novakovic P, et al. Classification of fetal resilience to porcine reproductive and respiratory syndrome (PRRS) based on temporal viral load in late gestation maternal tissues and fetuses. *Virus Res.* 2019;260:151-162.
  93. Vallet JL, Freking BA, Miles JR. Effect of empty uterine space on birth intervals and fetal and placental development in pigs. *Anim Reprod Sci.* 2011;125(1-4):158-164.
  94. Landis JR, Koch GG. The measurement of observer agreement for categorical data. *Biometrics.* 1977;33(1):159-174.
  95. Lin LI-K. A Concordance Correlation Coefficient to Evaluate Reproducibility. *Biometrics.*

- 1989;45(1):255.
96. PigChamp\_Knowledge\_Software. 2019 USA PigChamp Benchmarking Summaries.
  97. NAHMS. Part II: Reference of Swine Health and Health Management in the United States, 2012. 2016;II: USDA-A.
  98. Morrison Swine Health Monitoring Program CoVM U of M. PRRS aggregate prevalence of sow herd status.
  99. Nair MS, Yao D, Chen C, Pieters M. Serum metabolite markers of early *Mycoplasma hyopneumoniae* infection in pigs. *Vet Res.* 2019;50(1):1-10.
  100. Welle T, Hoekstra AT, Daemen IAJM, Berkers CR, Costa MO. Metabolic response of porcine colon explants to in vitro infection by *Brachyspira hyodysenteriae*: a leap into disease pathophysiology. *Metabolomics.* 2017;13(7):1-7.
  101. Gong W, Jia J, Zhang B, et al. Serum metabolomic profiling of piglets infected with virulent classical swine fever virus. *Front Microbiol.* 2017;8(APR).
  102. Yang T, Wilkinson J, Wang Z, Ladinig A, Harding J, Plastow G. A genome-wide association study of fetal response to type 2 porcine reproductive and respiratory syndrome virus challenge. *Sci Rep.* 2016;6:20305.
  103. Psychogios N, Hau DD, Peng J, et al. The human serum metabolome. *PLoS One.* 2011;6(2).
  104. Saude EJ, Slupsky CM, Sykes BD. Optimization of NMR analysis of biological fluids for quantitative accuracy. *Metabolomics.* 2006;2(3):113-123.
  105. Bahado-Singh RO, Akolekar R, Mandal R, et al. Metabolomics and first-trimester prediction of early-onset preeclampsia. *J Matern Neonatal Med.* 2012;25(10):1840-1847.
  106. Hagel JM, Mandal R, Han B, et al. Metabolome analysis of 20 taxonomically related benzylisoquinoline alkaloid-producing plants. *BMC Plant Biol.* 2015;15(1):220.
  107. Suleman M, Malgarin CM, Detmer SE, Harding JCS, MacPhee DJ. The porcine trophoblast cell line PTr2 is susceptible to porcine reproductive and respiratory syndrome virus-2 infection. *Placenta.* 2019;88.
  108. Havener LJ, Toback FG. Amino acid modulation of renal phosphatidylcholine biosynthesis in the rat. *J Clin Invest.* 1980;65(3):741-745.
  109. Holmsen H, Hindenes JO, Fukami M. Glycerophospholipid metabolism: Back to the future. *Thromb Res.* 1992;67(3):313-323.

110. Hanna VS, Hafez EAA. Synopsis of arachidonic acid metabolism: A review. *J Adv Res.* 2018;11:23-32.
111. Takikawa O, Yoshida R, Kido R, Hayaishi O. Tryptophan degradation in mice initiated by indoleamine 2,3-dioxygenase. *J Biol Chem.* 1986;261(8):3648-3653.
112. King NJC, Thomas SR. Molecules in focus: Indoleamine 2,3-dioxygenase. *Int J Biochem Cell Biol.* 2007;39(12):2167-2172.
113. Alex Pasternak J, MacPhee DJ, Harding JCS. Fetal cytokine response to porcine reproductive and respiratory syndrome virus-2 infection. *Cytokine.* 2020;126:154883.
114. Yang Q, Zhang Q, Tang J, Feng W hai. Lipid rafts both in cellular membrane and viral envelope are critical for PRRSV efficient infection. *Virology.* 2015;484:170-180.
115. Gault CR, Obeid LM, Hannun YA. An overview of sphingolipid metabolism: From synthesis to breakdown. *Adv Exp Med Biol.* 2010;688:1-23.
116. Hannun YA, Obeid LM. Sphingolipids and their metabolism in physiology and disease. *Nat Rev Mol Cell Biol.* 2018;19(3):175-191.
117. Chan FK-M, Luz NF, Moriwaki K. Programmed necrosis in the cross talk of cell death and inflammation. *Annu Rev Immunol.* 2015;33(1):79-106.
118. Thurmond RL, Gelfand EW, Dunford PJ. The role of histamine H1 and H4 receptors in allergic inflammation: The search for new antihistamines. *Nat Rev Drug Discov.* 2008;7(1):41-53.
119. Graham AC, Hilmer KM, Zickovich JM, Obar JJ. Inflammatory response of mast cells during Influenza A virus infection is mediated by active infection and RIG-I signaling. *J Immunol.* 2013;190(9):4676-4684.
120. Danial NN, Korsmeyer SJ. Cell death: critical control points. *Cell.* 2004;116(2):205-219.
121. Pasternak JA, MacPhee DJ, Harding JCS. Maternal and fetal thyroid dysfunction following porcine reproductive and respiratory syndrome virus2 infection. *Vet Res.* 2020;51(1).
122. Van Goor A, Pasternak A, Walker K, et al. Differential responses in placenta and fetal thymus at 12 days post infection elucidate mechanisms of viral level and fetal compromise following PRRSV2 infection. *BMC Genomics.* 2020;21(1):1-20.
123. Zhang Q, Yoo D. PRRS virus receptors and their role for pathogenesis. *Vet Microbiol.* 2015;177(3-4):229-241.

124. Kent-Dennis C, Pasternak A, Plaizier JC, Penner GB. Potential for a localized immune response by the ruminal epithelium in nonpregnant heifers following a short-term subacute ruminal acidosis challenge. *J Dairy Sci.* 2019;102(8):7556-7569.
125. Team RC. R: A language and environment for statistical computing. Published online 2020.
126. Wickham H. *Ggplot2: Elegant Graphics for Data Analysis*. Springer-Verlag New York; 2016.
127. Dhuriya YK, Sharma D. Necroptosis: A regulated inflammatory mode of cell death. *J Neuroinflammation.* 2018;15(1):1-9.
128. Cheon D-S, Chae C. Comparison of virus isolation, reverse transcription-polymerase chain reaction, immunohistochemistry, and in situ hybridization for the detection of porcine reproductive and respiratory syndrome virus from naturally aborted fetuses and stillborn piglets. *J Vet Diagnostic Investig.* 2000;12(6):582-587.
129. Cheon DS, Chae C. Distribution of porcine reproductive and respiratory syndrome virus in stillborn and liveborn piglets from experimentally infected sows. *J Comp Pathol.* 2001;124(4):231-237.
130. Amadori M, Razzuoli E. Immune control of PRRS: lessons to be learned and possible ways forward. *Front Vet Sci.* 2014;1.
131. Schönenberger MJ. Hypoxia signaling pathways: modulators of oxygen-related organelles. *Front Cell Dev Biol.* 2015;3:42.
132. Lee JW, Ko J, Ju C, Eltzschig HK. Hypoxia signaling in human diseases and therapeutic targets. *Exp Mol Med.* 2019;51(6):68.
133. Shimizu S, Eguchi Y, Kosaka H, Kamiike W, Matsuda H, Tsujimoto Y. Prevention of hypoxia-induced cell death by Bcl-2 and Bcl-xL. *Nature.* 1995;374(6525):811-813.
134. Goyal P, Weissmann N, Grimminger F, et al. Upregulation of NAD(P)H oxidase 1 in hypoxia activates hypoxia-inducible factor 1 via increase in reactive oxygen species. *Free Radic Biol Med.* 2004;36(10):1279-1288.
135. Forstermann U, Sessa WC. Nitric oxide synthases: regulation and function. *Eur Heart J.* 2012;33(7):829-837.
136. Hale LP, Braun RD, Gwinn WM, Greer PK, Dewhirst MW. Hypoxia in the thymus: Role of oxygen tension in thymocyte survival. *Am J Physiol - Hear Circ Physiol.* 2002;282(4

- 51-4):1467-1477.
137. Ohta A, Diwanji R, Kini R, Subramanian M, Ohta A, Sitkovsky M. In vivo T cell activation in lymphoid tissues is inhibited in the oxygen-poor microenvironment. *Front Immunol.* 2011;2(JUL):1-10.
  138. Malgarin CM, MacPhee DJ, Harding JCS. Fetal metabolomic alterations following porcine reproductive and respiratory syndrome virus infection. *Front Mol Biosci.* 2020;7.
  139. Christianson WT, Collins JE, Benfield DA, et al. Experimental reproduction of swine infertility and respiratory syndrome in pregnant sows. *Am J Vet Res.* 1992;53(4):485-488.
  140. Law SH, Chan ML, Marathe GK, Parveen F, Chen CH, Ke LY. An updated review of lysophosphatidylcholine metabolism in human diseases. *Int J Mol Sci.* 2019;20(5).
  141. Ošt'ádal B, Kolář F. *Cardiac Ischemia: From Injury to Protection.* Vol 4. Springer US; 1999.
  142. Chiong M, Wang Z V., Pedrozo Z, et al. Cardiomyocyte death: Mechanisms and translational implications. *Cell Death Dis.* 2011;2(12):1-11.
  143. Orogo AM, Gustafsson ÅB. Cell death in the myocardium: My heart won't go on. *IUBMB Life.* 2013;65(8):651-656.